NIRS-M-235

Karolinska Institutet

Proceedings of

Japanese-European Joint Symposium on Ion Cancer Therapy

and

NIRS-KI Joint Symposium on Ion-Radiation Sciences

September 9 & 10-11, 2010
Karolinska University Hospital, Solna
Stockholm, Sweden

Organized by

National Institute of Radiological Sciences, Japan

and

Karolinska Institute, Sweden

INDEX

INDEX

KI and NIRS Joint Symposium on Ion-Radiation Sciences

INDEX

4th Japanese-European Joint Symposium on Ion Cancer Therapy

Stockholm, 9th of September 2010

Preface

The light ions have a unique role in the development of modern radiation therapy where Biological Optimized Radiation Quality and Intensity Modulated Radiation Therapy (QMRT and IMRT) are increasingly coming into clinical use preferably through a systems biology approach to therapy optimization. The unique dose distributional qualities of light ions such as the sharp penumbra and high deep Bragg peak are ideally suited for high quality radiation therapy, and even more importantly their radiation biological properties are almost perfect for eradicating large complex generally hypoxic tumor volumes with minimal damage to surrounding normal tissues. The remaining challenge to a more wide spread clinical use of light ions are to improve the sensitivity and specificity of molecular tumor Imaging to more accurately localize the tumor tissues and to develop fast scanning systems that maximizes the fundamental biological and physical advantages of the light ions. For optimal application it is essential to modulate the ion beams and select the best possible ion species depending on the molecular and anatomic properties of the tumor and surrounding normal tissues and that is where systems biology will play a key role. For small hypoxic tumors the high apoptotic induction at the Bragg peak of lithium ions is ideal whereas large tumor masses may require carbon and oxygen ions and the microscopically invasive part of the tumor may be best treated by photons, electrons, protons or helium ions.

The National Institute of Radiological Sciences (NIRS) in Chiba, Japan, pioneered the clinical study of carbon ion radiotherapy using the Heavy Ion Medical Accelerator in Chiba (HIMAC). The HIMAC is the world's first heavy ion accelerator complex dedicated to cancer therapy. Since 1994 it has been the leading center for clinical and radiation physics research on carbon ion radiotherapy and more than 5,000 patients with a variety of tumors have been treated to date. This 4th Japanese-European joint meeting has been organized to stimulate the clinical and scientific interaction with the long-term goal of contributing to a more widespread use of the clinical advantages of carbon ion radiotherapy.

Hirohiko Tsujii, NIRS
Anders Brahme, Karolinska

Treatment Planning for Carbon-Ion Scanning at NIRS

Taku Inaniwa, Takuji Furukawa, Shinji Sato, Nobuyuki Kanematsu, Naruhiro Matsufuji, Shinichiro Mori, Eri Takeshita, Takeshi Himukai and Koji Noda

Research Center for Charged Particle Therapy, National Institute of Radiological Sciences, Chiba, Japan
Corresponding Author: Taku Inaniwa, e-mail address:taku@nirs.go.jp

Abstract

In order to use an intensity-controlled raster scan method at the new particle-therapy research facility in HIMAC, we have developed a software program dedicated to the planning of radiotherapy with a scanned ^{12}C beam. Inverse planning techniques are implemented in the software in order to obtain uniform biological dose distribution within the target as well as to reduce the dose delivered to the organs at risk. The scan trajectory is determined so that the path length will be minimized by applying a fast simulated annealing algorithm for scan trajectory optimisation. The dose delivered along the scan trajectory during the beam transition time from one spot to the next spot is integrated into the inverse planning to shorten the treatment time. The lateral dose distribution of the scanned carbon beam is expressed by a sum of three Gaussians in order to account for the dose reduction observed in the irradiation of a small target volume. The code also copes with the planning for intensity modulated ion therapy. The reliability of the software has been confirmed through irradiation experiments at HIMAC.

1. Introduction

A project to construct a new particle-therapy research facility as an extension of the existing Heavy-Ion Medical Accelerator in Chiba (HIMAC) has been initiated for further development of carbon-ion therapy at the National Institute of Radiological Sciences (NIRS). The facility will be equipped with three treatment rooms, two of which will provide the horizontal and vertical fixed beam ports, and another one a rotating gantry [1]. In all rooms, three-dimensional (3D) irradiation with pencil beam scanning will be used in order to make full use of the advantages of heavy-ion therapy such as the high dose concentration and high relative biological effectiveness (RBE) around the Bragg peak. This method has already been implemented for clinical use at the Paul Scherrer Institute (PSI) with protons [2] and the Gesellschaft für Schwerionenforschung mbH (GSI) with carbon ions [3]. Recently, it has also been used at the Heidelberg Ion Therapy Center (HIT) with carbon ions [4]. In these facilities, only patients with static tumors, e.g., tumors in the head and neck or in the spinal cord, have been treated. In the new particle-therapy research facility, we intend to treat not only static tumors, but also movable tumors by using gated irradiation and re-scanning methods [5]. Faster scanning methods will be key to completing the treatment irradiation within a few minutes. The range shifter plates will be used in the new facility because of their capability to change the beam range within a few hundred milliseconds. The effect of the additional beam spread and the increase of the projectile fragments due to the insertion of the range shifter plates have to be included in the dose response function of the scanned beam in the treatment planning. To address the problems pertaining to the developmental flexibly and to allow for the irradiation of movable tumors, we developed a treatment planning software program for carbon-ion scanning which is suitable for the unique scanning system designed at NIRS. This paper describes the basic principles of this software program.

2. Materials and Methods

2.1 Beam Model

In 3D irradiation with pencil beam scanning, the prescribed dose distribution is realized by superimposing the dose of the individual pencil beams *d* according to their optimized weights *w*. The Bragg peak of the pristine beam is slightly broadened to produce a "mini peak" by the ridge filter, and is used as a pencil beam. In the new facility, pristine beams with 11 different energies will be prepared between 140 MeV/u and 430 MeV/u. The dose distribution at (x_i, y_i, z_i) delivered by the pencil beam stopped at (x_0, y_0, z_0) can be represented as follows:

$$d(x_i, y_i, z_i; x_0, y_0, z_0) = D_1(x_i; x_0, y_i; y_0, \sigma_1(z_i; z_0))d_z(z_i; z_0). \quad (1)$$

Here, $d_z(z_i; z_0)$ is the planner-integrated dose at a depth of z_i, while $D_1(x_i; x_0, y_i; y_0, \sigma_1(z_i; z_0))$ is the two dimensional normalized Gaussian functions with standard deviations $\sigma_1(z_i; z_0)$ representing the beam spread at a depth z_i. The planner-integrated dose $d_z(z_i; z_0)$ and the lateral beam spread, i.e., $\sigma_1(z_i; z_0)$, were determined from the measured dose distribution with a large area parallel plate ionization chamber and a profile monitor, respectively. Then these measured data are fitted to simple formulae and incorporated into the planning software as shown in Figure 1. With this algorithm, the effect of the beam spread due to multiple scattering in the range shifter can be incorporated, at least for the primary particles. However, our recent research revealed that the dose delivered to the target is reduced according to the field-size in carbon ion scanning with range shifter plates [6]. The observed dose reduction is referred to as the 'field-size effect of dose' in this paper. In order to account for this effect, we adopted three-Gaussian forms of lateral dose distributions for the pencil beam model used in the treatment planning software. In this case, equation (1) can be rewritten as follows:

$$d(x_i, y_i, z_i; x_0, y_0, z_0) = d_z(z_i; t) \times$$
$$\left\{\left(1 - \sum_{j=2}^{3} f_j(z_i; t)\right) D_1(x_i; x_0, y_i; y_0, \sigma_1(z_i; t)) + \sum_{j=2}^{3}\left(f_j(z_i; t) D_j(x_i; x_0, y_i; y_0, \sigma_j(z_i; t))\right)\right\}, \quad (2)$$

where $f_j(z_i; t)$ is the fraction of integrated dose assigned to the *j*-th Gaussian component at a depth z_i delivered by the pencil beam with the range shifter plate of thickness *t*, and $D_j(x_i; x_0, y_i; y_0, \sigma_j(z_i; t))$ is a two dimensional Gaussian function describing the lateral spread of the *j*-th component at a depth of z_i with the standard deviation $\sigma_j(z_i; t)$. The parameters $\sigma_j(z_i; t)$ and $f_j(z_i; t)$ are experimentally determined and registered as the pencil beam parameters in the software. The lateral dose profile expressed with the three-Gaussian beam model is schematically shown in Figure 2, along with that of the single-Gaussian beam model. This allows for the option of using the three-Gaussian beam model in the dose optimization. The observed field-size effect of doses can be accounted for with this beam model. However, it is time-consuming to implement the three-Gaussian beam model in the iterative dose optimization. The 'predicted-dose scaling factor' is usually used as an alternative approach to account for the field-size effect of the doses [6].

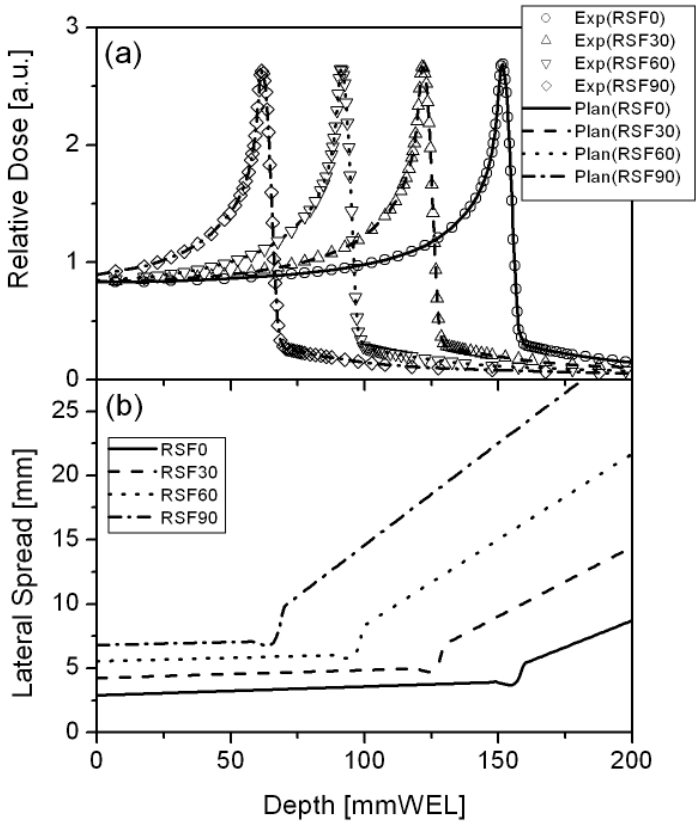

Figure 1. Pencil beam data for a 290-MeV/u carbon beam used by the treatment planning software. (a) Planner-integrated dose distribution d_z and (b) lateral beam spread σ_1 as a function of depth z_i for a range shifter of 0 (solid line), 30 (dashed line), 60 (dotted line) and 90 (dash-dotted line) mm water equivalent thicknesses.

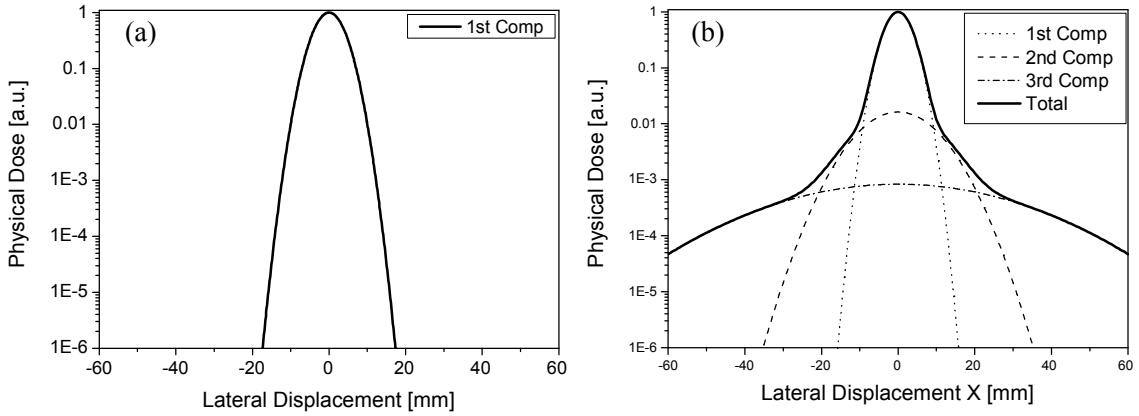

Figure 2. Schematics of the lateral dose distribution expressed by (a) a single-Gaussian beam model and (b) a three-Gaussian beam model.

2.2 Dose Optimization

The goal of dose optimisation in the treatment planning is to find the best particle numbers (weight) for each pencil beam, i.e. the best weighting matrix, so that the resulting dose distribution is as close as possible to the

prescribed dose distribution within the target volume and does not exceed the dose restrictions within the organs at risk. When determining the weighting matrix, the dose-based objective function $f(w)$ is minimized through an iterative optimisation process. The objective function can be described as;

$$f(w)=\sum_{i\in \mathrm{T}}\left(Q_{\mathrm{P}}^{\mathrm{o}}\left[D_{biol,i}(w)+U_i-D_{\mathrm{P}}^{\max}\right]_+^2+Q_{\mathrm{P}}^{\mathrm{u}}\left[D_{\mathrm{P}}^{\min}+U_i-D_{biol,i}(w)\right]_+^2\right)+\sum_{i\in \mathrm{O}}Q_{\mathrm{O}}\left[D_{biol,i}(w)+U_i-D_{\mathrm{O}}^{\max}\right]_+^2 \quad (3)$$

where $D_{biol,i}(w)$, $D_{\mathrm{P}}^{\max}$, $D_{\mathrm{P}}^{\min}$, $Q_{\mathrm{P}}^{\mathrm{o}}$, $Q_{\mathrm{P}}^{\mathrm{u}}$, $D_{\mathrm{O}}^{\max}$, Q_{O} is the biological dose at a point i obtained with matrix w, the maximum and minimum doses applied to the target T, the penalties for over- and underdosage specified for the target, the maximum dose allowed for the OAR and the penalty for overdosage in OAR, respectively. In raster scanning irradiation, the beam delivery is not switched off during the transition time from one spot to the next. Therefore, in this scheme, the extra dose is inevitably delivered to the sites between two successive spots during the beam spot transition, along the scan trajectory. The contribution of the extra dose is included in the dose optimization by adding the term U_i to the objective function representing the amount of the extra dose delivered to a voxel i [7]. For the dose optimization, we used a gradient-based algorithm with the quasi-Newton method.

2.3 Flow of treatment planning

By using the developed software, the treatment plans are produced according to the flowchart shown in Figure 3. Each task in the flowchart is briefly explained below.

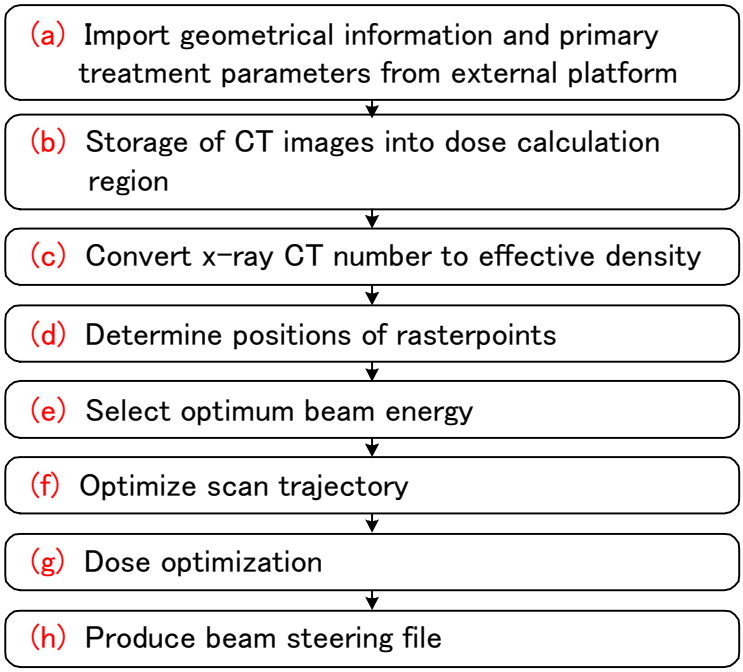

Figure 3: Flowchart of the treatment planning.

(a) Radio-oncologists delineate the PTV and OARs on the clinical CT images using an external platform, and determine the primary treatment parameters, e.g. isocenter, desired dose level, irradiation method (single field or IMIT), number of ports, and beam directions, based on the information about the position and type of tumor as well as critical structures. The isocenter in the CT coordinates coincides with the origin of the raster scanner system. The scanner step size in the lateral and orthogonal directions, Δx and Δy, and step size of range

shifter plate, Δz, are also determined at this stage. The CT images, geometrical information determined by the radio-oncologists and the primary treatment parameters are imported from the platform to the software program.

(b) The CT images are stored in the segmented region for dose calculation by using the tri-linear interpolation. The voxel size is determined taking both the precision and time required for the dose optimization into account. The voxels within the PTV and OARs are identified with different flags.

(c) The x-ray CT number stored in each voxel is converted to the stopping powers relative to the stopping power of water using a conversion table created based on the polybinary tissue model [8].

(d) The Bragg peaks are placed automatically by the software to account for the cold doses in the peripheral region of the PTV due to the finite size of the mini peak and beam width. In this step, the maximum range of the pencil beam is determined among all pencil beams placed within the PTV.

(e) From the maximum range determined in (d), the optimum beam energy is selected from 11 individual energies available from the HIMAC synchrotron.

(f) In the raster-scan method, the region of the raster-point was divided into slices of equal ion ranges. The beam scanning begins at the distal slice (highest energy) and laterally covers each slice on a discrete *x*-*y* grid, until the most proximal slice (lowest energy) is reached. In order to minimize the extra dose in raster scanning [7] and shorten the treatment time, we determined the scan trajectory on each slice so that the path-length would be minimized by applying a fast simulated annealing algorithm to scan trajectory optimization [9].

(g) The particle numbers (weight) for each raster-point are determined by the dose optimization method described in 2.2.

(h) Finally, the beam steering file is produced in which the position of the raster-point x_0, y_0, z_0, corresponding thickness of the range shifter plates *t*, and the particle numbers (weights) of all pencil beams are written in following the order of the optimized scan trajectory.

3. Results and Discussions

3.1 Correction of the field-size effect with the predicted-dose scaling factor

In order to account for the field-size effect of the doses, we tested the 'predicted-dose scaling factor'. Here, the physical dose distribution of 1 Gy was planned for the cylindrical target volume of 100 mm in diameter and 60 mm in spread-out Bragg-peak (SOBP) using the single-Gaussian beam model for the dose optimization. The dose distribution was recalculated with the three-Gaussian beam model only at the end of the optimization, and the 'predicted-dose scaling factor' was derived as a ratio of the averaged dose within the target volume for optimized dose distribution to that for the recalculated dose. The derived factor of 1.013 in the present case was multiplied with the spot-weights tabulated in the beam steering file. The irradiation experiments were carried out according to the derived beam steering file using the carbon-ion scanning system developed at HIMAC [10]. In Figure 4, the measured physical dose distribution along the beam axis is shown with the calculated distribution using the three-Gaussian beam model. Our calculation could reproduce the measured distribution within an inherent accuracy from point to point of less than 2%, including the errors pertaining to the irradiation and measurements. This result shows that the field-size effect of the physical doses can be corrected with a single 'predicted-dose scaling factor' derived by the three-Gaussian beam model.

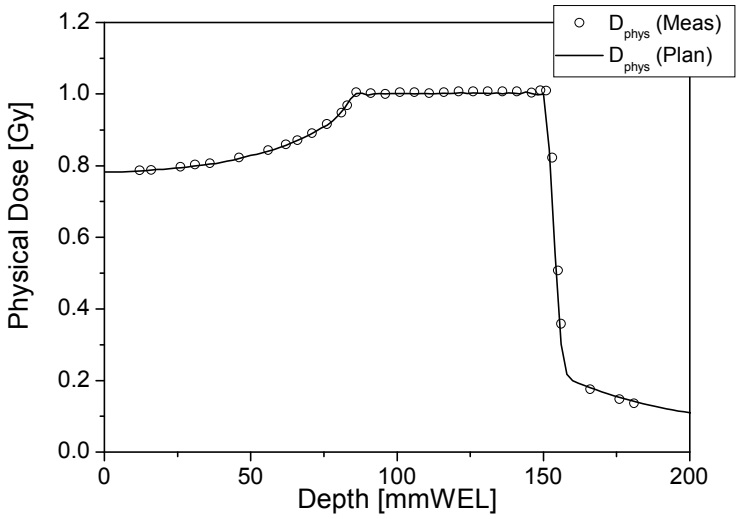

Figure 4. The measured physical dose distribution along the beam axis for the cylindrical target volumes of 100 mm in diameter and 60 mm in SOBP (open circles) are compared with the calculated distribution using the three-Gaussian form of the pencil beam model.

3.2 Treatment planning for patient data

In order to investigate the clinical applicability of the developed software program, treatment plans were produced based on data of a patient treated at HIMAC. As an example, a patient having a rectal tumor was selected (Figure 5(a)). The clinical dose of 4.6 GyE would be delivered from a single port in the anterior to posterior direction. In this plan, only the target volume is specified on the CT images and implemented for dose optimization. The size of the dose calculation voxel was set to $2 \times 2 \times 2$ mm^3, while the scanner step sizes and step size of range shifter plate were all set to 3.0 mm. The beam energy was determined to be 290 MeV/u, and the total number of pencil beams was 15659. In Figure 5(a), the planned biological dose distribution is shown with color-wash display on axial, sagittal and frontal CT images. To verify the treatment plan, we recalculated the physical dose distribution on a water phantom according to the produced beam steering file (Figure 5(b)). Then, the irradiation experiment was performed according to the same beam steering file. In the experiment, we use the verification system that consisted of a water phantom and 24 small thimble ionization chambers (PTW31015) connected to two 12 channels electrometers (Multidos, PTW) [11]. The positions of the ionization chambers within the water phantom are identified with open circles in Figure 5(b). The measured physical doses with the ionization chambers were compared with the recalculated ones in Figure 6. The error bars indicate the possible maximum and minimum doses caused by the setup errors of the mounting of the 24 ionization chambers. Here, we assumed the setup errors of ±0.5 mm, ±1.0 mm and ±1.5 mm in the lateral, orthogonal and beam directions as extreme cases, respectively. The deviations between the measured and the planned doses were less than 6% for all ionization chambers. These experimental results show the reliability of our treatment planning software, as well as the beam delivery system, for carbon-ion scanning developed at HIMAC [10].

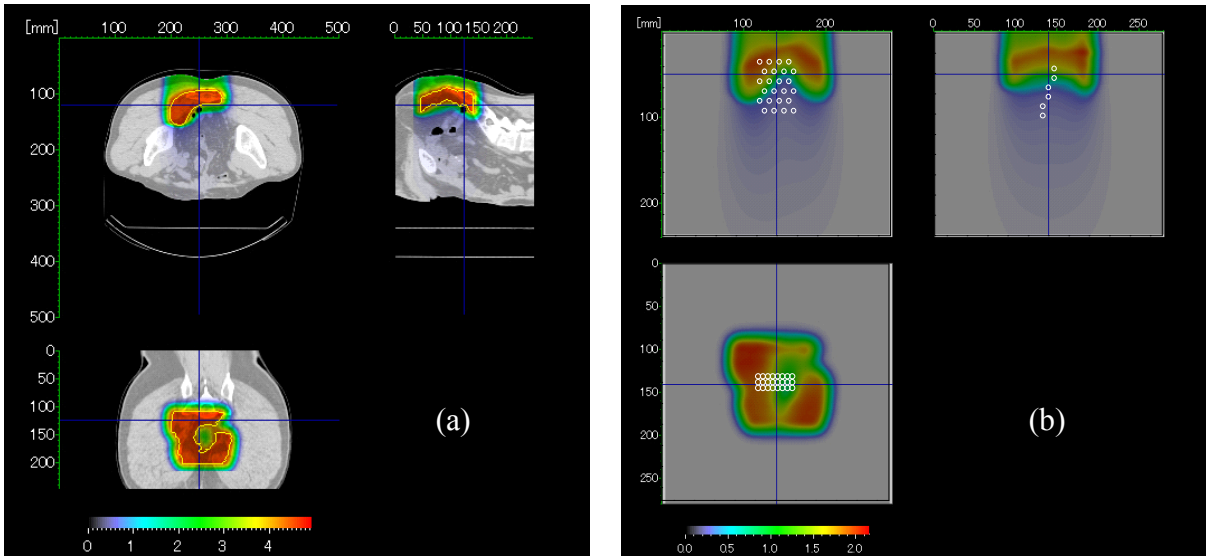

Figure 5. (a) Color wash display of clinical dose distribution for a patient with a rectal tumor. The yellow line encompassed the target volume. (b) The physical dose distribution recalculated on a water phantom. Positions of the 24 ionization chambers are indicated with open white circles.

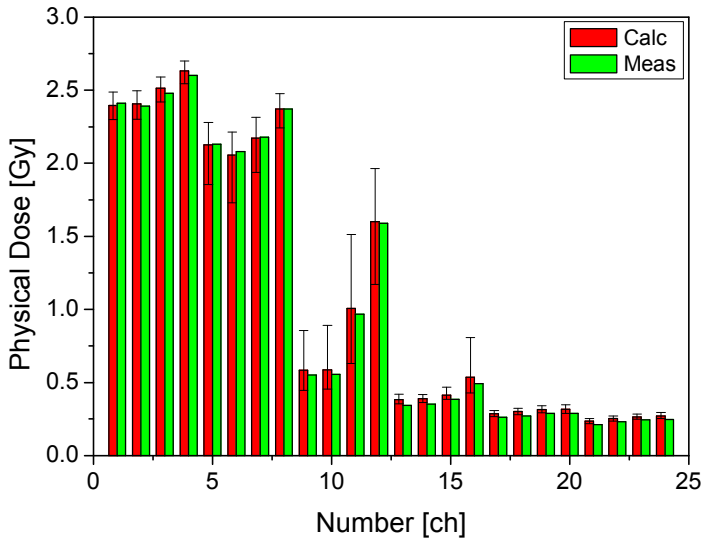

Figure 6. The comparison of dose values recalculated by the treatment planning software (red bars) and the dose values measured with the 24 ionization chambers (green bars) at the positions indicated with open circles in Figure 5(b).

4. Conclusions

We have developed a treatment planning software program dedicated to carbon-ion scanning. In the software, the lateral dose distribution of the scanned carbon beam is expressed by a single Gaussian or a sum of three Gaussians. By using the predicted-dose scaling factor derived with these two beam models, the field size effect of the physical doses could be corrected effectively. The maximum deviation between the measured and planned physical doses was less than 2% in the whole target region. The clinical applicability of the new software program was tested based on the patient with a rectal tumor treated at HIMAC. The verification

measurements were performed with the produced beam steering file. The good agreement between the measured and calculated doses shows the reliability of the treatment planning software program, in addition to that of the beam delivery system, for carbon-ion scanning developed at HIMAC.

References

［1］ Noda K, Furukawa T, Fujisawa T, et al. New accelerator facility for carbon-ion cancer-therapy. J Radiat Res. 2007; 48: Suppl. A43-A54.

［2］ Pedroni E, Bacher R, Blattmann H, et al. The 200 MeV proton therapy project at PSI: Conceptual design and practical realization. Med Phys. 1995;22:37-53.

［3］ Kraft G. Tumortherapy with ion beams. Nucl Instrum Methods Phys Res A. 2000;454:1-10.

［4］ Combs S E, Jäkel O, Haberer T and Debus J. Particle therapy at the Heidelberg Ion Therapy Center (HIT) – Integrated research-driven university-hospital-based radiation oncology service in Heidelberg, Germany. Radiat. Oncol. 2010; 95: 41-44.

［5］ Furukawa T, Inaniwa T, Sato S, et al. Design study of a raster scanning system with phase-controled rescanning toward conformal irradiation of moving target in heavy-ion radiotherapy. Med Phys. 2007;34:1085-1097.

［6］ Inaniwa T, Furukawa T, Nagano A, et al. Field-size effect of physical doses in carbon-ion scanning using range shifter plates. Med. Phys. 2009; 36: 2889-2897.

［7］ Inaniwa T, Furukawa T, Tomitani T, Sato S, Noda K, Kanai T, Optimization for fast-scanning irradiation in particle therapy. Med Phys. 2007;34:3302-3311.

［8］ Kanematsu N, Matsufuji N, Kohno R, Minohara S, Kanai T. A CT calibration method based on the polybinary tissue model for radiotherapy treatment planning. Phys Med Biol. 2003;48:1053-1064.

［9］ Kang J H, Wilkens J J, Oelfke U, Demonstration of scan path optimization in proton therapy. Med Phys. 2007;34:3457-3464.

［10］ Furukawa T, Inaniwa T, Sato S, et al. Performance of NIRS fast scanning system for heavy-ion radiotherapy Med. Phys. Submitted

［11］ Karger C P, Jäkel O and Hartmann G H. A system for three-dimensional dosimetric verification of treatment plans in intensity-modulated radiotherapy with heavy ions. Med. Phys. 1999; 26: 2125-2132

Fast IMRT with Narrow Scanned High Energy Photon Beams

Bjorn. Andeassen

Department of Cell and Molecular Biology, Karolinska Institutet, 171 76 Stockholm, Sweden

Abstract:

Radiation biologically optimized treatment planning generally requires that the Intensity distribution of the incoming beams are spatially Modulated (IMRT) thus significantly increasing the treatment outcome by increasing the tumor dose as far as possible while avoiding the sensitive normal tissues. Today conventional treatment units delivering 4 to 20 MV photon beams use flattening filters to create a homogeneous flat broad photon beams which then can be shaped by segmental Dynamic MultiLeaf Collimator (DMLC). Using DMLC to modulate an incoming broad photon beam is a proven technique for delivering IMRT and has been the subject of improvement and development since the early eghties. However, with a treatment unit based on the scanning narrow high energy (50 – 75 MeV) photon beams in combination with a Penumbra trimming MLC instead of a flattening filter and DMLC a more flexible and faster system for IMRT is possible.

Narrow photon beams can be produced by directing a low emittance high energy electron beam on a thin target of low Z material, and then cleaning the therapeutic photon beam from the large fraction of transmitted primary high energy electrons, and photon generated charged leptons, with a dedicated purging magnet placed directly downstream of the target. With a thin bremsstrahlung target the photon spectrum is harder and ideal for 3D in vivo treatment verification by PET-CT based imaging of photo nuclear reactions in human tissues. A scanning system is already available with the racetrack microtron MM50 where the intrinsic electron beam from 5 up to 50 MeV is stigmaticaly scanned so that the focus of the resulting bremsstrahlung beam is a fixed point source just below the upstream side of the bremsstrahlung target. In clinical practice this machine has been used with a full range bremsstrahlung target where no primary electrons are transmitted through the target and the stati c purging magnet removed the photon generated leptons produced in the downstream end of the target. For experimental purposes we used one of the present block collimators as electron collector which results in unwanted electron and photon contamination of the useful beam but it was deemed sufficient for experimental verification of the scanned beam techniques ability to create arbitrary dose distributions.

Measurements with fast narrow scanned photon beams indicates an interesting performance increase even though the measurements have been performed with hardware mainly designed for full range bremsstrahlung targets. The full width of the scanned photon beam at half maximum was 34 mm measured at 9.5 cm depth in water at isocenter (SSD 90.5 cm), 1 m from the 3 mm Be target, generating a collimated 80-20¥% penumbra of 9 mm at primary electron energy of 50 MeV. To generate suitable scan patterns we used a iterative deconvolution scheme that delivered a quasi continuous pencil beam intensity distribution across the entire field.

This was then discretized to a small number of equal intensity pencil beams spots using a Levenberg-Marquard optimizer with an analytical approximation of the pencil beam kernel and the analytical derivatives of the kernel. For a 10x10 cm2 field with a 3 mm Be target the number of accelerator pulses needed to deliver a homogeneous dose distribution across the entire field was typically around 50. By using the MLC as a penumbra trimmer and adding extra spots on the collimator edges the delivered field is markedly flatter at the edges as shown in a figure then with a conventional system.

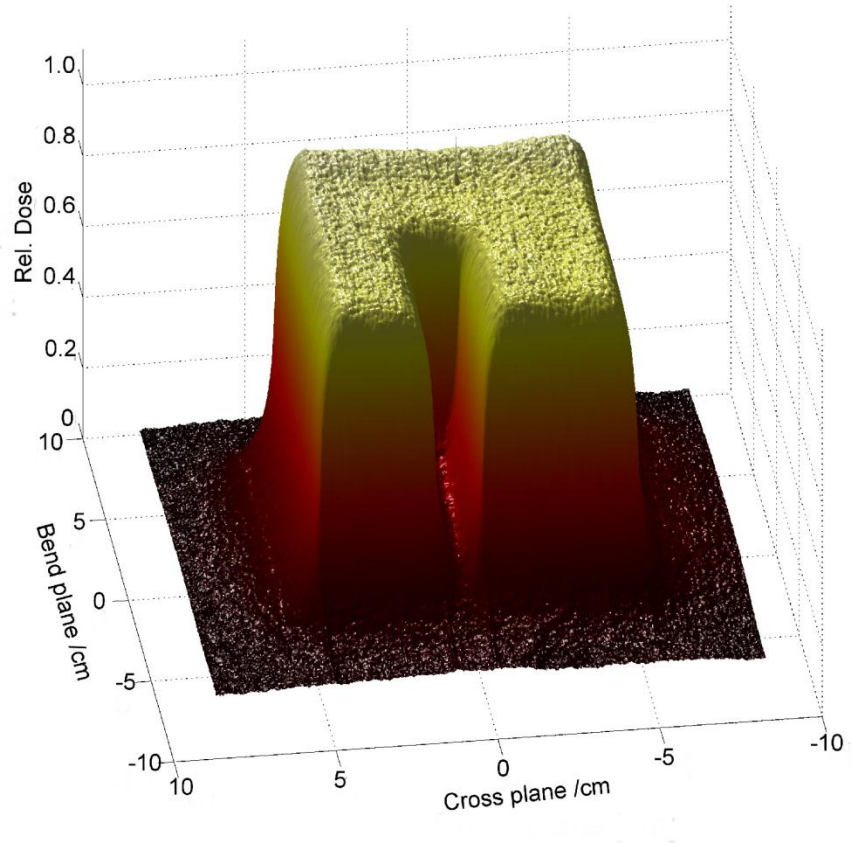

Overview of Carbon-ion Therapy at NIRS: 15 Years' Experience

Hirohiko Tsujii

National Institute of Radiological Sciences, Chiba, JAPAN
e-mail: tsujii@nirs.go.jp

In June 1994, the National Institute of Radiological Sciences (NIRS) initiated heavy particle radiotherapy using carbon ion beams obtained from the Heavy Ion Medical Accelerator in Chiba (HIMAC) that was built as part of the nation's "Overall ten-year anti-cancer strategy in Japan" starting in 1984. The construction was completed at the end of 1993 (Fig.1) and the facility was opened for carbon ion radiotherapy (C-ion RT) in the following year. Since then the HIMAC has been served as a multipurpose, shared facility jointly used for cancer therapy and for fundamental particle beam study by both Japanese and foreign researchers.

C-ion RT has been carried out for various types of malignant tumors at NIRS. [1),2),3)] It was approved from the Ministry of Health, Welfare and Labor as "Highly Advanced Medical Technology" in 2003. This means that C-ion RT has meanwhile achieved for itself a solid place in general practice after clinical experiences of cancer therapy since the beginning of clinical trials at NIRS.

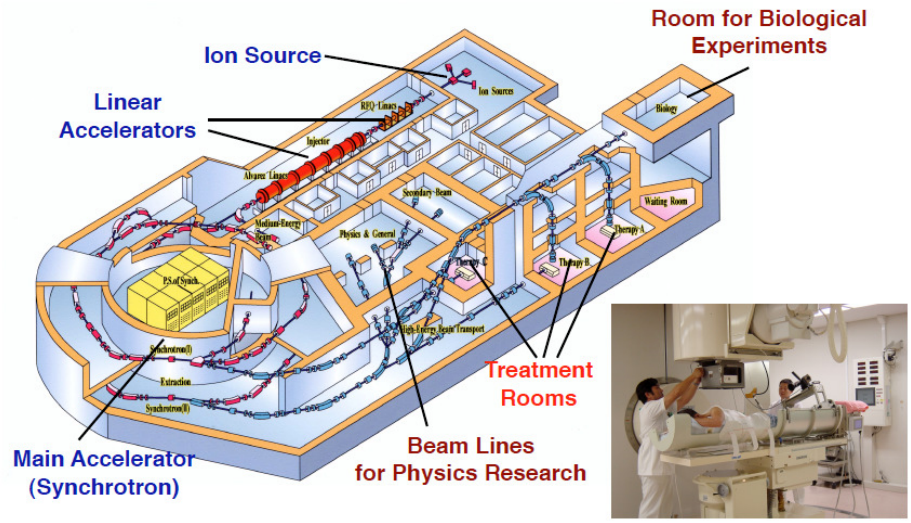

Fig.1 The bird's-eye view of the HIMAC (Heavy Ion Medical Accelerator in Chiba).

1. Expected benefit of carbon ion radiotherapy

Among various types of ion species, we have chosen carbon ion beams for therapy, which have two particular features (Fig.2).[4),5)] First, in marked contrast to photon beams showing an exponential attenuation behavior in the medium, carbon ions have the property of forming a high-dose range, a so-called Bragg peak, in the body (Fig.3). As a result of such dose concentration behavior, the carbon ion beam can be focused solely in the tumor. This property is extremely useful for radiotherapy, for even when there are critical organs in the vicinity of the lesion it is possible to safely concentrate a high dose in the lesion. Second, the ionization density along the trajectory of the carbon ion beams in the body, in other words, the energy given off per unit length (called LET), is higher than in the case of protons or photons. For this reason, the carbon ion beam has a high relative biological effectiveness (RBE) in the Bragg peak that is twice or three times greater than that of photons in clinical situation. [6),7)]

The peak area of the carbon ion beam has further advantageous biological features for cancer treatment in addition to its high RBE. These merits include the fact that radiation damage to cancer tissue will not easily recover, that the oxygen concentration in the tissue has little effect on radio-sensitivity, and that there are only small differences in radio-sensitivity among the different phases of the cell cycle. Furthermore, comparison of the ratio of the RBE in the peak portion to the RBE in the plateau portion of the different charged particle beams

shows that carbon ion beams have the highest value for this ratio among all particle beams (Table 1).[8] This means that carbon ion beams have the best balance of any particle beams in terms of both physical and biological dose distribution, leading to the biological background that the treatment period can be significantly shortened as compared with conventional treatment modalities.[9]

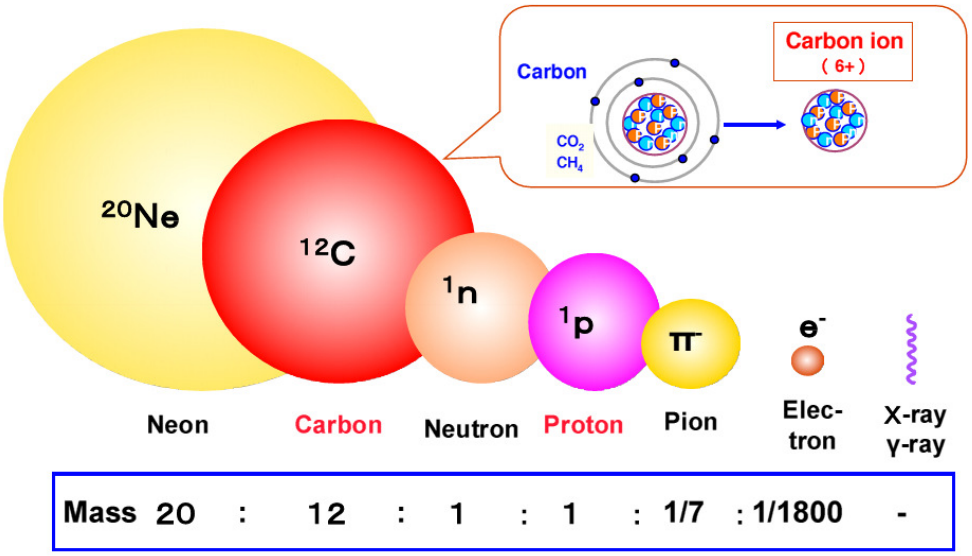

Fig. 2 Among various types of ion species, carbon ions are chosen for cancer therapy because they appeared to have the best balanced property in terms of both physical and biological dose distribution.

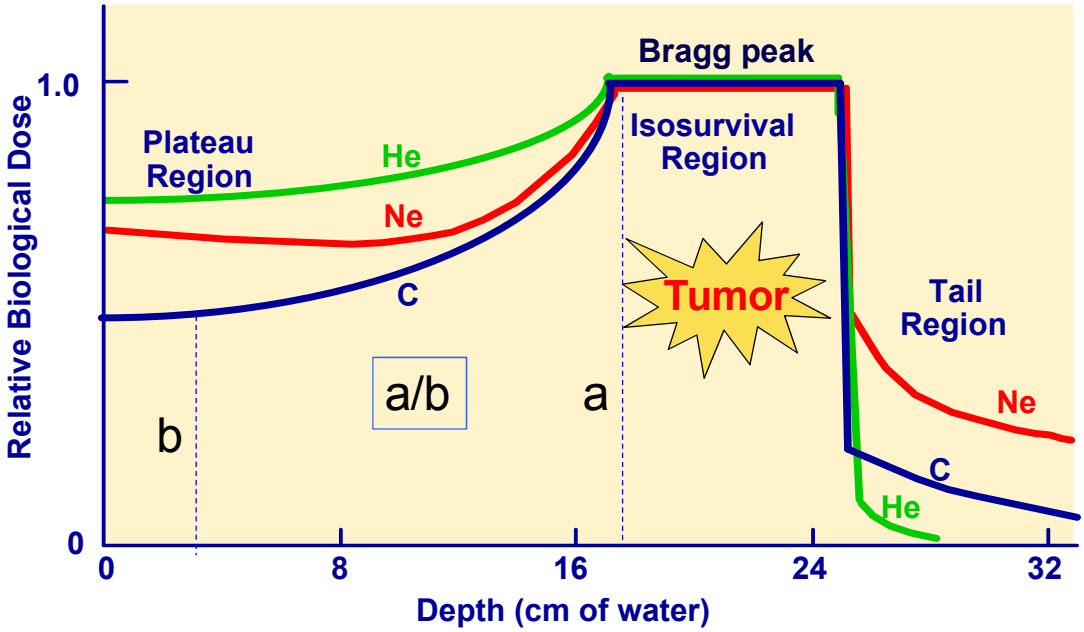

Fig.3 The carbon ions have the largest value for ratio of the RBE in the peak portion to the RBE in the plateau portion (a/b).

Table 1. The Peak-to-Plateau Ratio of RBE for Jejunal Crypt Cell is larger in carbon ions than other ion species (Goldstein et al.: Radiat. Res. 86, 542-558, 1981).

Ion	RBE_{sd}		RBE_2	
	Peak / Plateau	Ratio	Peak / Plateau	Ratio
Proton	1.2/1.1	1.1	1.3/1.2	1.1
Helium	1.2/1.1	1.1	1.5/1.3	1.2
Carbon	1.4~1.5/1.3	1.1~1.2	1.6~2.2/1.3	1.2~1.7
Neon	1.5~1.6/1.4	1.1	2.6~3.0/2.1	1.2~1.4
Argon	1.8~2.0/2.1	0.9	3.6~3.8/4.3	0.8~0.9

RBEsd : single dose, RBE2: fractionated

2. Framework for administration of carbon ion radiotherapy

Consistent efforts have been made at NIRS since the beginning to provide carbon ion radiotherapy on an ethically and scientifically sound basis under a number of Committees headed by the "Carbon Ion Radiotherapy Network Committee" as the supreme organ responsible for clinical studies. All clinical study protocols were first prepared by the Planning Teams, then evaluated by the disease-specific Subcommittees, and finally approved by the Network Committee after investigation by the Ethical Committee. An Evaluation Committee is appointed to deliberate on the validity of whether the individual clinical studies should be continued, and the results of all clinical studies are submitted to the Network Committee whose sessions are invariably held in public. All of the patients, without exception, were submitted to the Tumor Board for evaluation of criteria for C-ion RT as well as to Staff Meeting for evaluation of treatment planning (Fig.4).

The number of patients registered until the present is in excess of 5,100 as of February 2010. The number of patients continues to rise incessantly year after year, due not only to the way in which the irradiation techniques have been established and can be executed without problem but also as a result of the significant reduction in the number of fractions and the treatment time per patient (Fig.5).

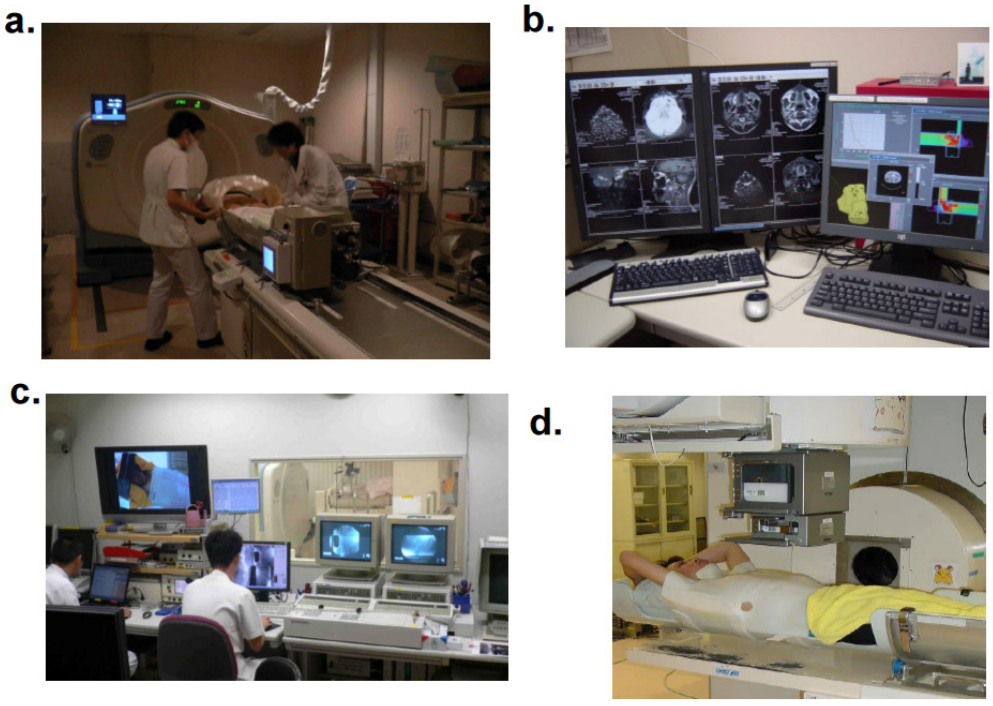

Fig. 4 Step by step procedures for C-ion Therapy. a. CT scans is done for treatment planning; b. Dose distribution is calculated and treatment parameter are determined in the treatment planning system; c. Patient positioning is confirmed in the simulation room; d. Treatment room.

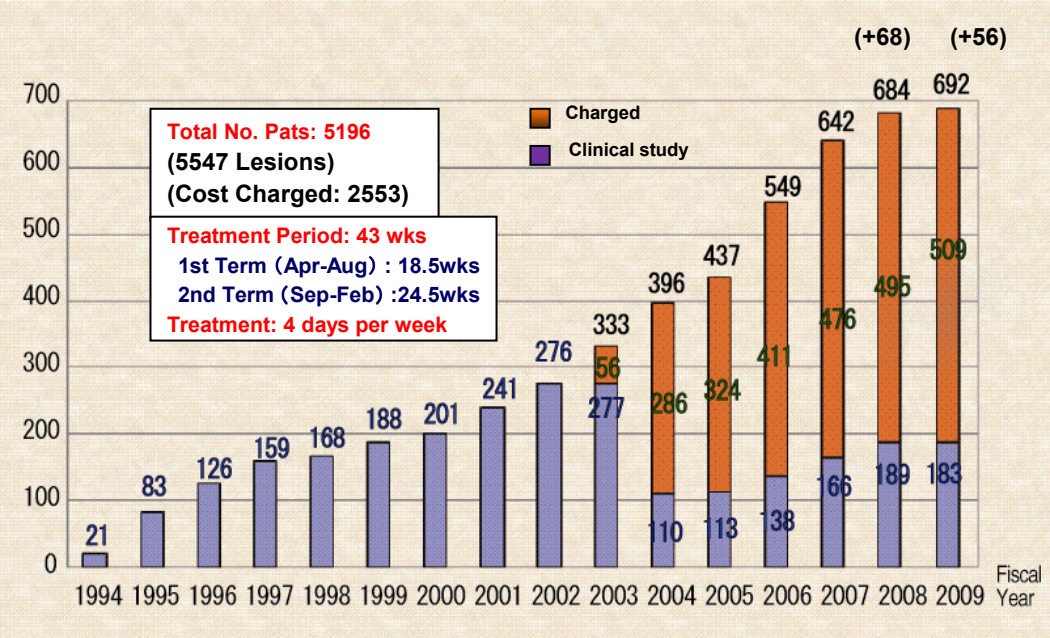

Fig. 5 Annual number of patients in C-ion RT at NIRS (June 1994～31 January 2010)

3. Clinical results of carbon ion radiotherapy

C-ion RT has been mainly applied to those tumors like brain tumors, head and neck cancer, lung cancer, hepatocellular carcinoma, prostate cancer, bone and soft-tissue tumors, uterine cancer, and rectal cancer (post-ope pelvic recurrences) that need further improvement in treatment results (Fig.6). In the first instance, phase I/II trials were carried out in order to confirm safety and obtain data about the anti-tumor effect of this treatment. Based on this evidence, the recommended dose was established by fixing both the fraction number and treatment time for each disease and escalating the total dose in successive increments of 5 to 10% at a time.

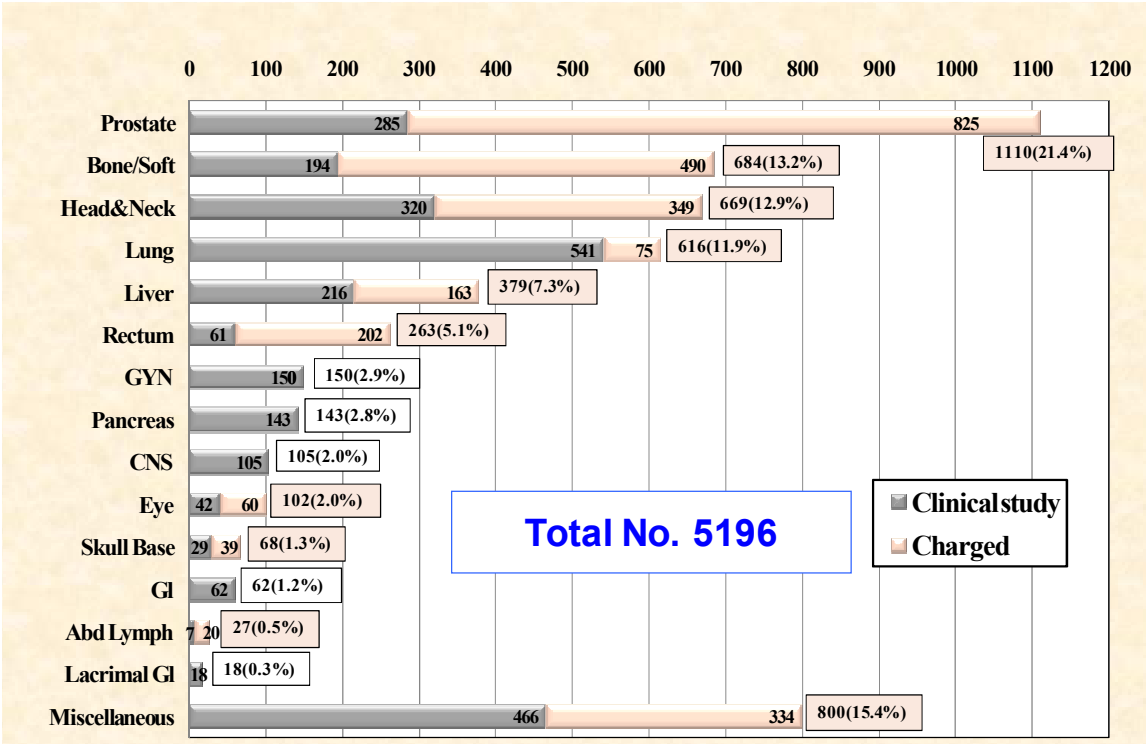

Fig. 6 Distribution of tumors in C-ion RT at NIRS.

Experiences to date indicate that carbon ion radiotherapy is advantageous for the following types of tumors.[1),2),3),10)]

1) Definite indications for C-ion RT

Advanced non-squamous cell cancer of the head and neck
(adenocarcinoma, adenoid cystic ca, malignant melanoma)
Bone/soft tissue sarcoma of the pelvis, paraspinal region, and head/neck
Postoperative pelvic recurrence of rectal cancer
Slow growing tumors

2) Elective indications for C-ion RT
Skull base tumors ----- Better result in long-term follow-up
Lung cancer ---- Single fraction RT in Stage I tumor,
Better result in T2 and locally advanced tumor
Prostate ca ----- Short course RX, better result in high risk group
Hepatoma ------ Two fraction RT, better result in large tumor
Choroidal melanoma -------- Less toxicity by CT-oriented planning

3) Promising results
Uterine adenoca, Pancreas ca, Renal cancer,
Malignant glioma, Locally confined recurrent tumor, etc

4) Hypofractionated RT in any types of tumors

Tumors located in the vicinity of critical organs such as the eye, spinal chord, digestive tract with a relatively large size or irregular shape are good indications. However, tumors that infiltrate or originate in the digestive tract itself are difficult to control with C-ion RT alone. Regarding dose-fractionations, it has been possible to complete a treatment in significantly short time (Table 2). For example, for stage 1 lung cancer and liver cancer, treatment is now available in only one or two irradiation sessions. Even for prostate cancer and bone and soft-tissue tumors requiring a relatively long course of radiotherapy, only 16 sessions of carbon ion therapy have been sufficient, roughly half the number of fractions required in the case of standard radiotherapy. This means that the facility can be operated more efficiently, offering treatment for a larger number of patients than is possible with other modalities over the same period of time. Currently, the number of irradiation sessions per patient averages 13 fractions spread over approximately three weeks in carbon ion therapy.

Examples of patients before and after the treatment is shown in Figure 7 and Figure 8

At present, NIRS provides treatment as the Highly Advanced Medical Technology to approximately 70% of the patients. For such tumors as glioblastoma and pancreatic cancer, for which it has not yet been possible to obtain satisfactory results, clinical trials are simultaneously carried out in an attempt to achieve even more favorable treatment results. As part of the great mission incumbent upon NIRS, there is a need to continue with clinical trials in order to achieve further improvements.

Table 2. Dose-fractionations determined by dose escalation studies for carbon ion RT at NIRS

Site		GyE / Fr./ Wk	GyE / fr	BED (α/β=10)	BED (α/β=2.5)
Head & Neck	Adenoca, ACC, MMM Sarcoma	57.6 / 16 / 4 70.4 / 16 / 4	3.6 4.4	78.3 101.4	140.5 194.3
Skull base	Chordoma & Chondrosarcoma	57.6 / 16 / 4	3.6	78.3	140.5
Lung	Peripheral	60.0 / 4 / 1 46.0 / 1 / 1dy	15.0 -	150.0 -	420.0 -
Lung	: Mediastinum Hilar : Superficial : Bulky	48.0 / 12 / 3 54.0 / 9 / 3 68.4 / 12 / 3	4.0 6.0 5.7	67.2 86.4 107.4	124.8 183.6 224.4
Liver	Hepatocellular ca Metastasis of Rectal ca	42.8 / 2 / 2dys > 46.0 / 1 / 1dy	21.4 -	134.4 -	409.2 -
Bone & Soft tissue	Sarcoma	70.4/ 16 / 4	4.4	101.4	193.4
Prostate	Low/Medium/High risk	57.6 /16/ 4	3.6	78.3	140.5
Pancreas	Pre-operative RT C-ion+ CDDP 1000mg/m^2	> 35.2 / 8 / 2 > 45.6 / 12 / 3	4.4 3.8	50.7 62.9	97.2 114.9
Rectum	Post-ope pelvic rec.	73.6 / 16 / 4	4.6	107.5	209.0
Standard photon RT		60 / 30 / 8	2.0	72	108

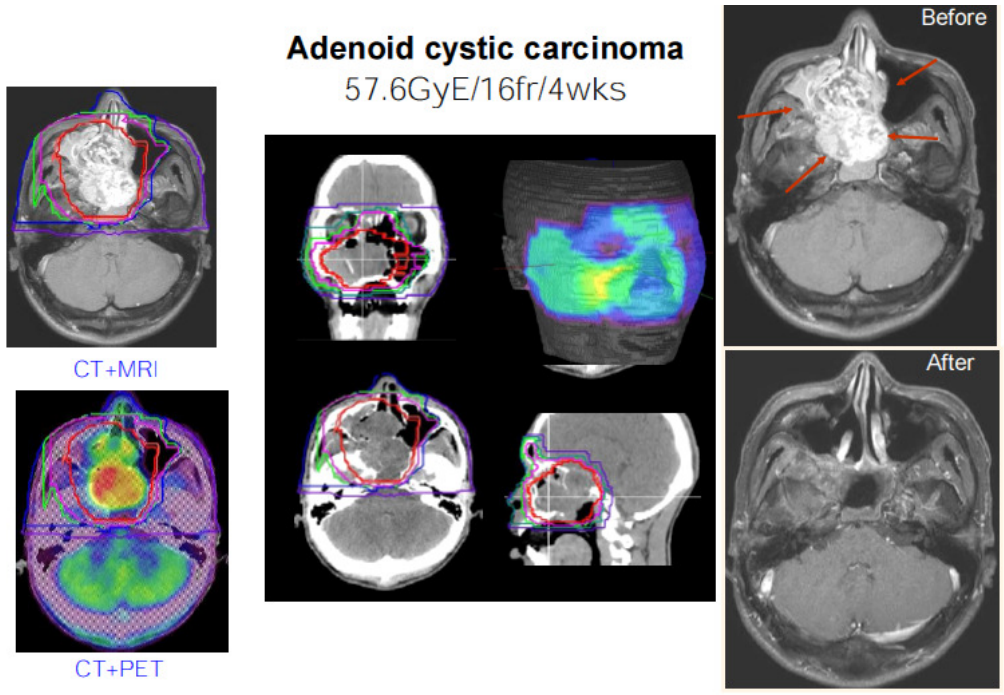

Fig. 7 An example is shown of treatment planning for head and neck cancer. Fusion images of CT+MRI and CT+PET are commonly used.

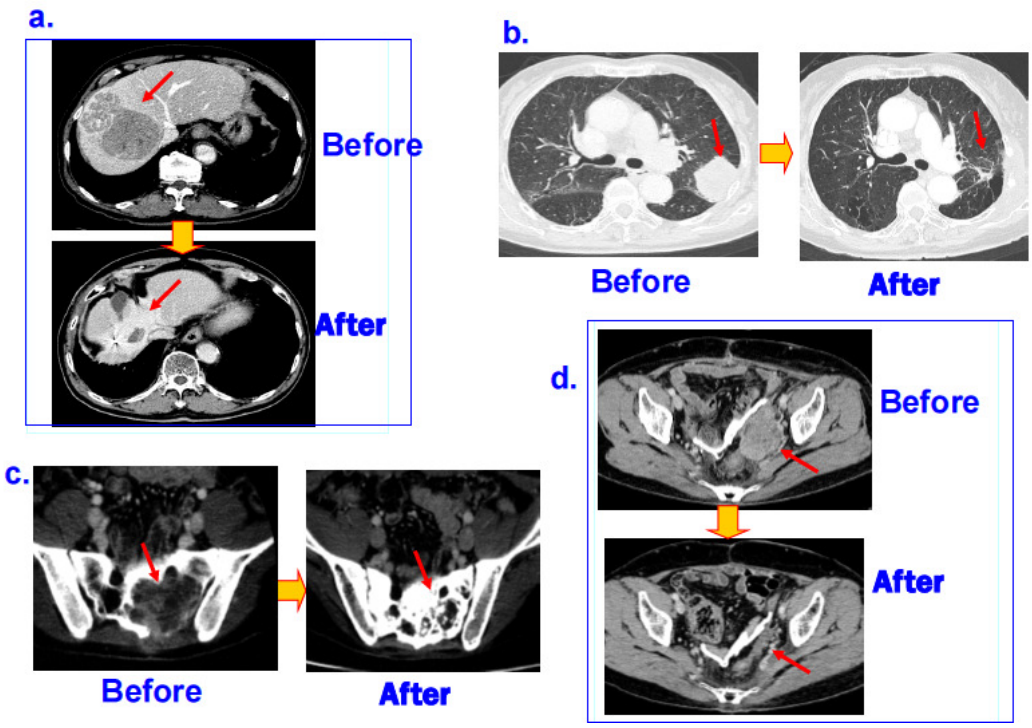

Fig. 8 Remarkable shrinkage of tumors was observed in hepatoma after two fractionated treatment (a), in Stage I lung cancer after single fraction treatment (b), and in post-operative pelvic recurrence of the rectal cancer (d). A patient with sacral bone sarcoma demonstrated re-calcification in the involved site after C-ion RT(c).

References

[1] Tsujii H, Kamada T, Baba M, et al: Clinical advantages of carbon-ion radiotherapy. New J Phys. 10: 1367-2630, 2008.

[2] Tsujii H, Minohara S, Noda K: Heavy-particle radiotherapy: System design and application. Reviews of Accelerator Science and Technology Vol 2 (ed. by Chao AW), Imperial College Press, UK, pp1-19, 2009.

[3] Okada T, Kamada T, Tsuji H, et al.: Carbon ion radiotherapy: Clinical experiences at National Institute of Radiological Sciences (NIRS). J Radiat Res. 51: 355-364, 2010.

[4] Chen GTY, Castro JR, Quivey JM: Heavy charged particle radiotherapy. Ann.Rev.Biophys.Bioeng. 10: 499-529, 1981.

[5] Kraft G: Tumor therapy with heavy charged particles. Prog Part Nucl Phys. 45: S473-S544, 2000.

[6] Kanai T, Furusawa Y, Fukutsu K, et al: Irradiation of mixed beam and design of spread-out Bragg peak for heavy-ion radiotherapy Rad Res. 147 78-85,1997.

[7] Kanai T, Endo, M, Minohara, S, et al: Biophysical characteristics of HIMAC clinical irradiation system for heavy-ion radiation therapy Int J Radiat Oncol Biol Phys. 44 201-10. 1999.

[8] Goldstein, et al.: Radiat. Res. 86, 542-558, 1981.

[9] Koike S, Ando K, Uzawa A, et al: Significance of fractionated irradiation for the biological therapeutic gain of carbon ions. Radiat Prot Dos. 99: 405-408, 2002.

[10] Schulz-Ertner D, Tsujii H: Particle radiation therapy using proton and heavier ion beams. J Clin Oncol. 25(8): 953-964, 2007.

Modeling the Biological Dose Response to Carbon Beams

Naruhiro Matsufuji, Mami Wada, Yuki Kase*, Akiko Uzawa, Koichi Ando**

Research Center for Charged Particle Therapy, National Institute of Radiological Sciences, Chiba, Japan

** Proton Therapy Research Center, Shizuoka Cancer Center, Mishima, Japan*

*** Gunma University Heavy Ion Medical Center, Maebashi, Japan*

Corresponding Author: Naruhiro Matsufuji, e-mail address: matufuji@nirs.go.jp

Abstract

A thorough understanding of the dose response is one of the keys for success in radiation therapy. Due to the relatively short history and increased fraction size resulting from hypofractionation by superior dose localization, verification of the appropriateness of the available dose response models for carbon ion radiotherapy is needed. In this study, the applicability of three dose response models, including the LQ, MT and RCR models was investigated for the endpoints of *in-vivo* mouse skin reaction and the clinical local control rate of non-small cell lung cancer with the carbon beam. We found that the RCR model is the most appropriate for determining the *in-vivo* skin reaction among the three models; however, the classical LQ model still gives the best reproducibility of the clinical results. The understanding of the difference between *in-vivo* and clinical data, as well as the uniqueness of single irradiation, is indispensable for establishing the optimum dose and technique for administering carbon ion radiotherapy in the future.

Introduction

The ability to administer hypofractionated irradiation is one of the advantages of carbon ions for cancer therapy realized by superior dose localization as a result of the fact that energy loss toward the range end can be elevated, and associated with increased biological effectiveness. At HIMAC (Heavy Ion Medical Accelerator in Chiba), the efficacy of hypofractionation has been investigated in most tumor sites, and ultimately, one-day irradiation has been tried against NSCLC (non-small cell lung cancer) [1].

Due to its simplicity and sufficient precision in conventional radiotherapy modality, the LQ (linear-quadratic) model has been preferred for estimating the biological or clinical response to radiation. In hypofractionated radiotherapy; however, the absorbed dose given to the tumor is far beyond the range where the LQ model has been experimentally verified. The RCR (Repairable-Conditionally Repairable) model recently proposed by Lind et al. of the Karolinska Institutet is expected to be applicable for a wider dose range [2]. In addition, the MT (multi-target two components) model [3] developed from hit-target theory is regarded as yet another approach for estimating the dose response. In this study, these models were applied to estimate the *in-vivo* findings, as well as the clinical, response to carbon ions.

Methods and Materials

1. Materials

From a single dose up to 6 fractionated irradiation experiments have been conducted at the HIMAC BIO cave with carbon ions of various LETs (13.6, 28.4, 43.0, 58.0 keV/μm) and X-rays to mice [4]. The main endpoint of the current study was the incidence of grade 2 skin reactions, *i.e.*, a complete epilation with or without slight edema. To assess the clinical response, the local control rate of NSCLC derived through a dose escalation study with carbon ions at HIMAC [5] was used.

2. LQ model

The LQ model gives the probability of cell killing by two components, one dependent on the dose and the other on the square of the dose. The linear term with regard to the absorbed dose is explained as the probability of a DNA double strand break (DSB) by a single track, while the quadratic term, related to the dose, shows the probability of two independent tracks. The cell survival S_{LQ} after exposure to the fractional dose d is calculated as:

$$S_{LQ} = \exp(-\alpha d - \beta d^2) \tag{1}$$

When the LQ model is valid, a linear relationship is expected between the dose per fraction and the reciprocal total dose on the same biological endpoint by different fractionations as shown below.

$$E = n(\alpha d + \beta d^2) \tag{2}$$

$$1/nd = \alpha/E + (\beta/E)d \tag{3}$$

When plotting the isoeffective reciprocal total dose (1/nd) as a function of dose per fraction (d) as known as the Fe-plot [6], the ratio of the intercept (α/E) to the gradient (β/E) corresponds to the α/β value.

3. MT model

The cell survival is expressed using the equation below in the MT model.

$$S_{MT} = \exp(-Ad)[1 - \{\exp(-d/d_0)\}^m] \tag{4}$$

The first exponential term corresponds to the "ion kill", *i.e.*, irrepairable cell killing by a single hit to a single target expected in the core of the ion track, while the rest of the equation shows the probability of the "gamma kill", *i.e.*, repairable cell killing by a shingle hit to multiple targets.

4. RCR model

The RCR model also uses the exponential expression, but in a different form.

$$S_{RCR} = \exp(-ad) + bd\exp(-cd) \tag{5}$$

The first term indicates the probability of "unhit" and the second term corresponds to the probability of cell survival after repairing the resulting damage.

5. Tumor control probability (TCP)

The LQ, MT and RCR models are, in their basic form, used for the estimation of cell survival probability. By taking the number of clonogens in a tumor into this estimation of cell survival, the TCP (tumor control probability) can be estimated. The TCP of a tumor containing N clonogens in n fractionated irradiation is given as:

$$TCP = exp(-NS^n) \tag{6}$$

Here, it is stated that the distributions of the parameter values are needed for realistic TCP modeling [7]. In this study, Gaussian distribution was introduced to one of the parameters in each model for the sake of simplicity.

$$\mathrm{TCP}_{LQ} = \frac{1}{\sqrt{2\pi}\sigma}\int\left[exp\left(-\frac{(\alpha-\alpha_0)^2}{2\sigma_\alpha^2}\right)\times exp\left(-\mathrm{N}\{\exp(-\alpha d-\beta d^2)\}^n + 0.693\frac{T-T_k}{T_d}\right)\right]d\alpha \tag{7}$$

$$\mathrm{TCP}_{MT} = \frac{1}{\sqrt{2\pi}\sigma}\int\left[exp\left(-\frac{(A-A_0)^2}{2\sigma_A^2}\right)\times exp(-\mathrm{N}\{\exp(-\mathrm{Ad})[1-\{\exp(-d/d_0)\}^m]\}^n)\right]dA \tag{8}$$

$$\mathrm{TCP}_{\mathrm{RCR}} = \frac{1}{\sqrt{2\pi}\sigma}\int\left[\exp\left(-\frac{(c-c_0)^2}{2\sigma_c^2}\right)\times\exp(-\mathrm{N}\{\exp(-\mathrm{ad})+bd\exp(-cd)\}^n)\right]\mathrm{dc} \tag{9}$$

In the case of the LQ model, the distribution is convoluted into the parameter α as the α is dominant in a typical fractionation size. The effect of cell repopulation is also taken into account in the equation by the tumor doubling time T_d and the kickoff time of the proliferation T_k. This formalism of TCP was proposed by Webb and Nahum [8]. The distribution is attributed to the parameter *A* in the MT model as the "ion kill", to extent of which is expressed with this *A*, and is considered to be the leading term for the carbon ion irradiation. In the RCR model, the parameter *c* is assigned for the distribution by assuming that the repair capacity represented has patient-dependent variation.

6. Data analysis

As for the *in-vivo* case, at first, the α/β value of the mouse skin for 58 keV/μm was determined to be 13.0 by giving a linear fit to the data on the Fe-plot while omitting the data point of the single irradiation. Then, by assuming the β as 0.05, the isoeffect *E* is calculated with the eq. (2). Then, the parameters in each model (eqs. (1), (4) and (5)) was determined for each different LET irradiation result by least square fit in order to obtain the same isoeffect E. Finally, the isoeffective dose estimated by the models was plotted on the Fe-plot together with the experimental data.

In the case of clinical data analysis, the parameters in each model (eqs. (7), (8) and (9)) were determined by least-square fit to the observed local control rate of NSCLC with carbon ions in 18 fractions at HIMAC. Then, using the parameters, the TCP in hypofractionation from 9 fractions down to a single fraction was estimated and compared with the clinical observations. The calculation in this study was powered by the *Wolfram Mathematica* © version 7 software program.

Results and Discussion

1. Applicability of the models for *in-vivo* mouse skin reactions

Figure 1 shows the Fe-plot of the *in-vivo* mouse skin reactions together with the estimates provided by the models. The experimental results of the mouse skin reaction tests show a drop in the Fe-plot following a single

dose of radiation. This drop is unique to carbon ion irradiation, and is not observed during X-ray irradiation. This means that the LQ model shows a dissociation in the response between single and multiple irradiations with carbon ions.

On the other hand, MT and RCR models both succeeded in reproducing the drop following the single irradiation. The RCR model shows more favorable reproducibility than the MT model for high LET data. The LET dependency of the parameters in the RCR and MT models are shown in Fig. 2. The LET dependency of parameters used in the RCR model suggests that cluster-like, less repairable lesions are produced significantly by high LET irradiation. The LET dependency of the parameters in the MT model suggests that there is an increase in the "ion-kill" and the decrease in "gamma-kill" with the elevation of LET, as would be expected.

2. Applicability of the models for clinical data

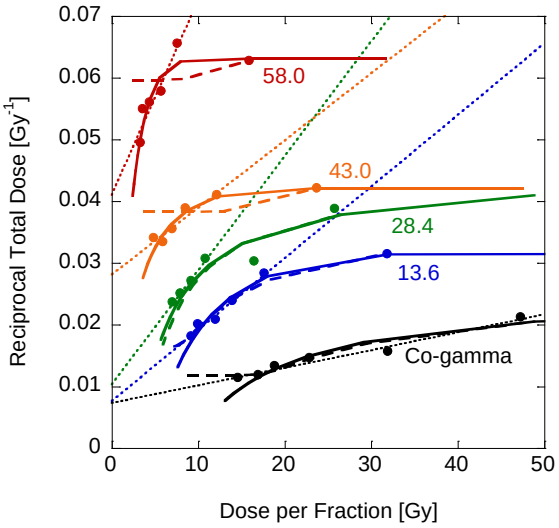

Fig. 1. Fe-plot of the *in-vivo* mouse skin reaction. The numbers in the figure correspond to the LET value of the carbon beam. The estimation of LQ, MT and RCR models are shown with narrow dashed, thick dashed and thick solid lines, respectively.

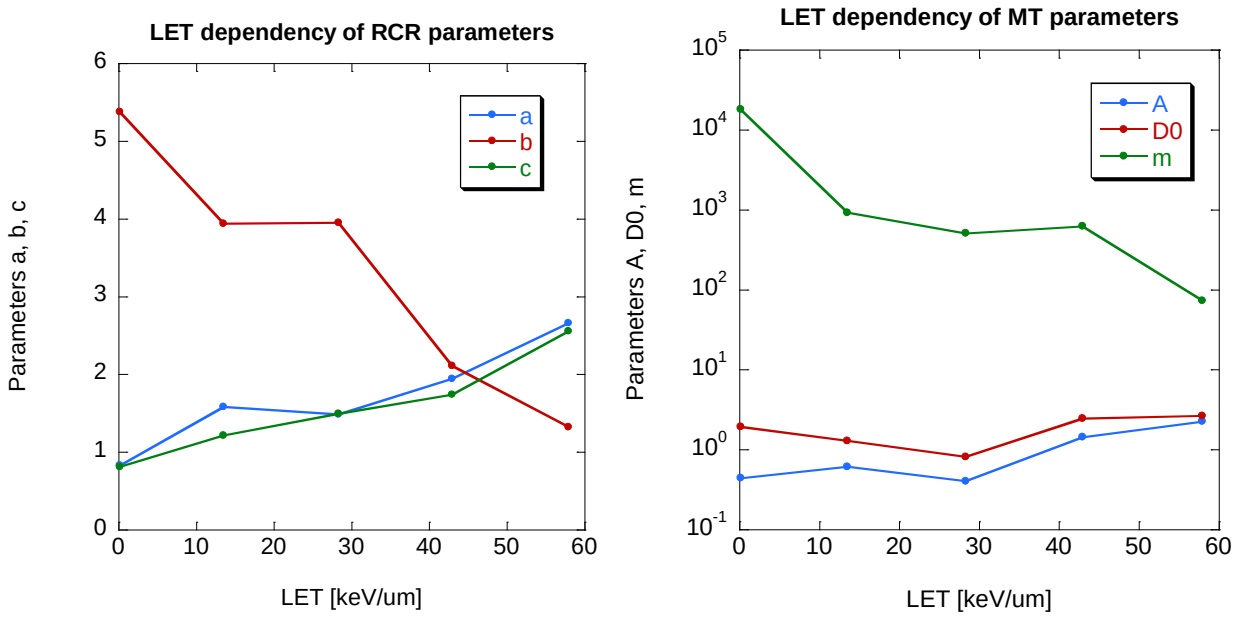

Fig. 2. LET dependency of the parameters in the RCR model (left) and the MT model (right).

Regarding their clinical application, all the three models succeeded in giving satisfactory fit to the local control rate for 18 fractionations, as shown in Fig. 3. The calculated parameters are summarized in Table 1. Interestingly, about 30% variation in sensitivity was found to give the best fit to the data.

The estimation of the hypofractionated clinical data is, however, not perfect (as shown in Fig. 4). The RCR model tends to underestimate the dose response in hypofractionation, while the MT model overestimates the response. The LQ model is, among the three models, the best, but is still not perfect. The disagreement between the models is found only on single irradiation. However, even in the case of a single irradiation, the 50% TCP level agrees to the clinical result. The dissociation at high TCP levels can be explained from the viewpoint of the TCP model, as there in an increase in the variation of radiosensitivity. It is necessary to investigate the reason for this unique increase in the variation in the case of single irradiation with the more detailed analysis of the clinical results.

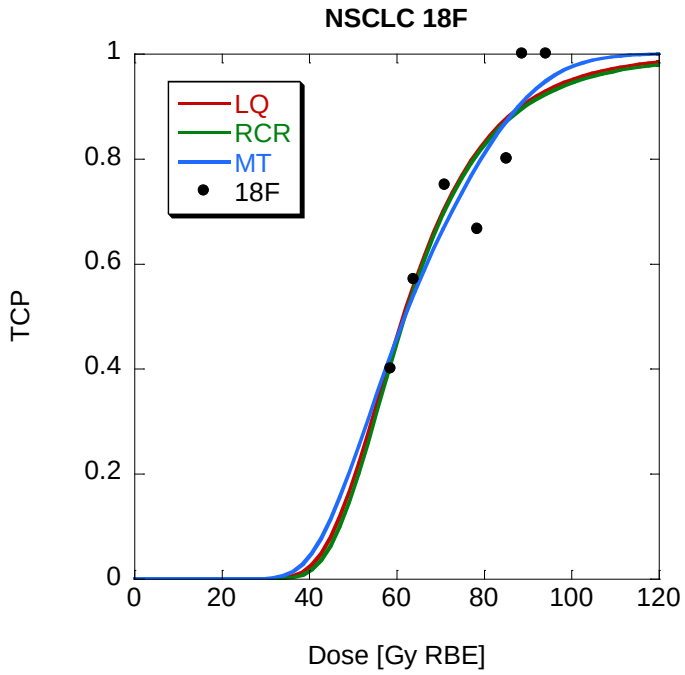

Fig. 3. TCP fitting by the LQ, RCR and MT models for the local control of NSCLC by 18 fractions

When considering the reason(s) for the contradiction in the applicability between the LQ and the MT or the RCR models between *in-vivo* and clinical data, the robustness of the parameters can play a role. The calculated parameters in the MT and the RCR models were highly sensitive to the initial value. This suggests that the obtained values are not in global, but in a local minimum. The applicability might be improved by finding the global minimum values; however, such oversensitivity makes the practical application of the MT and RCR models more difficult. The other possibility is that there are differences in the biological damage obtained during *in-vivo* and clinical data. While the clinical data is directly connected to the tumor cell killing, the damage from the *in-vivo* data is considered to be repairable. Further study is necessary in order to understand the mechanism behind the observed tendency toward differences in the *in-vivo* versus clinical data.

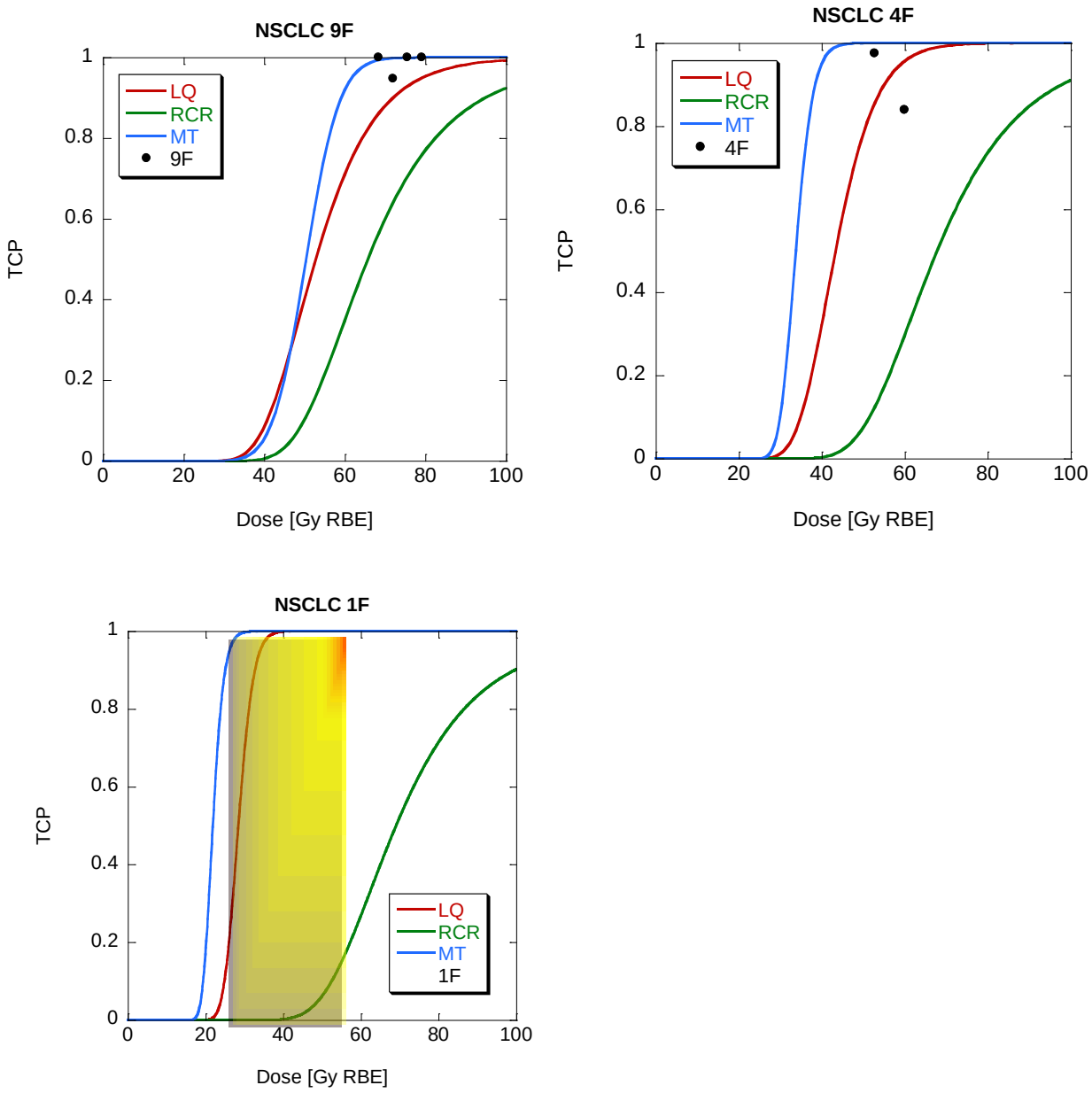

Fig. 4. TCP estimation of 9, 4 and single irradiations by the LQ, RCR and MT models with the parameters for the 18 fractions as summarized in Table 1. Due to the insufficient follow-up period, only the dose range is shown in the case of single irradiation.

Conclusion

The verification of the LQ, MT and RCR models has previously been tried using the cell survival response as an endpoint, and due to the experimental difficulties in the cell survival experiments, the dose range was limited to less than 10 Gy or 10^{-3} survival level. This aim of the present study was to verify the appropriateness of the models for the application of the dose prescribed in the practice of carbon ion radiotherapy. Regarding the fractionated *in-vivo* mouse skin reaction, while the LQ model failed to reproduce the experimental results of single irradiation by the carbon beam, the RCR model was found to be useful in the dose and fraction range used for the experiment. In contrast, for the clinical response, the LQ model was preferable to the other models. In

both the *in-vivo* and clinical cases, further study is necessary, especially on the dose response following a single irradiation.

Table 1. Parameters in LQ, RCR and MT models for the fit to the local control of NSCLC in 18 fractions

Model	**Variable**		**σ**	**Fitting parameters**				**Fixed parameters**
LQ	α	0.865	0.268 (31.0%)					β=0.076, T_d=7, N=10^9
MT	A	0.816	0.248 (30.4%)	D_0	0.498	m	115.3	N=10^9
RCR	c	0.729	0.171 (23.5%)	A	6.317	b	0.880	N=10^9

References

[1] Tsujii H, Kamada T, Baba M et al. Clinical advantages of carbon-ion radiotherapy. *New J. of Phys.* 2008;10:075009.

[2] Lind B K, Persson L M, Edgren M R, Hedlöf I and Brahme A. Repairable-conditionally repairable damage model based on dual Poisson processes. *Rad. Res.* 2003;160:366-375.

[3] Butts J J and Katz R. Theory of RBE for heavy ion bombardment of dry enzymes and viruses. *Rad. Res.* 1967; 30:855-871.

[4] Uzawa R, Ando K, Koike S et al. Research on the tumor control effect and complications of therapeutic charged beam. *2008 Annual Report of the Research Project with Heavy Ions at NIRS-HIMAC.* 2009; 47-49.

[5] Miyamoto T, Yamamoto N, Nishimura H, et al. Carbon ion radiotherapy for stage I non small cell lung cancer. *Radiother. Oncol.* 2003;66:127-140.

[6] Douglas B G and Fowler J F. The Effect of Multiple Small Doses of X Rays on Skin Reactions in the Mouse and a Basic Interpretation. *Radiat. Res.* 1976;66:401-426.

[7] Dasu A, Toma-Dasu I and Fowler J F. Should single or distributed parameters be used to explain the steepness of tumour control probability curves? *Phys. Med. Biol.* 2003;48:387-397.

[8] Webb S and Nahum A E. A model for calculating tumour control probability n radiotherapy including the effect of inhomogeneous distributions of dose and clonogenic cell density. *Phys. Med. Biol.* 1993;38:653-666.

Repairable Conditionally Repairable Damage Model

Bengt K. Lind

Karolinska Institutet and Stockholm University, Department of Medical Radiation Physics, 171 76 Stockholm, Sweden

The advent of intensity modulated radiation therapy makes it increasingly important to accurately model the therapeutic response when large volumes of normal tissues are irradiated by controlled graded dose distributions aimed at maximizing tumor cure and minimizing normal tissue toxicity. The so called Repairable Conditionally Repairable damage model (RCR) is very useful and flexible for accurate description of the response of healthy tissues as well as tumors in classical and truly radiobiologically optimized radiation therapy. The model distinguishes between two different types of damage namely the potentially repairable that may also be lethal i.e. non-repaired or misrepaired and the conditionally repairable, which may be repaired if the conditional damage has been repaired and if it has not been repaired correctly may lead to an apoptotic response. When potentially repairable damage is being repaired, for example by non homologous end joining, conditionally repairable damage may consequently be corrected by homologous repair. The induction of both types of damage is assumed to be described by Poisson statistics. The resultant cell survival expression has the unique ability to fit accurately most experimental data well both at low, (low-dose hypersensitivity), intermediate (the shoulder of the survival curve) and high dose levels (the quasi exponential high-dose survival). The complete Poisson expression can be accurately approximated by a simple bi-exponential cell survival $S(D) = e^{-aD} + bDe^{-cD}$, where the first term is due to undamaged cells and the last term represent completely repaired sublethal damage. Several constraints on the parameters *a*, *b* and *c* can be derived in order to keep the model consistent with the assumptions made in the derivation. Such constraint also regularizes the Maximum Likelihood or Least Square minimization problem used during the fit of the model to experimental data, thus facilitating the correct extraction of the parameters.

Analytical Description of the LET Dependence of Cell Survival Using the Repairable- Conditionally Repairable Damage Model

M. Wedenberg[1,2], B. K. Lind[1], I. Toma-Dasu[1], H. Rehbinder[2], A. Brahme[1]

[1]*Medical Radiation Physics, Stockholm University and Karolinska Institutet, 171 76 Stockholm, Sweden*
[2]*RaySearch Laboratories AB, Stockholm, Sweden*

The main goal in curative radiation therapy is to maximize tumor cells kill while avoiding radiation induced damage to the surrounding normal tissue. Today, most radiation therapy treatments are performed with photons and electrons, but there is an increasing interest in light ion radiation therapy mainly due to the improved dose conformity and the increased biological effectiveness compared to conventional radiotherapy. In light ion radiation therapy, not only the dose, but also the local energy spectrum, often characterized with the linear energy transfer (LET), must be considered. In biological outcome calculations and treatment optimization, it is advantageous to use a radiobiological model that analytically accounts for both dose and LET for the ion type of interest. With such a model the biological effect can be estimated also for dose and LET combinations for which there are no observations in the underlying experimental data. The aim of the present study was to develop a cell survival model where the cell survival dependence on both dose and LET is explicitly expressed. The advantages of the model are presented including its robustness and ability to estimate the fraction of surviving cells as a function of dose and LET for a given ion type and cell line.

The Repairable- Conditionally Repairable (RCR) damage model was extended by expressing its parameters as functions of LET to provide a radiobiological model that accounts analytically for both the dose and the LET for a given ion type and cell line. The LET-parameterized RCR model was fitted to experimental cell survival data of cells exposed to light ion radiation with LETs ranging from 25 eV/nm to LETs high enough to observe a reduced effectiveness in cell inactivation per unit dose, so called overkill effect. The cell survival data included HSG and V79 cells irradiated with carbon ions and T1 cells irradiated with helium ions. The robustness of the model was assessed by testing its ability to estimate cell survival curves for LETs where no data is available using other survival data. This analysis was performed by excluding cell survival data of a range of LETs, recreating them using the model and only a limited set of survival data of other LETs, and comparing the predictions with the actual experimental results.

The LET-parameterized RCR model was found to accurately fit the experimental cell survival data, including survival data for LET values not used in the fitting. The RBE as a function of LET obtained with the RCR model was also calculated. At the survival level of 10%, a maximum RBE of 2.9, 3.9 and 4.2 was obtained for HSG cells (C-ions), V79 cells (C-ions) and T1 cells (He-ions) at 150, 162 and 101 eV/nm, respectively.

The LET-parameterized RCR model is a cell survival model that can describe the fraction of surviving cells as a function of both dose and LET for a given ion type and cell line. From this cell survival model it is possible to also determine the RBE of the radiation. Since the model is able to provide good agreement to the experimental cell survival data and, moreover, is robust in the sense that it is able to estimate cell survival fractions for LETs for which there are no experimental data available, the model can be valuable in treatment planning for ions.

Cell Survival Modelling for Oxic and Hypoxic Cells for Light Ions in the Clinically Relevant LET Range Using the RCR Model

Laura Antonovic, Anders Brahme, Iuliana Toma-Dasu

Medical Radiation Physics, Stockholm University and Karolinska Institutet, 171 76 Stockholm, Sweden

Biological optimisation of radiation therapy requires a comprehensive radiobiological model for cell killing as a function of radiation dose accounting for the quality of radiation and the microenvironmental conditions.

The present study proposes a cell survival model for light ions in which the dependence on dose, LET and oxygenation status is explicitly described. The repairable-conditionally repairable (RCR) model has been previously modified in order to include the LET dependence of its parameters for oxic conditions. For the description of cell survival in hypoxic conditions, a global modification factor of the parameters valid for the oxic conditions was derived as a function of LET. The model was subsequently applied on experimental survival data for V79 cells irradiated with ^{12}C beams with LETs in the range 22.5 – 502 keV/μm in oxic conditions and hypoxic conditions.

The model was found to fit quite accurately both the oxic and the hypoxic experimental cell survival data within the investigated range of LETs. Therefore, the result of the study is a model able to predict the biological outcome for mixed populations of oxic and hypoxic cells irradiated with ^{12}C beams in the clinically relevant range of LETs.

If extended to clinically relevant cell lines, the proposed model for cell killing accounting for oxygen status and radiation LET could be used for estimating the tumour control probability in light ion radiation therapy. It could therefore be regarded as the basic tool in the biological optimisation of treatment plans for tumours with distinct hypoxic subregions.

Uniform Tumour Cell Kill and Absorbed Dose with Mixed Modality Light Ion Beams

Patrick Vreede and Anders Brahme

Medical Radiation Physics, Stockholm University and Karolinska Institutet, 171 76 Stockholm, Sweden

When treating patients with carbon ions, a spread out Bragg peek (SOBP) is normally used. The SOBP is obtained by placing several narrow carbon peaks one after each other, creating a SOBP with uniform biological dose, but differing absorbed dose and ionization density along the SOBP. This approach leads to low doses in the distal part of the SOBP and high doses to the proximal part in order to get a uniform biological dose, therefore the ionization density of the beam will wary and the effect of the treatment beam might not be the same in different parts of the SOBP.

To get a more homogenous absorbed dose and ionization density, we propose the use of mixed modality light ions beams i.e. mixing different light ions into a single beam, as shown in the figure below.

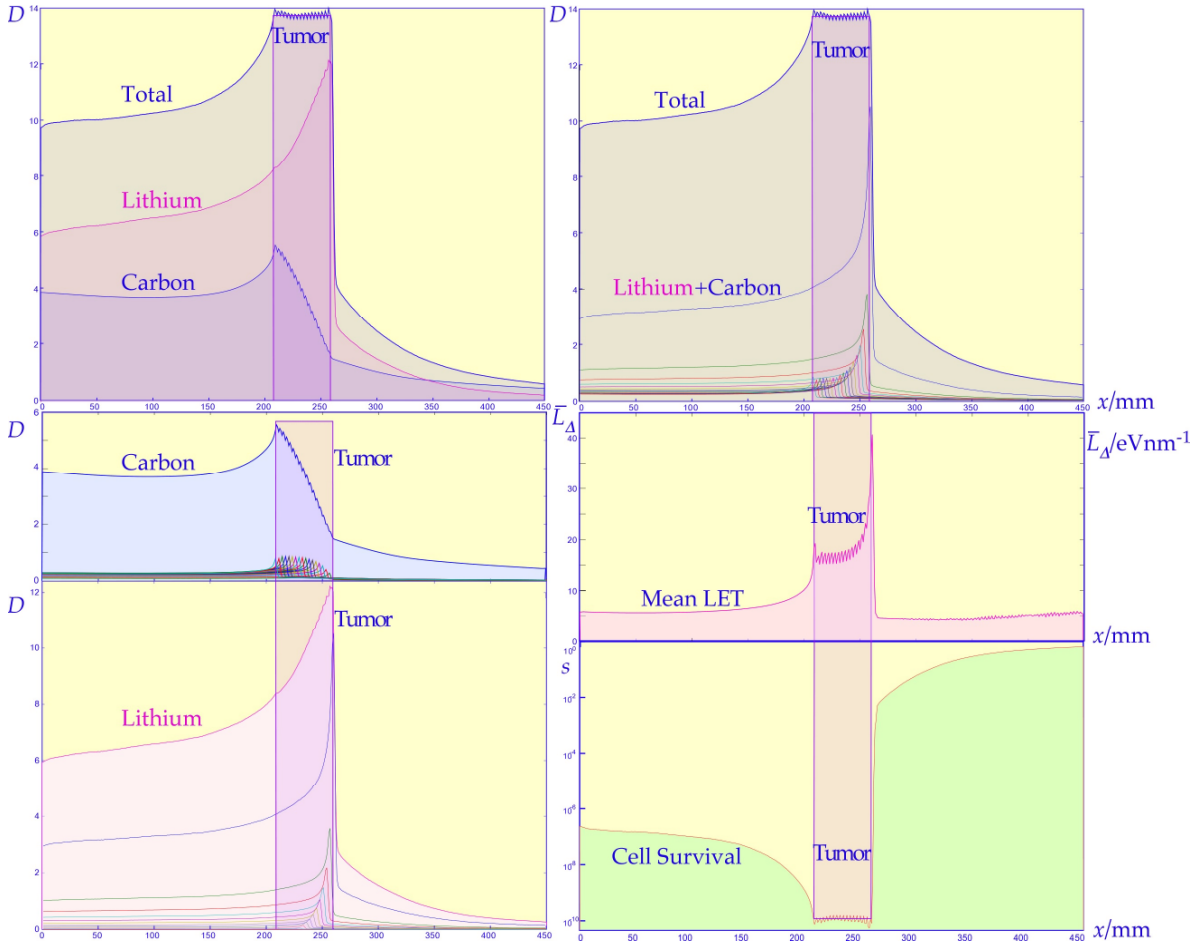

To calculate the combined effect of the different contributions of the ion beams we use Monte Carlo calculated dose and LET kernels combined with a modified version of the RCR model. By optimizing the fluence distribution between two different particles, using Matlab, we are able to find a mixed beam SOPB which gives a more homogenous absorbed dose distribution, as well as homogenous survival.

This approach could also be used to tailor the ionization density within the target region to e.g. have a higher ionization density in a hypoxic area.

Secondary Electron Productions from Ions – Simulations and Radiobiological Modeling

K. Wiklund[1], J. M. Fernández-Varea[2], B. K. Lind[1]

1Medical Radiation Physics, Stockholm University and Karolinska Institutet, 171 76 Stockholm, Sweden
2 Facultat de Física, Universitat de Barcelona, ES-08028 Barcelona, Spain

A Monte Carlo code for the event-by-event simulation of electron transport in liquid water is presented. The code, written in C++, can accommodate different interactions models. Currently it implements cross sections for inelastic collisions calculated with the model developed by Dingfelder *et al* (1998, 2008) and cross sections for elastic scattering computed within the static-exchange approximation (Salvat *et al* 2005). Other included interaction mechanisms are excitation by electron impact and dissociative attachment.

Various track penetration parameters, including the detour factor, are defined as useful tools to quantify the geometrical extent of electron tracks in liquid water. Results obtained with the present microdosimetry code are given in the form of probability density functions for initial electron kinetic energies ranging from 0.1 to 10~keV. The sensitivity of the simulated distributions to the choice of alternative physics models has been briefly explored.

The present MC microdosimetry code will be used for ion beam characterizations with track-segment condition as a continuation of the previous semi-analytical calculations carried out by Wiklund *et al* (2008). The goal is to develop an accurate characterization of beam quality and to model the cellular and sub-cellular response to radiation. Details of the spatial distribution of energy-transfer events at the nanometre scale are therefore needed. DCSs for bare light ions (H^+, He^{2+}, C^{6+}, etc) computed from the CDW-EIS approximation are going to be employed to describe the initially produced electrons. The results will be linked to cell survival by including information from spatial distribution in the `repairable conditionally repairable' model (Lind *et al* 2003).

Characterisation of Radiation Quality and Secondary Dose Distributions in Patients in Light Ion Therapy

Martha Hultqvist

Medical Radiation Physics, Stockholm University, Stockholm, Sweden

During light ion therapy, the primary ions are fragmented due to nuclear inelastic collisions with the atomic nuclei in the material. This process results in the production of secondary particles and attenuation of the primary beam intensity. In a cascade of events, the nuclear fragments in turn produce secondary particles through nuclear interactions during their transport. The organs and tissues of the patient are thus exposed to a complex secondary radiation field and secondary doses can be delivered to normal tissues both close to and relatively far from the treated volume. Monte Carlo simulations of ion and neutron transport in three dimensional heterogeneous phantoms offer the possibility to study the secondary dose distribution. Using the SHIELD-HIT07 code, the secondary doses have been simulated in the male phantom ADAM-HIT and in the phantom representing a 10-year-old female child, CHILD-HIT, for irradiation of prostate and brain tumor, respectively. The simulated irradiations were performed with 1H, 4He, 7Li, 12C and 16O ion beams in the energy range 100-400 MeV/u. The neutron contributions to the absorbed doses and the dose contributions from charged fragments that were not produced by neutron interactions in the phantoms have been studied, as well as the energy spectra of particles delivering the secondary doses.

The radiation quality, in terms of the dose-mean lineal energy, $\bar{y}_D$, has been evaluated in the primary radiation field in water for irradiation with 1H and 12C ions with initial energies 160 MeV and 290 MeV/u, respectively. The $\bar{y}_D$ was calculated from the energy distributions of primary and secondary ions, and from their energy-dependent $\bar{y}_D$-values. The energy distributions were obtained from simulations with SHIELD-HIT07 and the energy-dependent $\bar{y}_D$-values were obtained from ion-track simulations with PITS99 coupled with the electron transport code KURBUC. $\bar{y}_D$ depth profiles in water are presented for simulated object sizes 10-100 nm.

A Model of Carbon Ion Interactions in the Energy Range 1 keV/u to 10 MeV/u in Water

Thiansin Liamsuwan and Hooshang Nikjoo

Radiation Biophysics Group, Department of Oncology-Pathology, Karolinska Institutet, SE-17176, Stockholm, SWEDEN

Differences in the initial degree of damage by radiation arise from differences in structure of radiation tracks, which are the magnitude and the spatial distribution of the energy deposition in microscopic targets. To accurately describe track structures of ions, total and differential interaction cross sections are needed. In this talk, we present a model of electronic interactions of carbon ions in water at the energy range 1 keV/u-10 MeV/u, representative at and behind the Bragg peak. At this energy region, the scaling property of the interaction cross sections becomes less valid because charge-transfer processes (electron capture and electron loss) contribute increasingly to energy loss processes of ion tracks, and give rise to the presence of partially dressed projectiles such as C^{q+} with $q \leq 6$. To calculate the interaction cross sections of carbon ions, the Classical Trajectory Monte Carlo (CTMC) calculations were applied, taking into account ionization and charge transfer processes of all carbon charge states (C^0- C^{6+}). The method of calculation and the results in term of total, singly and doubly differential cross sections will be presented. The calculated cross sections are implemented in a Monte Carlo track structure simulation code for the full slowing-down carbon ion tracks.

OpenPET (1):
A New Geometry Enabling PET Imaging during Radiation Therapy

Taiga Yamaya[1] and Taku Inaniwa[2]

[1]*Molecular Imaging Center, National Institute of Radiological Sciences, Chiba, Japan*
[2]*Research Center for Charged Particle Therapy, National Institute of Radiological Sciences, Chiba, Japan*
Corresponding Author: Taiga Yamaya, e-mail address:taiga@nirs.go.jp

Abstract

The OpenPET geometry is our new idea to visualize a physically opened space between two detector rings. This geometry is expected to lead to realization of in-beam PET, which is a method for an *in situ* monitoring of charged particle therapy, by letting the beams pass through the gap. This geometry will also allow simultaneous PET/CT measurements of the same PET FOV as the CT FOV, in contrast to the conventional PET/CT where each FOV is separated by several tens of centimeters. In this paper, we review the original concept and simulation results of the OpenPET.

Introduction

The OpenPET geometry is our new idea to visualize a physically opened space between two detector rings [1]. As shown in fig. 1 (a), two detector rings of axial length W are separated by a gap G. When $G \leq W$, an axially continuous FOV of $2W+G$ is obtained. Axial spatial resolution, which is degraded with the extended gap due to the parallax error, can be recovered by use of depth-of-interaction (DOI) detectors. The OpenPET is expected to enable 1) PET image-guided radiation therapy by letting the beams pass though the gap (fig. 1 (a)), 2) real-time multimodal imaging by inserting another imaging device in the gap (fig. 1 (b)), and 3) extension of an axial field-of-view (FOV) with the limited number of detectors (fig. 1 (c)). In this paper, we review the concept and simulation results of the OpenPET.

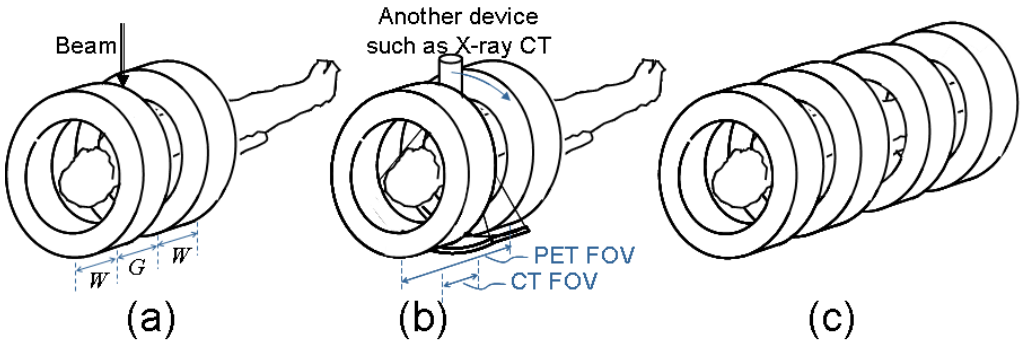

Fig. 1. An OpenPET geometry and its applications. For details, see the text.

Applications of the OpenPET

For the first, OpenPET is expected to realize in-beam 3D PET, which is a method for an *in situ* dose monitoring of charged particle therapy. Without injecting any PET tracer, positron emitters are produced through fragmentation reactions between the projectiles and the atomic nuclei of the tissue during patient irradiation [2]. Dual-head PET cameras limiting to 2D imaging have been studied [3]-[5], and the OpenPET is the first possible 3D geometry that does not interfere with the beam paths. Tracking a moving target such as a tumor in the lung will also become possible if the real-time image reconstruction becomes available. In addition, real-time monitoring of therapeutic gain might be possible in the future when a new PET tracer that quickly responds to radiotherapy is developed.

For the second, for example of combining with CT, OpenPET geometry allows simultaneous PET/CT to measure the same PET FOV as the CT FOV, in contrast to the conventional PET/CT where each FOV is separated by several tens of centimeters.

For the third, the OpenPET with two detector rings of axial length *W* extends an axial FOV up to 3*W*, because the maximum limit of the gap to obtain the axially continuous FOV is W. By multiplexing the OpenPET geometry, the axial FOV can be theoretically increased to an unlimited extent without increasing the number of detectors [6].

Numerical simulations

In order to evaluate the imaging performance of the OpenPET geometries, we simulated a dual HR+ like scanner (*D*=827.0 mm, *W*=153.6 mm) separated by a variable gap (*G* ranging from 0 to 2*W*) as shown in fig. 2 (a). The maximum gap size to have axially continuous FOV is *W*. In order to investigate the image quality when the gap exceeded the limitation, however, we varied the gap size up to 2*W*. Each one of the dual scanners consisted of 4 rings of 72 block-detectors. Each block-detector consisted of 8 x 8 array of BGO crystals with size 4.1 mm (transaxial) x 4.4 mm (axial) x 30.0 mm (depth). For comparison, we also simulated a dual-head PET scanner with the opening angle of 45 deg which is similar to the geometry proposed by Crespo et al 2006 [7]. For fair comparison, the number of crystal rings of the dual-PET scanner was increased to 85 (i.e., axial length of detector rings was 408.0 mm) so that the total number of crystals became equivalent, while the OpenPET had 64 rings. The dual-head PET scanner had two apertures of 408.0 mm x 316.0 mm on both sides.

We simulated a "warm" cylinder of 230.0 mm in diameter and 614.4 mm length which included 63 "hot" spheres of 4.0 mm diameter (fig. 2 (b)). The warm cylinder was filled with background activity and the hot spheres contained higher activity. The contrast between background and the hot spheres was 1:5. The mask for the gaps of *G*=0.0 mm, 76.8 mm, 153.6 mm, 230.4 mm and 307.2 mm was applied to the noise-free projection data. The masked 3D OS-EM with 8 subsets and 20 iterations was applied.

Reconstructed images for the OpenPET (*G* ranging from 0.0 to 307.2 mm) and the dual-head PET are shown in fig. 3. Since the coronal and the sagittal views are identical except for the dual-head PET geometry, only the sagittal views are displayed. In addition, two transaxial slices at the center and at 114.9 mm off-center are shown. Strong artifacts such as distortion along the y-axis are observed in the images by the dual-head PET geometry. On the other hand, the OpenPET geometry shows excellent performance. The central slices (slice A) of *G* ranging from 0.0 to 307.2 mm are very similar. The off-center slices (slice B) of *G* ranging from 0.0 to 153.6 mm are also similar. When *G*>153.6 mm (i.e., the maximum limitation for axially continuous FOV), however, blank areas where there is no LOR appear on both sides of the open space. With the blank areas, distorted point spread functions and low-frequent artifacts are also observed.

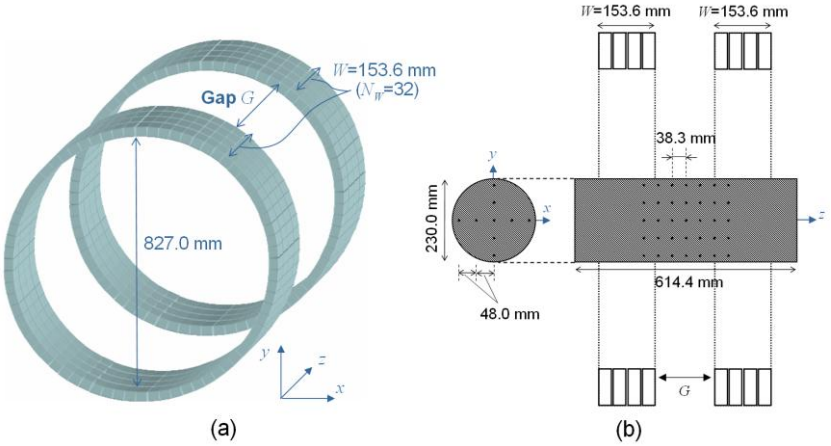

Fig. 2 The simulated OpenPET scanner (a) and the simulated cylinder phantom (b). Each scanner of the OpenPET has similar dimensions to the HR+ (N_W=32 crystal rings, *W*=153.6 mm axial length).

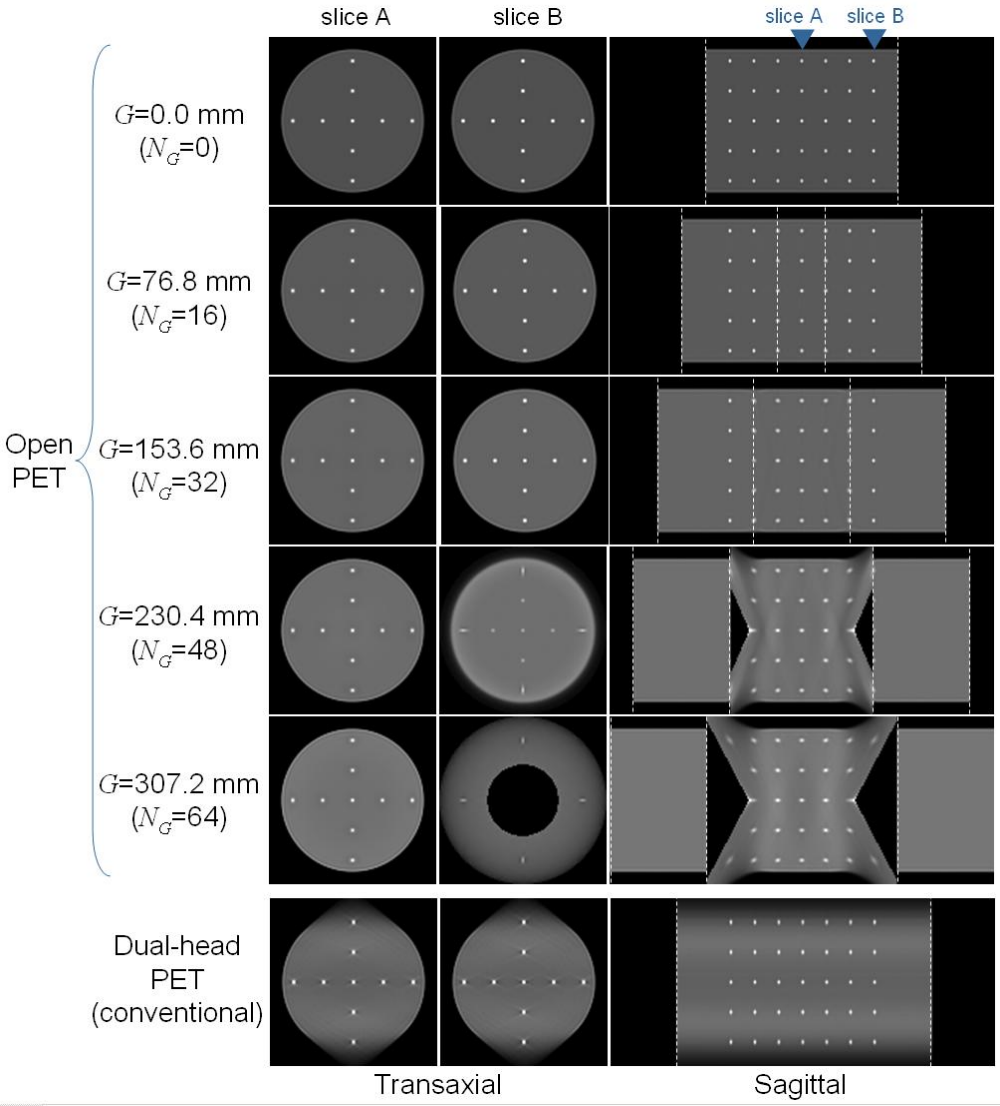

Fig. 3 Reconstructed images of the simulated phantom for the OpenPET (G ranging from 0.0 to 307.2 mm) and the dual-head PET. In addition to sagittal views, the central slice (slice A) and the off-center slice (slice B) are shown. White dotted lines represent the boundary of the area where detectors are located. N_G represents the number of rings corresponding to the gap.

Experiments using human data

We also tested the OpenPET geometry using experimental data obtained with the jPET-D4 [8], which is a prototype brain scanner that has five rings of 24 DOI detector blocks. We simulated the OpenPET geometry with a gap of 66 mm by eliminating data corresponding to one ring of blocks from the experimental data. Although some artifacts were observed at both ends of the open gap, the images obtained with and without the gap were very similar (fig. 4).

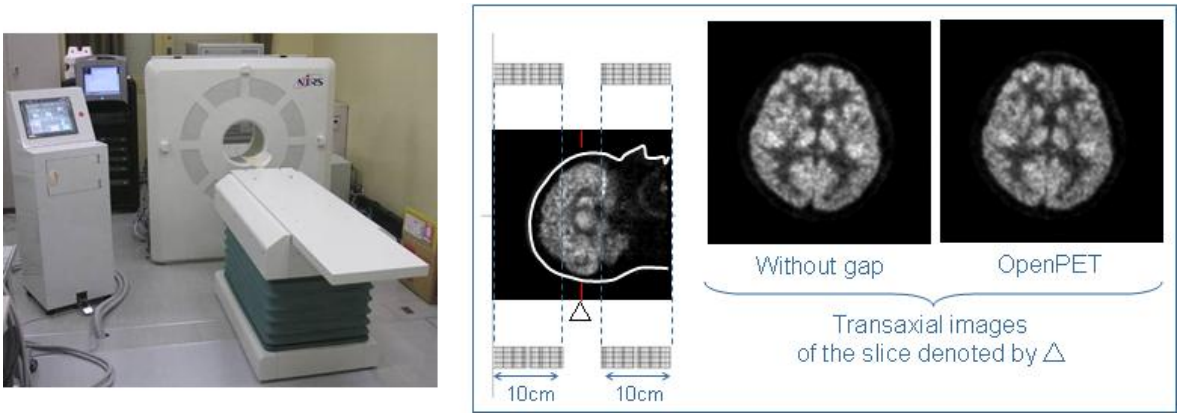

Fig. 4 Experimental testing of the OpenPET geometry using FDG-PET data acquired with the jPET-D4 (left). The images obtained with and without the gap were very similar.

Conclusions

In this paper, we reviewed our new idea of an OpenPET geometry, which consist of two axially separated detector rings. A long FOV including the open space is visualized by the masked 3D OS-EM. The OpenPET geometry is expected to help in realization of in-beam PET and simultaneous PET/CT as well as stress-less PET scanning.

Acknowledgement

This work is being supported by the NIRS President Grant Creative Scientific Research and the Grant-in-Aid for Scientists Research (A) of Kakenhi (20700417).

We would like to thank Drs. Mikio Suga, Hideaki Haneishi and Hideyuki Kawai in Chiba University, including their graduate students, for their excellent works to develop software and a small prototype. We would also like to thank Dr. Hiroyuki Kudo in Tsukuba University and Dr. Takashi Obi in Tokyo Institute of Technology for their advising on image reconstruction problems. For HIMAC experiments, we would like to thank NIRS colleagues in Research Center for Charged Particle Therapy, especially Drs. Koji Noda, Shinichi Minohara, Shinji Sato and Kyosan Yoshikawa. We also thank Mr. Yasunori Nakajima in Tokyo Institute of Technology. For animal imaging tests, we would like to thank NIRS colleagues in Molecular Imaging Center, especially Drs. Atsushi Tsuji, Mitsuru Koizumi, Ichio Aoki, Daisuke Kokuryo, Makoto Higuchi, Takayuki Obata. Finally we would like to thank all our Imaging Physics Team members; Dr. Eiji Yoshida, Dr. Naoko Inadama, Dr. Fumihiko Nishikido, Dr. Hideaki Tashima, Mr. Hidekatsu Wakizaka, Ms. Shoko Kinouch, Mr. Takayuki Mitsuhashi and Dr. Hideo Murayama.

References

［1］ Yamaya T, Inaniwa T, Minohara S, et al A proposal of an open PET geometry. Phys Med Biol. 2008; 53: 757-773.

［2］ Enghardt W, Crespo P, Fiedler F, et al. Charged hadron tumour therapy monitoring by means of PET. Nucl Instrum Methods Phys Res A. 2004; 525: 284–288.

［3］ Iseki Y, Mizuno H, Futami Y, et al. Positron camera for range verification of heavy-ion radiotherapy. Nucl Instrum Methods Phys Res A. 2003; 515: 840–849.

［4］ Crespo P, Barthel T, Frais-K¨olbl H, et al. Suppression of random coincidences during in-beam PET measurements at ion beam radiotherapy facilities. IEEE Trans Nucl Sci; 2005;52: 980–987.

［5］ Nishio T, Ogino T, Nomura K et al. Dose-volume delivery guided proton therapy using beam ON-LINE PET system. Med Phys. 2006;33: 4190–4197.

［6］ Yamaya T, Yoshida E, Inadama N, et al. A multiplex “OpenPET” geometry to extend axial FOV without increasing the number of detectors. IEEE Trans Nucl Sci. 2009;56: 2644-2650.

[7] Crespo P, Shakirin G and Enghardt W. On the detector arrangement for in-beam PET for hadron therapy monitoring. Phys Med Biol. 2006;51: 2143-2163.
[8] Yamaya T, Yoshida E, Obi T, et al. First human brain imaging by the jPET-D4 prototype with a pre-computed system matrix. IEEE Trans Nucl Sci 2008;55: 2482-2492.

OpenPET(2): Development of a Small Prototype for a Proof-of-Concept

Eiji Yoshida[1], Shoko Kinouchi[2,1], Taku Inaniwa[3], Shinji Sato[3], Yasunori Nakajima[4], Hideaki Tashima[1], Fumihiko Nishikido[1], Naoko Inadama[1], Hideo Murayama[1], Taiga Yamaya[1]

[1]Molecular Imaging Center, National Institute of Radiological Sciences, Chiba, Japan, [2]Chiba University, [3]National Institute of Radiological Sciences, Research Center for Charged Particle Therapy, [4]Tokyo Institute of Technology
Corresponding Author: Eiji Yoshida, e-mail address: rush@nirs.go.jp

Abstract

Objectives: We have proposed an OpenPET geometry which consists of two axially separated detector rings. The open gap would be suitable for in-beam PET, which is a method for in situ monitoring of charged particle therapy. In this work, we developed the first prototype of the OpenPET, especially for in-beam experiments using phantoms. The OpenPET prototype was designed with 2 detector rings of 8 detector blocks. Ring diameter was 110 mm and the minimum axial field-of-view was 99 mm. Distance between detector rings could be controlled. The DOI detector consisted of 784 LGSO crystals which were arranged in 4-layer of 14 x 14 arrays, coupled to a 64-ch FP-PMT. Each crystal element was 2.9 x 2.9 x 5 mm^3. Front-end circuits were separated from the detector head by 1.2 m coaxial cables. Front-end circuits were set under the detector rings and surrounded by lead and paraffin shields. **Results**: The system sensitivities were measured from a ^{22}Na point source. The system sensitivity without open gap was 7.2 %. On the other hand, the system sensitivity with open gap kept to 5.8 %. Count rate performance test utilized 8-cm cylinder phantom. Maximum count rate of prompt was 29 kcps at 0.1mCi. **Conclusions**: The small OpenPET prototype was succeed to get fully 3D images under the in-beam experiment. The OpenPET prototype has promises high sensitivity and enough performance for in-beam experiments.

I. INTRODUCTION

We have proposed an OpenPET geometry which consists of two axially separated detector rings [1]-[3]. The open gap would be suitable for in-beam PET, which is a method for *in situ* monitoring of charged particle therapy. Dual-head PET geometries have been studied for in-beam PET [4]-[5]. These geometries cannot avoid image artifacts due to missing lines-of-responses (LORs). In this work, we develop the first prototype of the OpenPET, especially for in-beam experiments using phantoms. The activity due to irradiation is generally low although the activity distribution is confined to a localized area in the body. Also, the number of annihilation photons from patient irradiation is limited to 1/100 of that in clinical PET. Therefore, highly sensitive PET scanners are required for in-beam PET. A depth-of-interaction (DOI) detector [6] can be designed for highly sensitive PET with high spatial resolution. On the other hand, we need to pay attention to protecting the detector and electronics circuits from damage by secondary particles [7]. We developed and evaluated the OpenPET prototype for in-beam PET experiments.

II. MATERIALS AND METHODS

A. OpenPET prototype

Fig. 1 shows the photograph of the small OpenPET prototype. The small OpenPET prototype was constructed with 2 detector rings of 8 detector blocks. Ring diameter was 110 mm and the minimum axial field-of-view (FOV) was 99 mm. Distance between detector rings could be controlled. (When distance between scintillator blocks was 44 mm, the open gap was 27 mm.) The DOI detector consisted of 784 $Lu_{2x}Gd_{2(1-x)}SiO_5$: Ce (LGSO, x=0.9) crystals (Hitachi Chemical Co., Ltd., Japan) which were arranged in 4-layer of 14 x 14 arrays, coupled to a 64-ch FP-PMT (Hamamatsu H8500) as shown in Fig. 2. In the OpenPET geometry, peripheral LGSOs near the open gap have higher sensitivity than other LGSOs. Size of LGSO block was smaller than sensitive area of the FP-PMT for all LGSOs must have enough spatial resolution.

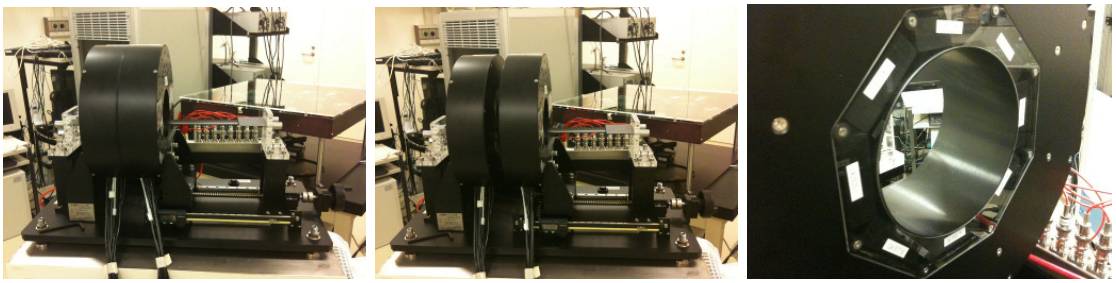

Fig. 1. Photographs of the small OpenPET prototype (Left: without open gap, Middle: with open gap, Right: Detector ring).

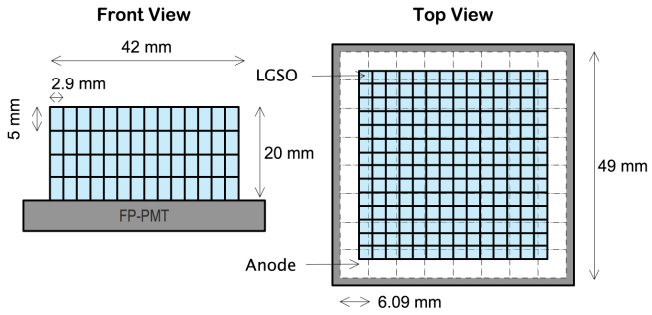

Fig. 2. Illustration of the 4-layer DOI detector.

Fig. 3 is the latest system architecture of the small OpenPET prototype. This system was designed to low cost, compact and portable. The small OpenPET prototype was designed as a system so as to be easily carried between PET areas and the Heavy Ion Medical Accelerator in Chiba (HIMAC). After 64 channels gain correction of the FP-PMT, output signals of two DOI detectors stacked axially were projected on one 2D position histogram by an Anger calculation. This signal processing can be reduced to the scale of a coincidence processer. Front-end circuits were separated from the detector head by 1.2 m coaxial cables. Front-end circuits were set under the detector rings and surrounded by lead and paraffin shields for in-beam PET experiments. Each DOI detector was in coincidence with the opposing 7 DOI detectors. Also, the coincidence circuits have delayed coincidence circuits for random estimation. Coincidence data were corrected only for the list mode.

Energy window was 400-600 keV and timing window was 60 ns. Table I shows specification of the small OpenPET prototype.

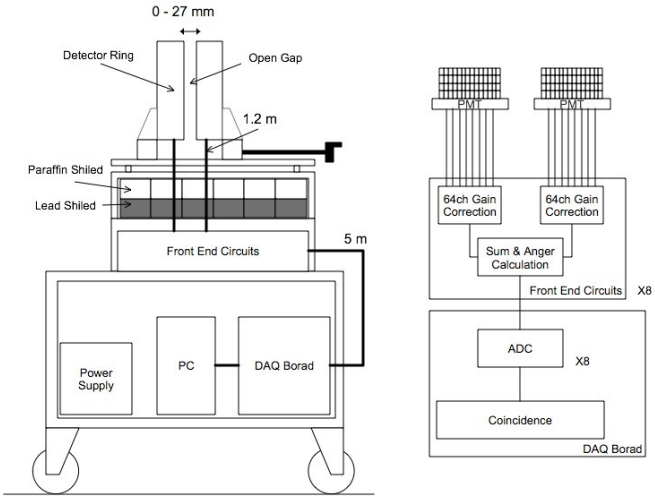

Fig. 3. System architecture of the small OpenPET prototype.

TABLE I

SPECIFICATION OF THE SMALL OPENPET PROTOTYPE

Scintillator material	LGSO
Number of scintillator	25,088
Size of scintillator	2.9 x 2.9 x 5 mm^3
Block size of the detector	42 x 42 x 20 mm^3
DOI	4
Photomultiplier tube	64 channel FP-PMT
Ring diameter	110 mm
Axial length	99 -126 mm
Data acquisition	List mode
Energy window	400 – 600 keV
Coincidence time window	60 ns

B. Performance evaluation

System sensitivity and sensitivity profile were measured from a ^{22}Na point source (0.64 MBq) and a 26-cm ^{68}Ge-^{68}Ga line source (0.34 MBq), respectively. Measurement times of the ^{22}Na point source and the ^{68}Ge-^{68}Ga line source are 10 and 60 minutes, respectively. These sources were placed in the center of the FOV. The open gap assumed virtual slices.

Count rate performance test utilized 8-cm cylinder phantom (4 cm diameter) for the small OpenPET prototype with 27-mm open gap. This cylinder phantom was filled with ^{18}F. This phantom was placed in the center of the FOV.

C. *In-beam PET experiment*

Fig. 4 shows ^{11}C irradiation experiment at HIMAC using the small OpenPET prototype. Open gap width was fixed to 27 mm. ^{11}C beam energy was selected as 330 MeV/u and ^{11}C beam intensity was about 5.0 x 10^6 pps. ^{11}C beam diameter was limited to 5 mm using the brass collimator. Target phantom was the PMMA cylinder (4 cm diameter and 10 cm length). Irradiation range was 2 cm into the PMMA cylinder using 145 mm PMMA range shifter. Irradiation time was 20 min and PET measurement time was 40 min after the start of ^{11}C irradiation. After normalized and random corrections, the fully 3D images were obtained by the MLEM reconstruction. A pixel pitch of reconstructed image was 1.5 mm.

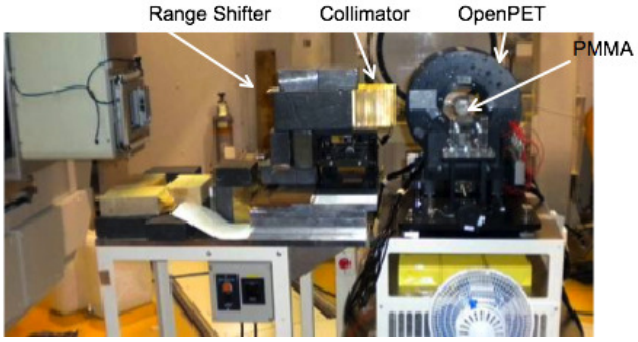

Fig. 4. ^{11}C irradiation experiment using the small OpenPET prototype.

III. RESULTS

A. *Performance Evaluation*

Fig. 5 shows the 2 dimensional (2D) position histogram from the 511-keV uniform irradiation (^{68}Ge-^{68}Ga line source). 1,568 crystals on a 2D position histogram could be separated clearly using the 1.2 m coaxial cables. Also, average energy resolution was 14 %. Timing resolution was very poor, but was not be optimized now. Therefore, timing window was 60 ns in this work.

Table II shows the system sensitivities with or without the open gap for the ^{22}Na point source. The sensitivity decreases by 19 % with the open gap. Fig. 6 shows sensitivity profile with 27 mm open gap for the 26-cm line source. The number of the slices is 83 and slice pitch is 1.475 mm. Sensitivity profile with the open gap are separated into three triangular distributions. Also, the center slice of open gap has maximum sensitivity.

Fig. 7 shows count rate performance with 27-mm open gap for the small OpenPET prototype. Prompt was saturated until 0.1 mCi, though this does not reach the peak due to the limitation of the data acquisition speed. Maximum cont rate of prompt was 29 kcps.

TABLE II

SYSTEM SENSITIVITY FOR THE OPENPET PROTOTYPE.

Open gap width (mm)	Sensitivity (%)
0	7.2
27	5.8

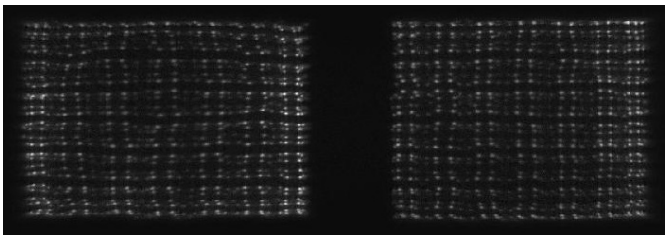

Fig. 5. 2D position histogram from the 511 keV uniform irradiation.

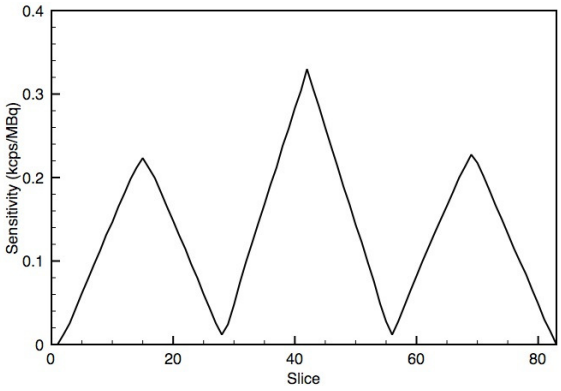

Fig. 6. Sensitivity profile with 27-mm open gap for the 26-cm line source.

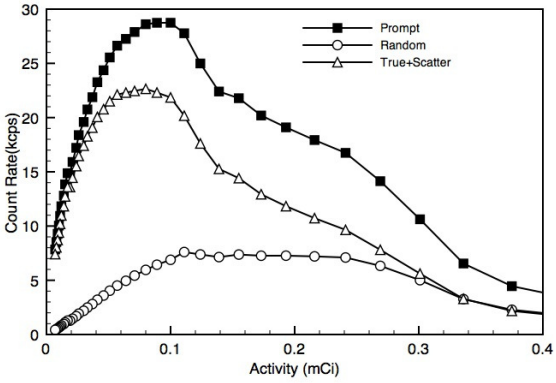

Fig. 7. Count rate performance with 27-mm open gap for the small OpenPET prototype.

B. In-beam PET experiment

Fig. 8 shows count rate of true coincidence after the start of ^{11}C irradiation. In the ^{11}C irradiation, the small OpenPET prototype was measured 3.3-sec cyclic peaks from prompt gamma ray. ^{11}C particles were stored into the PMMA cylinder after the start of irradiation. After irradiation, count rate was decayed with time. Fig. 9 shows reconstructed image from ^{11}C irradiation. Images of full data has artifact from prompt gamma ray as shown in Fig 9 a). After data was extracted to without cyclic peaks, obtained images were clear as shown in Fig. 9 b). Also, images of extracted data is almost same to off-beam data. Fig. 9 d) shows image profile to the direction of beam irradiation.

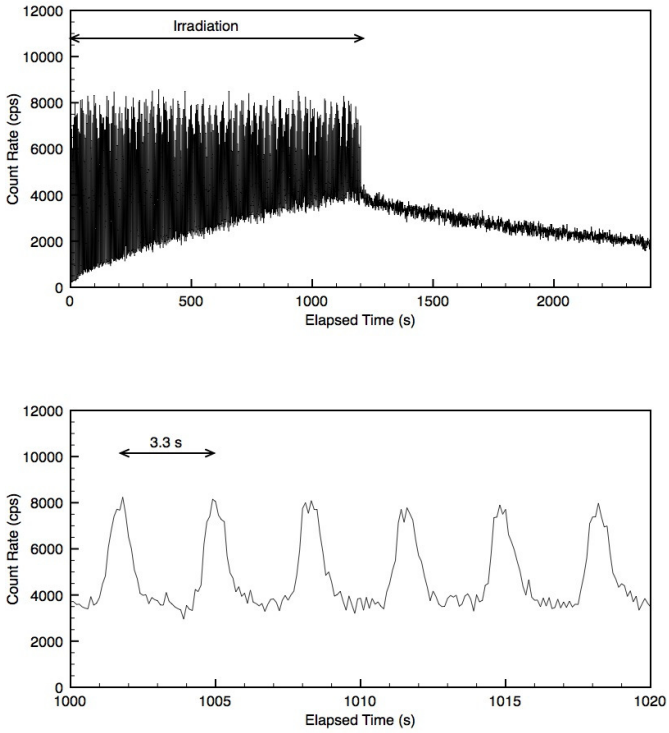

Fig. 8. Count rate of true coincidence after the start of ^{11}C irradiation.

(Top: all measurement time, Bottom: Expanded graph from 1000 s to 1020 s)

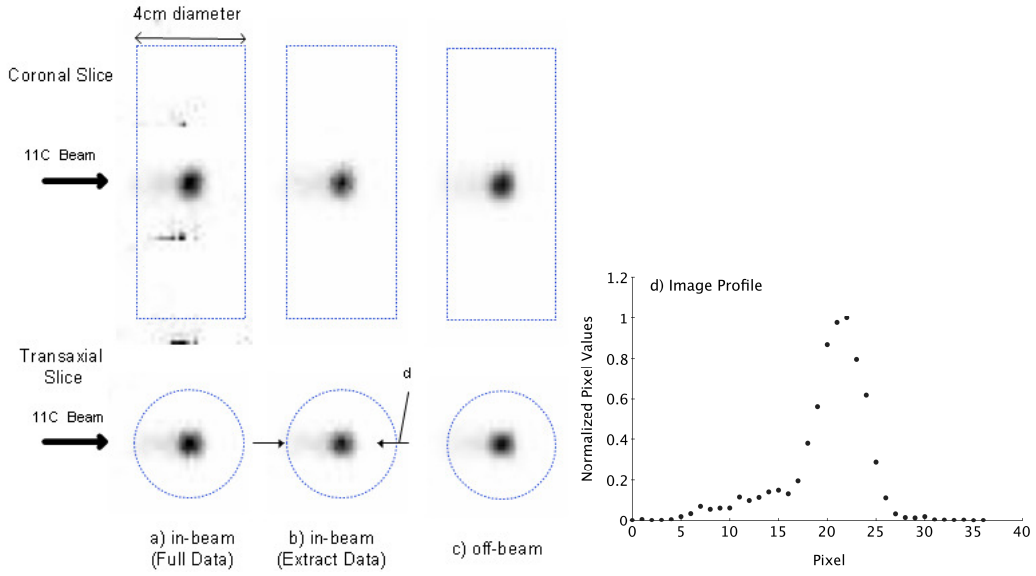

Fig. 9. Reconstructed images from ^{11}C irradiation using the small OpenPET prototype.

d) is image profile to the direction of beam irradiation.

IV. DISCUSSION AND CONCLUSION

We developed the small OpenPET prototype for in-beam PET experiments and demonstrated to OpenPET geometry for proof-of-concept. The small OpenPET prototype has high sensitivity, but limited to count rate performance. The small OpenPET prototype was succeed to get fully 3D images under the in-beam experiment.

The OpenPET prototype also promises enough performance for in-beam experiments. We will try to improve to count rate performance by optimized to timing resolution.

References

［1］ Yamaya T, Inaniwa T, Minohara S, et al A proposal of an open PET geometry. Phy. Med. Biol., 2008;53:757-773.

［2］ Yamaya T, Inaniwa T, Yoshida E, et al Simulation studies of a new 'OpenPET' geometry based on a quad unit of detector rings. Phys. Med. Biol., 2009;54:1223-1233.

［3］ Yamaya T, Inaniwa T, Yoshida E, et al Simulation studies of a new 'OpenPET' geometry based on a quad unit of detector rings. Phys. Med. Biol., 2009;54:1223-1233.

［4］ Crespo P, Barthel T, Frais-Kolbl H, et al Suppression of random coincidences during in-beam PET measurements at ion beam radiotherapy facilities. IEEE Trans. Nucl. Sci., 2005;52:980–987.

［5］ Nishio T, Ogino T, Nomura K,et al Dose-volume delivery guided proton therapy using beam on-line PET system. Med. Phys., 2006;33:4190-4197.

［6］ Tsuda T, Murayama H, Kitamura K, et al Performance Evaluation of a Subset of a Four-Layer LSO Detector for a Small Animal DOI PET Scanner: jPET-RD". IEEE Trans. Nucl. Sci., 2006;53;35-39.

［7］ Nishikido F, Yazaki Y, Osada H, et al Influence of secondary particles from heavy ion irradiation to in-beam OpenPET detectors. Conf. Rec. 2009 IEEE Nucl. Sci. Symp. Med. Imag. Conf., J04-5.

Carbon Ion Radiotherapy at Gunma University

Tatsuya Ohno, Takashi Nakano, Satoru Yamada, Tatsuaki Kanai

Gunma University Heavy Ion Medical Center, Gunma University, Japan
e-mail address :tohno@gunma-u.ac.jp

Abstract

The carbon ion radiotherapy project was launched at Gunma University in 2001, and the collaboration with the National Institute of Radiological Sciences (NIRS) was started in 2004. Based on the design and R&D studies at the NIRS, the construction (size: 45m x 65m) and operation costs of the accelerator system were reduced to one-third of those at the NIRS while maintaining its high performance. From the start of building construction (February of 2007) to treatment of the first patient (March of 2010) took approximately 3 years. As of July of 2010, a total 25 patients, including those with cancers of the prostate, head and neck, and lung have been treated with carbon ion radiotherapy at the Gunma University Heavy Ion Medical Center (GHMC). This short manuscript describes the clinical indications and cost analysis at the GHMC.

Facility

Carbon ion radiotherapy for the first patient at Gunma University was initiated in March of 2010. Our facility is the first university hospital-based facility in Japan, is supported by the Japanese and local governments, and is a compact prototype of a commercial design ready for distribution (Figures 1 and 2). The major specifications of the facility were determined based on the experience of clinical treatments at the NIRS. The main accelerator is a slow-cycling synchrotron with a diameter of 20m, and it accelerates carbon ions up to an energy range from 140 to 400 MeV per nucleon. A spiral wobbler system was adopted for the beam delivery system in order to improve the beam efficiency in a large irradiation field size. Among the 4 treatment rooms, one has a fixed horizontal beam line, one has a fixed vertical beam line, one has both fixed horizontal and vertical beam lines, and the remaining one is prepared for research and development of an advanced scanning technique for smaller targets.

Figure 1. Gunma University Heavy Ion Medical Center (GHMC)

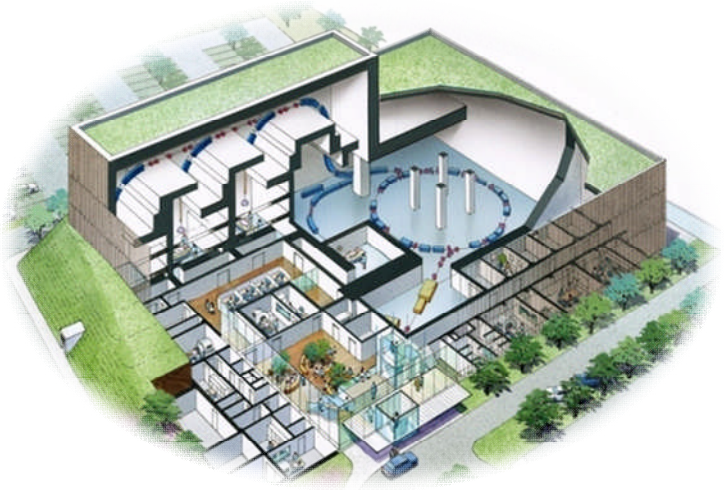

Figure 2. Bird's eye view of the GHMC

Clinical Indications of Patients Treated at Gunma University

Many phase I/II dose escalation and phase II studies for various tumor sites have been carried out at the NIRS since 1994 (1). Although promising clinical outcomes have been reported from the NIRS, it is of interest whether or not the efficacy of carbon ion radiotherapy from a single institution can be reproduced in other facilities when the optimal dose and fractionations are used for a similar patient population. In the GHMC, the efficacy and safety of carbon ion radiotherapy were reviewed for each tumor type, and then the best available dose and fractionation schedules determined at the NIRS were adopted for our clinical protocols (Table 1)

Table 1. Ongoing clinical protocols at the Gunma University Heavy Ion Medical Center

Site (protocol #)	Eligible patients	Treatment
Lung cancer (GUNMA0701)	・Histologically proven non-small cell lung cancer ・T1a-T2aN0M0 (peripheral type, TNM classification, 2009) ・Inoperable or decline surgery	*T1a-b:* 52.8 GyE/4 fr/1 week *T2a:* 60.0 GyE/4 fr/1 week
Prostate cancer (GUNMA0702)	・Histologically proven prostate cancer ・T1c-T3N0M0 (TNM classification, 2002) *Low risk group:* PSA <10ng/mL and Gleason score ≤6 and T1c-T2b N0 M0. *Intermediate risk group:* Other than low risk and high risk groups *High risk group:* PSA ≥20ng/mL or Gleason score ≥8 or T3 N0 M0	*Low risk group:* Carbon ion RT alone (57.6 GyE/16 fr/4 weeks) *Intermediate risk group* Hormone therapy (6-8 months) and Carbon ion RT *High risk group* Hormone therapy (2 years) and Carbon ion RT
Liver cancer (GUNMA0703)	・Histologically proven or compatible features on CT/MRI with hepatocellular carcinoma ・Single lesion ・No invasion of the main trunk of the portal vein ・T1-3N0M0 (TNM classification, 2002) ・Child-Pugh A or B	52.8 GyE/4 fr/1 week
Rectal cancer (GUNMA0801)	・Recurrent pelvic tumor after surgery for rectal cancer ・No metastases other than pelvic tumors ・Curative intent for primary surgery	73.6 GyE/16 fr/4 weeks
Head and neck cancer (GUNMA0901)	・Histologically proven non-squamous cell carcinoma ・T any N0M0 (TNM classification, 2002)	64.0 GyE/16 fr/4 weeks
Bone and soft tissue sarcoma (GUNMA0904)	・Histologically proven bone and soft tissue sarcomas ・Stage IA-III (TNM classification, 2002)	*Standard:* 70.4 GyE/16 fr/4 weeks *Sacral chordoma:* 67.2 GyE/16 fr/4 weeks *Spine tumor:* 64.0 GyE/16 fr/4 weeks

There needs to be a multi-institutional clinical study on carbon ion radiotherapy in order to establish powerful evidence that the protocols are safe and effective. At present, a prospective study of prostate cancer patients is under preparation among all proton and carbon ion radiotherapy facilities in operation in Japan. In this study, prostate cancer patients with the same eligibility criteria will be treated with protons or carbon ion beams at each prescribed dose and fractionation. The GHMC will take part in the clinical study.

Cost analysis

Although the increased development of advanced technologies such as carbon ion radiotherapy usually results in higher health care expenses, the cost-effectiveness of carbon ion radiotherapy has not been fully investigated for all indications. However, we previously evaluated the cost-effectiveness of carbon ion radiotherapy compared with conventional multimodality therapy in the treatment of patients with locally recurrent rectal cancer (2). In this study, 14 and 11 patients receiving treatment for the locally recurrent rectal cancer between 2003 and 2005 were retrospectively followed during the study period of 2 years at the NIRS and Gunma University Hospital (GUH), respectively. All patients received only radical surgery for primary rectal adenocarcinoma and had isolated unresectable pelvic recurrence. The direct costs for diagnosis, treatment of a recurrence of the cancer, supportive therapy, hospital admissions, complications, and follow-up visits were computed for each individual. Treatment was carried out with carbon ion radiotherapy alone at the NIRS, while multimodality therapy, including three-dimensional conformal radiotherapy, chemotherapy and hyperthermia was performed at GUH. The 2-year overall survival rate was 85% and 55% for carbon ion radiotherapy at NIRS and multimodality treatment at GUH, respectively. The mean cost was 4,803,946 JPY for the carbon ion radiotherapy group and 4,611,100 JPY for the multimodality treatment group. The incremental cost-effectiveness ratio for carbon ion radiotherapy was 6,428 JPY per 1% increase in survival. The median duration of total hospitalization of the treatment was 37 days for carbon ion radiotherapy and 66 days for the multimodality treatment group.

In conclusion, by calculating all of the direct costs, carbon ion radiotherapy was found to be a potentially cost-effective treatment modality compared to multimodality treatment for locally recurrent rectal cancer.

References

［1］ Okada T, Kamada T, Tsuji H, et al. Carbon Ion Radiotherapy: Clinical Experiences at National Instituteof Radiological Science (NIRS) J. Radiat. Res., 51: 355-364, 2010.

［2］ Mobaraki A, Ohno T, Yamada S, Sakurai H, Nakano T. Cost-effectiveness of carbon ion radiation therapy for locally recurrent rectal cancer. Cancer Sci. 101:1834-1989, 2010.

Tracking Target Motion

Shinichiro Mori, Motoki Kumagai, Suguru Dobashi, Nobuyuki Kanematsu, Hiroshi Imada, Makoto Shinoto, Kazuhiko Oonishi, Taku Inaniwa, Takuji Furukawa, Naoyoshi Yamamoto, Shigeo Yasuda, Shigeru Yamada, Susumu Kandatsu, Masayuki Baba and Koji Noda

Research Center for Charged Particle Therapy, National Institute of Radiological Sciences, Chiba, Japan
e-mail address: shinshin@nirs.go.jp

Abstract

Purpose: To quantify the magnitude of respiration-induced target motion, 4DCT and dynamic flat panel detector (DFPD) images were used.

Methods and Materials: Several tens of inpatients with lung, pancreas or liver cancer underwent 4DCT acquisition under free breathing conditions using a 256 multi-slice CT (256MSCT) in cine mode. For lung cancer cases, fluoroscopic images were acquired after 4DCT images. The patient respiratory signal was obtained by an external respiratory sensing monitor. For the 4DCT study, gross tumor volume (GTV) and normal tissues were contoured on the CT data set and the intrafractional motion was calculated. For the DFPD study, target motion was calculated by marker-less template matching and compared with the external respiratory signal.

Results: 4DCT images obtained with the 256MSCT improved the evaluation of tumor displacement without 4DCT artifacts that were observed using the conventional MSCT. The images were of sufficient quality to calculate particle dose distribution for layer-stacking irradiation, as well as scanning for target movement. The correlation between the external and internal intrafractional motions were slightly degraded.

Conclusions: It is necessary to capture intrafractional motion in both treatment planning and irradiation stages. By doing this, we can provide increased treatment accuracy.

Introduction

Worldwide, more than 28 particle treatment centers were operating in 2008, including three carbon ion beam centers, and the construction of new centers is set to continue. Compared with photon beams, charged particle beams provide superior dose conformation, and minimization of excessive dosing to normal tissues. These strengths are due to the characteristic increase in energy deposition of particle beams with penetration depth (proton and carbon ion beams) up to a sharp maximum at the end of the range (Bragg peak).

Organ motion due to respiration has been investigated using a variety of methods, including fluoroscopy, ultrasound (US), MRI, CT and PET, in the lung, liver, pancreas, kidney, and prostate sites. An understanding of motion characteristics in radiotherapy planning is useful for determining internal margins and optimizing beam parameters (beam angle, etc.), because the degradation of image quality due to respiratory motion affects radiotherapy planning and delivery of the treatment beam. We used 256 multi-slice CT (256MSCT), which employs a 12.8-cm wide cylindrical 2D detector system built into the frame of a conventional 16 multi-slice CT (Aquilion, Toshiba Medical Systems)(1), to evaluate organ motion. Within this 12.8-cm system, the 256 multi-slice CT obtains volumetric cine CT data without resorting to the respiratory phase. Motion artifacts due to breathing were frozen by a temporal resolution of 250 ms, allowing the tumor shape to be evaluated accurately.

Moreover, thinner slice thickness and a shorter total acquisition time helped determine target margins without 4DCT artifacts. Organ movement due to respiration may change the run of a charged particle beam that can result in degradation of dose conformation to the target. Moreover, treatment planning accounts for organ motion to avoid dose variation. Therefore, although the treatment beam sometimes misses due to movement of the target, better imaging will allow for better treatment accuracy. We herein introduce our approaches to capture images of a moving target and quantitatively assessing the potential problems in treatment planning due to organ movement.

Organ/target motion

We quantified organ and target motion due to respiration in the pancreas, liver and lung sites as a function of time using the 4DCT and DFPD. In the NIRS, patients receiving thoracic and abdominal treatments undergo carbon ion beam treatment with a custom-made immobilization device to improve patient positional reproducibility throughout the treatment course. To more accurately simulate typical clinical conditions, the same immobilization techniques were used during this study.

For the pancreatic site (irradiation in the supine position only), 3D visualization of the pancreas as a function of the respiratory phase is shown in Figure 1. Geometrical variation was greater around the pancreas tail than the pancreas body and head regions. The average pancreas head, body and tail displacement in the inferior direction for the ungated phase was 8.3 mm, 9.6 mm and 13.4 mm, respectively, which was minimized in the gated phase to 2.8 mm, 2.8 mm and 3.6 mm, respectively. For all six patients with pancreatic cancer, the average pancreas COM displacement relative to that at peak exhalation was mainly in the inferior direction, at 9.6 mm for the ungated phase and 2.3 mm for the gated phase (2).

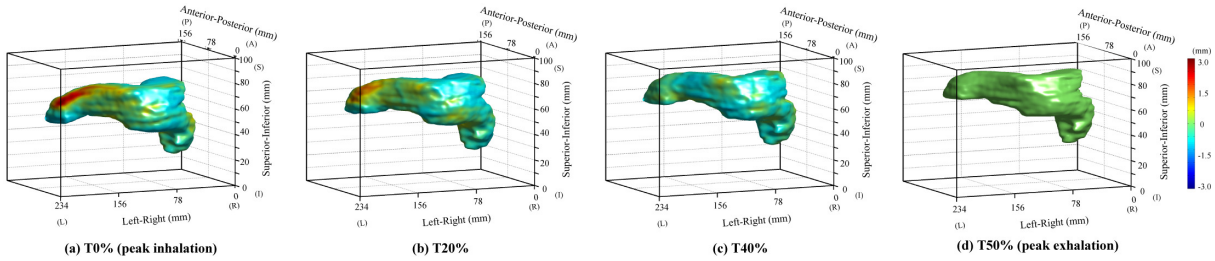

Figure 1. 3D-visualized pancreas, and the magnitude of geometrical variation from peak exhalation as a function of the respiratory phase. (a) T0 (peak inhalation), (b) T20, (c) T40, (d) T50 (peak exhalation).

With regard to the liver site (irradiation administered with patients in the prone position), after the 1st 4DCT were done, the patient couch was moved to the adjacent position to cover the entire liver. As a result, an approximately 25cm longitudinal scan range could be acquired. Geometrical changes due to respiration were quantified by a deformable registration between the reference and respective respiratory phases (Figure 3). The magnitude of the intrafractional displacement was increased close to the inhalation phase, with both AP and SI movement around the diaphragm. However, around the middle abdominal region, the movement was almost SI (Figure 2). Another visualization technique is the intrafractional motion curve shown in Figure 3. These visualizations were useful to understand the rich information provided in the 4DCT, and were useful for optimizing treatment planning.

The GTV-COM displacement average in 10 patients was 0.3mm (max: 1.8mm) in the left side, 2.2mm (max: 5.3mm) in the right side, 4.6mm (max: 10.8mm) in the anterior side, 0.1mm (max: 0.3 mm) in the posterior side, and 11.6 mm (max: 17.4mm) in the inferior side. No displacement was observed on the superior side.

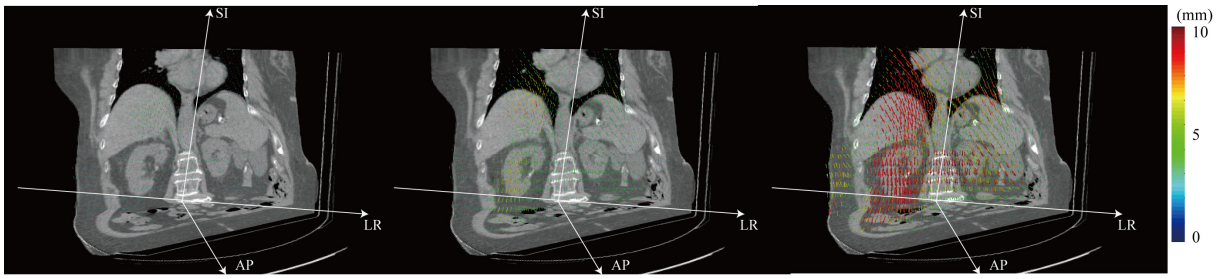

(a) Late exhalation (T40) (b) Mid-exhalation (T20) (c) Peak inhalation (T0)

Figure 2. Intrafractional motion map (shown as arrows) overlaid on the CT images (oblique view). (a) Late exhalation (T40), (b) mid-exhalation (T20) and (c) peak inhalation. Arrow starting and end points were peak exhalation (T50) and each phase, respectively. Large displacements were observed around the right liver region.

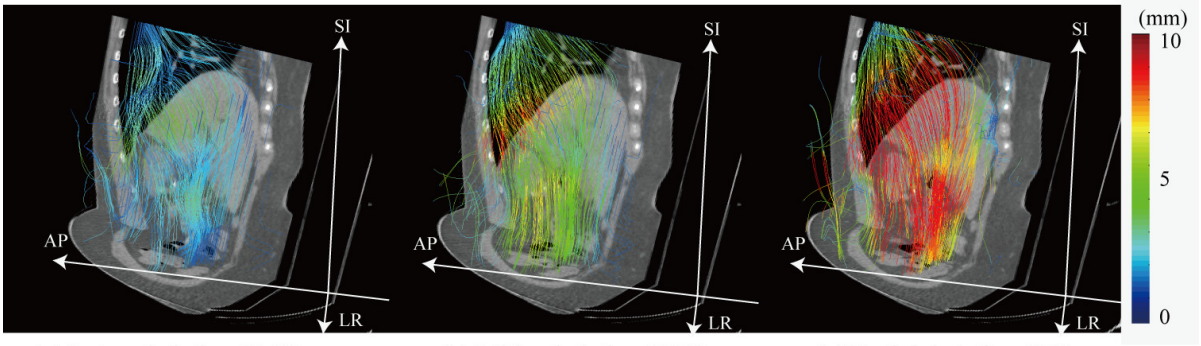

(a) Late exhalation (T40) (b) Mid-exhalation (T20) (c) Peak inhalation (T0)

Figure 3. Intrafractional motion curves overlaid on the CT images in oblique view. These curves represent the magnitude of displacement and motion direction from peak exhalation (T50) to respective phases (Tn).

A total of 14 lung cancer patients participated in the 4DCT immobilization study (supine position only). Volumetric cine imaging of the lungs showed continuous movement of the tumor in the axial and sagittal sections, and the carbon ion dose distribution of a beam with a 330 degree beam angle was overlaid for respiratory-ungated layer-stacking irradiation at respective phases (Figure 4). The average GTV-COM displacement relative to that at peak exhalation was 1.4 mm (range 0.5-2.3 mm) in the left-right, 2.2 mm (range 0.8-4.7 mm) in the anterior-posterior, and 6.6 mm (range 1.6-21.8 mm) in the superior-inferior direction.

Several centers have reported treatment approaches to a moving target using passive beam irradiation because it gives constant SOBP to the target during a whole irradiation. However, because layer-stacking and scanning irradiation involves irradiation with the respective beam as a function of time within the same layer and then changes to the next layer, repeating this process until the prescribed dose is delivered to the target will be less robust against motion than passive irradiation (3, 4). These findings highlight the importance of evaluating respiratory-induced dose variation, including deformable registration, in scanning and layer-stacking irradiation approaches.

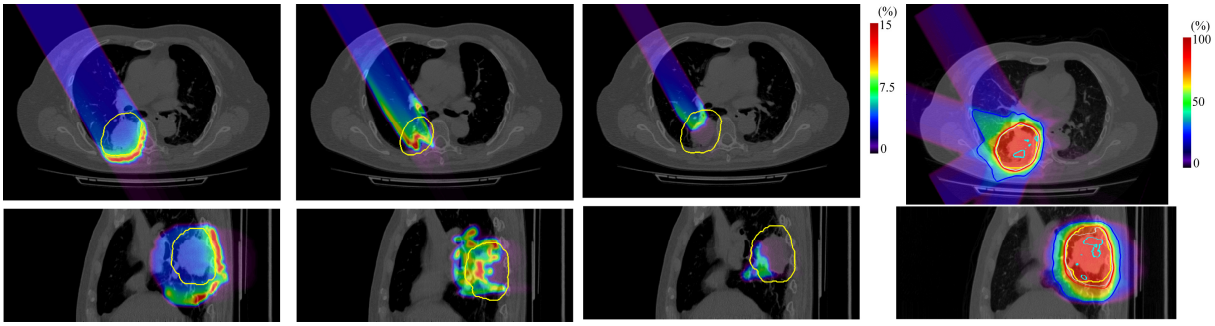

(a) Phase T40, 1st layer (b) Phase T90, 17th layer (c) Phase T50, 20th layer (d) Accumulated dose

Figure 4. Carbon ion beam distribution for respiratory-ungated layer-stacking irradiation. The beam angle was 330 degrees. (a) 1st layer at phase T40. (b) 17th layer at phase T90. (c) 20th layer at phase T50. (d) Accumulated dose including deformable registration. The yellow line is the planning target volume at the respective phase (PTV(Tn)).

Some limitations to irradiating a moving target warrant further discussion. While tumor movement as a result of respiratory motion is now well understood, little attention has been paid to movement due to bowel gas movement. Gas bubble movement is due to two physiological processes, respiration and peristalsis. Since the charged particle beam stopping position is strongly dependent on the radiological pathlength from the patient surface, replacing dense tissue with a low-density material such as bowel gas changes the radiological pathlength significantly, resulting in a perturbation in the beam stopping position from that originally planned. Quantitative analysis of dose variation due to bowel gas movement in the treatment course is a more challenging task in charged particle therapy than photon therapy.

In clinical situations, it takes a several minutes to complete treatment beam irradiation per fraction using the respiratory-gated strategy. Triple phase dynamic enhancement CT acquisitions were routinely acquired for diagnostic purposes under inhalation breath-holding. The scan interval time of the venous phase and delayed phase from the arterial phase were 35 s and 145 s, respectively. We defined the arterial phase CT data (scan interval time 0 s) as a treatment planning CT, and calculated the compensating bolus, which was then applied to the CT data sets at the other two phases. Since the bolus was designed to cover the CTV at the planning CT, over 95% of the dose was delivered to the CTV at 0 s. Although anatomical positions at each phase were similar, beam overshoot/undershoot was observed at 35 and 145 s due to extension/shortening of the radiological path length from the anterior and left directions against the planning CT. Since gas bubbles in the bowel may degrade dose conformation to the target, methods to appropriately deal with this issue are required (5).

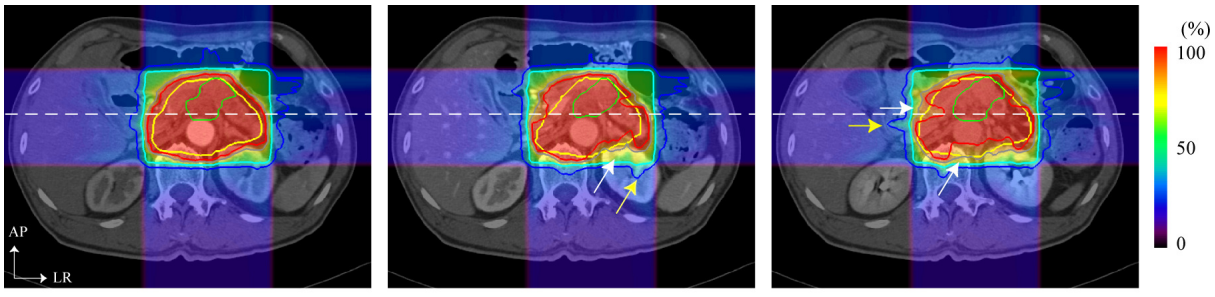

(a) (b) (c)

Figure 5. Carbon ion beam dose distribution in axial and coronal sections using contrast enhanced multi-phase CT images at time (a) 0 s (reference CT), (b) 35 s, and (c) 145 s. Green and yellow lines show gross tumor volume and clinical target volume contours, respectively.

Although the human respiratory cycle is not strictly regular, and generally varies in amplitude and period from one cycle to the next, for this study we assumed that the patient respiratory cycle, pattern and tumor position were reproducible throughout the course of treatment. Current treatment planning uses a single respiratory cycle only because the inclusion of respiratory patterns during irradiation cannot be accounted for. Respiratory pattern variations can be considered in treatment planning via the acquisition of 4DCT data for multiple respiratory cycles before treatment, although consideration needs to be given to the very high patient dose this entails. Several approaches to this problem are available. The first is to include respiratory pattern variations in treatment planning via the use of margins, etc. The second is real-time monitoring of target position using either an external marker or internal monitoring system. Owing to the imperfect reproducibility of the respiratory cycle, this relatively extended treatment period may result in inconsistencies between respiratory phase as determined using an external marker on the diaphragm and the movement of the internal anatomy. Thanks to its high temporal resolution and reproducibility of setup position, fluoroscopy is currently the better choice.

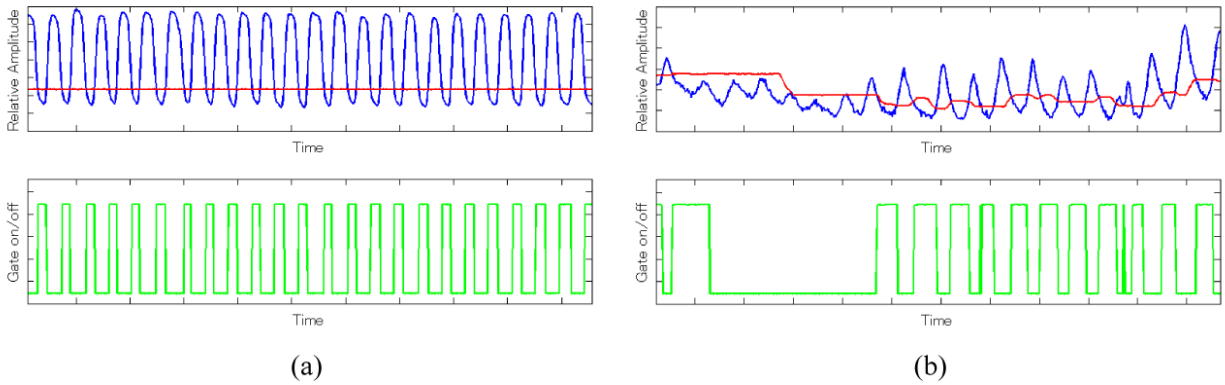

Figure 6. Respiratory signal obtained using an external respiratory sensing monitor (blue line), gating threshold (red line) and gating signal (green line). (a) Regular breathing pattern. (b) Irregular breathing pattern.

Real time tracking

However, although external systems facilitate the measurement of patient surface position as a function of time, and are in fact in routine use at several treatment centers, they do not provide internal target position. Rather, this can be obtained using 4DCT data and the respiratory signal during 4DCT acquisition. Owing to the imperfect reproducibility of the respiratory cycle, this relatively extended treatment period may result in inconsistencies between respiratory phase as determined using an external marker on the diaphragm and the movement of the internal anatomy. The problem, however, is that neither provides insights into how variable patients' breathing is during the few minutes of treatment. Current 4DCT scans acquire only a single respiratory cycle, so that, as a result, the patient's respiratory cycle and tumor position are not reproducible for all respiratory activity during treatment.

Fluoroscopic images using DFPD were acquired for lung cancer patients from a 45 degree oblique view. To minimize the skin dose, 6 s fluoroscopy with 15fps was repeated 8 times with an acquisition interval time of 12s, thus resulting in a total image acquisition time and study time of 48 s and 180s, respectively (Figure 7). Respiratory signals were obtained by an external respiratory sensing system. The target position was captured by using a multi-template matching method as follows: First, ten template images were binned using the first

respiratory cycle images (= 90 images). A bonding box sufficient to cover the target region was set on the template images. The target positions in the respective phase were calculated by using template images. The gating threshold was defined as 20% of the amplitude of the reference cycle (first respiratory cycle) and the external respiratory signal is shown in Figure 7.

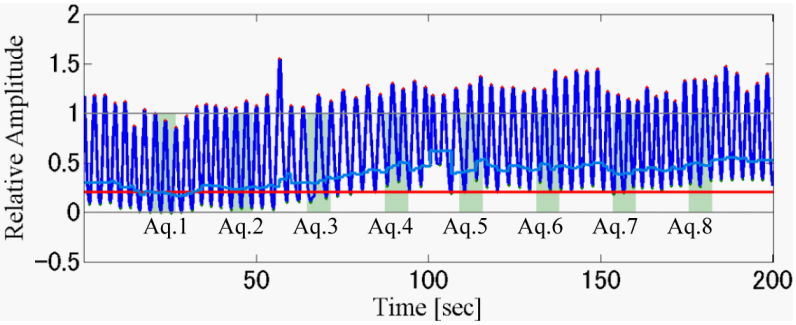

Figure 7. Respiratory signal obtained by the external respiratory sensing monitor (blue line). Red and light blue lines show the 20% gating threshold of the reference respiratory cycle and that of respective cycles. The green square region shows the DFPD image acquisition time.

DFPD images with the calculated bonding box are shown in Figure 8. The tumor was small, and not clearly observed on the images. Tumor displacement was almost entirely in the SI direction. Quantitative results in SI and AP displacement are summarized in Figure 9. With regard to SI motion, the external respiratory signal and internal target position were well correlated in the 1st DFPD acquisition. These correlations, however, were degraded after 3rd acquisition. For AP motion, the external and internal correlation was not good for any of the DFPD acquisition series, and the internal tumor position fluctuated because the tumor was close to the left atrium. As a result, the tumor position was also affected by the patient's heartbeat. In this patient, the SI motion determined by 4DCT was approximately 7 mm in a single respiratory cycle, however, that obtained by fluoroscopy was 17.5mm during a 180 s study time.

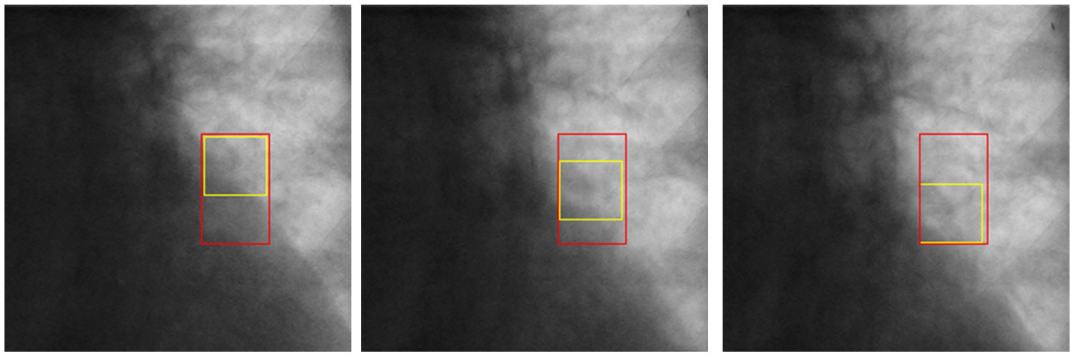

Figure 8. DFPD lung image as a function of respiratory phase. The yellow and red squares show the calculation region and the bounding box of calculation regions.

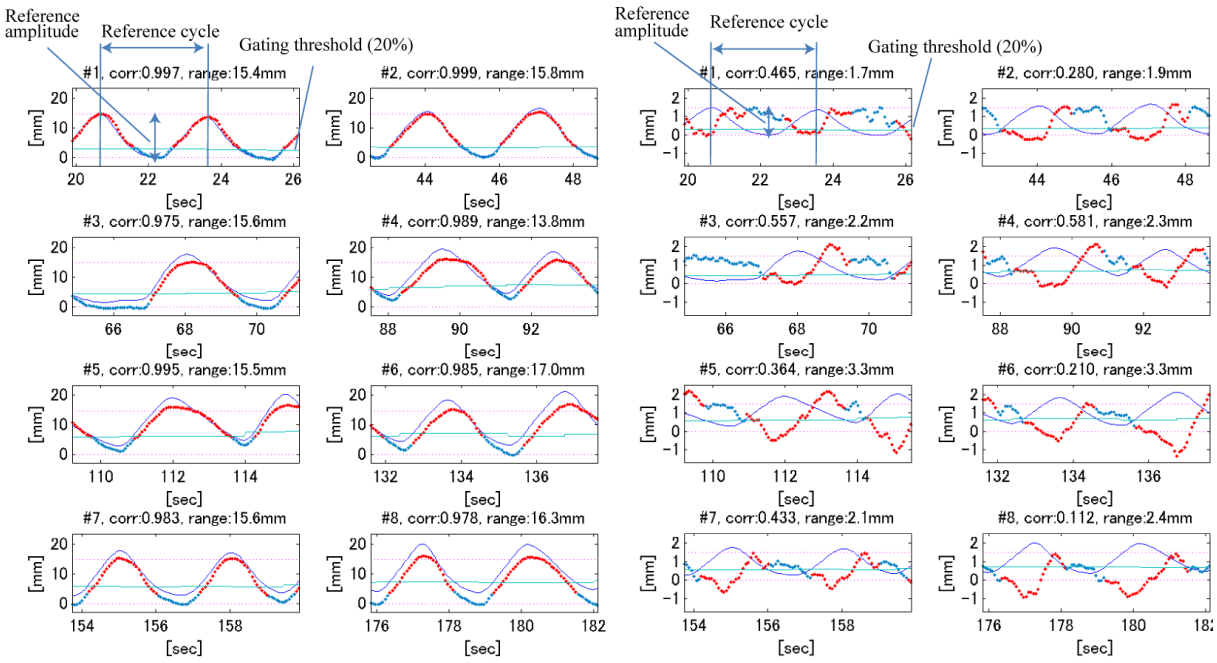

(a) SI motion (b) AP motion

Figure 9. The relationship between external respiratory signal (solid blue line) and tumor displacement obtained by DFPD images (dotted red/blue lines). (a) SI motion. (b) AP motion. The light blue solid line shows the gating threshold (20% of the external respiratory signal in each cycle). The tumor position during the gating window is shown by a dotted blue line.

Patient positional verification

Conventional patient positioning (patient setup) is commonly performed by use of a tattoo on the patient's skin for correct setup of the patient. Recently, several treatment centers have started using a laser marker on the treatment room wall or on the x-ray imaging system. However, patient positioning takes several minutes to complete, and adjustment of the rotational component of the coordinate transformation (yaw, pitch, roll) is more difficult than that for coordinate transformation (left-right, anterior-posterior, and superior-inferior). A more recently introduced patient positional system uses the 2D-3D image registration technique with a combination of 2D imaging, such as portal images, and volumetric CT data used for treatment planning, and it calculates patient positioning errors between the treatment and planning stages. Current CPUs have four or fewer cores in a single integrated circuit, limiting the performance of multithreading computation. An alternative approach, however, is to use a GPU (graphic processing unit) as a parallel computational architecture in place of the CPU. We were able to improve the patient positioning system by including a GPU-based auto-registration function programmed in C++ and CUDA (NVIDIA Corporation, CA, USA). The GPU-based version (a 500 MHz core clock, an 800 MHz memory clock, and 640 MB of memory, NVIDIA 8800 GTS board) gives a 50-fold faster calculation time than the CPU-based software program (2.0 GHz single quad-core CPU Intel Xeon processor, 4 GB physical memory)(6). As a result, auto registration could be finished in less than 30s, with 0.2 mm and 0.2deg geometrical accuracy. This shorter calculation time can help decrease patient positional changes during the setup procedure. Moreover, the high geometrical accuracy could improve dose conformation to the target.

Conclusions

We introduced the NIRS approaches to a 4D charged particle study. It is necessary to capture intrafractional motion in both treatment planning and irradiation stages in order to provide better treatment accuracy. We are presently constructing a new treatment facility which will allow the provision of raster-scanning irradiation, including thoracic and abdominal regions (7). We are convinced, however, that our approach to moving targets in charged particle therapy will be a decisive factor in overcoming problems with treatment accuracy, and will be useful for improving treatment using the scanning irradiation method.

References

［1］ Mori S, Endo M, Tsunoo T, et al. Physical performance evaluation of a 256-slice CT-scanner for four-dimensional imaging. Med Phys 2004; 31:1348-1356.

［2］ Mori S, Hara R, Yanagi T, et al. Four-dimensional measurement of intrafractional respiratory motion of pancreatic tumors using a 256 multi-slice CT scanner. Radiother Oncol 2009; 92:231-237.

［3］ Kanematsu N, Endo M, Futami Y, et al. Treatment planning for the layer-stacking irradiation system for three-dimensional conformal heavy-ion radiotherapy. Med Phys 2002; 29:2823-2829.

［4］ Inaniwa T, Furukawa T, Nagano A, et al. Field-size effect of physical doses in carbon-ion scanning using range shifter plates. Medical Physics 2009; 36:2889-2897.

［5］ Kumagai M, Hara R, Mori S, et al. Impact of intrafractional bowel gas movement on carbon ion beam dose distribution in pancreatic radiotherapy. Int J Radiat Oncol Biol Phys 2009; 73:1276-1281.

［6］ Mori S, Kobayashi M, Kumagai M, Minohara S. Development of a GPU-based multithreaded software application to calculate digitally reconstructed radiographs for radiotherapy. Radiol Phys Technol 2009; 2:40-45.

［7］ Noda K, Furukawa T, Fujisawa T, et al. New accelerator facility for carbon-ion cancer-therapy. Journal of Radiation Research 2007; 48:A43-A54.

Treatment planning Considering Macroscopic Heterogeneity in Sensitivity and Dose Based on PET Hypoxia Imaging

Iuliana Toma-Dasu

Medical Radiation Physics, Stockholm University and Karolinska Institutet, 171 76 Stockholm, Sweden

The progress in dose delivery and treatment planning for radiation therapy has opened new opportunities for advanced Intensity and Radiation Quality Modulated radiation therapy optimised on biological bases. One of the most important factors influencing the outcome of cancer treatment is the oxygenation of the tumour. Due to its importance many attempts have been made to characterise it for the quantitative modelling of treatment outcome. Theoretical simulation can be used to provide quantitative data on tumour oxygenation for a whole range of applications. The results could be used to study the influence of mixed radiation quality on the biological modelling of tumour response for treatment planning. Furthermore, the simulated tumour with respect to the microenvironment could also be an important tool for investigating the influence of microscopic heterogeneity of high LET radiation on the treatment outcome.

Given the clinically-proven importance of tumour microenvironment and in particular of tumour oxygenation for the result of the treatment, a computer model has been built in order to simulate realistic tumours with respect to the macroscopic heterogeneity in sensitivity given by the oxygenation. Furthermore, the oxygenation was also simulated at the cellular level. The oxygenation of heterogeneous tissues was modelled starting from basic physical processes and measurable parameters. The general equation that describes the oxygen transport in tissue under the influence of diffusion and consumption was used, allowing the description of tumour oxygenation in a rather broad range of tissues. The realistic tissue oxygenations obtained with this model have been used as input for simulations of tumour responses to various dose distributions. The results had shown the relative influence of the total amount and temporal change of the distribution of hypoxic regions on treatment outcome. Thus, it had been suggested that information on tumour hypoxia has to be taken into consideration for accurate treatment planning and can therefore be used for biologically-based treatment optimisation.

An example of a theoretically simulated tumour with respect to the microscopic heterogeneity in sensitivity is presented in figure 1.

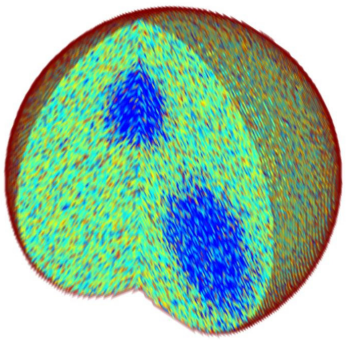

Figure 1. Simulated spherical tumour, 2 cm in diameter, with respect to oxygenation. The colour scale indicates the oxygen partial pressure ranging from the radiobiological hypoxia, 0 to 10 mmHg, (blue) to 40 mmHg (red). The tumour presents two macroscopic hypoxic regions surrounded by well oxygenated cells.

The model was further used in the development of an algorithm for optimising treatment planning based on positron emission tomography (PET) imaging of tumour hypoxia. The algorithm is based on the nonlinear conversion of image intensities into radiosensitivity maps and takes into account the heterogeneity and the

dynamics of the hypoxic regions during the treatment. The results have shown that incorporating hypoxia information from PET images into treatment planning is feasible. There are however considerable differences in the prescribed doses depending on the planning approach. Best results in terms of dose prescription appear to be obtained by using the uptake characteristics of the imaged tracers as they give the best interpretation of the intensity gradients.

The results also show that treatment planning considering macroscopic heterogeneity in sensitivity and dose based on PET hypoxia method could identify the difficult cases that would require very high doses of low LET radiation to the hypoxic regions or cases where the hypoxic regions might be located close to organs at risk and could thus not be irradiated with photons without producing unacceptable damage to the normal tissues nearby. Indeed, the proposed method identifies in the planning stage the patients from which suboptimal results could be obtained from radiation therapy with low LET radiation. These patients could therefore be directed rather early to alternative methods, such as light ion therapy, the use of radiosensitisers or other practical methods to overcome tumour hypoxia than dose escalation with low LET irradiation. This would result in increased benefit for both the patients that could thus receive an optimal treatment from the very beginning and for the oncology departments as they could use their resources directly for the most efficient treatment method.

Individualisation of the treatment based on the non-linear uptake of PET tracers for tumour hypoxia could therefore lead to improved treatment outcome while creating the premises for Intensity and Radiation Quality Modulated radiation therapy optimised on biological bases.

Design of an Open PET System with Therapeutic & Stereoscopic Phase-Contrast X-ray Capabilities

Anders Brahme

Medical Radiation Physics, Department of Oncology-Pathology, Karolinska Institutet

Background

The fast development of intensity, energy and radiation quality modulated radiation therapy (IMRT and QMRT) during the last two decades with photon and electron beams has resulted in a considerable improvement of radiation therapy, particularly when combined with radiobiologically based treatment optimization techniques. This development and the recent development of advanced tumor diagnostics based on PET-CT imaging of tumor clonogen density and hypoxia opens the field for new powerful radiobiologically based treatment optimization methods. The ultimate step is to use the unique radiobiological and dose distributional advantages of light ion beams for truly optimized bio-effect planning where the integral 3-dimensional dose delivery and tumor cell survival can be monitored early on in the treatment by PET-CT imaging and be corrected by adaptive therapy optimization methods.

Method

BIologically Optimized in vivo predictive Assay based adaptive Radiation Therapy (BIOART) is really the ultimate way to perform high precision radiation therapy using checkpoints on the integral dose delivery and the tumor response, and based on this information, performing compensating corrections of the dose delivery. By using biologically optimized scanned high-energy photon or ion beams it is possible to measure in vivo the 3 dimensional (3D) dose delivery using either the same PET-CT camera that was initially used for diagnosing the tumor spread or a dedicated system integrated with the treatment unit (cf the Fig). With the open PET design it is not only possible to integrate a scanned beam treatment unit but also to include a 3D or rather a 4D (including time) diagnostic system using high contrast X-rays based on phase contrast stereoscopic imaging (PSI). This technique will allow 4D imaging without the need for a large number of projections (around 300-400 with CT) and thus eliminates the need for rotation during 4D imaging and therapy. Generally the increased contrast makes two projections at 2-20 degrees angle enough to get sufficient 4D imaging information as shown in the image.

Result

This method thus opens up the door for truly 3D biologically optimized adaptive radiation therapy where the measured dose delivery to the true target tissues can be used to fine adjust the incoming beams so that possible early errors in the integral therapy process are practically eliminated towards the end of the treatment even when dynamic motions are present in the target volume. Interestingly enough all major error sources can be corrected for in this way such as organ motions, treatment planning errors, patient setup and tumor responsiveness errors, as well as dose delivery problems due to gantry, multileaf or scanning beam errors. When it is possible to quantify the surviving tumor clonogen density during the first week or so of therapy, this information can be used to account for uncertainties in the biological responsiveness of the tumor and really cover all clinical uncertainties at the same time as more accurate dose response data can be derived from the treatment. With the photonuclear or nuclear-nuclear reactions the response of the PET-CT or PET- PSI camera is related to the truly delivered integral dose with correct

temporal averaging, and thus if only small errors are seen, it is sufficient to adjust the last few treatment fractions. Thus, when using PET based tumor response monitoring, it is even possible to account for the uncertainty in known historical biological response for the disease of the patient and perform a truly optimized radiation treatment.

Conclusions

Using the recently available biologically based treatment optimization algorithms it is possible to improve the treatment outcome for advanced tumors by as much 10 – 40%. The adaptive BIOART process based both on 4D tumor cell survival and dose delivery monitoring has the potential of accurate tumor eradication, not least with 4D geometric Bragg peak scanning and intensity and radiation quality modulated ion beam dose delivery. There is no doubt that the future of radiation therapy is very promising and gradually more and more patients may not even need advanced surgery but instead could be cured by photon and electron IMRT and biologically optimized radiation quality modulated light ion therapy, QMRT as discussed previously, where the high LET-RBE Bragg peak is solely placed in the gross tumor volume.

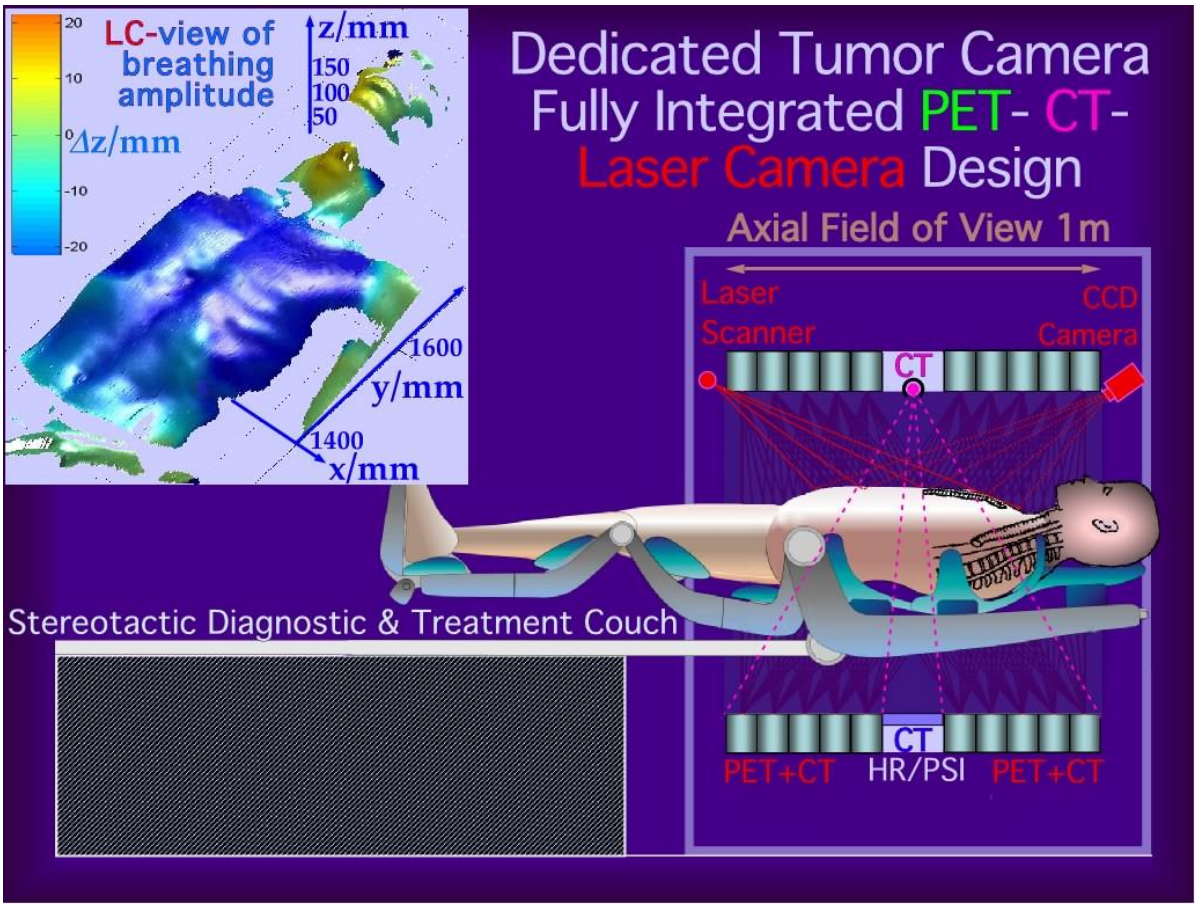

Cross-section through the PET-PSI imaging side of the proposed system with two dedicated high-resolution PSI detectors in the open region in the lower open part of the detector. Perpendicular to this horizontal cut is the therapeutic direction where the Carbon 11 beam can be used at the same time as the phase contrast X-rays are imaging the tumor region in 4D and the PET camera is imaging the therapeutic dose delivery also in 3D + time. When the beam is off the indicated narrow focus X-ray source can be rotated around the patient to make cone beam CT with the same detectors as used for the PET. The 4D Laser Camera will allow full correction for motion artifacts both during PET-PSI imaging and therapy.

Production of clinically useful positron emitter beams during carbon ion deceleration

M Lazzeroni and A Brahme
Division of Medical Radiation Physics, Department of Oncology-Pathology, Karolinska Institutet, Stockholm, Sweden

E-mail: Marta.Lazzeroni@ki.se

Abstract

The accurate monitoring of the dose delivery both to the tumour and surrounding normal tissues in the patient is one of the most challenging issues in external beam radiation therapy. In case of light ion beams this is particularly important due not only to their sharp depth-dose profile and the uncertainty of the stopping powers, but also to their high relative biological effectiveness at the end of the range (**1**,**2**). The use of PET or PET-CT imaging techniques in synergy with therapeutic positron emitter beams (e.g. ^{11}C) offers one of the best clinical solutions to this problem (**3-6**). However, so far the use of positron emitter beams has been mainly limited due to their low production efficiency. The purpose of the present study is therefore to investigate the choice of the optimal decelerating target material in order to maximize the production of a ^{11}C positron emitter beam.

The Monte Carlo code SHIELD-HIT07 (**7**,**8**) was used in order to evaluate the production of high energy ^{11}C fragments generated by the interaction of a primary monoenergetic ^{12}C beam with a cylindrical phantom of 300 cm in length and 10 cm in radius, divided in 1 cm thick slices. A quite wide range of target materials was considered.

Results describing the ^{11}C fluence build-up and mean energy variation with the depth in the phantom show that high levels in the fluence of ^{11}C fragments are reached in compounds where the fraction by weight of Hydrogen atoms is high, being the highest in Liquid Hydrogen . Furthermore, an analysis of the fluence build-up as a function of the mean energy of the secondary ^{11}C beam and correspondent range in a Water phantom was determined. Finally, it has been demonstrated that a sufficient intensity of the ^{11}C beam can be achieved if the primary ^{12}C beam intensity can be increased 10-20 fold over what is needed for carbon therapy.

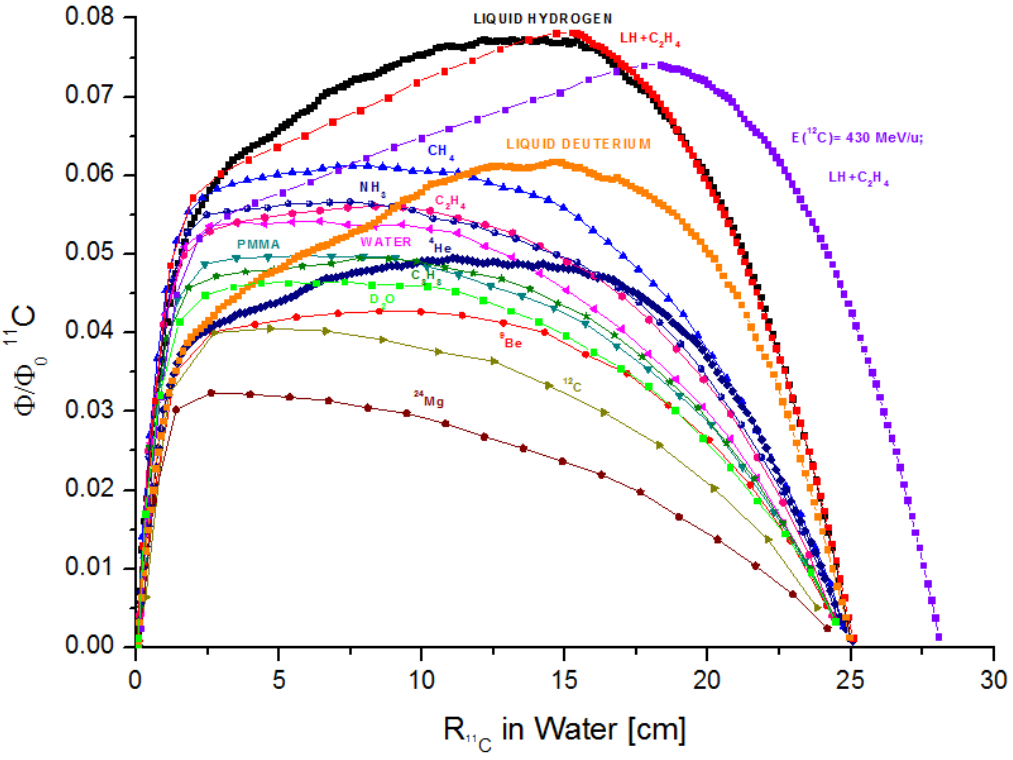

Fig. 1 *Fluence of ^{11}C ions normalized to the production at the surface level as a function of the range of the beam in a water phantom.*

References:

1. Brahme A. 1982 Physical and biologic aspects on the optimum choice of radiation modality, *Acta Radiol Oncol.* **21**(6),469-79.
2. Tsujii H. et al., 2008 Clinical advantages of carbon-ion radiotherapy *New Journal of Physics* **10** 075009 (16pp)
3. Tomitani T. et al., 2003 Washout studies of ^{11}C in rabbit thigh muscle implanted by secondary beams of HIMAC *Phys. Med. Biol.* **48** 875-889
4. Urakabe E. et al., 2001 Spot scanning using radioactive ^{11}C beams for heavy-ion radiotherapy *Jpn. J. Appl. Phys.* **40** 2540-2548
5. Kanazawa M. et al., 2002 Application of an RI-beam for cancer therapy: In-vivo verification of the ion-beam range by means of positron imaging *Nuclear Physics A* **701** 244c-252c
6. Iseki Y. et al., 2004 Range verification system using positron emitting beams for heavy-ion radiotherapy *Phys. Med. Biol.* **49** 3179-3195
7. Gudowska I., Sobolevsky N., Andreo P., Belkic D. and Brahme A. 2004 Ion beam transport in tissue-like media using the Monte Carlo code SHIELD-HIT *Phys. Med. Biol.* **49** 1933-1958
8. Geithner O., Andreo P., Sobolevsky N., Hartmann G. and Jäkel O. 2006 Calculation of stopping power ratios for carbon ion Dosimetry *Phys. Med. Biol.* **51** 2279-2292

Direct and Indirect Actions to High-LET Radiations

Ryoichi Hirayama[1], Yoshitaka Matsumoto[1], Yuki Kase[1,2], Miho Noguchi[3], Nobuhiro Takase[1,4,5], Akiko Uzawa[1], Atsushi Ito[4], Naruhiro Matsufuji[1], Koichi Ando[6], Ryuichi Okayasu[1], Yoshiya Furusawa[1]

[1]*Research Center for Charged Particle Therapy, National Institute of Radiological Sciences, Chiba, Japan*
[2]*Proton Therapy Division, Shizuoka Cancer Center Research Institute, Nagaizumi, Japan*
[3]*Advanced Science Research Center, Japan Atomic Energy Agency, Tokai, Japan*
[4]*School of Engineering, Tokai University, Hiratsuka, Japan*
[5]*Therapy-Level Dose Calibration Center, Association for Nuclear Technology in Medicine, Chiba, Japan*
[6]*Heavy Ion Medical Center, Gunma University, Maebashi, Japan*
Corresponding Author: Ryoichi Hirayama, e-mail address: hirayama@nirs.go.jp

Abstract

The biological effects of radiation originate principally from damages to DNA. DNA damage by photon radiation as well as heavy ions, is induced by a combination of direct and indirect actions. The contribution of indirect actions in cell killing can be estimated from the maximum degree of protection by dimethylsulfoxide (DMSO), which suppresses OH radical-mediated indirect action, without affecting the direct action. Exponentially growing Chinese hamster V79 cells were exposed to high LET radiation of 20 to 2106 keV/µm in the presence or absence of DMSO, and their survival was determined using a colony formation assay. The contribution of indirect action to cell killing decreased with increasing LET. However, the contribution did not reach zero even at very high LETs, and was estimated to be 32% at an LET of 2106 keV/µm. Therefore, even though the radiochemically estimated *G* value of OH radicals was nearly zero at an LET of 2000 keV/µm, indirect action by OH radicals substantially contributed to the biological effects of high LET radiations. The RBE determined at a survival level of 10% increased with LET, reaching a maximum value of 3 at around 100 keV/µm, and decreased thereafter. When the RBE was estimated separately for direct action and indirect action, the RBE resulting from indirect action had a peak at around 70 keV/µm with a gradual decrease with increasing LET. In contrast, the RBE of direct action peaked at around 200 keV/µm. Furthermore, the peak value for direct action (~6) was much higher than for indirect action (~2.5). Therefore, the direct action contributes more to the high RBE of high LET radiations than indirect action.

Introduction

Indirect action due to water-derived radicals plays an important role in the induction of biological effects by low linear energy transfer (LET) radiation including X-rays and γ-rays. Roots and Okada reported that various alcohols and SH compounds protect mammalian cells against radiation-induced of single-strand breaks in DNA [1]. They concluded that 71% of all DNA damage is induced by indirect action mediated by hydroxyl radicals (OH radical), and that OH radicals are the most important of all other radicals such as H and e_{aq}^-. They also showed that 65% of the radiation-induced cell killing of mouse L5178Y cells is mediated by indirect action conferred by OH radicals [2]. Ashwood-Smith demonstrated that dimethylsulfoxide (DMSO) provides 70% protection against X-ray-induced lethality in mice [3].

Chapman et al. indicated that indirect actions of radiation also contribute to cell killing even for high LET radiation. The extent of protection by 2 M DMSO against carbon ions with an LET of 180 keV/µm was 50% [4]. Roots et al. analyzed the contribution of indirect action in cell killing of Chinese hamster ovary cells for the LETs ranging from 16 to 682 keV/µm, using 2 M ethylene glycol as an OH radical scavenger [5]. They estimated the contribution of indirect action to be approximately 20-25% at an LET of 682 keV/µm. Ito et al. estimated the contribution of indirect action to cell killing for LETs up to 440 keV/µm using the DMSO method proposed by

Shinohara et al. in which the contribution of indirect action was estimated from the degree of protection (DP) at the infinite DMSO concentration obtained by the extrapolation of data points [6, 7]. The above reports demonstrated that although the contribution of indirect action decreases with increasing LET, it still remains a major factor even for a high LET of 682 keV/μm.

Although these reports suggested that indirect action plays a major role in the cell killing induced by high LET radiation, radiochemical analysis showed that the G value of OH radicals in aqueous solution is almost zero at LETs above 1000 keV/μm [8-10]. Therefore, the contribution of indirect action to cell killing for LETs above 1000 keV/μm needs to be examined in order to reconcile the discrepancy between biological studies and the radiochemical analyses.

In this report, we estimated the contribution of indirect action to cell killing by the DMSO method for very high LET of up to 2106 keV/μm. Furthermore, the LET-RBE (relative biologic effectiveness) relationship was assessed separately for direct and indirect actions of radiation. In addition to our experimental results, we also discuss the contribution and the mechanisms of direct and indirect actions of high LET radiation to the RBE.

Methods and Materials

1. Cells and irradiation

Chinese hamster V79 cells were grown in Ham's F12 medium supplemented with 10% fetal bovine serum and antibiotics (100 U/ml penicillin and 100 μg/ml streptomycin) under humidified air with 5% CO_2 at 37˚C. Cultured cells were harvested with 0.2% trypsin and seeded onto 35 mm (Φ) culture dishes for oxic condition and 38 mm (Φ) glass dishes for hypoxic condition at a concentration of 2-4 × 10^5 cells per dish. The cells were cultured for 24 hours prior to irradiation. X-irradiation was done using an X-ray generator (SHIMADZU, PANTAC HF-320S) operating at 200 kVp and 20 mA with a filter of 0.5 mm aluminum and 0.5 mm copper at a dose rate of 3.5 Gy/min. Exposure of samples was done at a room temperature. Helium, carbon and iron ions with a dose-averaged LET of 2.2, 20 and 200 keV/μm were provided by 150, 290 and 500 MeV/nucleon beams, respectively by the Heavy-ion Medical Accelerator in Chiba (HIMAC) at the National Institute of Radiological Sciences (NIRS). Iron ions with LETs of 797, 1298 and 2106 keV/μm were provided by 90 MeV/nucleon beams from the RIKEN Ring Cyclotron (RRC) at the Institute of Physical and Chemical Research (RIKEN). The energy of these beams was modulated by inserting absorbing materials (PMMA for HIMAC, Al for RRC) to obtain appropriate LETs. The dose-averaged LET included the contribution of fragmented particles.

DMSO has been used to scavenge radiation-induced free radical species, in particular OH radical. Cells growing on plastic dishes were covered with 2 ml of medium with DMSO at final concentrations of 0-1.0 M and were equilibrated at room temperature for 1 hour. The medium was discarded prior to irradiation, and then dishes were covered by a polyvinyl chloride film to prevent drying, and the dishes were irradiated from the cellular side. In the case of hypoxic irradiation, the cells were cultured with 0.9 ml of medium alone or with medium containing different concentrations of DMSO at molarities of 0-1.0 M, and then transferred into the irradiation chamber. The chamber was flushed for more than 1 hour just before irradiation with 1000 ml/min of 95% pure N_2 and 5% pure CO_2 that had passed through a bubbling bottle to maintain high humidity. Oxygen levels in the chamber of hypoxic samples were less than 0.2 mmHg as detected using an oxygen electrode to measure medium pO_2. An oxygen enhancement ratio (OER) obtained for mammalian cells of 2.5-3 showed that radiobiological hypoxia was routinely achieved, indicating that oxygen levels were below 0.7 mmHg (about 0.1% oxygen) [11, 12].

After irradiation, the cells were harvested by trypsinization and seeded in triplicate onto 60 mm (Φ) culture dishes at densities that would give approximately 150 colonies per dish. After 7-8 days of incubation, the colonies were fixed with 10% formalin and stained with 1% methylene blue in water. Colonies consisting of more than 50 surviving cells were scored.

2. Calculation of the protectable fraction by DMSO (DMSO method)

The protectable fraction was defined as a maximum protection level by an infinite concentration of DMSO. This method of calculation was originally proposed by Shinohara et al. [7]. Briefly, the maximum protection was calculated by the extrapolation of reciprocals of survival fractions over those of experimental DMSO concentrations. For the calculation of the degree of protection (DP) for helium ions, we used the data points beyond the shoulder region of survival curves where the curves decreased exponentially. DP was defined by equation (1), and the regression curve was drawn in the plots of DP as a function of the DMSO concentration

$$DP = (\ln SF_0 - \ln SF_x)/(\ln SF_0) \quad (1)$$

where SF_0 and SF_x are surviving fractions at 0 and x M of DMSO, respectively. The DP is expressed as the increase of the surviving fraction in the presence of DMSO normalized by the surviving fraction in the absence of DMSO. A regression line was also drawn in the graphs of the reciprocals of DP plotted against those of the DMSO concentration, as shown in equation (2). The maximum DP can be obtained as the value at the point of intersection of the regression at the infinite concentration of DMSO as shown in the equation (2).

$$1/DP = k\cdot(1/x) + y_\infty;$$
$$y_\infty = 1/DP;(x \rightarrow \infty, 1/x = 0) \quad (2)$$

where y_∞ and k are the inverse of DP at an infinite concentration and slope of the regression line of DP, respectively. The k-value means $[D + I]I^{-1}k_S[S]k_D^{-1}$ (M), where k_S, k_D and $[S]$ were defined as the reaction constant of OH radicals with target cellular molecules ($M^{-1}s^{-1}$), that of OH radical with DMSO and the concentration of the cellular reaction site (target cellular molecules) responsible for cell killing (M), respectively [6]. D and I are the components of direct and indirect action in the "effective dose" contributing to cell inactivation. The portion of indirect action was calculated according to equation (3)

$$IA = 1/y_\infty \times 100 \quad (3)$$

where IA is the contribution of indirect action. IA is expressed the maximum protectable fraction by an infinite concentration of DMSO.

Results and Discussion

1. Contribution of indirect action of low and high LET radiation under oxic and hypoxic conditions

The contributions of OH radical-mediated indirect action for low LET radiations under oxic and hypoxic conditions were 44-65% (average 56%) and 9-30% (average 19%), respectively (Table 1 and 2). Other studies [6, 7, 13-15], however, made estimates of 63-93% (average 80%) in the presence of oxygen and 52% in its absence when the DMSO method was used (also listed in Tables 1 and 2 for comparison). The maximum contributions of indirect action for high LET radiation by the DMSO method were higher than that by fixed concentrations of a 2 M scavenger at the same LET value (Table 2). Thus, the estimate is sensitive to the DMSO concentration and the use of the infinite concentration is likely to be an accurate estimate for both low and high LET radiation values, validating the use of the DMSO method.

We observed that the contribution of indirect action to cell killing decreased with increasing LET (Table 2). However, indirect action still played a significant role in cell killing and contributed to around 30% of cell killing even at an LET of 2106 keV/μm. In contrast, radiolysis experiments using a radical scavenger yielded G value of OH radicals of almost zero at LETs around 1000 keV/μm [8-10]. One of the reasons for the non-zero contribution of indirect actions in our study is that radiation from the beams was contaminated by low LET components coming from fragmentation products of primary ions, and these fragments constituted a significant fraction of the radiation dose and number for heavy ion beams [16, 17].

Another reason for the difference between the analysis of radiolysis and our present experiments is that the former study used a chemically homogeneous aerated solution, and the concentration of the target molecule was relatively low. In contrast, the concentration of target molecules such as DNA in the cellular nucleus is very

high, with highly heterogeneous distributions in the nucleus. These differences may have contributed to the larger fraction of protection by DMSO in the previous studies.

The track structure is important in cell killing. According to Schöpfer et al., the level of the oxygen effect for cell killing on yeast cells decreases with increasing LET. Interestingly, the effect reappears at the very high LET region of energy above 4.4 MeV/u [18]. The track of the ion path is composed of a core with high density ionizations, and a penumbra with scattered δ-rays. The penumbra of very high LET particles with energy of 4.4 MeV/u is composed of δ-rays reaching a range of approximately 1 μm. The contribution of indirect action is thought to be significant in this penumbra range and this is particularly so when the LET becomes very high. Thus, the 30% contribution of indirect action in cell killing seems to be reasonable for iron ions (LET of 2106 keV/μm) with a specific energy of 16 MeV/nucleon on the target.

Table 1. The contribution of indirect action to cell killing of photon radiations and electron beam

Cell line	Radiation	OH contribution %		Scavenger	(*M*)	Reference
		Oxic	Hypoxic			
V79	250 kV X-rays	62	30	DMSO	3.5	Chapman et al.,(1973)[28]
L5178Y	1 MV X-rays	65		Ethylene glycol	2.0	Roots and Okada (1975)[2]
V79	4.3 MV electrons	57	16	DMSO	2.0	Millar et al.,(1981)[29]
V79	4.3 MV electrons	54	21	Glycerol	2.0	Millar et al.,(1981)[29]
HA1	225 kV X-rays	55	20	Ethylene glycol	2.0	Roots et al.,(1982)[30]
CHO	270 kV X-rays	44	9	DMSO	2.0	Skov(1984)[31]
V79	200 kV X-rays	59	18	DMSO	2.0	Sapora et al.,(1991)[32]
		Ave 56	Ave 19			
HeLa	150 kV X-rays	93		Cysteamine	∞	Shinohara et al.,(1996)[7]
HeLa	150 kV X-rays	73		DMSO	∞	Shinohara et al., (1996)[7]
HeLa	^{60}Co γ-rays	89		Cysteamine	∞	Shinohara et al., (1996)[7]
HeLa	^{60}Co γ-rays	88		DMSO	∞	Shinohara et al., (1996)[7]
HL-60	4 MV X-rays	85		DMSO	∞	Ito et al.,(2006)[6]
HeLa	^{60}Co γ-rays	89		DMSO	∞	Ito et al., (2006)[6]
HeLa	^{137}Cs γ-rays	87		DMSO	∞	Ito et al., (2006)[6]
HeLa	80 kV X-rays	72		DMSO	∞	Ito et al., (2006)[6]
HeLa	12.4 kV X-rays	63		DMSO	∞	Ito et al., (2006)[6]
L5178Y	^{137}Cs γ-rays	68		DMSO	∞	Miyazaki et al., (2007)[13]
V79	200 kV X-rays	76		DMSO	∞	Hirayama et al., (2009)[14]
		Ave 80				

Table 2. The contribution of indirect action to cell killing of heavy ions

Cell line	Radiation / LET	OH contribution %		Scavenger	(*M*)	Reference
		Oxic	Hypoxic			
HA1	Helium / 16 keV/μm	35		EG*	2.0	Roots et al.,(1985)[5]
HA1	Carbon / 17.8 keV/μm	44		EG	2.0	Roots et al.,(1985)[5]
HL-60	Carbon / 20 keV/μm	92		DMSO	∞	Ito et al(2006)[6]
V79	Carbon / 20 keV/μm	65		DMSO	∞	Hirayama et al.,(2009)[14]
HA1	Neon / 41 keV/μm	50		EG	2.0	Roots et al.,(1985)[5]
HA1	Carbon / 52.1 keV/μm	42		EG	2.0	Roots et al.,(1985)[5]
HA1	Lithium / 52.5 keV/μm	25		EG	2.0	Roots et al.,(1985)[5]
HL-60	Carbon / 60 keV/μm	84		DMSO	∞	Ito et al(2006)[6]
HL-60	Carbon / 80 keV/μm	79		DMSO	∞	Ito et al(2006)[6]
HA1	Carbon / 95.3 keV/μm	38		EG	2.0	Roots et al.,(1985)[5]
HL-60	Silicon / 100 keV/μm	71		DMSO	∞	Ito et al(2006)[6]
HA1	Neon / 113.5 keV/μm	42		EG	2.0	Roots et al.,(1985)[5]
HA1	Argon / 114.3 keV/μm	43		EG	2.0	Roots et al.,(1985)[5]
HA1	Carbon / 129 keV/μm	25		EG	2.0	Roots et al.,(1985)[5]
V79	Carbon / 180 keV/μm	56		DMSO	2.0	Chapman et al.,(1979)[4]
HA1	Neon / 184.5 keV/μm	28		EG	2.0	Roots et al.,(1985)[5]
HA1	Carbon / 186 keV/μm	25		EG	2.0	Roots et al.,(1985)[5]
V79	Iron / 200 keV/μm	50		DMSO	∞	Hirayama et al.,(2009)[14]
HL-60	Silicon / 200 keV/μm	66		DMSO	∞	Ito et al(2006)[6]
HL-60	Silicon / 300 keV/μm	65		DMSO	∞	Ito et al(2006)[6]
HA1	Argon / 305.7 keV/μm	25		EG	2.0	Roots et al.,(1985)[5]
HL-60	Iron / 440 keV/μm	62		DMSO	∞	Ito et al(2006)[6]
HA1	Argon / 491.1 keV/μm	25		EG	2.0	Roots et al.,(1985)[5]
HA1	Neon / 682 keV/μm	25		EG	2.0	Roots et al.,(1985)[5]
V79	Iron / 797 keV/μm	52		DMSO	∞	Hirayama et al.,(2009)[14]
V79	Iron / 1298 keV/μm	39		DMSO	∞	Hirayama et al.,(2009)[14]
V79	Iron / 2106 keV/μm	32		DMSO	∞	Hirayama et al.,(2009)[14]
V79	Helium / 2.2 keV/μm		52	DMSO	∞	Hirayama et al.,(2009)[15]

*EG:Ethylene glycol

2. RBEs of cell killing induced by direct and indirect actions

We have estimated RBEs of cell killing separately for direct action as RBE_D and for indirect action as RBE_I. RBE_D increased with increasing LET, and had a peak value of around 6 at 200 keV/μm. RBE_I peaked at 70 keV/μm, but with a value of around 2.5. Thus, direct action of heavy ion beams gives a higher RBE for cell killing than indirect action. The high LET ion has a track of ionization with core and penumbra. The core is generated mainly by a direct hit of high energy ions, while the penumbra is gnerated the scattering δ-rays. Thus, it can clearly be envisaged that the core region of the track cannot be protected by radical scavengers such as DMSO and gives the DNA damage with multiple local lesions. In contrast, the effect of scattering δ-rays can be efficiently protected by DMSO, and the DNA damage produced in the penumbra region is less complex than that

by the core. DNA damages with multiple lesions are called clustered damage as proposed by Goodhead and others, and this damage is known to be more refractory to repair and more efficient in cell killing [19-21]. Indeed, heavy ion beams were shown to generate DNA damages with more severe biological effects [22-27].

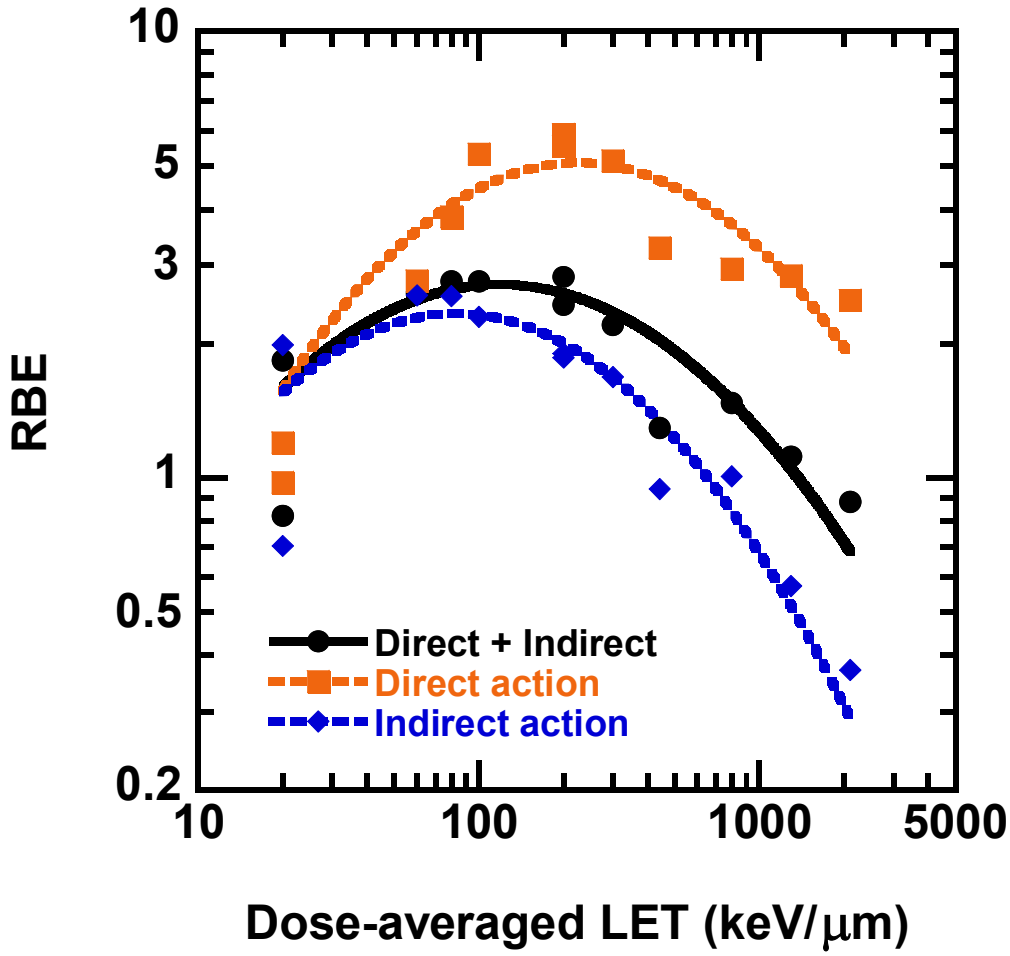

Fig. 1 The LET-RBE relationships for direct and indirect actions of radiation. RBEs were calculated from the 10% survival data. [6, 14].

Conclusions

The results from this report indicate that indirect action by OH radicals contributes at least 30% or the cell killing effect at the very high LET region where radiochemical analysis indicated that the *G* value of OH radicals was zero. In addition, direct action of heavy ions is the major reason for the higher RBE of high LET radiation, suggesting a new therapeutic application of particle radiation with ultra-high RBEs.

Acknowledgements

We thank Drs. Ohtsura Niwa (NIRS), Jürgen Kiefer (Giessen Univ.), Kunio Shinohara (Waseda Univ.), Hiroshi Ohara (NIRS), Gen Kobashi (NIRS) and Shin-ichi Yamashita (JAEA) for helpful discussions. We also thank all staff members in the Heavy-Ion Radiobiology Research Group and the synchrotron crews at NIRS and the cyclotron crews at RIKEN for providing steady beams during the experiments. This work was partly supported by the Research Project with Heavy Ions at NIRS-HIMAC (11B424, 15B248, 18B468, 21B468) and RIKEN-RRC. This work was also supported by the Japan Society for the Promotion of Science (JSPS) Grant-in-Aid for Young Scientists (B) [KAKENHI (20790923)].

References

[1] Roots R, Okada S. Protection of DNA molecules of cultured mammalian cells from radiation-induced single-strand scissions by various alcohols and SH compounds. Int J Radiat Biol. 1972;21: 329-342.

[2] Roots R, Okada S. Estimation of life times and diffusion distances of radicals involved in x-ray-induced DNA strand breaks of killing of mammalian cells. Radiat Res. 1975;64: 306-320.

[3] Ashwood-Smith MJ. The radioprotective action of dimethyl sulphoxide and various other sulphoxides. Int J Radiat Biol. 1961;3: 41-48.

[4] Chapman JD, Doern SD, Reuvers AP, et al. Radioprotection by DMSO of mammalian cells exposed to X-rays and to heavy charged-particle beams. Radiat Environ Biophys. 1979; 16: 29-41.

[5] Roots R, Chatterjee A, Chang P, et al Characterization of hydroxyl radical-induced damage after sparsely and densely ionizing irradiation. Int J Radiat Biol. 1985;47: 157-166.

[6] Ito A, Nakano H, Kusano Y, et al. Contribution of indirect action to radiation-induced mammalian cell inactivation: dependence on photon energy and heavy-ion LET. Radiat Res. 2006; 165:703-712.

[7] Shinohara K, Nakano H, Ohara H. Detection of Auger enhancement induced in HeLa cells labeled with iododeoxyuridine and irradiated with 150 kV x-rays--Effects of cysteamine and dimethylsulfoxide. Acta Oncol. 1996; 35:869-875.

[8] Bisby RH, Cundall RB, Sims HE, et al The inactivation of papain by high LET radiations. Int J Radiat Biol. 1984; 46:261-268.

[9] Taguchi M, Kojima T. Yield of OH radicals in water under high-density energy deposition by heavy-ion irradiation. Radiat Res. 2005;163: 455-61.

[10] Uehara S, Nikjoo H. Monte Carlo simulation of water radiolysis for low-energy charged particles. J Radiat Res. 2006;47: 69-81.

[11] Hirayama R, Furusawa Y, Fukawa T, et al Repair kinetics of DNA-DSB induced by X-rays or carbon ions under oxic and hypoxic conditions. J Radiat Res. 2005;46: 325-332.

[12] Sprong D, Janssen HL, Vens C, et al Resistance of hypoxic cells to ionizing radiation is influenced by homologous recombination status. Int J Radiat Oncol Biol Phys. 2006;64: 562-572.

[13] Miyazaki N, Nakano H, Ito A, et al Different contributions of the indirect effects of gamma-rays on the cytotoxicity in M10 and XRCC4 transfected M10 cells. Radiat Environ Biophys. 2007;46: 237-246.

[14] Hirayama R, Ito A, Tomita M, et al. Contributions of Direct and Indirect Actions in Cell Killing by High-LET Radiations. Radiat Res. 2009;171: 212-218.

[15] Hirayama R, Matsumoto Y, Kase Y, et al. Radioprotection by DMSO in Nitrogen Saturated Mammalian Cells Exposed to Helium Ion Beams. Radiat Phys Chem. 2009;78: 1175-1178.

[16] Matsufuji N, Fukumura A, Komori M, et al Influence of fragment reaction of relativistic heavy charged particles on heavy-ion radiotherapy. Phys Med Biol. 2003;48: 1605-1623.

[17] Matsufuji N, Komori M, Sasaki H, et al. Spatial fragment distribution from a therapeutic pencil-like carbon beam in water. Phys Med Biol. 2005;50: 3393-3403.

[18] Schöpfer F, Schneider E, Rase S, et al. Heavy ion effects on yeast cells: reappearance of the oxygen effect with very high LET. Int J Radiat Biol. 1984;46: 305-316.

[19] Goodhead DT. Initial events in the cellular effects of ionizing radiations: clustered damage in DNA. Int J Radiat Biol. 1994;65: 7-17.

[20] Nikjoo H, O'Neill P, Goodhead DT, et al. Computational modelling of low-energy electron-induced DNA damage by early physical and chemical events. Int J Radiat Biol. 1997;71: 467-483.

[21] Sutherland BM, Bennett PV, Sidorkina O, et al. Clustered DNA damages induced in isolated DNA and in human cells by low doses of ionizing radiation. Proc Natl Acad Sci USA. 2000;97: 103-108.

[22] Durante M, Furusawa Y, George K, et al. Rejoining and misrejoining of radiation-induced chromatin breaks. IV. Charged particles. Radiat Res. 1998;149: 446-454.

[23] Gudowska-Nowak E, Nasonova E, et al. Chromosome fragmentation after irradiation with C ions. Radiother Oncol. 2004;73 Suppl 2: S123-126.

[24] Anderson RM, Stevens DL, Sumption ND, et al. Effect of linear energy transfer (LET) on the complexity of alpha-particle-induced chromosome aberrations in human CD34+ cells. Radiat Res. 2007;167: 541-550.

[25] Terato H, Tanaka R, Nakaarai Y, et al. Quantitative analysis of isolated and clustered DNA damage induced by gamma-rays, carbon ion beams, and iron ion beams. J Radiat Res. 2008;49: 133-46.

[26] Asaithamby A, Uematsu N, Chatterjee A, et al. Repair of HZE-Particle-Induced DNA Double-Strand Breaks in Normal Human Fibroblasts. Radiat Res. 2008;169: 437-446.

[27] Hada M, Georgakilas AG. Formation of Clustered DNA Damage after High-LET Irradiation: A Review. J Radiat Res. 2008;49: 203-210.

[28] Chapman JD, Reuvers AP, Borsa J, et al Chemical radioprotection and radiosensitization of mammalian cells growing in vitro. Radiat Res. 1973;56: 291-306.

[29] Millar BC, Sapora O, Fielden EM, et al. The application of rapid-lysis techniques in radiobiology. IV. The effect of glycerol and DMSO on Chinese hamster cell survival and DNA single-strand break production. Radiat Res. 1981;86: 506-514.

[30] Roots R, Chatterjee A, Blakely E, et al. Radiation responses in air-, nitrous oxide-, and nitrogen-saturated mammalian cells. Radiat Res. 1982;92: 245-254.

[31] Skov KA. The contribution of hydroxyl radical to radiosensitization: a study of DNA damage. Radiat Res. 1984;99: 502-510.

[32] Sapora O, Barone F, Belli M, et al. Relationships between cell killing, mutation induction and DNA damage in X-irradiated V79 cells: the influence of oxygen and DMSO. Int J Radiat Biol. 1991;60: 467-482.

Tumor Metastasis Exposed to High-LET Radiations

Yoshitaka Matsumoto[1], Akiko Uzawa[1], Ryoichi Hirayama[1], Sachiko Koike[1], Ryuichi Okayasu[1], Koichi Ando[2], Shin-ichiro Masunaga[3], and Yoshiya Furusawa[1]

[1]Research Center for Charged Particle Therapy, National Institute of Radiological Sciences, Chiba, Japan
[2]Heavy Ion Medical Center, Gunma University
[3]Particle Radiation Oncology Research Center, Research Reactor Institute, Kyoto University
[3]Heavy Ion Medical Center, Gunma University
Corresponding Author: Yoshitaka Matsumoto, e-mail address: y_matsu@nirs.go.jp

Abstract

Purpose: The aim of this study is to clarify the effect of carbon ion beams (C-ion) on metastatic potential of melanoma *in vitro* and *in vivo*.

Materials and Methods: A highly metastatic mouse malignant melanoma cell line B16/BL6 were maintained in RPMI-1640 medium supplemented with 10% FBS and antibiotics. [*in vitro*] Samples were prepared 2 days before and then irradiated with C-ions or X-rays. Surviving fractions were obtained using colony formation assay. Migration and invasion activity as metastatic potentials of the cells were examined using the Boyden-chamber method and the Matrigel invasion assay. [*in vivo*] The cells were implanted in right-leg of C57BL/6J mice at $1x10^6$ cells/mouse 9-10 days before irradiation. Tumors were irradiated at the center of 6cm-SOBP of C-ions, or γ-rays. Radiosensitivity for whole tumor was obtained by the tumor growth delay method, and that for individual cell in a tumor was obtained by an in vivo-in vitro assay. The metastatic effects were analyzed with the spontaneous lung metastasis model. The dose averaged LET values of carbon beams were approximately 50 keV/μm.

Results: [*in vitro*] Survival curves showed higher cytotoxic effects of C-ions compared with X-rays, and the RBE values were 1.96. The potential of migration and invasion were suppressed by C-ions at all dose points (0.50 to 8.0 Gy) tested, however it was enhanced by X-rays at low dose points (0.50 and 1.0 Gy) than non-irradiated controls. The RBE values obtained from migration and invasion test were higher than that from cell killing. [*in vivo*] C-ions significantly suppressed the tumor growth, and the RBE was 2.64. The numbers of lung metastatic nodules after tumor-irradiations decreased with the dose, and C-ions were more effective compared with γ-rays. The metastatic potentials of survived cells in a tumor after irradiation was analyzed with the number of metastatic lung colony from implanted tumors and survival of irradiated and explanted cells from a tumor. Smaller number of metastasis was found for C-ions than γ-rays when the numbers were compared with biological equivalent dose.

Conclusion: It might suggest that C-ion inhibit metastasis at radiotherapy compared with low-LET photons.

Contents in this proceeding was submitted for a journal.

Introduction

Heavy-ion beams with high linear energy transfer (LET) have advantages of good dose distribution for tumor and increasing relative biological effectiveness (RBE) with depth [(1)]. The Heavy Ion Medical Accelerator in Chiba (HIMAC) was constructed at the National Institute of Radiological Sciences (NIRS). Clinical trials have been demonstrated using carbon-ion beams for different cancers, lung cancer, bone & soft tissue sarcomas, hepatomas, prostate cancer, choroidal cancer, rectal cancer and head and neck cancer since July 1994 [(2, 3, 4)]. Up to February 2010, over 5000 patients have been treated including over 2500 patients subject to Advanced Medical Technology program. On the whole, carbon-ion therapy for various tumor sites has conducted successfully [(2, 5)]. However, malignant melanomas or osteosarcomas could not achieve satisfactory 5-year survival in contrast of very high 5-year local control as examples. Malignant melanoma showed high local control of about 75%, whereas the overall survival was

not enough and was about 36% at 5-years [6]. A most important reason of these clinical results is distant metastasis. Metastasis, the biggest threat to survival for patients with solid tumors. It is an important subject to control tumor distant metastasis for heavy-ion radiotherapy in especial.

Ionizing radiation has been established as a highly effective modality used in the local control of tumor. However, several papers have reported that photon beam irradiation, X-rays or γ-rays enhanced metastatic processes of malignant tumor cells at sub-lethal dose [7-11]. Particle beams, carbon-ion beams (C-ions) are new modality of cancer therapy. C-ions have been shown more effective than conventional photon for cytotoxic effects [12-14]. Several studies have been reported the anti-metastatic effects of C-ions *in vitro* and *in vivo* [15-19], however the biological basic data about the exquisite effects are scarce.

In this study, we compare the effect of particle beams (C-ions) to photon beams (X-rays or γ-rays) for metastatic potential of melanoma *in vitro* and *in vivo*. Additionally, the anti-metastatic effects for local melanomas are re-analyzed depend on the surviving fraction of cells in the tumor.

Materials and Methods

Culture of cells

B16/BL6 murine melanoma cells (RIKEN Bioresource Center, Tsukuba, Japan) derived from C57BL/6 mice were maintained in RPMI-1640 medium (Sigma-Aldrich Japan Co., Tokyo, Japan) supplemented with 10% fetal bovine serum (FBS) and penicillin/streptomycin. Exponentially growing cells were seeded in flasks in CO_2 incubator at 37 ºC and cultured for about 1-2 days prior to exposure for all *in vitro* experiments.

Irradiation

X-rays were produced by a generator operated at 200 kVp and filtered with each 0.5 mm Al and Cu with a dose rate of about 0.8 Gy/min, and γ-rays were by Cs-137 with dose rate of about 1.0 Gy/min. X-rays and γ-rays data were used for the reference to compare the biological effects of C-ions on each end point *in vitro* or *in vivo* assay, respectively. C-ions provided by 290 MeV/nucleon beams at NIRS-HIMAC. Cells were irradiated with mono-peak C-ions having dose-averaged LET of 50.7 keV/μm (depth at 143.6 mmH_2O), and tumors were placed at the center of 6cm SOBP C-ions (depth at 116.4 mmH_2O, and 50 keV/μm of the dose averaged LET).

Clonogenic cell survival assay *in vitro*

Survival curves of cells were obtained by means of colony formation assay. After irradiation, cells were harvested, counted and seeded in three dishes, and then incubated for 12 days. Colonies containing more than 50 cells were counted as survivors.

Chemotaxis assay

Chemotaxis was assessed with a 24-well cell culture insert companion plate (BD Falcon, 353504) and cell culture insert (BD Falcon, 353097) with a polycarbonate filter of 8 μm pores coated with 10 μg/ml fibronectin. After irradiation, cells were washed and re-suspended in serum-free medium. The cell suspension were added to the upper well, which was placed into a lower well containing 10 % fetal bovine serum as a chemoattractant. After 6 hours of incubation, cells that had migrated to opposite surface of the filter were fixed and stained. Cell migration was quantified by counting the number of stained nuclei in five random fields with a microscope.

Matrigel Invasion assay

Invasion of tumor cells assessed by measuring the invasion of cells through transwell inserts with 8 μm pores coated with Matrigel (BD Falcon, 356230). Irradiated cells were suspended in a serum-free medium. The cell suspension was added to the upper well in a medium with 10% fetal bovine serum as a chemoattractant. The number of cells that had invaded to the opposite surface of the Matrigel-coated membrane was counted in five random fields under a microscope.

Mice and tumor

B16/BL6 cells were inoculated subcutaneously into the right hind leg of 7-10 weeks old syngeneic female C57BL/6J mice (Japan SLC, Inc., Shizuoka, Japan). Nine or ten days later, the tumors with approximately 7-8

mm in diameter, were employed for the irradiations [20]. The study protocol was reviewed and approved by the NIRS Institutional Animal Care and Use Committee (protocol no. 08-2017). Incidentally, the p53 status of B16/BL6 tumor cells is the wild [21].

Tumor growth delay assay

After irradiation for right-hind legs bearing tumors with γ-rays or C-ions on the 9 or 10 days after inoculation, the size of the tumors implanted in the right hind legs of some tumor bearing-mice was measured with calipers in three orthogonal axes 3 times a week for about 35 days. Tumor volume was calculated using the formula: $V = (\pi/6)*abc$, where *a, b* and *c* are the three orthogonal diameters.

***In vivo-in vitro* colony assay**

After irradiation, mice were sacrificed by cervical dislocation and tumors were excised under aseptic conditions. Tumors were minced with scissors, and spin and trypsinized for 20 min at 37 ºC. The suspension was then filtered through a cell strainer (BD Falcon, 352340). After counting of viable cells, appropriate numbers of viable cells were plated onto 60-mm cell culture dishes with 5 ml media and incubated for 12 days following irradiation. The colonies were then fixed with 10 % formalin solution and stained with 1 % methylene blue.

Metastasis assessment

As the lungs are the primary sites of metastatic spread from B16/BL6 tumors in the legs, the development of pulmonary metastases was also assessed. At three days after irradiation, implanted local tumors of right legs were surgically amputated to avoid dying of mice. At 25-26 days after irradiation, the tumor-bearing mice were sacrificed by cervical dislocation. Then, their lungs were fixed in Bouin's solution for an overnight. The lungs were stored in buffered 10 % formalin solution until metastatic colonies were counted. Visible lung metastatic colonies were counted under a dissection microscope [22]. Five mice were used to assess each treatment per dose, and each experiment was repeated at least three times.

Statistical analysis

To examine the differences between pairs of values, Student's *t*-test was used when variances of the two groups could be assumed to be equal. *P*-values are from two-sided tests. A *P*-value of < 0.05 was considered statistically significant.

Results

In vitro Survival curves

Dose-response of B16/BL6 cells exposed to X-rays or carbon-ion beams were fitted by the LQ equation. The curves of X-rays showed a big shoulder, and the shoulder became very small for C-ions. The relative biological effectiveness (RBE) calculated by the D_{10} values was 1.96 (Fig. 1). Surviving fractions against physical doses were plotted and fitted to survival curves using the following linear-quadratic model equation: $SF = \exp(-\alpha D-\beta D^2)$, where SF is the surviving fraction and D is the physical dose. The symbols and bars are the mean and SE calculated from at least independent three experiments for each radiations.

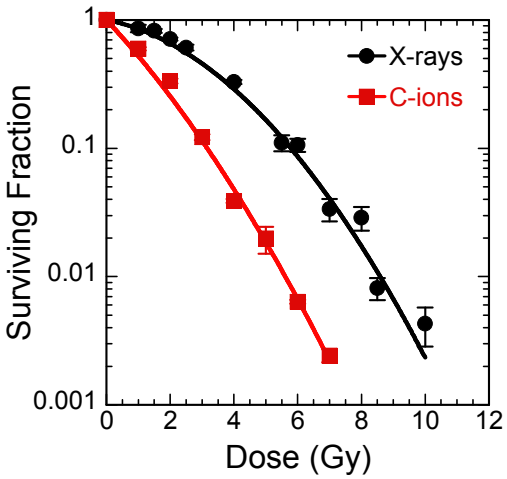

Figure 1 Clonogenic cell survival curves of B16/BL6 melanoma cells exposed to carbon-ion beams or X-rays.

Migration and invasion

To assess the effects of C-ions and X-rays on cell mortality, the migration of B16/BL6 melanoma cells after irradiation were examined using chemotaxis assay. C-ions suppressed migration of cells in a dose-dependent manner at 6 hours after irradiation (Fig. 2). On the other hand, X-rays showed the

tendency of increase the ability at very low dose region (0.5 and 1.0 Gy) after irradiation. The number of cells migrated to opposite surface of control samples was 182±28 cells. Cells were irradiated with X-rays or C-ions with the 50 keV/μm LET. Vertical axis shows number of migrated cells (percentage of control), and horizontal axis shows physical dose. Symbols and bars show mean and SD calculated from at least independent three experiments. *, $p < 0.05$; **, $p < 0.01$ (student's *t*-test, compared irradiated samples with control samples).

Invasive capacity of B16/BL6 melanoma cells after irradiation using Matrigel invasion assay. C-ions significantly reduced the invasion ability depend on the increment of dose at 24 hours after irradiation (Fig. 3). Meanwhile, X-rays promoted cell invasion even at the dose levels below 1 Gy. Remarkably, X-rays enhanced the invasive capabilities of melanoma cells 28 % compared to non-irradiated cells at low dose region. X-rays with high dose (4 and 8 Gy) decreased the migration and invasion of cells as compared with control samples. The number of cells invaded to opposite surface of control samples was 157±19 cells. Cells were irradiated with X-rays or C-ions at 50 keV/μm. Vertical axis shows number of invaded cells (percentage of control), and horizontal axis shows physical dose. Symbols and bars show mean and SD calculated from at least independent three experiments. *, $p < 0.05$; **, $p < 0.01$ (student's *t*-test, compared irradiated samples with control samples).

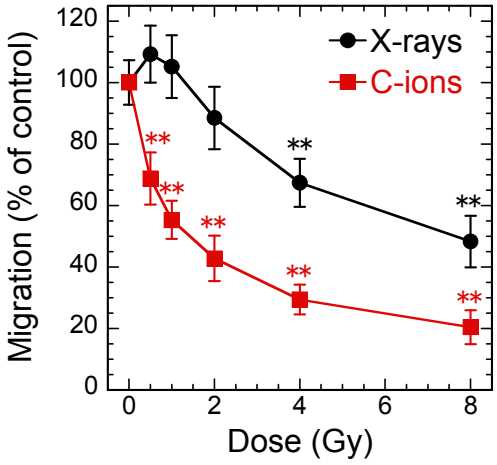

Figure 2 Effects of irradiation on cell migration of B16/BL6 melanoma cells.

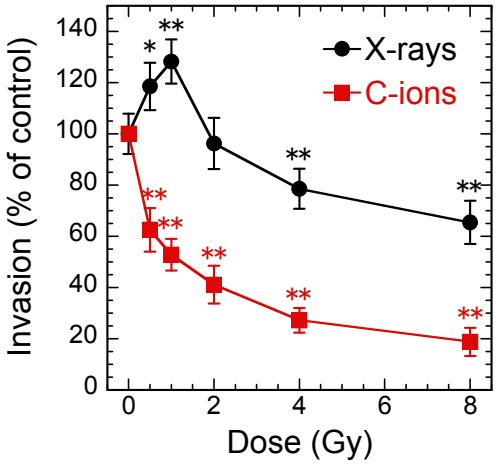

Figure 3 Effects of irradiation on cell invasion of B16/BL6 melanoma cells.

Growth of B16/BL6 tumors

Tumor growth delay (TGD) of B16/BL6 melanomas was measured after irradiation with C-ions and γ-rays (Fig. 4). The TGD time increased with the radiation dose for both radiations. The binomial function was used to fit the data, and the iso-effect doses to produce a TGD time of 10 days were 39.4 and 14.9 Gy for γ-rays and C-ions, respectively. The RBE value calculated from TGD analysis was 2.64. This value is so bigger than the RBE value obtained from *in vivo-in vitro* cell survival assay.

Cell survival in a tumor

Survival curves of clonogenic cells in tumors after γ-ray or C-ions irradiation were obtained using *in vivo-in vitro* assay (Fig. 5). Local tumors on right hind-legs of mice were irradiated with γ-rays or C-ion beams at the center of 6-cm SOBP. Cells in tumors showed big shoulders in survival

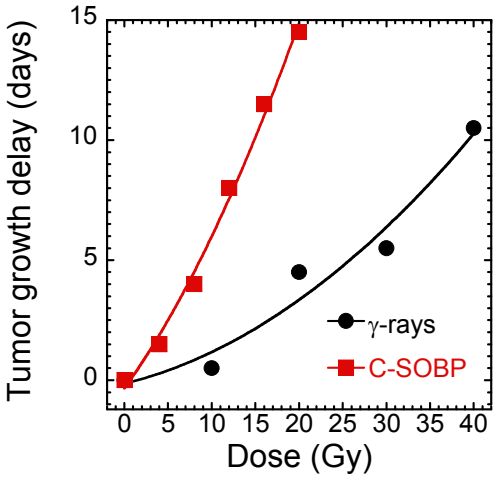

Figure 4 Dose-responses of B16/BL6 tumor growth delay after irradiation.

curves for γ-rays and C-ions. The biological equivalent dose, D_{10} were 20.4 Gy for γ-rays and 10.7 Gy for C-ions, and the RBE calculated from D_{10} values was 1.91. Both survival curves were fitted to survival curves using the following LQ equation. The symbols and bars are the mean and SE calculated from independent three experiments.

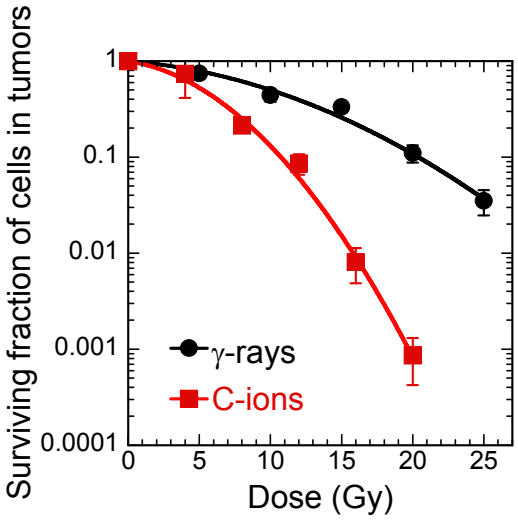

Figure 5 Surviving fractions of cells in B16/BL6 tumors were measured using *in vivo-in vitro* assay.

Lung metastasis

To elucidate the effects of radiations to metastases made after irradiation for local tumors, number of colonies produced among the interval between inoculation and irradiation were obtained. The numbers made before irradiation was 8.3 ± 3.0. Figure 6 shows the numbers of metastases subtracted the metastases before irradiation from total metastases at 35 days after inoculation as a function of the dose of γ-rays and C-ions. Lung metastases were not significantly decrease at the dose range of 10-30 Gy for γ-rays, and the statistical differences were found at high dose region of 40 - 60 Gy. On the other hand, the numbers of lung colonies markedly decreased for C-ions at low dose region between 10 and 30 Gy (Fig. 6). However, the decrease of metastases was saturated at 40 Gy, and the saturated level was same with the metastases made before irradiation. This figure showed that C-ions were more effective for inhibition of metastases compared with γ-rays even when comparing the effects using biological equivalent dose on cell survival. Symbols and bas represent mean and SD calculated from at least independent three experiments.

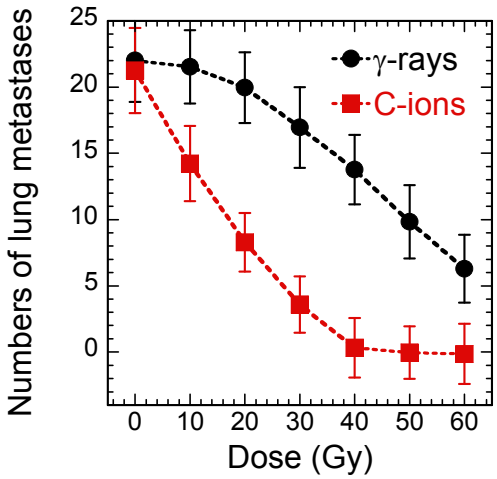

Figure 6 Subtracted numbers of macroscopic metastases in the lung on 35days after tumor cell inoculation as a function of the dose of γ-rays or C-ions.

Discussion

Our ultimate goal is to treat the primary local tumor and to control any underlying metastases. In the present study we found that C-ions irradiation for primary local tumors inhibited the incidence of lung metastases effectively more than photon beam irradiation. Carbon-ion radiotherapy might be useful tool to cancer therapy on not only local tumor control but also suppression of metastases.

Carbon-ion radiotherapy has established its efficacy in previous reports [1-5]. It is thought that the advantage of carbon-ion beam therapy over conventional photon beam therapy mostly depends on the superior physical dose distribution. However, the effects of heavy-ion beams for metastatic potentials of tumor cells are not yet well known. We think that heavy-ion beams including C-ions might suppress metastatic potential for particle beam specific biological effects.

Firstly we focused on the effects of C-ions on migration and invasion of tumor cells compared with X-rays. Cell migration and invasion are fundamental components of tumor metastasis. It was reported that sublethal dose of X-rays induced the expression of the $\alpha V\beta V_3$, β_3 or β_1 integrin in many kinds of tumor cells (glioblastoma, osteosarocoma, glioma, or colon carcinoma) and enhance the cell migration [6, 15, 16]. In the current study, X-rays promotes migration and invasion capabilities of melanoma cells at low dose level, however C-ions markedly suppress the both capabilities in as the increment of dose (Fig. 2 and 3). It is known that X-rays enhance MMP-2

activity that related to the invasive ability of tumor cells, whereas C-ions and proton strongly inhibit the activity after irradiation [15]. These data is supportive for our results. Additionally, we obtained cell survival curves of B16/BL6 melanoma cells exposed to C-ions or X-rays (Fig. 1), and RBE values were calculated from all in vitro experimental end points, cell death, inhibition of cell migration and inhibition of cell invasion. As a result by the comparison of these RBE values, C-ions were more effective to invasion and migration compared with cell death. Ogata et al reported that the ant-migration effects of C-ions were more strongly than X-rays compared using biological equivalent dose on cell death [15]. These findings mean that there are many cells without enough migration capabilities after C-ions even if cells are survive.

C-ions irradiation significantly decreased lung metastases in a dose-dependent manner *in vivo* experiments (Fig. 6), however γ-rays need very large dose to decrease the metastases. Previous study has shows superior anti-metastatic effect of C-ions over X-rays for lung metastases made from cells injected by tail vein [15]. Tamaki et al reported, however that C-ions and γ-rays similarly inhibited metastasis from primal NR-S1 fibrosarcomas [17]. As a reason of this discrepancy, we focused the difference of local tumor radiosensitivity for C-ions and γ-rays. B16/BL6 melanomas used in our study is too radioresistant on tumor growth delay. The RBE values are 2.6 or 1.6 for B16/BL6 melanomas or NR-S1 fibrosarcomas, respectively (Fig. 4). Additionally, Masunaga et al. reported that B16/BL6 tumors with 7-8 mm φ contain more than 50 % quiescent (Q) cells showed radioresistace [23]. It is not known the percentage of Q cells in NR-Si tumors, however these differences about radioresistance of tumors might be related this discrepancy.

On the other hand, C-ions showed remarkably suppression of metastases after irradiation, however about 8 metastatic colonies were found at very large dose region, 40 - 60 Gy. This saturation level conformed to subtraction number of metastases as background. It can be said that these residual metastases is "pre-irradiation metastases" departed from primary tumors before the irradiation. These metastases remained up to large dose of C-ions, and it is important to control the metastases for advancement of C-ion cancer therapy. Immediate future, it is necessary that combination therapy with both C-ions and other treatment to aim at metastases control.

After irradiation, tumors include cells for both the surviving and the dying. Therefore, we wanted to evaluate the frequency of metastases of only survived cells. Employing the data of cell survival in tumors obtained with *in vivo-in vitro* assay (Fig. 5) and change of metastases number (Fig. 6), correlations of subtracted numbers of microscopic lung metastases with surviving fraction of cells in tumors after C-ions or γ-rays were estimated. It is noteworthy that anti-metastatic effect of C-ions was effective more than γ-rays even if comparing the effects using biological equivalent dose (Fig. 7). This means the anti-metastatic effect of C-ions superior to γ-rays depend on not only cell death but also cell mortality or other functions of cells, for example migration, invasion, adhesion, or angiogenesis end so on. Additionally, it was reported that the effects of γ-rays for metastasis was enhanced by nicotinamide that release hypoxic region to oxic [23]. It is known C-ions show low OER and more effective for hypoxic tumors *in vitro* and *in vivo*, and the effective suppression of metastases after C-ions might be involved in the difference of OER.

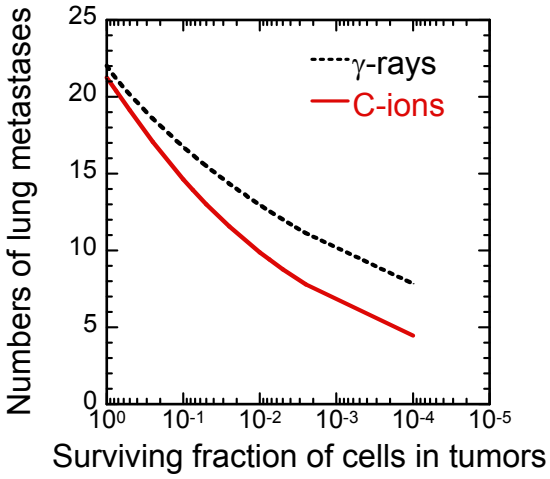

Figure 7 Correlation of number of lung metastases with surviving fraction of cells in tumors.

In conclusion, we aimed to study the effects of C-ions irradiation on metastasis from local melanoma tumors and found that C-ions more effective to radiotherapy for primary tumors to inhibit the incidence of lung metastasis compared with photon beams.

Acknowledgements

This work was supported in part by a Grant –in-Aid from the Ministry of Education, Culture Sports, Science and Technology and by the Special Coordination Funds for Research Project with Heavy Ions at the National Institute of Radiological Sciences-Heavy-ion Medical Accelerator in Chiba (NIRS-HIMAC). We acknowledge all staff members in the Heavy-Ion Radiobiological Research Group for their kind help and suggestions and the HIMAC crews for their kind operation at sample irradiation.

References

［1］ Tsujii H, Mizoe J, Kamada T, et al. Clinical Results of Carbon Ion Radiotherapy at NIRS. J Radiat. Res. 2007; 48 Suppl. A: A1-13.

［2］ Kamada T, Tsujii H, Tsuji H, et al. Efficacy and safety of carbon ion radiotherapy in bone and soft tissue sarcomas. J. Clon. Oncol. 2002; 15: 4466-71.

［3］ Miyamoto T, Yamamoto N, Nishimura H, et al. Carbon ion radiotherapy for stage I non-small cell lung cancer. Radiother. Oncol. 2003; 66: 127-40

［4］ Kato H, Tsujii H, Miyamoto T, et al. Results of the first prospective study of carbon ion radiotherapy for hepatocellular carcinoma with liver cirrhosis. Int. J. Radiat. Oncol. Biol. Phys. 2004; 59: 1468-76

［5］ Tsuji H, Yanagi T, Ishikawa H, et al. Hypofractionated radioptherapy with carbon ion beams for prostate cancer. Int J Radiat Oncol Biol Phys 2005; 63: 1153-60.

［6］ Yanagi T, Mizoe J, Hasegawa A, Mucosal malignant melanoma of the head and neck treated by carbon ion radiotherapy. Int J Radiat Oncol Biol Phys 2009; 74: 15-20.

［7］ Wild-Bode C, Weller M, Rimner A, et al. Sublethal irradiation promotes migration and invasiveness of glioma cells: implication for radiotherapy of human glioblastoma. Cancer Res 2001; 61: 2744-50.

［8］ Sonveaux P, Brouet A, Havaux X, et al. Irradiation induced angiogenesis through the up-regulation of the nitric oxide pathway: implications for tumor radiotherapy. Cancer Res 2003; 63: 1012-19.

［9］ Qian LW, Mizumoto K, Inadome N, et al. Radiation stimulates HGF receptor/c-Met expression that leads to amplifying cellular response to HGF stimulation via upregulated receptor tyrosine phophorylation and MAP kinase activity in pancreatic cancer cells. Int J Cancer 2003; 104: 542-9.

［10］ Qian LW, Mizumoto K, Urashima T, et al. Radiation induced increase in invasive potential of human pancreatic cancer cells and its blockeade by a matrix metalloproteinase inhibitor, CGS27023. Clin Cancer Res 2002; 8: 1223-7.

［11］ Onoda JM, Piechocki MP, Honn KV, Radiation induced increase in expression of the α IIb β3 integrin in melanoma cells: effects on metastatic potential. Radiat Res 1992; 130: 291-8.

［12］ Cox R, Thackr J, Goodhead DT, et al. Mutation and inactivation of mammalian cells by various ionizing radiations. Nature 1977; 267: 425-7.

［13］ Goodhead DT, Thacker J, Cox R, Non-rejoining DNA breaks and cell inactivation. Nature 1978; 272: 379-80.

［14］ Suzuki M, Kase Y, Yamaguchi H, et al. Relative biological effectiveness for cell-killing effects on various human cell lines irradiated with heavy-ion medical accelerator in Chiba (HIMAC) carbon-ion beams. Int J Radiat Oncol Biol Phys 2000; 48: 241-50.

［15］ Takahashi Y, Teshima T, Kawaguchi N, et al. Heavy ion irradiation inhibits *in vitro* angiogenesis even at sublethal dose. Cancer Res 2003; 63: 4253-7.

［16］ Ogata T, Teshima T, Kagawa K, et al. Particle irradiation suppresses metastatic potential of cancer cells. Cancer Res 2005; 65: 113-120.

［17］ Goetze K, Sholz M, Taucher-sholz G, et al, The impact of conventional and heavy ion irradiation on tumor cell migration *in vitro*. Int J Radiat Biol 2007; 83: 889-96.
［18］ Tamaki T, Iwakawa M, Ohno T, et al. Application of carbon-ion beams or gamma-rays on primary tumors does not change the expression profiles of metastatic tumors in an *in vivo* murine model. Int J Radiat Oncol Biol Phys 2009; 74: 210-8.
［19］ Akino Y, Teshima T, Kihara A, et al. Carbon-ion beams irradiation effectively suppresses migration and invasion human non-small-cell lung cancer cells. Int J Radiat Oncol Biol Phys 2009; 75: 475-81.
［20］ Ando K, Koike S, Uzawa A et al. Biological gain of carbon-ion radiotherapy for the early response of tumor growth delay and against early response of skin reaction in mice. J Radiat Res 2005; 46: 51-7.
［21］ Duan X, Zhang H, Liu B, et al. Apoptosis of murine melanoma cells induced by heavy-ion radiation combined with Tp53 gene transfer. Int J Radiat Biol 2008; 84: 211-7.
［22］ De Jaeger K, Kavanagh MC, Hill RP, Relationship of hypoxia to metastatic ability in rodent tumours. Br J Cancer 2001; 84: 1280-5.
［23］ Masunaga S, Matsumoto Y, Hirayama R, et al. Significance of manipulating intratumor hypoxia in the effect on lung metastases in radiotherapym with reference to its effect on the sensitivity of intratumor quiescent cells. Clin Exp Metastasis 2009; 26: 693-700.

Track Structure Considerations of Heavy Ions in the Low Dose Effects of Ionizing Radiation

Hooshang Nikjoo

Radiation Biophysics Group, Department of Oncology-Pathology, Karolinska Institutet, Stockholm, Sweden

Estimates of the effects on humans from exposures to low doses and low dose rates of ionizing radiations are of critical importance for the risk assessment in radiation protection, and radiation therapy. The main effects are the induction of tumour, and germ cell mutation believed to arise from damage to a single cell. It is postulated that biological effects of radiation track may be correlated with the severity of initial damage. Damage from radiation track arises from energy depositions in the form of isolated or clustered ionizations and excitations forming inhomogeneous events in the genetic material in the cell nucleus. These energy deposition events lead to induction of biological damage. Among many different types of damage to the genome double strand breaks (DSB) and clustering of DSBs are considered the most severe types of damage induced by the radiation track. This presentation examines features of heavy ions tracks in the cell nuclei by visual means and biophysical calculations, and their biological consequences. Of crucial importance in practical term is the question how cells may respond to the passage of a single particle track of low or high LET.

On the Use of the Interaction Density as a Measure of the Biological Efficiency of Ionizing Radiation

Bengt K. Lind

Karolinska Institutet and Stockholm University, Department of Medical Radiation Physics, 171 76 Stockholm, Sweden

Background

It is well known that the absorbed dose alone is not enough to quantify the biological effect from ionizing radiation. This is due to the varying spatial distributions of energy depositions on a microscopic scale. Historically, various approaches have been taken to characterize the differences seen in beam qualities, for example by the use of Specific Primary Ionization (SPI) or Linear Energy Transfer (LET). Most widespread today for this purpose is perhaps the use of LET, despite inherent shortcomings such as the fact that different charged particles, *i.e*. ions such as *p+*, *C* and *Li* etc, with the same LET can have different biological efficiency.

Provided that the spatial distribution of energy deposits (disregarding the amount of energy per deposit) is the most important characteristic, a concept more in line with SPI than LET should be aimed at. Such a measure could be the average (and higher moments) nearest neighbor distance in 3D space. In order to account for both inter and intra track distances the particle fluence should also be included. Following this lines of thoughts, the least biological efficiency would be expected for completely uniform density of energy deposits. An expression for the average nearest neighbor distance in *n* dimensions is thus needed.

Theory

Assuming Poisson distributed interactions along parallel tracks with the density ρ of energy deposits per unit *n*-volume, the average nearest neighbor distance r can be expressed as $r = (n/(\rho k_n))^{1/n}\Gamma(1+1/n)$. Here Γ is the gamma function and k_n is a constant given by a closed-form expression and takes, *e.g.* the values 2, 2π and 4π for the first three dimensions.

Given the expression for the average nearest neighbor distance, one can for example calculate which fluence, Φ, is needed to achieve uniform density of energy deposits from charged particles with mean (inelastic) free path $\bar{\lambda}$. The following expression for the fluence can be derived $\Phi = (2\Gamma(3/2)/\bar{\lambda})^2/\pi = 1/\bar{\lambda}^2$.

Discussion

For absorbed doses used in therapeutic radiation therapy (some tens of Gray), high energy electrons, in the MeV range, have an almost uniform density of energy deposits. On the contrary high LET charged particles deviate largely from the purely random distribution. Different approaches to quantify this deviation from uniformity, and thus, the increases biological efficiency then seen will be shown and discussed.

A Mathematical Model for the Non-homologous End Joining (NHEJ) Repair Pathway

Reza Taleei and Hooshang Nikjoo

Radiation Biophysics Group, Department of Oncology-Pathology, Karolinska Institutet,
Box 260, Stockholm SE17176, Sweden

Abstract

Ionizing radiation induces a variety DNA damage including single strand breaks (SSB), double strand breaks (DSB), and base lesions in human cells. DSB are considered to be the most critical lesions to be repaired. Human cells employ a complex repair system to retain their genome integrity. The unrepaired DSB may lead to mutation or consequently cancer. The main competitive pathways to repair the DSB are non-homologous end joining (NHEJ), homologous recombination (HR), and single strand annealing (SSA). NHEJ and SSA pathways are error prone, while HR is conservative. NHEJ is the main repair pathway in higher eukaryotes and it is active through the whole cell cycle. In this work we have proposed a biochemical kinetic rate model to describe the NHEJ repair pathway. The model consists of a system of nonlinear ordinary differential equations describing the repair processes. The model was benchmarked with the repair kinetics of the chicken B (DT40) and mouse embryo fibroblast (MEF) cells irradiated with doses ranging from 20 Gy to 80 Gy. Similar to the experimental DSB repair kinetics, the NHEJ model results show fast and slow DSB repair kinetics. This presentation describes the elements of the mathematical model, and compares the results with experimental data.

Clinical Use and Basic-Science Programs at HIMAC

Takeshi Murakami, Akifumi Fukumura, Kiyomi Eguchi-Kasai [*a], Toshiaki Kokubo*[b],
Kyosan Yoshikawa, Shigeru Yamada

Research Center for Charged Particle Therapy, National Institute of Radiological Sciences, Chiba, Japan
*[*a] Research Center for Radiation Protection, National Institute of Radiological Sciences, Chiba, Japan*
*[*b] Fundamental Technology Center, National Institute of Radiological Sciences, Chiba, Japan*
Corresponding Author: Takeshi Murakami, e-mail address: muraka_t@nirs.go.jp

Abstract

HIMAC is the first large accelerator constructed for medical purposes, and has been successfully carrying out cancer treatments using carbon beams since 1994. The facility is operated 24 hours a day. HIMAC supplies the various heavy-ion beams to basic-science programs during the night and on weekends, while the daytime is devoted to clinical use. Although changing the accelerator condition twice a day is a heavy burden for scheduling and everyday operation, it allows for an efficient use of the facility, and produces much outcome. The present status of the facility and an outline of the basic-science programs are described in this review.

Construction of HIMAC

The Japanese government launched a campaign entitled the "Comprehensive 10 Year Strategy for Cancer Control" in 1983. Heavy Ion Medical Accelerator in Chiba (HIMAC), proposed by NIRS, was approved as one of the major projects supported by this campaign. It was the first large accelerator, a high-energy heavy-ion accelerator, constructed for medical purposes in the world. The purpose of HIMAC was to investigate both the effectiveness and extent of heavy-ion therapy for cancer treatment. The construction of HIMAC was completed in 1993 [1]. After half a year of accelerator conditioning and pre-clinical studies of the physical and biological properties of heavy ions, clinical studies began in June of 1994.

Accelerators that can deliver heavy-ion beams with energies of around a few hundred MeV/nucleon are very rare in the world. Supplying HIMAC beams to other fields without interfering with the daily clinical use was therefore strongly desired. High-quality treatment also requires detailed knowledge concerning beam-material interaction processes. Thus, basic-science programs involving researchers from both inside and outside of the institute started in the fall of 1994.

The dual clinical/research use of the accelerator was highly challenging subject in two ways. The first was the feasibility of applying a large accelerator for clinical use. Obviously, the instruments of clinical use must be reliable and stable. Many people cast doubt on applying a large and complex accelerator, such as HIMAC, to a medical site. The second challenge involves the feasibility of coexisting clinical use and basic-science programs. Basic-science studies require a variety of ion beams, i.e. ion species, energies, intensities, and spot sizes, while clinical studies employ the same beam under definite conditions. Thus, all accelerator conditions must be changed from one purpose to another.

Sixteen years after starting the treatment/research programs, it has been shown that difficulties could be overcome. In fact, the cooperation between the different disciplines has proven to be very productive and innovative. The research activities at HIMAC include radiology, nuclear physics, atomic and molecular physics, radiation chemistry, engineering, and biology, in addition to medical applications.

Accelerator and irradiation rooms

1. Accelerator structure

The requirements for ion beams from a medical point of view are listed in Table 1. Ions from He to Ar were requested as ion species to be accelerated. A maximum range of 30 cm in soft tissue leads to be the maximum energy, for example, of 800 MeV/nucleon for Si. The development and improvement of ion sources and accelerators, including supplying new ion species, sophisticating the beam-transport system as pulse operation, and constructing a new beam course, continued after the official inauguration of the facility. Now, ion species that are available for basic-science studies range from the proton to Xe, including some unstable nuclei. A brief outline of the accelerator is given in Table 2.

Particle species	He, C, Ne, Si, Ar
Penetrating range	30 cm in tissue
Dose rate	5 Gy / min.
Max. field size	22 cm in diameter
Beam direction	Vertical and horizontal

Table 1. Requirements of the facility from a medical point of view

Ion source	PIG, 10GHz-ECR, and 18GHz-ECR	8 keV/nucleon
		Ion species: p to Xe
Injector	RFQ linac (0.6 m ϕ x 7.3 m long)	800 keV/ nucleon
	Alvarez linac (2.2 m ϕ x 24 m long)	6 MeV/ nucleon
Main accelerator	Synchrotron (42 m ϕ)	100 - 800 MeV / nucleon
		repetition rate: 3.3 seconds
Irradiation rooms	3 treatment rooms	
	4 experiment rooms	

Table 2. Outline of the accelerator parameters

Figure 1 gives a cut-away view of the HIMAC facility. HIMAC comprises ion sources, an injector, a synchrotron, a beam-transport system, three treatment rooms, and four experiment rooms. The major parts of the accelerator were constructed 20 m underground, because the facility is located in a densely populated area, and thus the outside appearance is important.

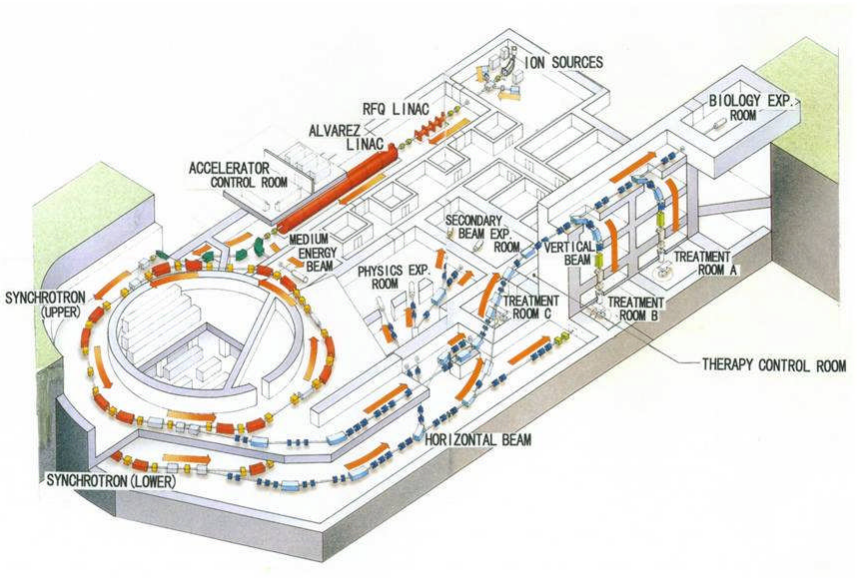

Fig.1 Cut-away view of the HIMAC facility

It is a distinctive feature of HIMAC that the synchrotron has two “identical” rings (upper and lower rings). Three ion sources are in operation, and all of magnets of the injector section are pulse-operated. The beams from the injector are deflected from pulse to pulse in three directions, i.e. direct use of the injector beams and injection into the two rings. Thus, three user groups can share the beam time. The versatility of the facility is very high, because three user groups can request different ion species, and the beam energies of the two rings are independent.

2. Beam-delivery system for treatment

There are three clinical-treatment rooms, which are equipped with horizontal (rooms B and C) and vertical courses (rooms A and B), and therefore there are four beam courses. In medical applications, very “broad and thick” irradiation fields are required. HIMAC employs “a wobbling system” and “a ridge filter” [2]. A pair of AC-operated magnets (wobbling magnets) followed by a scatter produces an irradiation field that is uniform within ±2%, with a maximum size of 22 cm in diameter. A block collimator and a multi-leaf collimator define the cross-sectional shape of the beam. An energy absorber having many “ridges” spreads the beam energy so as to form a broadened Bragg peak, called a Spread-Out-Bragg-Peak (SOBP). A dose monitoring system is installed in the course. Once the preset dose level is reached, the beams are automatically stopped. The upper and lower rings are assigned to two of three treatment rooms, or four courses, when a patient is ready to be irradiated.

3. Experiment rooms

There are four experiment rooms: the general-physics experiment room, the secondary beam experiment room, the biology experiment room, and the medium-energy experiment room.

3.1. General-physics experiment room

The highest and most intensive beams are available in the general-physics experiment room, shown in Fig. 2. Two beam courses, PH1 and PH2, are introduced into this room under vacuum all the way. In many cases, the targets and detectors are placed under atmospheric pressure, because the beams have a long residual range in air. Some groups prepare an irradiation chamber of their own style, directly connected to the beam line in order to avoid any slight change in the energy or scattering of the ions or electrons.

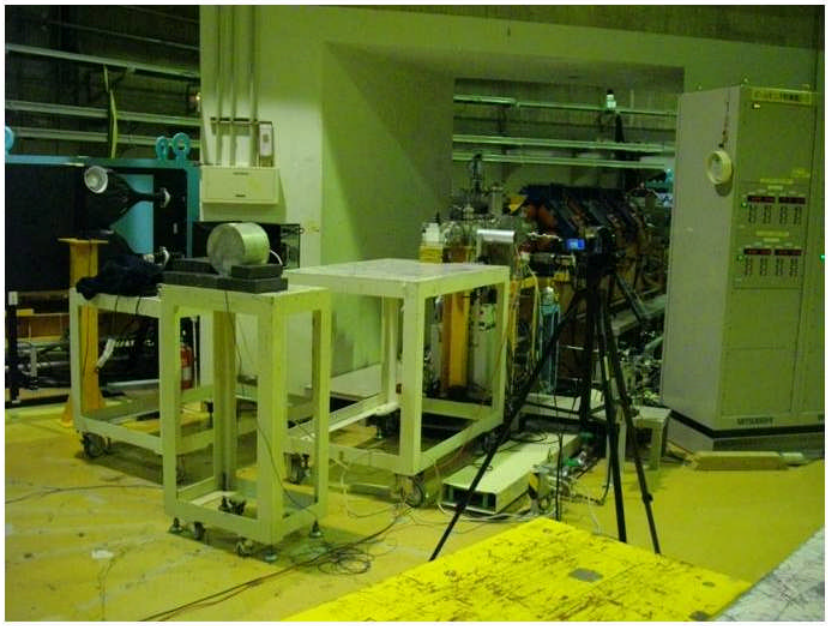

Fig.2 General physics experiment room

3.2. Secondary beam experiment room

Secondary beams produced by projectile fragmentation processes are introduced into the secondary beam experiment room [3]. Beams ranging from Li through Mn isotopes, as well as ^{11}C, have been used in various experiments. There are two beam courses. One is equipped with a pair of large scintillation detectors, and is mainly used for medical-related experiments. A scanning system was also installed for this beam course. The first-phase study concerning a project of the "next generation irradiation system" [4] were carried out using this beam course. In the other course, beams are transported under vacuum, and can be extracted through a thin window, similar to PH1 or PH2. Users prepare the entire measuring system when using this course.

3.3. Biology experiment room

The biology experiment room is equipped with a beam-delivery system similar to those in the treatment rooms. It delivers a uniform field with a diameter of typically 10 cm for various ion species. The residual range can be varied by an energy degrader made of acrylic resin. Small animals, such as mice and rats, as well as cultured cells, can be irradiated in the biology experiment room. In order to reduce the extra time needed for sample changing, a "sample changer", which is a remote controlled sliding bed that holds irradiation sample holders, can be installed, as shown in Fig. 3. Combining the dose-monitoring system and the sample changer, several sample holders can be set and be irradiated in a predetermined sequence. Some of the instruments necessary for biology experiments, including incubators, clean benches, a flow cytometer, and microscopes, are available in a working room next to the irradiation room. These instruments and equipment are indispensable, especially for outside users.

Recently, users of a uniform large field available in the biology experiment room have been expanding into the fields of chemistry or physics, i.e. non-biology researchers. These groups are called PIB, or Physics In Biology experiment room. For example, in some chemistry experiments, the desired data involve determining the relation between LET, or dose, and the quantity of some reaction products. Apparatus in the biology experiment room easily realize these measurements. Similarly, experiments related to space science, studying cosmic-ray effects on radiation detectors, etc. also often use the equipment in the biology experiment room.

Fig.3 Biology experiment room

3.4. Medium-energy experiment room

The beams from the injector, 6 MeV/nucleon, are directly transported to the medium-energy experiment room. It is a unique feature of this beam course that various ion species with the same velocity, i.e. the 6 MeV/nucleon, can be obtained.

Present status of HIMAC and an outline of the basic-science programs

1. Operation schedule

HIMAC is operated Monday through Saturday. In the daytime, from 9:00 through 19:00, from Tuesday through Friday, it is devoted to clinical use or related work. Monday is mainly used for the maintenance and conditioning of new beams, etc. Experiments on basic science are carried out during the night and on weekends. The schedules for these studies are illustrated in Fig. 4.

One year is divided into two periods: the 1st term is roughly from April through July, and the 2nd term is from September through the following February. The period depends on the fiscal year system in Japan. August and March are reserved for large-scale maintenance. Remodeling of the accelerator or target rooms and installing new apparatus are carried out during these maintenance periods.

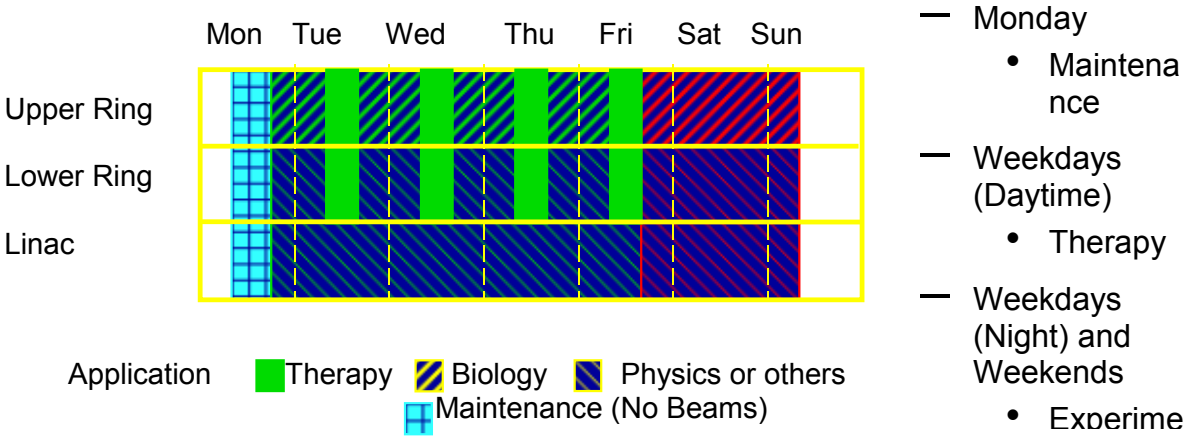

2. Summary of operation

The operation of the HIMAC accelerator in FY2009, from April 2009 through February 2010, is summarized in Fig. 5. The accelerator was operated for about 5,300 hours total. The "supply" of synchrotron rings indicates the time during which HIMAC supplied beams for therapy or basic science. The injector supplies beams to the synchrotron or the medium-energy experiment room: "direct use". It should be noted that the unscheduled downtime, denoted as "trouble", was less than 1% of the time. In FY2009, the beam time supplied for clinical use was roughly 1,600 hours for each of the upper and lower ring, the remaining hours were dedicated to basic science.

Concerning the basic-science programs, a summary of the beam time becomes more complex. A maximum of three user groups can share the beam time, each group with its own beams. The starting and ending time of each experiment is not the same. Thus, it seems straightforward to sum up the beam time "independently", because each group seems to occupy the whole accelerator. The summary of the beam times from 1994 through 2009 are summarized in Fig. 6, categorized as Physics or Biology. The biology time was used for experiments employing cells and small animals. The times of other experiments are categorized as the physics time. More than 5,000 hours were supplied in total. This beam time can be compared to other accelerator facilities dedicated to basic science.

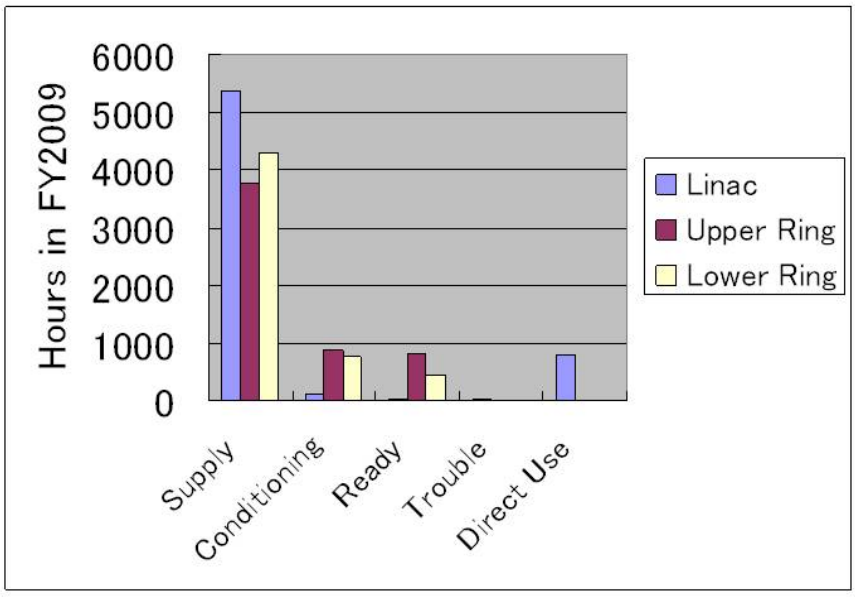

Fig.5 Operation hours of FY 2009

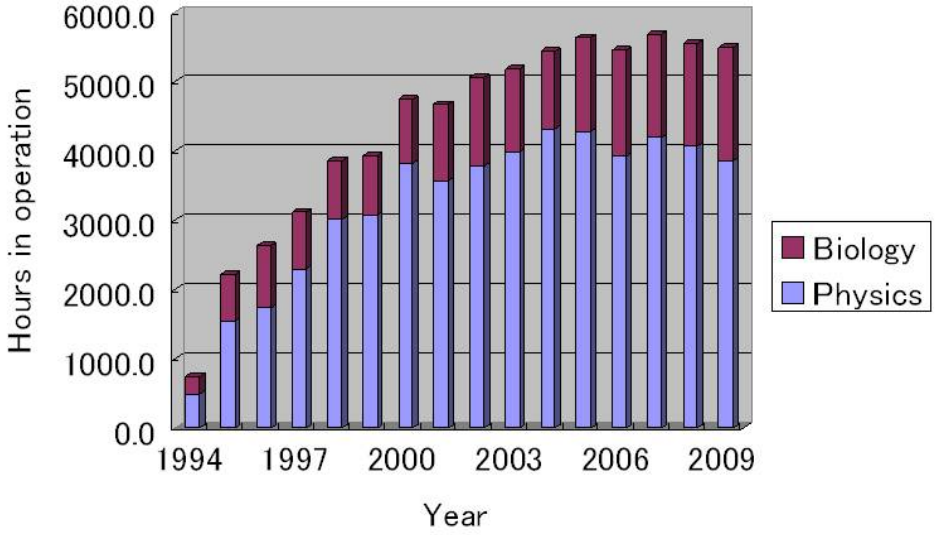

Fig.6 Beam time for Physics and Biology for each year

The reasons why Biology uses the beam for a shorter time than Physics in spite of two ring structures include the following: First, several groups are scheduled in one night for biology experiments, since the irradiation time used for biology experiments is typically 1 or 2 hours each. As a result, un-assigned beam time is not negligible. The other reason is the fact that the groups categorized as PIB are included in the physics time.

3. Evaluation of the proposals

Calls for proposals are posted twice a year. At HIMAC, collaboration with outside users is highly promoted in order to carry out basic science in a wide range of fields. Thus, NIRS accepts proposals on an equal footing, from inside or outside NIRS, and from Japanese and foreign investigators. All proposals are evaluated by PAC. All PAC members are researchers outside NIRS, mainly nominated by scientific societies or science institutes.

The number of accepted proposals per year has been around 120 in recent years, and roughly half of these involve biology.

The number of participants in last 10 years is shown in Fig. 7. About 620 users outside of NIRS and 160 users from NIRS participated in the basic-science programs last year. About 10% of the participants were non-Japanese.

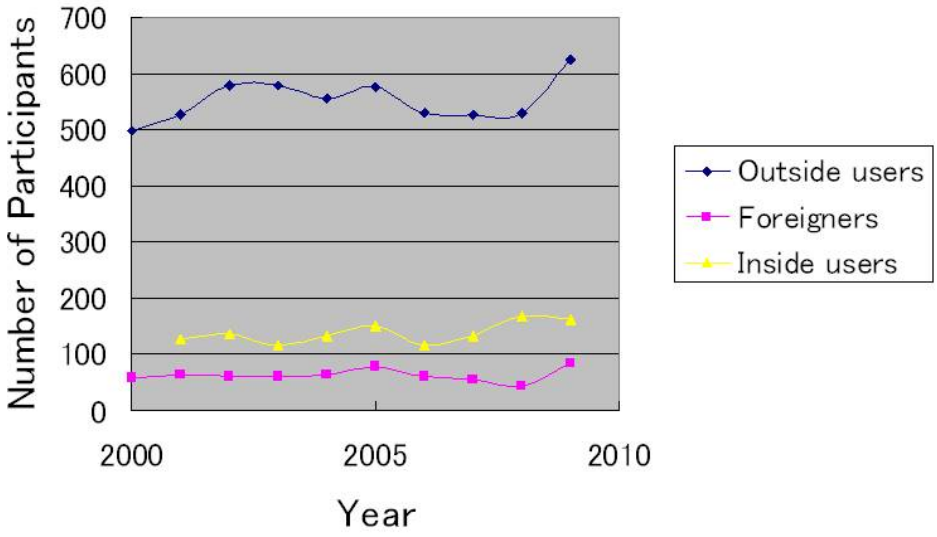

Fig.7 Number of participants in the basic science programs

4. Support system

Due to the broadness of the disciplines of the participants, the researchers involved in the basic-science programs are not necessarily users accustomed to conducting ion-beam experiments. Therefore, a support system, except for accelerator operation, is very important not only for clinical use but also for basic-science programs. Furthermore, it is essential that the experiment rooms and preparation rooms are kept clean and everything is properly arranged in order to carry out all experiments effectively, since many outside users are involved. The jobs for supporting researchers include: (1) assistance in operating the instruments in the biology experiment room, (2) assistance in necessary measures to carry out animal experiments, (3) maintenance of instruments installed in the experiment rooms, (4) detailed scheduling of the experiment rooms and preparation rooms, (5) consultation for arrangements of the measurement system, (6) consultation concerning the beam characteristics and the method of beam tuning, etc. These jobs are carried out by supporting staff from a contracted company.

5. Advantages and drawbacks to the dual use of the accelerator facilities

As shown above, HIMAC is used for two different purposes, clinical use and basic-science programs. Thus, the accelerator must change twice every day. This is a heavy burden on the accelerator staff, which is one of the major drawbacks of this use and management of the facility.

However, it has been found that there are also advantages to the dual-purpose use. First, it provides opportunities for the operators to practice setting up the different conditions, which is especially useful for recruits. The operator's skill and knowledge tend to increase as they continue observing and changing the settings. Second, since reducing the conditioning time is highly important, it provides motivation for improving the operation processes. Third, experiments for basic science require accelerator operation under extreme conditions, such as the highest or lowest energies, most or least-intense beams, extraordinarily stable beam extraction, etc., while relatively fixed conditions are employed in clinical use. Operation under extreme conditions leads to improving the tuning processes as well as upgrading the hardware. Those improvements result in a more stable operation and higher-quality beams for clinical use. Furthermore, dormant problems tend to become known in an early stage.

Research activities

Some of the experiments are briefly described here. Readers should refer to the annual report [5] for more information.

1. Irradiation corrected for respiration motion

Some human organs, such as the lungs and liver, change their positions by as much as 2 cm as a result of the autonomous respiratory motion. This movement results in a large margin of the target volume in treatment planning, leading to unnecessary exposure of normal tissue. The system of irradiation corrected for respiration motion is now commonly used in the everyday treatment of patients [6], providing an example of the success of inter-disciplinary groups in basic-science programs. The studies that provided this system were carried out by medical physicists in cooperation with accelerator physicists, electronics engineers, and of course, medical doctors.

2. Radiobiology experiments

It is impressive that such a large biology group, including both inside and outside users, can be organized. Concerning basic data, such as RBE values determined using cultured cells, different tumor cells show different responses to radiation. It is therefore easily imaginable that a sizable effort must be paid to obtain systematic data.

Mice are the most common small animals used in biology experiments at HIMAC. About 4,000 mice were utilized last year. Cages for mice or rats are prepared for temporary use before and after irradiation. Necessary processes for animal experiments, including the evaluation of experiments and the prevention of contamination, are strictly applied.

3. Application of high-quality beams

A project concerning atomic physics has shown the excellent quality of the high-energy heavy-ion beams from HIMAC, including the observation of a phenomenon so-called “channeling”. The beams must be parallel with an angular divergence of less than 1 mrad and have a small momentum width, and the beams must be very stable for an order of 100 hours to observe this phenomenon. Furthermore, they employed ions with one or two electrons remaining, such as Ar^{17+} or Fe^{25+} ions, for observing resonance phenomena. It is a challenging theme to accelerate such ions to high energies.

4. Nuclear physics

Several experiments related to the nuclear physics, including the use of radioactive nuclear beams, are currently ongoing. They include: (1) measurements of the cross section of a projectile and target fragmentation, (2) measurements of nuclear properties, such as magnetic and quadrupole moments, of unstable nuclei, (3) testing of instruments used in unstable nuclear beam experiments at RIKEN.

5. Simulation of cosmic rays

High-energy heavy-ion beams are good simulators of cosmic rays. Thus, many groups from foreign countries, as well as from Japan, have conducted experiments to test the effects of cosmic rays. These include: (1) the calibration of many types of detectors used by astronauts, (2) the response of detectors installed in man-made satellites, (3) determination of the response of semiconductor devices to cosmic rays, (4) evaluation of the response of biological samples to cosmic rays, and (5) basic data for predicting the response of satellite walls, etc to cosmic rays.

Summary

HIMAC, the first medical accelerator, has been satisfactorily carrying out clinical studies since 1994. It also has been delivering heavy-ion beams for research programs in a broad range of basic science areas. The interest in and applications of HIMAC are due to the high quality of beams, the excellent operation of the facility, and the good support system.

References

[1] Sato K, Yamada S, Ogawa H, et al. Performance of HIMAC. Nucl Phys. 1995;A588: 229c-234c.

[2] Kanai T, Endo M, Minohara S, et al. Biophysical characteristics of HIMAC clinical irradiation system for heavy-ion radiation therapy. Int J Radiation Oncology Biol Phys. 1999;44: 201-210.

[3] Kanazawa M, Kitagawa A, Kouda S, et al. Secondary beam course for the medical use at HIMAC. Proc EPAC98 1998; 2357-2359.

[4] Noda N, et al., this Proc.

[5] 2008 Annual Report of the Research Project with Heavy Ions at NIRS-HIMAC. NIRS-M-226, HIMAC-132. 2009.

[6] Minohara S, Kanai T, Endo M, Noda K, Kanazawa M. Respiratory gated irradiation system for heavy-ion radiotherapy. Int J Radiation Oncology Biol Phys. 2000;44: 1097-1103.

Carbon Ion Therapy for Patients with Locally Recurrent Rectal Cancer

Shigeru Yamada, Makoto Shinoto, Kazuhiko Ohnishi, Shigeo Yasuda, Hiroshi Imada, Tadashi Kamada, and Hirohiko Tsujii,

Hospital, Research Center for Charged Particle Therapy, National Institute of Radiological Sciences, Chiba, Japan, e-mail: s_yamada@nirs.go.jp.

Abstract

Purpose: To evaluate the tolerance for and effectiveness of carbon ion radiotherapy in patients with locally recurrent rectal cancer.

Patients and Methods: We conducted a phase I/II dose escalation study of carbon ion radiotherapy. One hundred twenty-nine patients with 134 sites of locally recurrent cancer receiving carbon ion radiotherapy were analyzed. Fifty-eight relapses originated in the presacral region, 45 in the pelvic sidewalls, 20 in the perineal region and 9 in the colorectal anastomosis. The total dose ranged from 67.2 to 73.6 gray equivalent (GyE) and was administered in 16 fixed fractions over 4 weeks (4.2 to 4.6 GyE/fraction).

Results: None of the 104 lesions treated with the highest total dose of 73.6 GyE experienced National Cancer Institute - Common Toxicity Criteria grade 3 to 5 acute reactions. The local control rate in patients treated with 73.6 GyE in the present study was 98% at one year and 95% at 5 years. The dose escalation was then halted at this level. The median survival in the patients treated with 73.6 GyE was 54 months (range, 7 to 82 months), and the overall survival rates were 74% at 3 years and 45% at 5 years, respectively.

Conclusion: Carbon ion radiotherapy seems to be a safe and effective modality in the management of locally recurrent rectal cancer, providing good local control and offering a survival advantage without unacceptable morbidity.

Introduction

The major recurrence patterns after surgery for rectal cancer include liver metastasis and local recurrence, with the rate of local recurrence (LR) for rectal cancer ranging from 10 to 40% [1-3]. Although the use of pre- or postoperative radiation therapy has reduced the incidence of LR, 10-15% of patients still develop recurrence. Patients with locally recurrent rectal cancer have low rates of subsequent local control and overall survival. Surgical resection remains the only potentially curative treatment. Curative surgery for LR is technically difficult, and the rates of complications and surgical mortality are relatively high. In fact, surgery for LR is seldom feasible, and most patients are referred for radiotherapy (Table1). External-beam radiation therapy is generally considered a palliative treatment. LR is generally resistant to conventional radiotherapy, and is located close to critical organs.

The carbon ion beam possesses unique physical and biologic properties [4,5]. It has a well-defined range and insignificant scatter in tissues, and the energy release is enormous at the end of its range. This well-localized energy deposition (high-dose peak) at the end of the beam path, called the Bragg peak, is a unique physical characteristic of charged particle beams, as is the induction of more cell cycle- and oxygenation-independent, irreversible cell damage than that observed with low-LET radiation. To improve both the long-term local control and survival of locally recurrent rectal cancer, we have initiated a radiation dose-escalation trial using carbon ion beams.

Table 1. Resection Rates and Survival Rates by Recurrence Sites

	Resction Rate	5-y Survival
Local Recurrence	10-30%	30-45%
Liver Metastasis	40-50%	35-45%
Lung Metastasis	20-30%	40-50%

Patients and Methods

Patient Eligibility

Patients were included in the study if they were confirmed to have locally recurrent rectal cancer without distant metastasis by computed tomography (CT), magnetic resonance imaging (MRI), and carbon-11 methionine positron emission tomography (PET) findings, had adenocarcinoma of the rectum, and had a potentially curative resection of the primary tumor and regional lymph nodes performed with neither gross nor microscopic residual disease. Patients who had undergone chemotherapy within 4 weeks before carbon ion radiotherapy or those who had prior radiation therapy at the same site were excluded from the study. The tumor had to be grossly measurable, but the size could not exceed 15 cm. Eligibility criteria included a Karnofsky performance status score higher than 60 and an estimated life expectancy of at least 6 months. The exclusion criteria included having another primary tumor, infection at the tumor site, and presence of the digestive tract in contact with the clinical target volume. A complete history was obtained, and a physical examination was performed before registration, including CT, MRI and PET, to determine the extent and size of the tumor. Chest and upper abdominal CT scans were mandatory at the time of entry into the trial. All patients signed an informed consent form approved by the local institutional review board.

Carbon Ion Radiotherapy

The Heavy Ion Medical Accelerator in Chiba (HIMAC) is the world's first heavy ion accelerator complex dedicated to medical use in a hospital environment. The features of the accelerator and carbon ion beam have been described previously [6,7]. In brief, carbon ion radiotherapy was given once daily, 4 days a week (Tuesday to Friday), for fixed 16 fractions in 4 weeks. Patients were treated with two to five irregularly shaped ports (median, three ports). The clinical target volume (CTV) was determined by setting the margin 5mm outside the gross tumor volume (GTV) and included the regional lymph nodes (LN). The LN areas that were considered part of the target volume included the internal iliac, external iliac and presacral nodes. The dose constraints of the maximum dose for the intestine and bladder were 30 GyE in 9 fractions and 60 GyE in 16 fractions, respectively. The prophylactic nodal areas of risk are usually treated with 37.8-41.4 GyE in 9 fractions of 4.2-4.6 GyE before irradiation field are reduced in size.

Dose Escalation and Toxicity Criteria

At least three patients were treated at the same dose level, and then a 10% escalation of the total dose was carried out after careful observation of normal tissue responses using the NCI-CTC (National Cancer Institute - Common Toxicity Criteria Version 2.0) guidelines. Dose adjustment was planned if there was any acute RTOG

grade 3 or higher toxicities. We followed the standard phase I dose escalation methods. If no dose-limiting toxicity (DLT) was observed in any of the three patients at a given dose level, the dose level was increased for the next cohort. If DLT was observed in no more than one in three patients, then three more patients were treated at the same dose level. If no further cases of DLT were seen in the additional patients, then the dose level was increased for the next cohort. Otherwise, dose escalation was stopped. Three patients at any dose level had to be followed up for at least 3 months before a subsequent dose escalation. We used 67.2 GyE in 16 fractions, with 4.2 GyE/fraction as the starting dose. For late reactions, the Late Effects of Normal Tissues/Subjective, Objective, Management, and Analytic scoring system was used in addition to the RTOG/European Organization for Research and Treatment of Cancer late scoring system. Scores for late reactions were the highest observed 3 months or later after carbon ion radiotherapy.

Toxicity

Toxicity of the treatment to organs such as the skin, bladder and digestive tract was assessed according to NCI-CTC Version 2.0 (April 30, 1999) and RTOG/EOTRC (late) classification.

Tumor Response and Local Control Criteria

The tumor response was defined as the maximum tumor response observed according to the RECIST scoring system during the first 6 months after the initiation of carbon ion radiotherapy. A complete response (CR) was defined as the disappearance of all measurable tumor in the treatment volume. A partial response (PR) meant a 30% or greater decrease in tumor size (longest diameter). Stable disease was defined by a less than 30% decrease or a less than 20% increase in tumor size. Progressive disease was defined as a 20% or greater increase in tumor size. The absence of local failure in the treatment volume based on CT, MRI, and PET scans was described as local control. Local recurrence was defined in terms of lesions occurring in the tumor bed.

Follow-Up

All patients were seen on a regular basis during follow-up. The initial evaluation of tumors using CT, MRI, and PET scans was performed within 1 month after the completion of carbon ion radiotherapy. Thereafter, the patients were followed up by CT or MRI every 1 or 2 months for the next 6 months, and then the intervals between imaging and follow-up were extended to 3 to 6 months. PET was not performed regularly after the initial evaluation.

Statistical analyses

The duration of survival and local control were defined as the interval between the initiation of carbon ion radiotherapy and the date of death, or the date of diagnosis of local failure, respectively. The survival and local control curves were generated by the Kaplan-Meier method, and the log-rank test was used for comparisons.14,15 Results were considered significant at $P < 0.05$.

Results

Patient Characteristics

Between April 2001 and August 2009, 130 patients (138 lesions) were enrolled in this study. One patient was excluded because of a subarachnoid hemorrhage before treatment. Thus, 129 of the 130 eligible patients were treated with carbon ion radiotherapy. Two more patients were excluded from analysis because of peritoneal dissemination or lymph node metastasis of the mediastinum. Therefore, 134 lesions in 129 patients (88 men and 41 women) were analyzed. Patient characteristics are summarized in Table 2. The median patient age was 62.5 years (range 27 to 83 years). All patients presented with adenocarcinoma at initial surgery. Abdominoperineal resection had been performed in 70 patients, anterior resection in 57, and Hartmann's resection in two. Fifty-five

relapses originated in the presacral region, 45 in the pelvic sidewalls, 20 in the perineal region, and 9 in the colorectal anastomosis. Carbon beams of 290, 350 and 400 MeV/nucleon energy were generated by the HIMAC synchrotron. Carbon ion therapy was given once daily, 4 days a week, for a fixed 16 fractions in 4 weeks. The dose was set at 67.2 GyE (4.2 GyE per fraction) and escalated to 73.6 GyE (4.6 GyE) in 5% increments.

Toxicity

The toxicities in the 129 patients (137 lesions) receiving carbon ion therapy are listed in Table 3. They were relatively few and mild in these patients. All patients completed the scheduled treatment course. No grade 3 to 5 acute toxicity was observed. Two grade 3 late skin and one gastrointestinal reaction were observed among the 124 lesions.

Table2 . Patient Characteristic

Characteristics	No. of Pts. (N=129,134lesions)
Age, years	
Median	62.5
Range	27-83
Female/Male	88/41
Primary tumor operation	
abdominoperineal excision	70
low anterior resection	57
Hartmann's resection	2
Tumor sites (n=59)	
presacral	55 (+1)
lymph nodes	45 (+2)
perineal	20 (+1)
anastomotic	9 (+1)

Table 3. Acute and Late Toxicities as Assessed by the NCI-CTC and RTOG/EORTC Scoring System

	Acute (NCI-CTC)						**Late (RTOG/EORTC)**					
	No. of lesions	Gr0	Gr1	Gr2	Gr3	Gr4	No. of lesions	Gr0	Gr1	Gr2	Gr3	Gr4
Skin	**127**	**24**	**102**	**8**	**0**	**0**	**137**	**63**	**71**	**1**	**2**	**0**
GI tract	**127**	**135**	**1**	**1**	**0**	**0**	**137**	**135**	**0**	**1**	**1**	**0**
Urinary	**127**	**136**	**1**	**0**	**0**	**0**	**137**	**135**	**0**	**2**	**0**	**0**

A MTD of 73.6 GyE had been indicated for patients with bone and soft-tissue sarcomas in the pelvis by a phase I/II dose escalation study of carbon ion radiotherapy. The local control rate in patients treated with 73.6 GyE in the present study was 98% at one year and 95% at 3 years, significantly better than the previously reported local control rates. The patients in our series had mostly been considered to have tumors for which there were no other effective local treatments. Despite such dire conditions, patients experienced good tumor control and a relatively low incidence of complications with carbon ion radiotherapy. To confirm these findings, a phase II clinical trial using 73.6 GyE is warranted.

Despite the fact that various types of chemotherapies were applied before or after carbon ion radiotherapy, there were no obvious effects of chemotherapy on the incidence of toxicities in this series.

Tumor Response

Evaluation of the tumor response was not considered the primary endpoint of this study, however, the tumor response was evaluated in 133 lesions. One patient was excluded from tumor response analysis because of difficulty in imaging evaluation. A CR was observed in 18 lesions and a PR in 37 (Table 4). Seventy-eight lesions remained stable. The overall tumor response rate (CR+PR) was 41%. Remarkable anti-tumor effects were observed.

Table 4. The Response of 133 Lesions

Total dose (GyE)	No. of lesions	CR	PR	SD	PD
67.2	10	4	1	5	0
70.4	19	0	6	13	0
73.6	104	14	30	60	0

The overall actuarial local control rates at five years were 35%, 89% and 95% at 67.2 GyE, 70.4 GyE and 73.6 GyE, respectively. Ten in-field recurrences were observed among the recurrent patients (Fig.1).

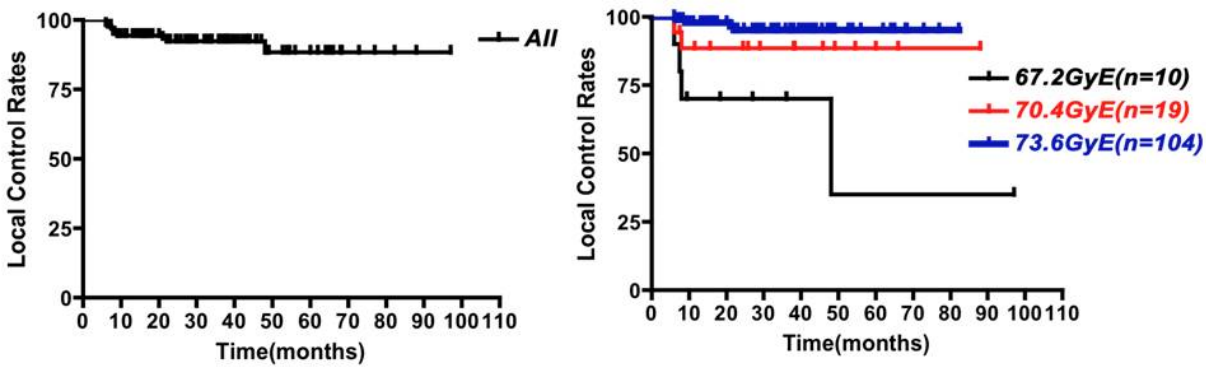

(a) (b)

Fig. 1. Local control rates a) in all 133analyzed lesions, b) by total dose

In terms of symptomatic response within 3 months after treatment, pain improved in 97% of the symptomatic cases. Pain relief was maintained at one year in 67%, 91% and 100% of the patients treated with 67.2GyE, 70.4GyE and 73.6GyE, respectively. In general, symptoms tended to improve during the course of radiation rather than worsen. While most authors agree that irradiation is frequently an effective therapy for symptomatic pelvic tumors, it has also been established that the response usually persists for only about 3-6 months. Symptomatic response rates range from 50% to 94% [10-15].

The overall survival estimates for the 119 patients analyzed during our study are shown in Fig 2. The three-year and five-year overall survival rates were 68% and 42%, respectively. The overall survival rates at three years were 36% at 67.2 GyE, 57% at 70.4 GyE, and 74% at 73.6 GyE. There was a clear correlation between the overall survival rates and total dose. Our 5-year overall survival rate at the recommended dose of 73.6GyE was 45%, which is nearly the same as for surgical resection [9,16-19].

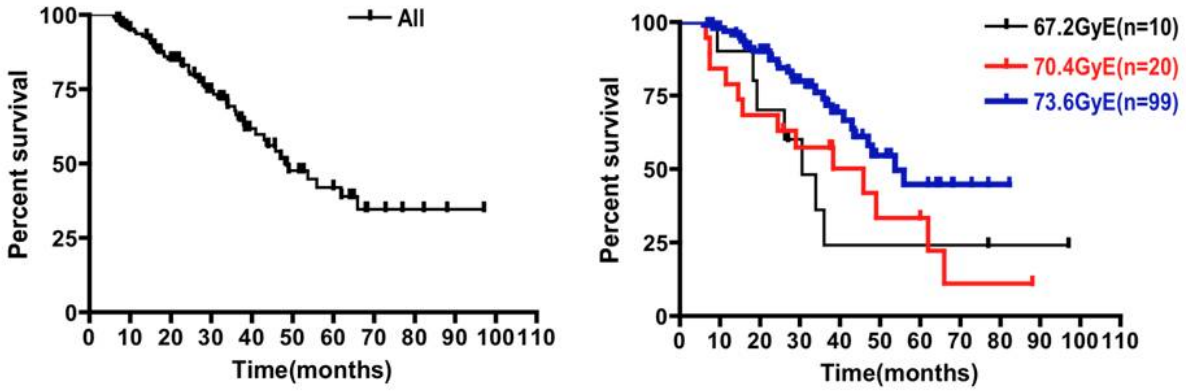

Fig 2. Overall survival rates a) in all 129 analyzed patients, b) by total dose

The above results substantiate the superior usefulness of heavy ion radiotherapy in the treatment of recurrent rectal cancer compared to conventional photon radiotherapy or combinations with chemotherapy.

Discussion

In this study, carbon ion radiotherapy was well tolerated and demonstrated substantial activity against locally recurrent rectal cancer. These results were obtained in patients with advanced and/or chemoresistant gross lesions not suited for surgical resection. We found a dose-response relationship for local control. The rate of actuarial local control increased as the total dose increased from 67.2 to 73.6 GyE, reaching more than 90% in patients treated with 73.6 GyE at one year. The 3-year local control rate for patients receiving either 70.4 GyE or 73.6 GyE was similar, at 89 or 95%, significantly better than that for those receiving 67.2 GyE (Fig. 3). Surgery is considered to be the standard treatment for rectal cancer patients, but it is only possible in a very small number of cases. Curative surgery for recurrent rectal cancer has resulted in higher than 50% long-term local control rate [8,9]. However, most patients must be referred for radiotherapy.

There have been several attempts to improve the duration and quality of response in advanced cancers by combining radiation treatment with chemotherapy [10-13]. Previous studies reported local control rates in patients with locally recurrent rectal cancer treated by all types of radiotherapy including other particle beams of less than 50% [14,15]. The local control rate of our 73.6 GyE group could be among the best achieved without surgical resection.

Although the focus of this study was not directed at survival, nonetheless, it is noteworthy that the improved local control resulted in better survival. We found a dose-response relationship for the survival rate. The 2-year

overall survival rate increased as the total dose increased from 67.2 to 73.6 GyE. The 2-year overall survival rates were 80% and 87% respectively. In the literature, the reported 2-year survival rate for patients with locally recurrent rectal cancer treated by external-beam radiation was 45% or less (Table 4). External-beam radiation therapy alone or in combination with chemotherapy provides palliation and modest prolongation of life, but has only a minimal curative potential in patients with locally recurrent rectal cancer. The reported 2- year and 5-year overall survival rates in patients with locally recurrent rectal cancer treated by curative surgery were 62-78% and 20-39% respectively (Table5). This level of survival achieved with carbon ion RT can be considered as equivalent to or better than a surgical resection.

Table 5. Results of Radiation Therapy for Locally Recurrent Rectal Cancer

Study and Reference		Number of patients	Radiation dose(Gy)	Survival rate 2 y	Survival rate 5y	Local control rate
Ciatto S[10]	1982	108	35-50Gy	5%(3y)	3%	
O'Connell[11]	1982	17	50	45%	0%	24%(2y)
Wong CS[12]	1991	22	45-50	27%	16%	9%(5y)
Lybeert MLM[13]	1992	76	6-66	61%(1y)	13%(3y)	28%(3y)
Knol HP[14]	1995	50	60	27%	8%	
Murata[15]	1997	18	12-60	44%(1y)		46%
NIRS	2010	99	73.6	87%	45%	95%(5y)

Table 6. Results of Surgical Treatment of Locally Recurrent Rectal Cancer

Study and Reference		Number of patients	Survival rate 1 y	Survival rate 2 y	Survival rate 5y
Wanebo[9]	1999	53	91%	62%	31%
Salo JC[16]	1999	71	88%	75%	31%
Saito N[17]	2003	43	91%	78%	39%
Moriya[18]	2004	48	95%	76%	36%
Melton[19]	2007	29	92%	65%	20%
NIRS	2010	99	97%	87%	45%

Wendling has clearly shown that the oxygenation of differential rectal adenocarcinoma is distinctly lower than that of the normal rectal mucosa, and tissue hypoxia or even anoxia are common features of these tumors [16]. Furthermore, Hockel showed that there is significantly greater hypoxia in pelvic recurrence than in primary tumors [17]. Improvements in tumor response and control have been sought through efforts to overcome the radioresistance of the hypoxic tumor cells identifiable in rectal cancers. These aspects might give high-LET particles a particular advantage, no matter whether this is due to a lower oxygen enhancement ratio (OER) or other intrinsic factors. Therefore, high-LET particle radiotherapy, such as that using carbon ions or neutrons seems to be effective against hypoxic recurrent tumors. Twenty patients with recurrent rectal cancer were treated

using the d,T generator in Munster by combined neutron-radiotherapy [18]. The radiation schedule most often used for palliation involves giving 40 Gy photon and 10 Gy neutron doses (14 MeV). Initiation of pain relief seems to occur faster with neutrons than with photons alone. Pain relief was achieved in 11 of 15 patients (73%), and the probability of a pain-free period is 46% for 9 months. It remains to be proven if the frequency of pain relief and the pain-free period, as well as the progression-free period, last longer with neutrons than with photons. The incidence of acute toxicity was 30% and late toxicity 10%. All toxicity was seen in the skin. A higher neutron dose will give better results, but may cause local radiation side-effects.

Carbon ion therapy offers the potential advantages of improved dose localization and enhanced biological effects [19]. Our results have shown that carbon ion therapy has the potential to deliver a sufficient dose to the tumor with acceptable morbidity in the surrounding normal tissues. Tumors that appear to respond favorably to carbon ions include locally advanced tumors with a non-squamous histology such as adenocarcinoma [20,21]. Carbon ion therapy may very well improve the tumor control of recurrent rectal cancer.

In conclusion, carbon ion radiotherapy is considered to be an effective local treatment for patients with locally recurrent rectal cancer, and it seems to represent a promising alternative to surgery. The morbidity rate of carbon ion radiotherapy has so far been acceptable, although the long-term safety of this approach for patients with sarcomas will still need to be elucidated.

References

［1］ Kapiteijin E, Marijnen CAM, Colenbrander AC et al. Local recurrence in patients with rectal cancer diagnosed between 1988 and 1992. Eur J Surg Oncol 24:528-535, 1998

［2］ Galandiuk S, Wieand HS, Moertel CG, et al. Patterns of recurrence after curative resection of carcinoma of the colon and rectum. Surg Gynecol Obstet 174: 27-32, 1992

［3］ Bozzetti F, Mariani L, Micel R, et al. Cancer of the low and middle rectum: local and distant recurrence and survival in 350 radically resected patients. J Surg Oncol 62: 207-213, 1992

［4］ Blakely EA, Ngo FQH, Curtis SB, et al. Heavy ion radiobiology: Cellular studies. Adv Radiat Biol 11:295-378, 1984

［5］ Hall EJ. Radiobiology for the Radiologist. Philadelphia, PA, JB Lippincott, 1988, pp 281-291

［6］ Sato K, Yamada H, Ogawa K, et al. Performance of HIMAC. Nuclear Physics A 588:229-234, 1995

［7］ Kanai T, Endo M, Minohara S, et al. Biophysical characteristics of HIMAC clinical irradiation system for heavy-ion radiation therapy. Int J Radiat Oncol Biol Phys 44:201-210, 1999

［8］ Lopez-Kostner F, Fazio VW, Rybicki LA et al. Locally recurrent rectal cancer: Predictors and success of salvage surgery. Dis Colon Rectum 44: 173-178, 2001

［9］ Wanebo HJ, Antoniuk P, Koness RJ et al. Pelvic resection of recurrent rectal cancer. Dis Colon Rectum 42: 1438-1448, 1999

［10］ Ciatt S, Pacini P. Radiation therapy of recurrences of carcinoma of the rectum and sigmoid after surgery. Acta Radiol Oncolo 21: 105-109, 1082

［11］ O'Connel MJ, Child DS, Moertel CG. A prospective controlled evaluation of combined pelvic radiotherapy and methanol extraction residue of BCG for locally unresectable or recurrent rectal cancer. Int J Radiat Oncol Biol Phys 8: 1115-1119, 1982

［12］ Wong CS, Cummings BJ, Keane TJ. Combined radiation therapy, mitomycin C, and 5-Fluorouracil for locally recurrent rectal carcinoma. Int J Radiat Oncol Biol Phys 21: 1291-1296, 1991

［13］ Lybeert MLM, Martijin H, DE NEVE W. Radiotherapy for locoregional relapses of rectal carcinoma after initial radical surgery. Int J Radiat Oncol Biol Phys 24:241-246,1992

［14］ Knol HP, Hanssens J, Rutten HJT. Effect of radiation therapy alone or in combination with surgery and/or chemotherapy on tumor and symptom control of recurrent rectal cancer. Strahlenther Onkol 173: 43-49, 1997

［15］ Murata T, Fujii I, Yoshino M. Radiation therapy with or without chemotherapy and hyperthermia for recurrent rectal cancer. J Jpn Soc Ther Radiol Oncol 9: 63-71, 1997

［16］ Salo JC, Paty PB, Guillem J. Surgical salvage of recurrent rectal carcinoma after curative resection .

Ann Surg Oncol 6: 171-177,1998
［17］ Saito N, Koda K, Takiguchi N. Curative surgery for local pelvic recurrence of rectal cancer Dig Surg 20:192-200, 2002
［18］ Moriya Y, Akasu T, Fujita S. Total pelvic exenteration with distal sacrectomy for fixes recurrent rectal cancer in the pelvis. Dis Colon Rectum 47: 2047-2054,2004
［19］ Melton GB, Paty PB, Boland PJ. Sacral resection for recurrent rectal cancer. Dis Colon Rectum 49: 1099-1107, 2006
［20］ Wendling P, Manz R, Thews G, et al. Heterogeneous oxygenation of rectal carcinomas in humans. Advances in Experimental Medicine & Biology 180: 293-300, 1984
［21］ Hockel M, Schlenger K, Hockel S. Tumor hypoxia in pelvic recurrences of cervical cancer. Int J Cancer 79, 365-369, 1998
［22］ Eising E, Potter R, Haverkamp U. Neutron therapy for recurrence of rectal cancer Strahlenther. Onkol 166: 90-94, 1990
［23］ Ando K, Koike S, Ohira C, et al. Accelerated reoxygenation of a murine fibrosarcoma after carbon-ion radiation. Int J Radiat Biol 75: 505-512, 1999
［24］ Kamada T, Tsujii H, Tsuji H, et al. Efficacy and safety of carbon ion radiotherapy in bone and soft tissue sarcomas. J Clin Oncol 20: 4466-4471, 2002
［25］ Miyamoto T, Yamamoto N, Nishimura H, et al. Carbon ion radiotherapy for stage I non-small cell lung cancer. Radiother Oncol 66: 127-140, 2003

Carbon Ion Radiotherapy for Pancreatic Cancer

Shigeru Yamada, Makoto Shinoto, Kazuhiko Ohnishi, Hiroshi Imada, Shigeo Yasuda, Tadashi Kamada, And Hirohiko Tsujii

Hospital, Research Center for Charged Particle Therapy, National Institute of Radiological Sciences, Chiba, Japan, e-mail: s_yamada@nirs.go.jp

.

Abstract

The Heavy Ion Medical Accelerator in Chiba (HIMAC) is the world's first heavy ion accelerator complex dedicated to medical use in a hospital environment. Carbon ion therapy offers the potential advantages of improved dose localization and enhanced biological effects. It has been suggested that carbon ion therapy is effective against radioresistant pancreatic cancer. In April 2000, clinical studies examining the treatment of pancreatic cancer with carbon ions were begun at the HIMAC. As of February 2010, 48 patients treated with preoperative carbon ion radiotherapy and 89 patients treated for locally advanced pancreatic cancer were enrolled into the clinical trials. Both protocols are still ongoing. The interim results of these clinical trials suggest that carbon ion radiotherapy provides good local control and offers a survival advantage for patients with otherwise hard to cure pancreatic cancer, without unacceptable morbidity.

Introduction

Adenocarcinoma of the pancreas continues to be a significant source of cancer mortality in Japan, resulting in approximately 19,000 deaths a year. It is the fifth leading cause of cancer-related deaths in Japan, with a less than 5% 5-year expected survival rate[1)]. About 70-75% of patients with pancreatic cancer present with locally advanced disease or distant metastases, and have a median survival of only 6 months. For unresectable pancreatic cancer, the median survival for patients treated with external beam radiation (EBRT) was better than with surgical bypass[2)] or stents alone[3)]. The median survival of patients who received EBRT alone was 4 to 7 months[4)]. The median survival for those treated with combined EBRT and chemotherapy for locally unresectable tumors was 8 to 10 months[5)]. Local failure of these combined therapies was still 26 to 48%. On the other hand, surgery with curative intent is undertaken in 15-20% of patients. Even after resection, the predicted 5-year survival rates are still less than 20%[1)]. Local recurrence in the pancreatic bed is seen in 50% of the patients undergoing presumed curative resection[6)].

We examined the effect of carbon ion therapy in terms of reducing the rate of local recurrence in patients with locally advanced adenocarcinoma of the pancreas or in those who were undergoing resection for adenocarcinoma of the pancreas.

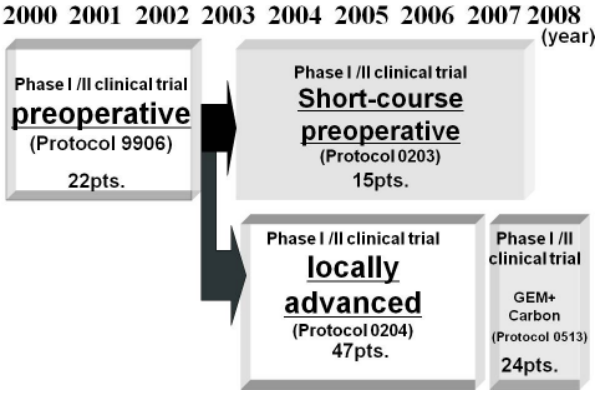

Fig.1 NIRS sequencing trial: schema

Protocols for Carbon Ion Therapy for Pancreas Cancer

A phase I/II clinical trial of carbon-ion therapy for patients with preoperative pancreatic cancer (9906) was carried out on surgically resectable patients from June 2000 through February 2003. This was followed by a Phase I/II clinical trial of short-course carbon-ion therapy for patients with preoperative pancreatic cancer (0203), commencing in April 2003 for similar surgically resectable patients, with a fractionation regimen from 16 (4 weeks) to 8 (2 weeks) fractions. Concurrently, a phase I/II clinical trial of carbon-ion therapy for patients with locally advanced pancreatic cancer (0204) was conducted for surgically non-resectable patients with local progressive disease without distant metastasis from April 2003 through February 2007. This was followed by a phase I/II clinical trial of gemcitabine combined with carbon-ion therapy for patients with locally advanced pancreatic cancer (see Figure 1).

A. Preoperative pancreatic cancer (Protocol 9906, 16 fractions/4 weeks)

Purpose: We examined the effects of preoperative carbon ion therapy in terms of reducing the rate of local recurrence in patients undergoing resection for adenocarcinoma of the pancreas.
Patients and Methods: Twenty-two patients were enrolled in this trial. The median patient age was 63 years. Carbon ion therapy was given once daily, 4 days a week, for a fixed 16 fractions in 4 weeks. The dose was set at 44.8 GyE and was escalated to 48.0 GyE at 5% increments.
Results: All patients completed the scheduled treatment course. Three grade 3 acute reactions and two grade 3 late reactions occurred in 16 of the patients treated with a total dose of 48.0 GyE. The two grade 3 late reactions were thought to be caused by the carbon ion therapy. Of the 22 patients, 15 (68%) underwent resection. All tumor specimens pathologically revealed evidence of grade 2 treatment effects with significant fibrosis, hyalinization, and necrosis (pathological grade 2 is defined as less than 33% active cancer cells). Remarkable antitumor effects were observed. The overall local control rates were 100% and 87% at 1 year and 2 years of follow-up, respectively. No local failure was observed in any of the 22 enrolled patients.
Conclusion: Carbon ion radiotherapy seems to be a safe and effective modality for the management of resectable pancreatic carcinoma, providing good local control and offering a survival advantage without unacceptable morbidity.

Patients and Methods

Patient Eligibility

Between April 2000 and February 2003, 22 patients judged according to the staging criteria of the Japanese Committee on Cancer as being at clinical stages I, II, III or IVa, equivalent to stages I, II or III by the TNM staging criteria, were enrolled in this trial. Criteria for trial eligibility were pathologic confirmation of ductal adenocarcinoma, age 18 years or more, an ECOG performance score of 0, 1, or 2, and adequate hematologic, hepatic, renal, and cardiopulmonary function to allow for pancreatectomy. Exclusion criteria were having another primary tumor, and infection at the tumor site. Patients who had undergone chemotherapy before carbon ion radiotherapy or those who had prior radiation therapy at the same site were excluded from the study. The tumor had to be grossly measurable, but its size could not exceed 15 cm, and the patients were evaluated by surgical consultation with three surgical investigators as to the resectability of the lesion. Chest and upper abdominal CT scans were mandatory at the time of entry into the trial. All patients signed an informed consent form approved by the local institutional review board.

Carbon Ion Radiotherapy

The features of the accelerator and the carbon ion beam have been described previously[7,8].

Carbon ion therapy was given once daily, 4 days a week, for a fixed 16 fractions over 4 weeks. The dose was set at 44.8 GyE and was increased to 48.0 GyE at 5% increments. The protocol specifications for carbon ion radiotherapy were as follows: The target volumes were established by CT scan. Field arrangements were generally designed using a 3-field or 4-field plan. The clinical target volume (CTV) included the gross tumor volume (GTV) and regional lymph nodes, which included the celiac, superior mesenteric, peri-pancreatic, portal and para-aortic

(celiac-IMA) nodes for pancreatic head cancer and splenic nodes for pancreatic body and tail cancer. The CTV was defined as the gross volume plus 1.0 cm or 0.5 cm (for tumors in contact with the gut). At least 50% of the functioning renal parenchyma was limited to 15 GyE or less. The spinal cord dose was limited to 30 GyE or less.

Surgery

Surgical resection was to be performed 2 to 4 weeks after the completion of carbon ion radiotherapy if there was no disease progression to an unresectable status as determined by repeated abdominal CT scans, a prohibitive decline in performance status, or other evidence of metastatic disease. The median time from the last day of carbon ion radiotherapy to surgical resection was 21 days (range, 20 - 26 days).

Tumor Response and Local Control Criteria

The tumor response was defined as the maximum tumor response observed by the RECIST scoring system during the first 6 months after the initiation of carbon ion radiotherapy. A complete response (CR) was defined as the disappearance of all measurable tumor in the treatment volume. A partial response (PR) was characterized by a 30% or greater decrease in tumor size (longest diameter). Stable disease was defined as a less than 30% decrease or a less than 20% increase in tumor size. Progressive disease was defined as a 20% or greater increase in tumor size. Local recurrence was defined in terms of lesions occurring in the treatment volume based on CT, MRI, and PET scans. The development of a new, low-density mass in the region of the pancreatic bed was considered evidence of local recurrence even in the absence of symptoms, and cytologic or histologic confirmation of recurrent disease was not required. The absence of local recurrence was described as local control.

Histological evaluation of the effects of carbon ion therapy included assessment of cytologic changes in conjunction with quantification of the amount of viable residual carcinoma cells (Table 1). Upon completion of specimen analysis, all cases were reviewed by the same histopathologist.

Table 1. Grading system for radiation treatment effects

Grading system for radiation treatment effects

Grade	Histological appearance
0	No tumor cell destruction evident
1	Less than two-thirds of tumor cells are destroyed
2	More than two-thirds of tumor cells are destroyed
3	No viable tumor cells present

Statistical analyses

The durations of survival and local control were defined as the interval between the initiation of carbon ion radiotherapy and the date of death or the date of diagnosis of local failure, respectively.

Results

Patient Characteristics

None of the 22 patients initially registered in this trial were excluded from the analysis. The patients consisted of 14 males and 8 females, with a median age of 63 years (range, 42 - 77 years). Thirty cancers originated in the head of the pancreas, 8 were in the body of the pancreas, and one was in both the head and body (Table 2).

Table 2. Patient characteristics

Characteristics		Number of patients (%)
Age (years)	Median (range)	**22** (42-77)
Gender	male	14
	female	8
ECOG performance score	0	18
	1	4
Tumor location	head	13
	body-tail	8
	head and body	1
Tumor size by CT (mm)		
Stage (preoperative, TNM))		
T3N0		4
T3N1		18

Toxicity

The toxicities in the 22 patients receiving carbon ion therapy are listed in Table 3. The toxicities were relatively few and mild. All patients completed the scheduled treatment course. Three grade 3 acute reactions and two grade 3 late reactions occurred among 12 of the patients treated with a dose of 48.0 GyE. One patient had cholangitis, easily resolved by a radiologic stent change and antimicrobials. Two were postoperative complications: one patient had leakage at the choledochojejunostomy, requiring percutaneous drainage, and the other had gastrojejunostomy leakage, requiring percutaneous drainage. Both leakages occurred outside of the treatment fields and were not considered likely to be related to the carbon ion therapy. There were no grade 3 to 5 blood or bone marrow reactions. Both of the grade 3 late reactions were post-surgery portal vein stenoses, and both underwent portal vein resections.

Table 3. Acute and Late Toxicities by NCI-CTC and RTOG/EORTC Scoring System

	Acute (NCI-CTC)						Late (RTOG/EORTC)					
	No. of patients	Gr0	Gr1	Gr2	Gr3	Gr4	No. of patients	Gr0	Gr1	Gr2	Gr3	Gr4
Skin	22	22	0	0	0	0	20	20	0	0	0	0
GI tract	22	18	3	1	0	0	20	20	0	0	0	0
Bile duct	22	20	0	1	1	0	20	20	0	0	0	0
Portal vein	22	20	0	2	0	0	20	18	0	0	2	0
Leakage	22	20	0	0	2	0	20	20	0	0	0	0

Tumor Response

Evaluation of tumor response was not considered the primary endpoint of this study. However, all 22 patients had CT scans before registration and 2-4 weeks after completion of the carbon ion radiotherapy. On the basis of the CT scans, only one patient showed a complete response, and one also showed a partial response. Twenty patients (91%) had stable disease, and none had local tumor progression.

Surgical Results

Of the 22 patients, 15 (68%) underwent resection. One of the 22 eligible patients did not undergo surgery. CT scan restaging after carbon ion radiotherapy revealed new liver metastases in this patient. Of the 21 patients undergoing exploratory celiotomy, 5 did not undergo a resection. Two had metastases to the liver and three to the peritoneum. Therefore, the remaining fifteen eligible patients had pancreatic resection; 10 underwent modified Child procedures, two had total pancreatectomies, and three distal pancreatectomies were performed. In addition, one patient also underwent solitary liver resection for a small isolated liver metastasis discovered intraoperatively after pancreaticoduodenectomy. This patient, who had a pancreatectomy that was not considered a potentially curative resection, was included in this analysis. The median time from completion of carbon ion radiotherapy to surgery was 22 days (range, 13 - 29).

Table 4. Pathological results of the 15 resected specimens

Total dose (GyE)	No. of patients	Grade0	Grade1	Grade2	Grade3
44.8	5	0	0	5	0
48.0	10	0	0	10	0

Pathological Results of Resected Specimens

The pathological characteristics of the 15 resected specimens are listed in Table 3. All tumor specimens revealed evidence of grade 2 treatment effects with significant fibrosis, hyalinization and necrosis, meaning that more than two-thirds of the tumor cells were destroyed. The resection margins were examined in all specimens. No patient had a grossly or microscopically positive resection margin.

Patient Outcome

The overall local control rates for all 22 patients were 100% at 1 year and 87% at 2 years of follow-up, respectively. One local failure was observed in the residual pancreas at 18 months after pancreaticoduodenectomy. There was no local and regional recurrence within the treatment fields of any of the patients. The 1-year overall survival rates were 62% for all patients and 90% in the resected patients, and median survival was 13.4 months and 21 months, respectively, for these patients, with a median follow-up of 13 months (range, 3.3 - 51 months) (Fig. 2). Two patients are currently alive without evidence of disease. Twenty patients have died; 19 of whom had metastatic relapse or carcinomatosis. In the nonresected patients, the 1-year overall survival rate and median survival were 30% and 6.3 months. This level of survival rate achieved with carbon ion RT alone can be considered as equivalent to chemoradiation (Table5).

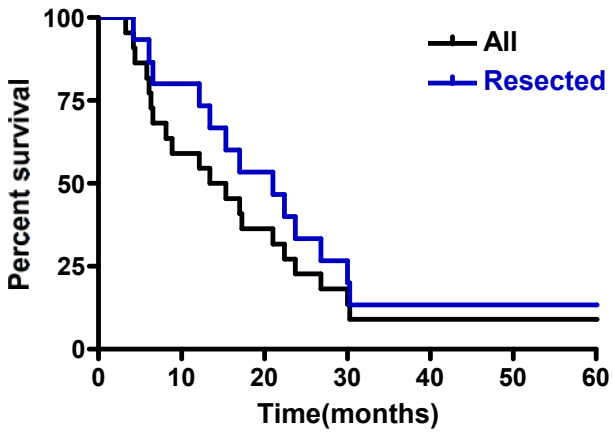

Fig.2 Overall survival for all 22 patients and the resected patients

Table 5. Results on the preoperative radiotherapy for resected pancreatic Cancer

Author	year	No	EBRT DOSE	Chemo	Median	1-y Surv.	Local Failure
Staley CA	1996[7]	39	50.4	5FU	19	81%	11%
Hoffman JP	1998[8]	24	50.4	5FU	15.7	71	13
Pister PWT	2002[9]	20	30	PAC	19	75	
Maginin V	2003[10]	19	50.4	5FU	30	81	
NIRS	2010	14	44.8-48.0	-	21	86	0

B. Short-course (8 fractions/2 weeks) preoperative treatment of pancreatic cancer (Protocol 0203)

The phase I/II trial of preoperative carbon ion radiotherapy (8 fractions/2 weeks) for pancreatic cancer prior to surgery was performed with the purpose of establishing the safety of carbon ion radiotherapy, determining the recommended dose, and substantiating its preoperative efficacy.

At present, we are giving 36.8GyE for a short-course trial, and patient enrollment in the trial is in progress, with the outcomes pending further follow-up and analysis. The 19 eligible patients were analyzed. Fifteen (79%) of the 19 patients underwent resection. The toxicities were relatively few and mild. All patients completed the scheduled treatment course. These early data indicate the same high level of local control as the 9906 protocol. However, the histological effect is showing a tendency of being somewhat inferior to the 9906 protocol, suggesting that the dose is not adequate. The 3-year overall survival rates were 37% for all patients and 52% in the resected patients. Although this trial is still ongoing, it appears that carbon-ion radiotherapy provides good local control and offers a survival advantage, without unacceptable morbidity. In view of the reports in the literature on drugs with a sensitizing effect in conjunction with heavy particle beams, further studies are scheduled to search for an even more effective treatment modality.

C. Locally advanced pancreatic cancer (Protocol 0204, 12 fractions/3 weeks)

The phase I/II trial of carbon ion radiotherapy (12 fractions/3 weeks) for locally advanced pancreas cancer was performed so as to establish the safety of carbon ion radiotherapy, determine the recommended dose, and confirm its efficacy.

Patients and Methods

Between April 2003 and February 2007, 47 patients judged according to the staging criteria of the Japanese Committee on Cancer as being clinical stages IVa or IVb without distant metastasis were enrolled in this trial. As one patient was excluded because they had received chemotherapy before treatment, 46 patients were eligible for analysis. Patients eligible for study entry had been histologically or cytologically confirmed to have locally advanced unresectable pancreatic ductal carcinoma. Th eligibility criteria were: confirmation of ductal carcinoma by CT findings, age 80 years or younger, an ECOG performance score of 0, 1, or 2, and hepatic, renal and cardiopulmonary function sufficient for undergoing surgery. The criteria of the CT findings for non-resectability of the tumor included tumor encasement of the celiac trunk and/or superior mesenteric artery. Carbon ion therapy was given once daily, 4 days a week, for a fixed 12 fractions over 3 weeks. The dose was set at 38.4 GyE and escalated to 52.8 GyE in 5% increments.

Results

The toxicity to organs such as the skin, bladder and digestive tract was assessed according to the NCI-CTC (acute) and RTOG/EOTRC (late) classifications. Tumor response was defined by the RECIST scoring system as the maximum tumor response observed during the first 6 months after the initiation of carbon ion radiotherapy. Local recurrence was defined in terms of lesions occurring in the tumor bed.

Survival was calculated as the time from the initiation of carbon ion therapy until death. Survival curves were estimated by the Kaplan-Meier method. All toxicities in the 46 patients receiving carbon ion therapy are listed in Table 8. All patients completed the scheduled treatment course. Seven grade 3 acute and one grade 3 late toxicities were observed. Six of the 7 patients with grade 3 acute toxicities were anorexic, and one patient had developed cholangitis. Tumor response was evaluated in 46 lesions. A CR was observed in one lesion, a PR in 7, SD in 37, and PD in one. The local control rates at 1 year in the 46 analyzed patients and in the patients receiving 45.6 GyE or more were 76% and 95%, respectively (Fig.3). The overall survival estimates for the 46 analyzed patients and the patients receiving 45.6 GyE are shown in Fig. 4. One-year overall survival was 43%.

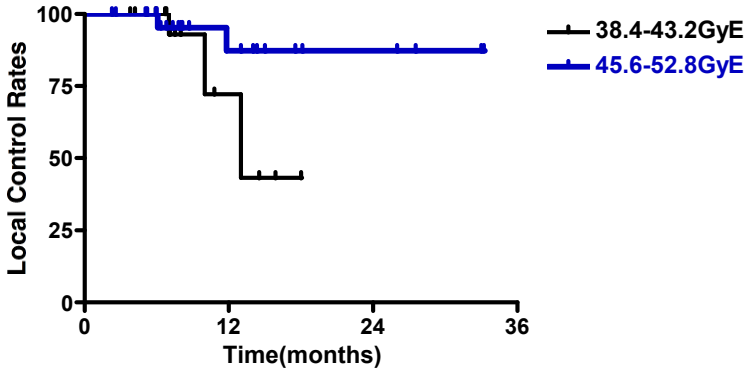

Fig. 3 Local control rates for all 46 patients by total dose

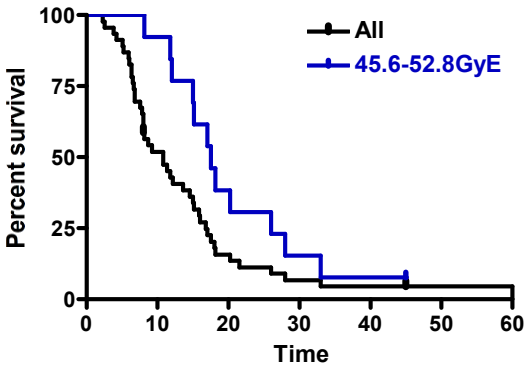

Fig.4 Overall survival for all 46 patients and the higher dose group

A maximum acute reaction of grade 3 was observed in two-thirds of the patients (67%) at 52.8 GyE. From these results, we concluded that the maximum tolerated dose of carbon ions is 52.8 GyE/12 fractions/3 weeks.

On the basis of the literature on drugs with a sensitizing effect in conjunction with heavy particle beams, further studies were scheduled in an effort to find even more effective treatment modalities based on a combination of chemo- and radiotherapy. We started a phase I/α clinical trial of gemcitabine combined with carbon-ion therapy for patients with local advanced pancreatic cancer in April 2007.

D. Combination therapy with gemcitabine and carbon-ion therapy (Protocol 0513, 12 fractions/3 weeks**)**

From the results of the 0204 clinical study, it could be concluded that carbon ion radiotherapy considerably improved the control of locally advanced pancreatic cancer with acceptable morbidity in the surrounding normal tissues, but a sufficient survival benefit was not be achieved. On the basis of the literature on drugs with a sensitizing effect in conjunction with heavy particle beams, further studies were scheduled in an effort to find even more effective treatment modalities based on a combination of chemo- and radiotherapy. We thus started a phase I/II clinical trial of gemcitabine combined with carbon-ion therapy for patients with locally advanced pancreas cancer in April 2007.

The dose escalation schedule of gemcitabine combined with carbon ion radiotherapy is shown in Fig. 5. First the dose of carbon ion radiation was fixed at 43.2 GyE and the dose of gemcitabine was increased from 400 mg to 1000 mg; then the dose of gemcitabine was fixed at 1000 mg and the dose of carbon ion radiation was increased from 45.6 Gye to 50.4 GyE. Carbon ion therapy was given once daily, 4 days a week, for a fixed 12 fractions over 3 weeks. Gemcitabine was given once weekly (Fig.6).

At present, we are giving 1000 mg/m^2 of gemcitabine combined with 50.4 GyE of carbon ions. All patients completed the scheduled treatment course. Gemcitabine combined with carbon ion radiotherapy is well tolerated by patients with pancreatic cancer. The 1-year overall survival rates were 82% for 12 patients given 1000 mg/m^2 combined with 43.2 GyE of carbon ions. While the trial is still ongoing, carbon-ion radiotherapy seems to provide good local control and offer a survival advantage without unacceptable morbidity.

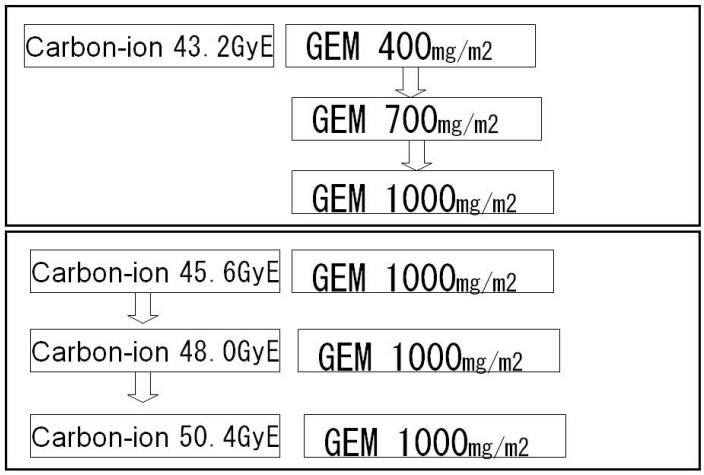

Fig. 5 Dose Escalation Schedule (0513)

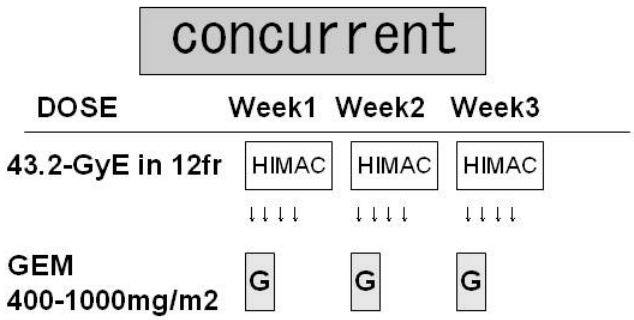

Fig.6 Treatment schema for combination Of gemcitabine andcarbon-iontTherapy

References

［1］ Registration committee of pancreatic cancer. Annual Report of Nationwide Survey of Pancreatic Cancer. J of Jpn Panc Surg. 18: 101-169, 2003

［2］ Lillemoe KD, Cameron JL, Hardacre JM et al. Is prophylactic gastrojejunostomy indicated for unresectable periampullary cancer? Ann Surg. 230: 322-330, 1999

［3］ Prat F, Chapat O, Ducot B et al. A randomized trial of endoscopic drainage methods for inoperable malignant stricture of the common bile duct. Gastrointest Endosc. 47: 1-7, 1998

［4］ Roldan GE, Gunderson LL, Nagorney DM et al. External beam versus intraoperative and extrabeam irradiation for locally advanced pancreatic cancer: Cancer. 61:1110-1116, 1988

［5］ Moertel CG, Gundeson LL, Mailliard JA et al. Early evaluation of combined fluorouracil and leucovorin as a radiation enhancer for locally unresectable, residual, or recurrent gastrointestinal carcinoma. J Clin Oncol. 12:21-27, 1994

［6］ Griffin JF, Smalley SR, Jewell W et al. Patterns of failure after curative resection of pancreatic carcinoma. Cancer. 66: 56-61, 1990

［7］ Staley CA, Lee JE, Cleary KR et al. Preoperative chemoradiation, pancreaticoduodenectomy, and intraoperative radiation therapy for adenocarcinoma of the pancreas head. Am J Surg 171:118-126,1996

［8］ Hoffman JP, Lipsitz S, Pisansky T. Phase II trial of preoperative radiation therapy and chemotherapy for patients with localized, resectable adenocarcinoma of the pancreas. J Clin Oncol 16: 317-323, 1998

［9］ Pisters PWT, Janjan WNA, Cleary KR. Preoperative paclitaxiel and concurrent rapid-fraction radiation for resectable pancreas adenocarcinoma. J Clin Oncol 20:2537-2544, 2002

［10］ Magnin M, Mountardier V, Giovannini MH, Neoadjuvant preoperative chemoradiation in patients with pancreatic cancer. Int J Radiation Oncology Biol Phys 55: 1300-1304, 2003

［11］ Sato K, Yamada H, Ogawa K, et al. Performance of HIMAC. Nuclear Physics A. 588:229-234, 1995

［12］ Kanai T, Endo M, Minohara S, et al. Biophysical characteristics of HIMAC clinical irradiation system for heavy-ion radiation therapy. Int J Radiat Oncol Biol Phys. 44:201-210, 1999

Carbon Ion Radiotherapy for Liver Cancer

Hiroshi Imada, Shigeo Yasuda, Shigeru Yamada, Makoto Shinoto, Kazuhiko Oonishi, Tadashi Kamada, and Hirohiko Tsujii

Hospital, Research Center for Charged Particle Therapy, National Institute of Radiological Sciences, Chiba, Japan
e-mail address: h_imada@nirs.go.jp

Abstract

The objective of this paper is to present a summary of a clinical study on carbon ion radiotherapy (C-ion RT) for hepatocellular carcinoma (HCC) conducted from April 1995 to August 2005 at the Research Center for Charged Particle Therapy, National Institute of Radiological Sciences, in Japan. A total of 193 patients with HCC were enrolled in the clinical trial of carbon ion beams. In the first and second phase I/II clinical trials, dose escalation experiments were carried out in incremental steps of 10%, resulting in the confirmation of both the safety and efficacy of short-course regimens of 12, 8 and 4 fractions. Based on the results, a phase II clinical study with fixed fractionation, that is, 52.8 GyE/4 fractions, was performed. A total of 47 patients were treated during this phase II study, which resulted in low toxicity and attained a high local control rate (96%) for 5 years after treatment. The last clinical study was conducted from April 2003 to August 2005 with a more hypofractionated regimen of 2 fractions/2 days, in which 36 patients were safely treated within a dose escalation range from 32.0 GyE to 38.8 GyE. The 2-fraction therapy protocol is continuing under the license of Highly Advanced Medical Technology. There have been no therapy-related deaths and no severe adverse events. We can conclude that, because of the low toxicity and high local control rate, C-ion RT has a promising potential as a new, radical, and minimally invasive therapeutic option for HCC.

Introduction

Hepatocellular carcinoma (HCC) is one of the most common malignant malignancies with the third highest annual mortality of 598,000 throughout the world (2002). This disease is especially prominent in Asia and Africa, as well as a number of countries in Europe, including Spain, Italy, Greece, and France. Worldwide, some 626,000 new cases were reported in 2002. In recent years, the incidence of HCC has shown an increasing trend in Australia, India, Israel, Canada, Italy, Spain, Finland and the USA. HCC is associated with liver cirrhosis in 80% of all HCC patients. This disease is thus often an advanced form of hepatic disorder resulting from hepatitis C or B viral infection. HCC patients often require repeated treatments owing to the multicentric nature of carcinogenesis in the cirrhotic liver. Therefore, both radical effect and minimal invasiveness are essential for the treatment of HCC. A variety of therapies are currently available for the treatment of HCC, but each of them has its specific limitations. So far, none has brought on the market any agent that satisfies the two essential requirements (radicality and minimal invasiveness) for the treatment of HCC tumors of any size encountered in practice.

Methods and Materials

1. Outline of carbon ion radiotherapy for HCC -Clinical Trials to Medical Treatment – (Table 1)

Clinical trials with carbon ion radiotherapy (C-ion RT) for HCC were initiated in April 1995 (1). A total of 193 patients with HCC were enrolled in the trials. In the first and second phase I/II clinical trials, dose escalation

studies were carried out in incremental steps of 10% each in order to find the optimum dose. In the first of these trials, 24 patients were treated with a 15-fraction regimen at a total dose range of 49.5-79.5 GyE. In the second trial, 86 patients were treated with short-course regimens, at total dose ranges of 54.0-69.6 GyE in 12 fractions, 48.0-52.8 GyE in 8 fractions, and 48.0-52.8 GyE in 4 fractions. Based on the results of these studies, a third protocol was established to implement a phase II clinical trial using a fixed total dose of 52.8 GyE spread over 4 fractions of 13.2 GyE each (2). The fourth protocol, a phase I/II clinical study, was performed using an even more hypofractionated regimen of 2 fractions/2 days at total dose levels ranging from 32.0 GyE to 38.8 GyE (3). The eligibility criteria common to all four of these protocols were as follows: (a) biopsy-proven HCC (histological diagnosis); (b) no tumor thrombosis of the main trunk of the portal vein; (c) no multiple viable lesions outside the planning target volume; (d) no previous treatment to target tumors by other forms of RT; (e) ECOG performance status of 0–2; (f) no other active cancers; and (g) digestive tract not in contact with the clinical target volume. Most of the subjects enrolled under these protocols had been judged as not amenable to, or as having had recurrence after, other treatments, or as having no prospect of an adequate treatment effect with any of the existing therapies. This 2-fraction therapy is currently ongoing according to guidelines allowing careful step-wise dose escalations at a 5% increase rate under the license of Highly Advanced Medical Technology.

Table 1. Outline of carbon ion radiotherapy for HCC

Carbon Ion Radiotherapy for HCC

April, 1995～March, 2010 **Total n=272**

Protocol	Disease	Category	Fractionation	Period	Number
1. 9401	HCC	Phase I/II study	15f/5w	1995.4～1997.3	24
2. 9603	HCC	Phase I/II study	12f/3w	1997.4～2001.3	34
			8f/2w		24
			4f/1w		28
3. 0004	HCC	Phase II study	4f/1w	2001.3～2003.3	47
4. 0202	HCC	Phase I/II study	2f/2days	2003.4～2005.8	36
Guideline	HCC	Highly Advanced Medical Technology	4f/1w	2005.9～	10
			2f/2days	2006.4～	69

2. Carbon ion radiotherapy

2-1. Preparation for treatment

One or two metal markers (0.5 × 3 mm) made of iridium wire were inserted near the tumor under ultrasound imaging guidance as landmarks for target volume localization. The irradiation fields were established with a three-dimensional therapy plan based on 5-mm-thick CT images. CT planning was performed using the HIPLAN, which was originally developed for 3D treatment planning (4). The clinical target volume was defined according to the shape of the tumor plus a 1.0-1.5-cm margin. The median target volume was 159 ml (range: 37-1466 ml). Double right-angled field geometry was used for irradiation in most patients (double right-angled field: 77%, double oblique field: 7%, 3-field: 14%, 4-field: 2%). The supine or prone position was selected

according to the location of the tumor. Respiration gating was employed in the CT scan planning and irradiation stages (5).

2-2. Verification of patient position and target volume localization

To accurately reproduce the patient position, a low-temperature thermoplastic sheet and a customized cradle were used. Patients were immobilized on a rotating couch to permit either vertical or horizontal beam irradiation from any angle. To assess the accuracy of patient position and target volume localization, orthogonal fluoroscopy and radiography were used immediately prior to each treatment session.

3. Follow-up and evaluation criteria

All patients were assessed according to a predetermined schedule. After C-ion RT, patients were evaluated on the basis of physical examinations and blood tests once a month for the first year, once every 3 months for the following year, and once every 3–6 months thereafter. Contrast-enhanced CT or MRI was performed every 3 months for the first 2 years and every 6 months thereafter. Local control was defined as no sign of regrowth or new tumors in the treatment volume. Local recurrence was defined as failure of local control. Overall survival was measured from the starting date of treatment until the date of death from any cause. Acute and late toxicities were assessed using the National Cancer Institute Common Criteria, version 2.0, and the Radiation Therapy Oncology Group/European Organization for Research and Treatment of Cancer late radiation morbidity scoring scheme. In addition, liver toxicity was assessed by Child-Pugh score, a commonly used marker of hepatic functional reserve in chronic liver disease, on a rating scale from 5 to 15 points, with the score increasing with a deterioration of hepatic function.

Results

The clinical trial results up to the 4-fraction regimen for which observation has been continued for 5 years or longer are described below. The results of the 2-fraction therapy protocol were not included in this analysis because the study is still ongoing and the post-treatment observation time has been relatively brief..

1. Toxicities

No therapy-related deaths occurred. There was no grade 4 hepatic toxicity. With regard to the Child-Pugh score, an increase in score count associated with C-ion RT remained within 1 point or below in many patients in the early (within 3 months of the start of radiotherapy) and late phases (after 3 months) (Fig. 1). This demonstrated that changes in liver function remained minor after C-ion RT was initiated. The number of cases reported with a score increase of 2 points or more in the late phase, which is of particular clinical significance, tended to be smaller with decreasing fraction numbers. No serious adverse effects were noted in the digestive organs.

2. Anti-tumor effect

HCC develops in a successive manner, fostered by the underlying cirrhosis of the liver. Patient survival is therefore determined by the overall results, including the treatment of recurrent lesions and also the treatment of hepatic insufficiency in cases where there is a decline in liver function. As a result, the survival rate does not reflect the efficacy of any particular treatment alone. In comparing the effectiveness of the different therapies for HCC, it is therefore easier to make a judgment on the basis of the local control rate rather than the survival rate. In the present clinical trials, other treatments proved ineffective or led to recurrence in 57% of the patients, and as the phase I/II trials were conducted as dose escalation studies to determine the recommendable dose, there is a possibility that some of the patients may have been treated with a dose that was less than optimal. It is therefore not possible to make a simple comparison of the survival rates achieved in these clinical trials with other treatments.

In this study, only patients who had been observed for 5 years or longer after the initiation of C-ion RT were eligible for analysis, and the local control rates for the analyzed lesions are shown separately according to protocol and fractionation regimen (Table 2). There were no significant differences in the control rate among the

different fractionation schedules.

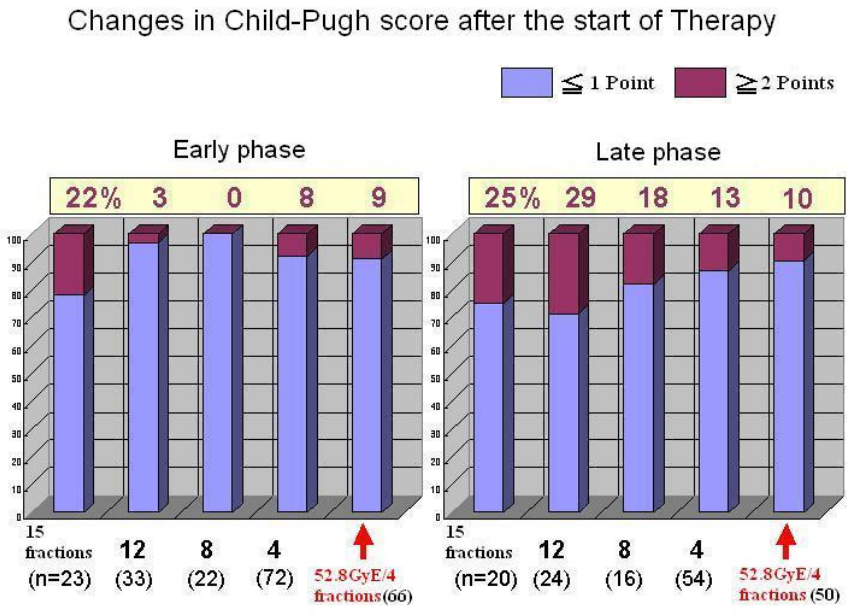

Fig. 1: Changes in Child-Pugh score before and after C-ion RT

Variations in the Child-Pugh score, an international standard used to assess the degree of hepatic insufficiency before and after irradiation, were studied. The degrees of hepatic insufficiency can be evaluated with the Child-Pugh score on a scale from 5 to 15 points. The score increases as the degree of hepatic insufficiency increases.

The increase in score associated with C-ion RT remained within 1 point or below in many patients in the early (within 3 months of start of radiotherapy) and late phases (after 3 months).

Table 2. Results of clinical trials for HCC with C-ion RT

Trial		Phase I/II	Phase I/II			Phase II	52.8GyE/4f
Number of fractions		15	12	8	4	4	4
Total dose (GyE)		49.5-79.5	54.0-69.6	48.0-58.0	48.0-52.8	52.8	52.8
Number of lesions		24	34	24	28	47	69
Maximum tumor diameter (cm)	Median	5.0	3.7	3.1	4.6	3.7	4.0
	Range	2.1-8.5	1.5-7.2	1.2-12.0	2.2-12.0	1.2-7.5	1.2-12.0
Recurrent Tumor	yes	18 (75%)	18 (53%)	16 (67%)	18 (64%)	20 (43%)	35 (51%)
	no	6 (25%)	16 (47%)	8 (33%)	10 (36%)	27 (57%)	34 (49%)
1-year local control (%)		92	97	91	89	96	94
3-year local control (%)		81	86	86	89	96	94
5-year local control (%)		81	86	86	89	96	94

Discussion

1. Standard therapies for HCC

The standard therapies for HCC are hepatectomy, transcatheter arterial embolization (TAE), percutaneous ethanol injection (PEI), radio-frequency ablation (RFA), and liver transplantation. According to the Survey and Follow-up Study of Primary Liver Cancer in Japan, the relative use of these therapies in the treatment records of

all patients for the two-year period from January 1, 2004 through December 31, 2005 were: hepatectomy 32%, TAE 32%, and percutaneous local therapy involving PEI, percutaneous microwave coagulation therapy (PMCT), and RFA 31%. Each of these procedures have their respective merits and drawbacks. For example, while hepatectomy provides the best certainty of removing cancer cells, the procedures also results in serious stress on both the liver and the body as a whole. TAE is clinically useful and has a relatively low degree of invasiveness, but is of limited radicality. PEI and RFA, on the other hand, are simple procedures offering a high degree of radicality but their effect is limited to comparatively small tumors (less than 3 cm in diameter). The use of radiotherapy for HCC has been considered difficult in view of the problems of radiation-induced hepatic insufficiency (6, 7). Progress in the development of irradiation devices in recent years, however, has made it possible to achieve highly localized irradiation. This has spurred advances in radiotherapy research for liver cancer (8-15).

2. Optimal candidates for C-ion RT

We have already reported that C-ion RT used for the treatment of HCC is safe and effective, and that it causes only minor liver damage (1). We investigated the reason why liver function is retained, then, non-irradiated lesion of liver is considered to contribute to the retention of liver function (16). For patients with extensive infiltration and those with multiple lesions it is difficult to achieve radicality with C-ion RT alone. C-ion RT is indicated for patients with a level of liver function corresponding to medium or better (Child-Pugh grade A or B). For small lesions 3 cm or less, however, other minimally- invasive, effective, and low-cost therapies, such as PEI and RFA, are available. In contrast, lesions larger than 3 cm are difficult to treat with PEI or RFA alone, making them ideal targets for C-ion RT. Especially for patients with locally concentrated lesions over 3 cm and up to 5 cm, the local control rate was 90% at 1 to 5 years, and the overall survival rate was 93% at 1 year, 57% at 3 years, and 40% at 5 years for C-ion RT. In addition, when the patient had relatively good liver function of Child-Pugh grade A, the overall survival rate was 88% at 1 year, 75% at 3 years and 63% at 5 years (Fig. 2).

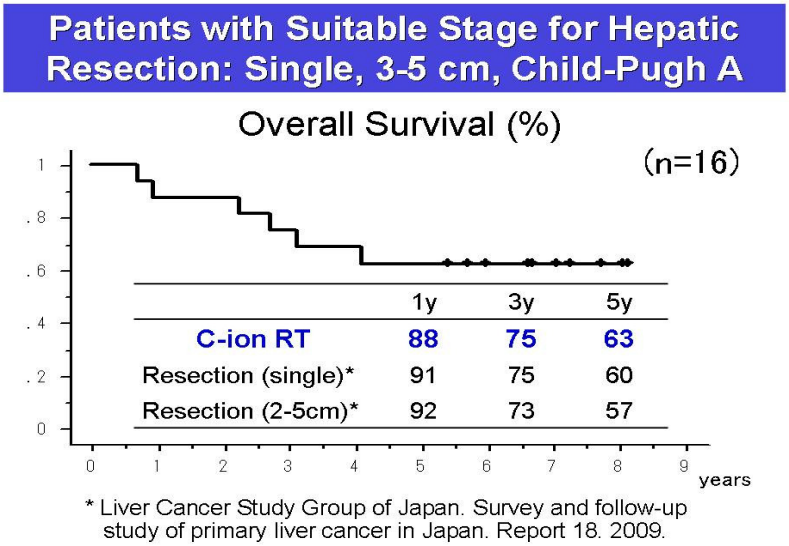

Fig. 2: Overall survival rates in patients suitable for C-ion RT: those with 3-5cm lesion and Child-Pugh grade A status

These outcomes seem to be comparable to those achieved with other therapies, for example, hepatectomy, for which overall survival rates of 91% at 1 year, 75% at 3 years, and 60% at 5 years after treatment for a single lesion, and of 92% at 1 year, 73% at 3 years, and 57% at 5 years for tumors 2 to 5 cm in diameter, have been

reported (17). These data suggest that the patients with locally concentrated lesions over 3 cm, and up to 5 cm, are the best candidates for C-ion RT.

In terms of HCC adjacent to the porta hepatis, minimally- invasive treatment without complications is an important issue. We compared the efficacy and toxicity of C-ion RT of 52.8GyE in 4 fractions for patients with HCC in terms of tumor location (adjacent to the porta hepatis or not). There were no significant differences in liver toxicity. Excellent local control was obtained independent of tumor location. Therefore, in certain patients with a higher risk of injury to the bile duct when undergoing RFA, C-ion RT appears to offer a promising therapeutic alternative (18).

Conclusion

C-ion RT is safe and effective, and it seems to have promising potential as a new, radical, and minimally invasive therapeutic option for HCC. However, further careful follow-up is still needed to confirm its clinical efficacy in practical medicine.

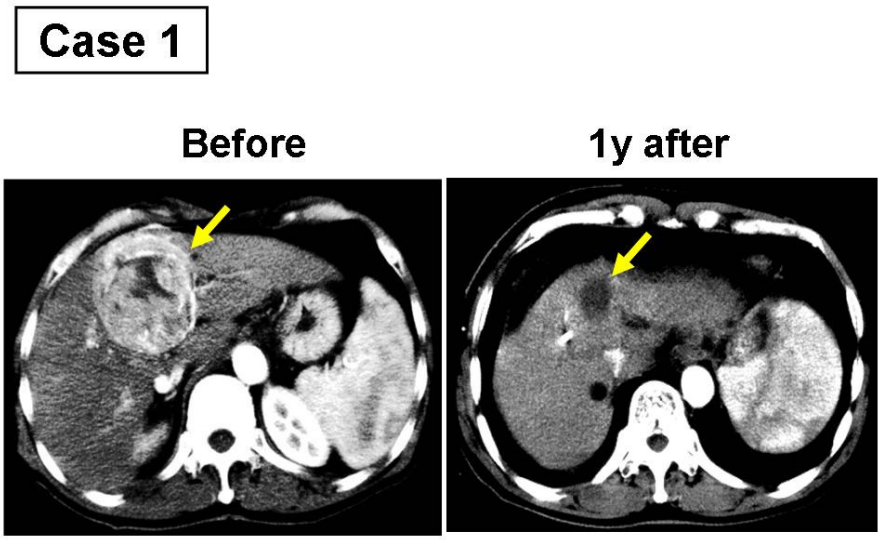

Fig. 3: Case 1
A 67-year-old male had a HCC of 7 cm in diameter in segment IV. He survived for 5 years after C-ion RT of 72.0 GyE in 15 fractions.

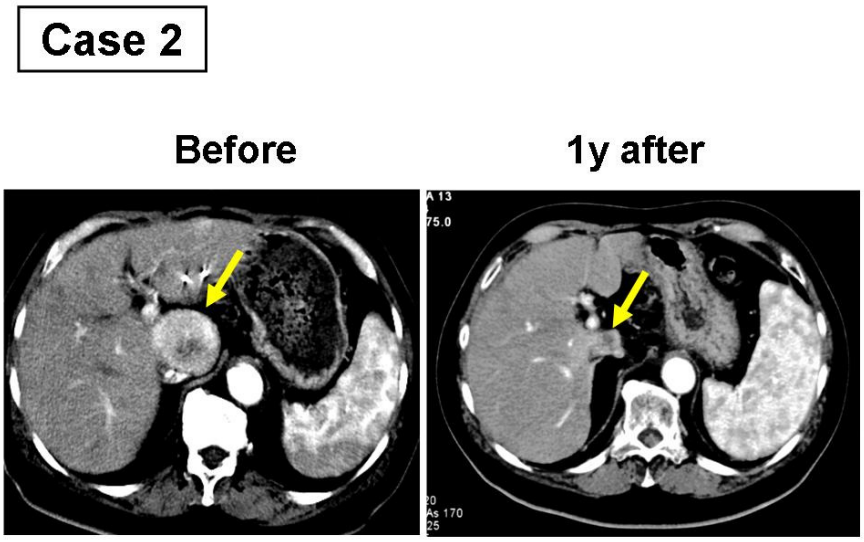

Fig. 4: Case 2
A 72-year-old male had a HCC of 4.6 cm in diameter in segment I. He remained alive for 8 years after C-ion RT of 52.8 GyE in 4 fractions.

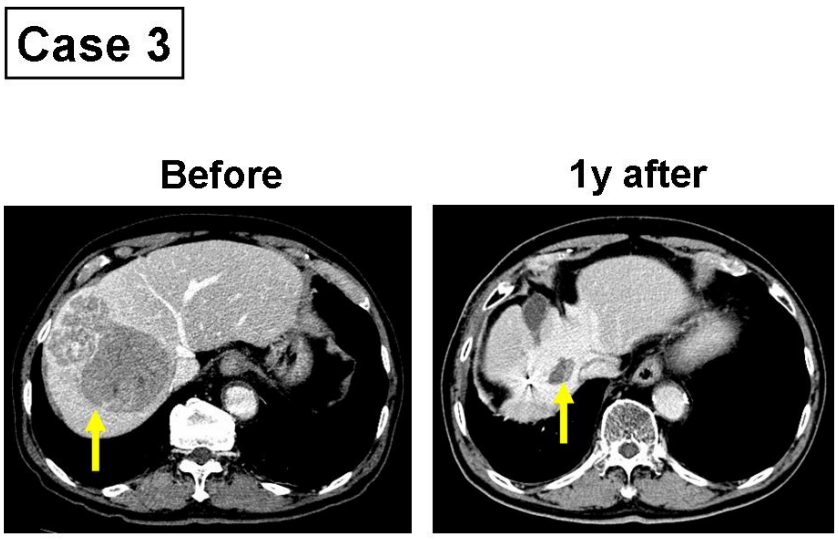

Fig. 5: Case 3
A 77-year-old man had a HCC of 10.5×7.7 cm in the right hepatic lobe. He is still alive 3 years after C-ion RT of 38.8 GyE in 2 fractions.

References

[1] Hirotoshi Kato, Hirohiko Tsujii, Tadaaki Miyamoto, et al. Results of the first prospective study of carbon ion radiotherapy for HCC with liver cirrhosis. Int J Radiat Oncol Biol Phys 2004; 59: 1468-1476.

[2] Hirotoshi Kato, Shigeru Yamada, Shigeo Yasuda, et al. Phase II study of short-course carbon ion radiotherapy (52.8GyE/4-fraction/1-week) for HCC. HEPATOLOGY 2005;42,Suppl.1:381A.

[3] Hirotoshi Kato, Shigeru Yamada, Shigeo Yasuda, et al. Two-fraction carbon ion radiotherapy for HCC: Preliminary results of a phase I/II clinical trial. J Clin Oncol 2005;23,Suppl.:338s.

[4] Endo M, Koyama-Ito H, Minohara S, et al. HIPLAN-A HEAVY ION TREATMENT PLANNING SYSTEM AT HIMAC. J. Jpn. Soc. Ther. Radiol. Oncol. 1996; 8: 231-238.

[5] Minohara S, Kanai T, Endo M, et al. Respiratory gated irradiation system for heavy-ion radiotherapy. Int J Radiat Oncol Biol Phys 2000;47: 1097-1103.

[6] Ingold DK, Reed GB, Kaplan HS, et al. Radiation hepatitis. Am J Roentgenol 1965;93:200-208.

[7] Phillips R, Murikami K. Primary neoplasms of the liver. Results of radiation therapy. Cancer 1960;13:714-720.

[8] Ohto M, Ebara M, Yoshikawa M, et al. Radiation therapy and percutaneous ethanol injection for the treatment of HCC. In: Okuda K, Ishak KG, editors. Neoplasm of the Liver. Tokyo: Springer-Verlag; 1987. p. 335-341.

[9] Robertson JM, Lawrence TS, Dworzanin LM, et al. Treatment of primary hepatobiliary cancers with conformal radiation therapy and regional chemotherapy. J Clin Oncol 1993;11:1286-1293.

[10] Yasuda S, Ito H, Yoshikawa M, et al. Radiotherapy for large HCC combined with transcatheter arterial embolization and percutaneous ethanol injection therapy. Int J Oncol 1999;15:467-473.

[11] Cheng J C-H, Chuang VP, Cheng SH, et al. Local radiotherapy with or without transcatheter arterial chemoembolization for patients with unresectable HCC. Int J Radiat Oncol Biol Phys 2000;47:435-442.

[12] Guo W-J, Yu E-X. Evaluation of combined therapy with chemoembolization and irradiation for large HCC. Br J Radiol 2000;73:1091-1097.

[13] Matsuzaki Y, Osuga T, Saito Y, et al. A New, Effective, and Safe Therapeutic Option Using Proton Irradiation for HCC. GASTROENTEROLOGY 1994;106:1032-1041.

[14] Kawashima M, Furuse J, Nishio T, et al. Phase II Study of Radiotherapy Employing Proton Beam for HCC. J Clin Oncol 2005;23: 1839-1846.

[15] Chiba T, Tokuue K, Matsuzaki Y, et al. Proton Beam Therapy for HCC: A Retrospective Review of 162 Patients. CCR 2005;11:3799-3805.

[16] Imada H, Kato H, Yasuda S, et al. Compensatory enlargement of the liver after treatment of hepatocellular carcinoma with carbon ion radiotherapy – Relation to prognosis and liver function. Radiother Oncol 2010;96:236-242.

[17] Liver Cancer Study Group of Japan. Survey and follow-up study of primary liver cancer in Japan. Report 18. Kyoto: Shinko-Insatsu; 2009

[18] Imada H, Kato H, Yasuda S, et al. Comparison of efficacy and toxicity of short-course carbon ion radiotherapy for hepatocellular carcinoma depending on their proximity of the porta hepatis. Radiother Oncol 2010;96:231-235.

Carbon Ion Radiotherapy for Prostate Cancer

Hiroshi Tsuji, Tohru Okada,
Tadashi Kamada, Hirohiko Tsujii,
and the Working Group for Genitourinary Tumors

Research Center Hospital of Charged Particle Therapy, National Institute of Radiological Sciences, Chiba, Japan
e-mail address:h_tsuji@nirs.go.jp

Abstract

Purpose: An up-to-date analysis of the results of hypofractionated conformal carbon ion radiotherapy (C-ion RT) for localized prostate cancer was performed to determine the normal tissue morbidity, biochemical relapse-free rate (bNED), and patient survival.
Methods and Materials: Nine hundred and three prostate cancer patients who received the C-ion RT that had been established by two prior dose-escalation studies were analyzed with regard to toxicity, survival, and bNED.
Results: Only 1 out of 818 patients followed up for at least 12 months developed grade 3 genitourinary toxicity, and no grade 3 or higher toxicities were observed in the rectum. The incidence of grade 2 rectum and GU morbidity were only 2.0% and 5.6%, respectively. The incidence of late toxicity in the patients treated with C-ion RT for 16 fractions was lower than that for patients who received 20 fractions. The overall bNED at 5 years was 90.9%, with only five local recurrences. The bNED of the 16-fraction C-ion RT was comparable to that of 20 fractions. The Gleason's score, T-stage, and initial PSA were significant prognostic factors for bNED, and the T-stage and initial PSA were also significant prognostic factors for the overall survival rate. C-ion RT with the established dose fractionation regimen yielded satisfactory bNED with very few local recurrences, and with minimal morbidity. Therefore, C-ion RT in 16 fractions could offer an even lower incidence of toxicities than 20 fractions, without any decrease in the biochemical control of the disease.

Introduction

Prostate cancer is a slow-growing tumor occurring in advanced-age male patients, but the incidence and mortality rate are both rapidly increasing in Asian as well as Western countries. Radiotherapy is one of the treatments of choice for localized or locally-advanced tumors of the prostate. In order to obtain satisfactory results, sufficient efficacy with a tolerable dose of radiation is required. Prostate tumors are relatively radio-resistant, and severe damage to adjacent normal tissues will have deleterious effects on the quality of life after the treatment, thus making radiotherapy challenging.

Carbon ion radiotherapy (C-ion RT) may be the ideal radiation treatment for prostate cancer because of the unique physical and biological advantages of carbon ion beams (1). The successful results obtained with novel conformal radiotherapy techniques, such as three-dimensional conformal radiotherapy (3DCRT) and intensity modulated radiotherapy (IMRT) (2-4), are evidence that dose conformity confers clear advantages to the radiotherapy of prostate cancer compared to conventional methods. Carbon ion beams offer superior dose conformity in the treatment of deep-seated tumors compared to the state-of the-art techniques of X-ray therapy,

and therefore C-ion RT possesses a greater potential of further improving the treatment outcome for prostate cancer patients (1).

In this respect, high-linear energy transfer (LET) radiation therapy with fast neutrons was found to yield an excellent tumor control rate. Its unacceptably high toxicity (5,6), however, has stood in the way of this therapy coming into wider use. The high incidence of morbidity associated with fast neutron therapy was mainly due to an inferior dose concentration of neutron beams. This problem, however, can be solved by the use of heavy charged particle beams, such as carbon ions, without foregoing the radiobiological advantages of high LET radiation.

To establish an appropriate dose fractionation regimen for C-ion RT, two phase I/II clinical studies have been performed (7-9) at the National Institute of Radiological Sciences in Chiba, Japan (NIRS) since 1994, using carbon ion beams generated by the Heavy Ion Medical Accelerator in Chiba (HIMAC). A phase II clinical study was then started in April 2000, using the established treatment method of hypofractionated C-ion RT with the recommended dose of 66.0GyE in 20 fractions over 5 weeks that had been proven effective in the phase I/II studies (10,11). The safety and efficacy of this treatment strategy was further confirmed by this phase II study, and approval for the use of this modality as a highly advanced medical technology was obtained in November of 2003. This article presents the methods and updated outcomes of this established C-ion RT, and also describes its future prospects at the NIRS.

Materials and Methods

1. Protocols

Up to now, a total of 1,106 patients have been enrolled in the study, 97 patients in the first two phase I/II studies, 176 in the phase II study, and 833 after official approval for the application of the procedure as a highly advanced medical technology (Table 1). Of this total, 903 patients received the established treatment of C-ion RT, and were followed up for at least 6 months, and their data was analyzed.

Patients were eligible if they had histologically proven prostatic adenocarcinoma, that is, stage T1, T2 or T3 primary tumors (12) without radiologically detectable distant metastasis (M0), involvement of regional lymph nodes (N0, pN0), or solitary, non-fixed involvement of regional lymph nodes diagnosed by staging pelvic lymphadenectomy (pN1). Eligible patients were required to be treatment-naive, except for hormone therapy. All patients signed an informed consent form approved by the local institutional review board. Pathological specimens were reviewed centrally before registration, and those of the phase I/II studies were reviewed retrospectively.

Until September 2005, patients were stratified into two subgroups, high-risk and low-risk, according to their T-staging, Gleason's score (GS), and initial serum PSA. Thereafter, the high-risk group was further divided into two groups — an intermediate-risk group and a true high-risk group. For the true high-risk group patients, those with a T3 primary tumor, GS $\geq$ 8 or a serum PSA value $\geq$ 20 ng/ml, long-term ($\geq$ 24 months) hormonal therapy was applied in combination with C-ion RT. Patients in the low-risk group, who had T1/T2a tumors with GS $<$ 7 and serum PSA $<$ 20 ng/ml, received only C-ion RT. For the intermediate-risk group of patients, consisting of those with a serum PSA value $<$ 20 ng/ml and a T2b primary tumor or GS of 7, combined treatment with C-ion RT and short-course (6 months) hormonal therapy was performed (Fig.1).

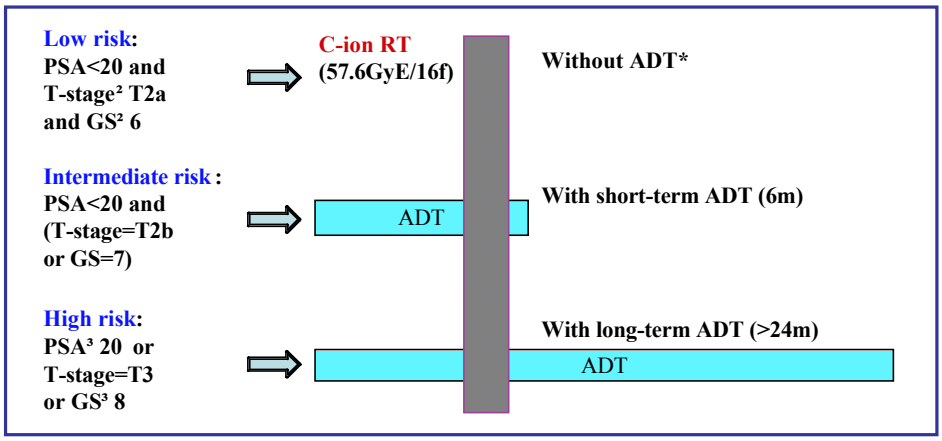

*ADT; Androgen Deprivation Therapy

Figure 1 Current treatment strategy for prostate cancer at NIRS
Patients were divided into three groups of high, intermediate, and low according to their T-stage, initial PSA, and centrally reviewed Gleason score.

Table1. Clinical studies of C-ion RT for prostate cancer at NIRS

Protocol	Study Design	T-stage	Period (C-ion RT)	Total Dose (Gy RBE/f)	Hormone therapy	Number of patients
9402	Phase I / II Dose escalation	T2b~T3	95.6～97.12	54.0～72.0/20	(+)	35
9703	Phase I / II Dose escalation	T1~T2a	98.1～00.2	60.0～66.0/20	(-)	20
	Fixed dose	T2b~T3		66.0/20	(+)	42
9904	Phase II Fixed dose	T1~T3	00.4～03.11	66.0/20	High*(+) Low* (-)	176
		T1~T3	03.12~10.2	66.0, 63.0/20 57.6/16	High* >24m Interm* =6m Low* (-)	833
Total			95.6～10.2			1,106

*Stratified by risk factors; Clinical stage, initial PSA, and Gleason score

2. Carbon Ion Radiotherapy

1) Treatment techniques

In order to make good use of the excellent dose concentration of the carbon ion beam, new techniques were developed to maintain the high precision and sufficient reproducibility in the patient positioning and field placement. The techniques that were applied include:

a) Rigid immobilization

b) Volume control of the rectum and the bladder

c) Precise field-localization with bony structures

Rigid immobilization required the feet and head of the patients to be positioned in customized cradles (Moldcare; Alcare, Tokyo, Japan), and their pelvis was immobilized with a low-temperature thermoplastic 3 mm in thickness (Shellfitter; Keraray Co, Ltd, Osaka, Japan), which can give mild pressure on the lower abdominal

wall and reduce organ motion in the pelvis. With this method of immobilization, the intra-fractional motion of the prostate was evaluated to be less than 2 mm.

To ensure volume control of the rectum and bladder, the bladder was filled with 100ml of sterilized water both at the time of CT acquisition and at each treatment session in the case of beam irradiation in the vertical direction. The patient was instructed to empty the rectum as much as possible just before the treatment and a laxative or enema was used if necessary. The amount of gas in the rectum was carefully observed by positioning images, and the set-up was repeated when necessary.

Precise field-localization with bony structures required that at every treatment session, the patient's position was verified with a computer-aided, on-line positioning system. The patient was positioned on the treatment couch with the immobilization devices, and digital orthogonal x-ray television images were taken in that position and transferred to the positioning computer. The positioning images were compared with reference images, which were checked to confirm their match with the digitally reconstructed radiograph (DRR). Any differences, if found to exist, were measured. The treatment couch was then moved to the matching position until the largest deviation of all points was less than 2mm.

2) Treatment Planning

A set of 2.5-mm-thick CT images was taken for treatment planning, with the patient placed in immobilization devices. Three-dimensional treatment planning was performed using HIPLAN software (National Institute of Radiological Sciences, Chiba, Japan) (13). The clinical target volume (CTV) was defined as consisting of the prostate and the seminal vesicles (SV) demonstrated by CT images, irrespective of the T-stage or other risk factors. A MRI was also taken for all the patients and used as a reference for defining the CTV. However, the whole SV was not always be included in the CTV, in the case of patients with low risk. Thus, for example, the CTV of the patients staged as T1 or T2a did not cover the SV tips. Further, anterior and lateral safety margins of 10mm and a posterior margin of 5mm were added to the CTV to create the initial planning target volume (PTV-1). In order to reduce the dose to the anterior rectal wall, a rectum-sparing target volume (PTV-2) was used for the latter half of the C-ion RT, where the posterior margin was reduced to the anterior boundary of the rectum. Evaluation of the plan was routinely performed at the case conferences before the actual treatment, using the dose-volume histograms (DVH) for the CTV, PTV-1, PTV-2, and the rectum. In particular, the DVH of the rectum was evaluated by comparing the reference DVH that was obtained from the analysis using actual DVH data from the prior dose-escalation studies. If the rectal DVH of the new patient was beyond the reference DVH at the high dose area, the treatment planning was revised.

C-ion RT was given once a day, 4 days a week. One port was used in each session. Patients were treated from 5 irregularly shaped ports, one anterior-posterior port and a pair of lateral ports for the PTV-1, and another pair of lateral ports for the PTV-2. One hundred percent of the prescribed dose was given at the maximum dose point of each portal. The PTV-2 was covered by at least 90% of the prescribed dose, and the minimum dose of the PTV-1 was more than 50% of the maximum dose and depended on the volume spared by the PTV-2.

The dose was expressed in Gray-Equivalent (GyE = physical carbon ion dose (Gy) x Relative Biological Effectiveness {RBE}). Irrespective of the size of the Spread-Out Bragg Peak (SOBP), the RBE value for carbon ions was estimated to be =3.0 at the distal part of the SOBP. The compensation bolus was fabricated for each patient to make the distal configuration of the SOBP similar to the PTV. The multi-leaf collimator or a customized brass collimator defined the margins of the PTV. Fig. 2 shows the representative dose distribution.

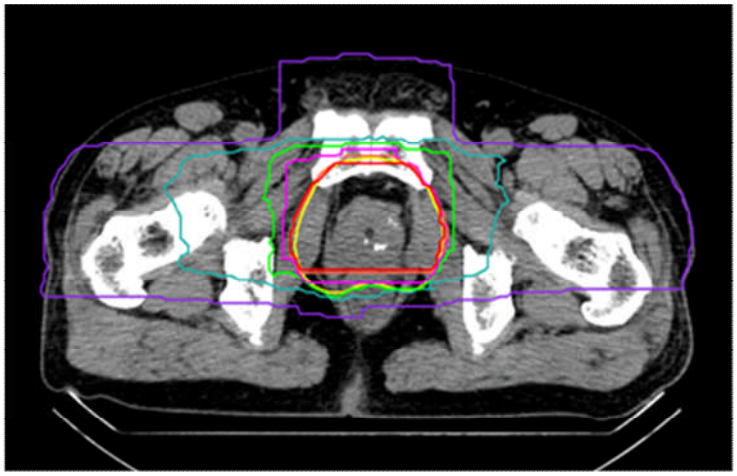

Figure 2

Typical dose distribution of carbon ion radiotherapy

The irradiation dose was fixed at 63.0GyE or 66.0GyE/20 fractions, which was the recommended dose fractionation schedule established by the two previous phase I/II studies (11). In addition, a more hypofractionated schedule of 57.6GyE/16 fractions was applied since September 2007. This newly applied fractionation had been tested in other patients who could not enrolled to the clinical studies because of their prolonged neoadjuvant hormonal therapy since April 2003. At present, a new clinical trial of C-ion RT in 12 fractions over 3 weeks is also ongoing, but the data were not included in this analysis because the trial has just been started.

3) Androgen Deprivation Therapy (ADT)

Before C-ion RT, neoadjuvant androgen deprivation therapy (ADT), such as medical or surgical castration with or without antiandrogen, was applied for 2 to 6 months for the patients in the high-risk and intermediate-risk groups. Adjuvant ADT was continued for a duration of 6 months for the intermediate-risk patients and for more than 24 months for the high-risk patients. The median duration of ADT of the 744 patients receiving combined treatment was 24.0 months; 7.4 months for the intermediate-risk and 29.0 months for high-risk patients. The remaining 159 patients received C-ion RT only.

Results

Of the 903 analyzed patients, 501 (55.5%) were categorized as high-risk, 243 (26.9%) as intermediate-risk, and 159 (17.6%) as low-risk according to our definition of risk grouping. The average pretreatment PSA value was 24.9 ng/ml, with a median of 12.6 ng/ml and a range of 3.4-810.0 ng/ml. Three hundred and eleven (34.4%) patients had an initial PSA value greater than or equal to 20 ng/ml. Two hundred and eighty six (31.7%) patients had T3 primary tumors, and the remaining 617 (68.3%) had T1 or T2 tumors. Two hundred and twenty two (24.7%) patients had a GS of less than or equal to 6, 424 (47.2%) had a GS of 7, and 252 (28.1%) had a GS greater than or equal to 8. The median follow-up period was 36.8 months at the time of analysis.

1) Toxicity

The cumulative incidence of late rectum and genitourinary morbidities in the 818 patients treated with either the 20 fractions or the 16 fractions and followed up more than 12 months are summarized in Table 2. Only one patient, who developed grade 3 bleeding the the bladder bleeding, developed a grade 3 or higher morbidity as of the latest follow-up. Grade 2 morbidities of the genitourinary system and rectum were observed in 5.6%

and 2.0% of the patients, respectively. Regarding the effect of alteration in the dose fractionation, both the rectal and GU toxicity in 57.6.GyE/16f were substantially less frequent than those in patients treated with 66.0GyE/20f or 63.0GyE/20f.

Table 2. Late gastrointestinal and genitourinary morbidity after C-ion RT in patients followed up for more than 12 months

Dose GyE/f.	No.pts.	Rectum				Bladder/urethra			
		Grade0	G1	G2	G3	Grade0	G1	G2	G3
66.0/20	250	196	46	8	0	103	120	27	0
	(%)	(78.4)	(18.4)	(3.2)	(0)	(41.2)	(48.0)	(10.8)	(0)
63.0/20	216	187	24	5	0	112	93	10	1
	(%)	(86.6)	(11.1)	(2.3)	(0)	(51.9)	(43.1)	(4.6)	(0.5)
57.6/16	352	326	23	3	0	187	156	9	0
	(%)	(92.6)	(6.5)	(0.9)	(0)	(53.1)	(44.3)	(2.6)	(0)
Total	818	709	93	16	0	402	369	46	1
	(%)	(86.7)	(11.4)	(2.0)	(0)	(49.1)	(45.1)	(5.6)	(0.1)

2) Survival and Tumor Control

The Kaplan-Meier estimates of overall and biochemical relapse free (bNED) survival for the 903 patients at five years were 94.9% and 90.9%, respectively (Fig. 3). By the date of analysis, 30 patients had died; 7 of metastasis from the prostate, and 23 of other malignancies or comorbid diseases. Up to now, none of the patients belonging to the low-risk or intermediate-risk groups has died of prostate cancer.

A total of five patients, three presenting with slowly elevating PSA and positive biopsies at 24 months, 38 months, and 48 months after C-ion RT, and two with apparent growth of the tumor on the MRI images, were judged as having local recurrence. By the date of analysis, 52 patients met the Phoenix criteria of biochemical failure: a more than 2.0 ng/ml rise of PSA from the nadir. Of these 52 patients, 30 patients were diagnosed as having metastasis: 14 in the bone, 2 in the lungs and 14 in the paraaortic or pelvic lymph nodes at 2 to 67 months after biochemical relapse. Five were judged to have a local recurrence, and the remaining 22 patients had no clinical evidence of recurrent lesions at the date of analysis.

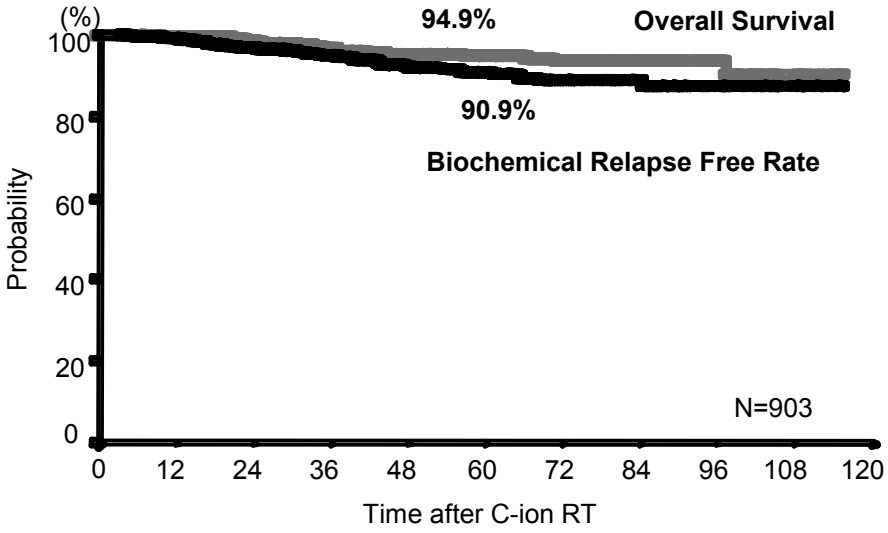

Figure 3 Overall and biochemical relapse free survival curves of all analyzed patients. Figures indicate 5-year rate.

3) Prognostic factors

Additional analyses were carried out to evaluate the influence of several prognostic factors on bNED and overall survival (OS), such as pretreatment serum PSA, GS, clinical stage, and dose fractionation. As a result, it was concluded that an initial PSA level of 20.0ng/ml or higher was a significant factor for lower bNED and OS. The five-year bNED and OS in T1/2 patients were significantly better than those in T3 patients. However, the 5-year bNED of 89.6% was remarkably high compared to other radiotherapy series for T3 patients.

Table 3. Biochemical relapse free rate (bNED) and onerall survival rate (OS) according to risk factors

			5-year rates (%)			
		No.pts.	bNED	p-value	OS	p-value
All		713	91.0		94.7	
Stage	T1/2	498	94.2	0.0001	97.8	0.0064
	T3	215	84.5		88.8	
PSA	< 20	478	93.1	0.0725	97.0	0.0151
	20 ²	235	87.9		91.2	
Gleason score	² 6	180	91.9		96.7	
	7	331	94.3	0.0023	95.2	n.s.
	8 ²	202	84.1		91.3	

The centrally reviewed GS also had a significant influence on the bNED, as the 5-year bNED of the patient subgroup with GS ≥ 8 was significantly lower than those of the subgroups with GS ≤ 6 and GS = 7, though their OS was not significantly different (Table 3).

Regarding the effect of altered fractionation on bNED, there was no significant difference among the patients treated with 20f and those treated with 16f (Fig. 4). On the basis of these results on bNED and toxicity, and the relatively lower toxicity with comparable bNED in 16 fractions, we started to treat all new patients with a dose fractionation of 57.6GyE/16f in September of 2007.

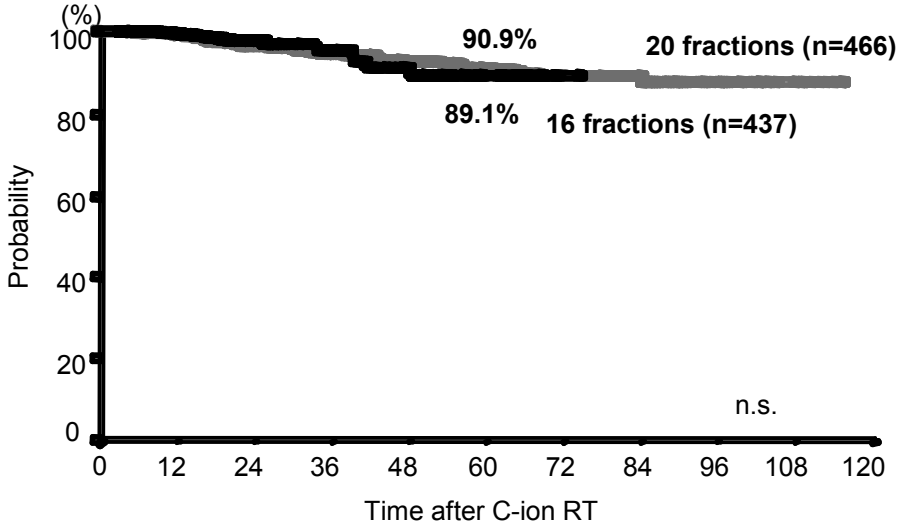

Figure 4 bNED according to altered fractionation of carbon ion radiotherapy

Discussion

In this article, the toxicity and survival outcomes of prostate cancer patients treated with the carbon ion radiotherapy (C-ion RT) procedure established in our phase I/II clinical studies were analyzed. The results have demonstrated that C-ion RT achieves a high biochemical control rate with a relatively low morbidity. A high rate of biochemical control was achieved as a result of the excellent dose concentration associated with C-ion RT and the efficient application of hormonel therapy. A number of studies using radiation therapy in combination with hormone therapy have also indicated a high rate of biochemical control (13-14). Comparing our results with meta-analysis of the RTOG study, survival rates in all patient subgroups were even better than those obtained using combinations of hormone therapy and conventional photon radiotherapy (Table 4). We presume that the higher survival rate was due to the positive impact of carbon ion beams on local tumor control, even in the high-risk patients.

Table 4. Comparing the Overall Survival Rate of C-ion RT with the Results of Meta Analysis of RTOG studies

Studies	Dose (Gy/fr.)	Overall Survival Rate					
		Group 2		Group 3		Group 4	
		No. pts.	5-y OS	No. pts.	5-y OS	No. pts.	5-y OS
RTOG Meta Analysis*							
RT alone	65-70/30-35	443	82%	338	68%	324	52%
RT + Hormone	65-70/30-35	114	76%	138	79%	103	63%
Carbon + Hormone	66-63/20 or 57.6/16	299	99%	210	93%	184	87%

*RTOG: Radiation Therapy Oncology Group; IJROBP 2000; 47(3): 617-627, MackToach III et al

During photon radiotherapy, the rate of local recurrence can be affected by the actual volume or pathological differentiation of the tumor tissue. However, high LET radiation is expected to be more effective for large volume, poorly differentiated tumors compared to photon irradiation, and, in fact, very few local recurrences were actually observed in our series, even in the patients with T3 tumors and a high GS. A substantially higher survival rate in the high-risk group (Group 4 in Table 4) could be achieved only by substantially more effective treatment than conventional photon radiotherapy.

A very low incidence of rectum morbidity was recorded, and this is ascribable to the physical properties of heavy charged particles in terms of dose conformity. This also substantiates the validity of our methods of patient positioning and target setting, and of our irradiation techniques. In addition, the acceptable incidence of genitourinary morbidity and the high efficacy against local tumors confirms the accuracy of our dose calculation, the biological advantage of carbon ion beams, and the effect of a relatively high dose given in a hypofractionated schedule. The incidence of late radiation toxicities in various radiotherapies are summarized in Table 5. IMRT and proton therapy had lower incidences than 3DCRT, and C-ion RT, particularly of 57.6GyE/16f, could achieve even an even lower incidence of both rectal and GU system toxicity.

Table 5. The Incidence of Late Radiation Toxicity Induced by Various Radiotherapy of the Prostate

Institutes	Radiotherapy	Dose(Gy/f)	No. of pts.	Morbidity ³ G2	
				Rectum	GU
Christie H. [1)]	IMRT	60/20	60	9.5%	4.0%
Princess Margaret H. [2)]	IMRT	60/20	92	6.3%	10.0%
Cleveland CF. [3)]	IMRT	70/28	770	4.4%	5.2%
Stanford U.[4)]	SRT	36.25/5	41	15.0%	29.0%
RTOG9406[5)]	3DCRT	68.4-79.2/38-41	275	7-16%	18-29%
	3DCRT	78.0/39	118	25-26%	23-28%
Loma Linda U.[6)]	Proton	75.0/39	901	3.5%	5.4%
NIRS	Carbon	63.0/20	216	1.9%	4.6%
	Carbon	57.6/16	274	0.7%	2.6%

1) JH Coote et al. IJROBP 74, 2009 2) JM Martin et al. IJROBP 69, 2007

3) PA Kupelian et al. IJROBP 68, 2007 4) CR King et al. IJROBP 73, 2009

5) JM Michalski et al. IJROBP 76, 2010 6) RW Schulte et al. Strahlenther Oncol 176, 2000

A further move in the direction toward a more hypofractionated regimen of 16 fractions over 4 weeks has already been made. In 437 patients treated with a C-ion dose of 57.6 GyE in 16 fractions, the bNED was comparable to that of 66.0GyE/20f or 63.0GyE/20f, and the incidence of GU toxicity was even lower. Therefore, this new dose fractionation is applied for all new patients at the NIRS. Further, a new clinical study with more hypofractionated C-ion RT of 51.6GyE/12f has just been started at our institute.

Conclusions

In conclusion, carbon ion radiotherapy administered using a hypofractionated schedule is an effective and safe option for the treatment of localized prostate cancer. With an appropriate use of hormone therapy, satisfactory biochemical control can be achieved even in high-risk patients. Trials with greater hypofractions have started at NIRS with the aim of establishing even more sophisticated methods of C-ion RT.

References

[1] Nikoghosyan A, Schulz-Ertner D, Didinger B, et al: Evaluation of therapeutic potential of heavy ion therapy for patients with locally advanced prostate cancer. Int J Radiat Oncol Biol Phys 58(1): 89-97, 2004

[2] Perez CA, Michalski J: Outcome of external-beam radiation therapy for localized carcinoma of the prostate (stages T1b, T2, and T3). In: Greco C, Zelefsky MJ, editors. Radiotherapy of prostate cancer. Amsterdam: Harwood Academic Publishers; p.155-184, 2000

[3] Hanks GE, Hanlon AL, Pinover WH, et al: Dose escalation for prostate cancer patients based on dose comparison and dose response studies. Int J Radiat Oncol Biol Phys 2000; 46: 823-832.

[4] Zelefsky MJ, Fuks Z, Hunt M, et al: High-dose intensity modulated radiation therapy for prostate cancer: Early toxicity and biochemical outcome in 772 patients. Int J Radiat Oncol Biol Phys 2002; 53: 1111-1116.

[5] Laramore GE, Krall JM, Thomas FJ, et al: Fast neutron radiotherapy for locally advanced prostate cancer: final report of a Radiation Therapy Oncology Group randomized clinical trial. Am J Clin Oncol 1993; 16: 164-167.

[6] Haraf DJ, Rubin SJ, Sweeney P, et al: Photon neutron mixed-beam radiotherapy of locally advanced prostate cancer. Int J Radiat Oncol Biol Phys 1995; 33: 3-14.

[7] Tsujii H, Morita S, Miyamoto T, et al: Preliminary results of phase I/II carbon-ion therapy at the National Institute of Radiological Sciences. J Brachytherapy Int 1997; 13: 1-8.

[8] Akakura K, Tsujii H, Morita S, et al: Phase I/II clinical trials of carbon ion therapy for prostate cancer. Prostate 2004; 58: 252-258.

[9] Tsuji H, Yanagi T, Ishikawa H, et al: Hypofractionated radiotherapy with carbon ion beams for prostate cancer. Int J Radiat Oncol Biol Phys 2005; 63(4): 1153-1160.

[10] Ishikawa H, Tsuji H, Kamada T, et al; A phase II trial using carbon ion radiotherapy (C-ion RT) for prostate cancer. JCO 23(16) part 1 Supple. 2005; 410S-410S.

[11] Ishikawa H, Tsuji H, Kamada T, et al: Carbon Ion Radiation Therapy for Prostate Cancer: Results of a Prospective Phase II Study. Radiother Oncol in press.

[12] International Union Against Cancer (UICC). TNM Classification of Malignant Tumours, 5th ed. New York: Wiley-Liss, Inc. 1997; p 170-173.

[13] Bolla M, Gonzalez D, Warde P, et al: Improved survival in patients with locally advanced prostate cancer treated with radiotherapy and goserelin. N Engl J Med 1997; 337: 295-300.

[14] Roach MIII, Lu J, Pilepich MV, et al: Predicting long-term survival, and the need for hormonal therapy: a meta-analysis of RTOG prostate cancer trials. Int J Radiat Oncol Biol Phys 2000; 47: 617-627.

Plans for Ion Radiation Therapy at Karolinska Institute and University Hospital

Anders Brahme

Medical Radiation Physics, Department of Oncology-Pathology, Karolinska Institutet

Abstract

Recent developments in radiation therapy have made it possible to optimize the high dose region to cover almost any target volume and shape at the same time as the dose level to adjacent organs at risk is acceptable. Further implementations of IMRT (Intensity Modulated Radiation Therapy), and inverse treatment planning using already available technologies but also foreseeable improved design of therapy accelerators delivering electron- and photon beams, will bring these advances to the benefit of a broad population of cancer patients. Protons will therefore generally not be needed, except possibly with microscopically invasive tumors, since in most situations the improvement will be insignificant or moderate, partly due to the large lateral penumbra with deep proton therapy and the low biological efficacy. A further step would be to use He-ions, which have only half the penumbra width of protons and still a fairly low-LET in the spread-out Bragg peak. There is however still a group of patients that cannot be helped by these advances as the tumor might be radioresistant for the presently utilized low ionization density beam qualities. The ultimate step in the therapy development process should therefore be to optimize the beam quality for each tumor-normal tissue situation. To facilitate beam quality modulated radiation therapy (QMRT) optimization light ions are needed. It is argued that in many radioresistant tumors a mean LET of 25-40 eV/nm in the target would be optimum as then tumor cells will be lost in the highest proportion through senescent or apoptotic cell inactivation and the superficial tissues will still be irradiated with a fairly low LET. Combination of Light ion beams such as He, Li, Be, B, and C would then be the ideal choice. In this paper a light ion facility is outlined for the Karolinska University Hospital facilitating both dose distribution and beam quality optimization using the cost efficient excentric gantry design simultaneously allowing laser cameras, cone beam CT and PET in four treatment rooms.

Introduction

Radiation therapy at the "Radiumhemmet", the oncological clinic of the Karolinska University Hospital, has traditions from the early years of the 20th century through pioneers like Thor Stenbeck, Gösta Forssell and Rolf Sievert and has continuously been involved in important developments of treatment techniques, most recently radiobiologically based treatment optimization, IMRT and stereotactic techniques (1,8). Throughout the last century radiation therapy has increased as an important tool for cancer treatments. During the last decade the yearly number of cases treated with radiotherapy in Sweden increased with 70% (10) and radiation therapy is now given to about 50% of all cancer patients in Sweden. Still the total cost of external beam radiation therapy is low, only 5% of all the cost for cancer care in the country. The development during the last century was based on improved dose distributions using low-LET radiation in combination with advances in the field of tumor diagnostics, radiation biology, as well as radiation detector and accelerator physics. The future challenge will be to optimize the radiation quality to have the best LET-distribution to maximize complication free tumor control (2,3). This is the radiobiological and clinical basis for the clinical introduction of light ion therapy.

It has been estimated that at least 10-20% will experience substantial improvements and maybe as many as 30% or more of all cancer cases would benefit from the use of light ion treatments (5,6,11) mainly all those patients that are lost due to lack of local cure. In Sweden 45 482 new cancers were diagnosed in year 2000. Assuming similar incidence in the rest of the Nordic countries would give about 120 000 new cancer cases per year. In addition also the neighboring new northern EU-members ought to be considered as a possible uptake region for patients. One light ion facility could not cover all this population, but at least there should be a possibility to select the patients, who would have the highest possible benefit from this form of therapy.

Light ion beams require a large accelerator and a new structure for the radiation therapy organization of the country level. The present merge of two radiotherapy centers in the Stockholm region to one very large department should help to establish the required "critical mass" for the development of an advanced comprehensive oncologic department.

Therapy optimization by radiation quality modulation

In addition, to the above basic LET related properties light ions have unique properties with regard to inducing senescent or apoptotic cell inactivation in tumors. In principle every patient should be planned by radiobiological treatment optimization methods so that factors such as the degree of local hypoxia or general radiation resistance will be taken into account and influence the locally selected LET distribution to maximize the complication free cure. The higher ion fluence per unit dose and sufficiently high microscopic energy deposition density are probably the main reasons why a medium LET induces the highest probability of an apoptotic or senescent response per unit dose at a given survival level (7,9) as shown in Fig. 1 at 1h - 3 days after irradiation. Senescence and apoptosis are the most desirable way of inactivating tumor cells with a minimum of normal tissue side effects and apoptosis is also nature's own preferred way of eliminating cells, for example during organ development. A lower degree of inflammatory reactions at a given level of cell kill should therefore be expected with medium LET beams and less microscopic energy deposition fluctuations (7).

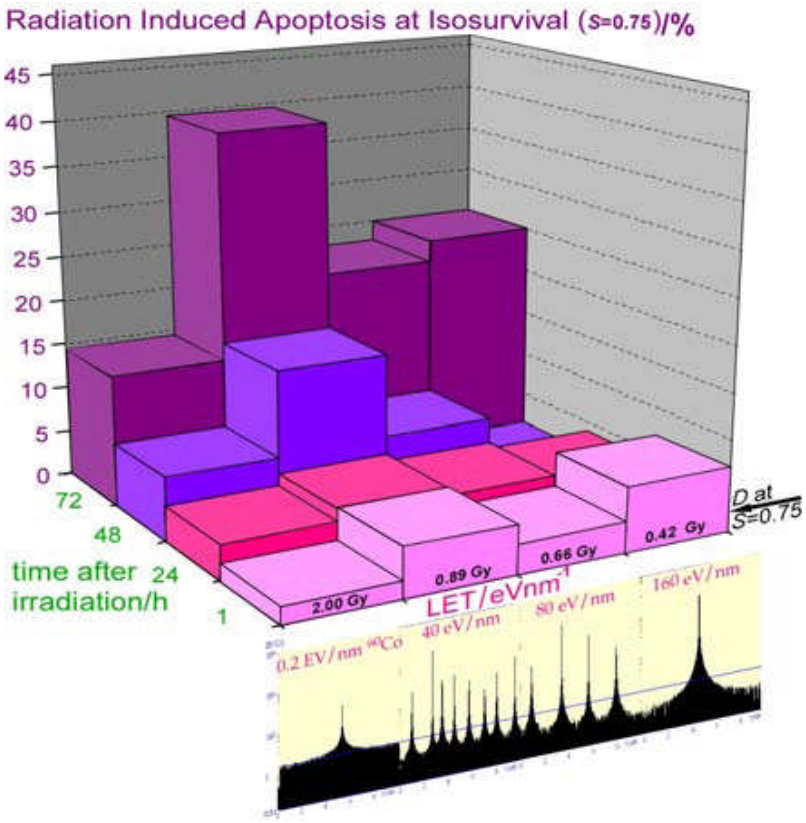

Figure 1. Variation of the apoptotically killed cell fraction as a function of time and LET after irradiation by 60Co γ-rays (0,2 eV/nm) and boron ions. The DNA damage induced apoptosis at 1h – 3 days after boron ion irradiation with a dose giving a clonogenic survival of 75% is shown as a function of the LET. A broad maximum is seen around a LET of 50 eV/nm indicating that a medium LET may be most efficient and beneficial for tumor eradication due to the larger number of dense energy depositions at a fixed dose of 2 Gy in the cell nucleus (10 μm, lower panel). The study was made with AA Melanoma cells with wild type p53. It is interesting that a fair amount of apoptosis is induced also in cell lines with mutant p53 due to p53 independent pathways active with light ions. 9

The dose distribution properties of narrow pencil beams are of prime interest to understand the clinical value of different radiation modalities for inverse biologically optimized treatments. As shown in Fig. 2 narrow pencil beams or so called dose distribution kernels are the building blocks of therapy planning as they show how the dose of an incoming pencil beam is distributed inside the patient. The larger the part of the dose distribution that falls in the tumor and the smaller the dose to surrounding tissues the better and more useful is the radiation modality for biologically optimized intensity modulated dose delivery. This becomes increasingly clear when

also the biological effectiveness of the beam varies in a similar manner with increased biological effectiveness in the region where the dose is high.

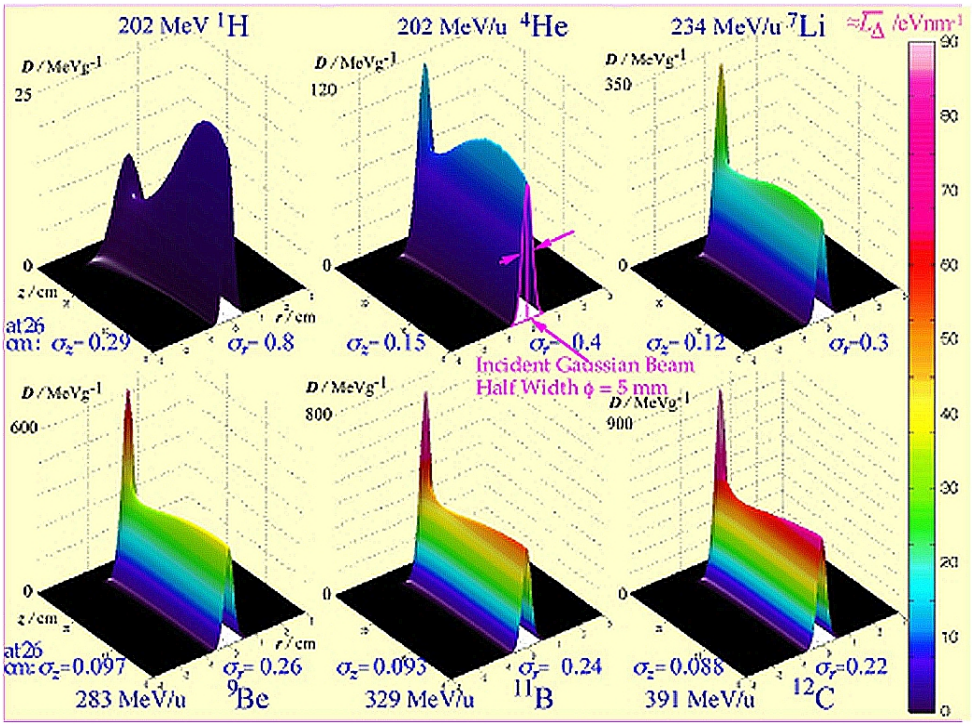

Figure 2. Illustration of the clinical usefulness for biologically optimized therapy planning with different light ion pencil beams all having an incident 1/e width of 5 mm. With protons the dose to normal tissues in front of the tumor is then about twice the tumor dose whereas it is only a small fraction of the tumor dose for the light ions from about lithium and above. The grey scale illustrates the ionization density and thus the increased biological effect in the tumor. The lower dark grey region represents essentially low LET damage whereas the higher grey region causes increasing high LET damage. σr and σz are the radial and longitudinal standard deviation due to multiple scattering and range straggling respectively in mm at the Bragg peak (depth 260 mm). The effect is somewhat reduced if the Bragg peak depth is at 10 - 15 cm, but still large enough to prevent Lars Leksell from using protons for brain treatment and instead develop the gamma knife.

The pencil beam dose distributions in Fig. 2 show that when the dose to a small part of the tumor needs to be increased by a certain amount, protons generally require an almost 2-fold increase in dose to shallow normal tissue, whereas with light ions, the increase is often around 50%. Thus, in a small tumor segment, a 4-times higher normal tissue load is obtained with protons, mainly because most of the protons have been multiply scattered out from the Bragg peak normally found in broad proton beams. This property determines the figure of merit of a given pencil beam kernel for therapy optimization. Obviously, the factor 4 is reduced substantially if the region of the tumor that needs extra dose is much larger than the 5 mm in Fig. 2. However, it should be kept in mind that the dose to surrounding normal tissues will be increased simultaneously, so Fig. 2 really depicts the most important dose distributional properties of our 6 lightest ions when it comes to biologically based dose delivery optimization. It is also seen that as the tumor LET increases, the LET in the entrance regions is simultaneously increased. This may increase the damage to shallow normal tissues as the atomic number is increased.

Taking all the above aspects together it is quite clear that all light ions from the hydrogen ions: proton, deuteron and tritium, through helium, lithium, beryllium and boron up to carbon and possibly oxygen have all their own special physical, biological and clinical advantages. With increasing atomic number and mass the lateral multiple scattering decreases rapidly and so does the longitudinal range straggling at the same time as the width and height of the high LET Bragg peak increases from a few cell nuclei to several mm. This increases the RBE and OGF and decreases the OER monotonically over this range, and thus increases their biological selectivity except possibly longitudinally distal to the tumor where the increasing particle fragmentation reduces the advantage of the heavier ions like carbon and oxygen for tumors in front of sensitive and serially organized normal tissues (2). To deliver an optimal biological effect distribution, we should ideally have two to three different ions available as discussed recently, one low LET ion preferably with high physical selectivity from the first part of the above listing such as protons or preferably helium ions for microscopic invasive tumors in sensitive normal tissues (3,7). An intermediate light ion like lithium or beryllium with close to optimal LET spectrum for optimal

apoptosis induction in small to medium size tumors and for eradicating hypoxic and radiation resistant tumors with beams with a very low LET in the plateau region and negligible fragmentation tail beyond the Bragg peak. Finally, a higher LET ion in the range from boron to oxygen is desirable for highest biological specificity in large hypoxic tumors like sarcomas. These high LET light ions are also useful with small localized resistant tumors and for boost therapy, in combination with the more conventional radiation modalities such as external beam intensity modulated electron, photon, proton or brachytherapy, to also cover possible well oxygenated microscopic tumor invasion in organs at risk.

Proposed outline of the Nordic Light Ion Center.
The preliminary layout of the light ion center is shown in Fig. 3. To allow high beam currents and a compact design a superconducting cyclotron is planed as accelerator. Ions from protons to carbon are planned to allow QMRT particularly with lithium and carbon ions. One ion species of special interest is 11C+6, which will allow direct PET-CT imaging of the delivered Bragg peak distribution.

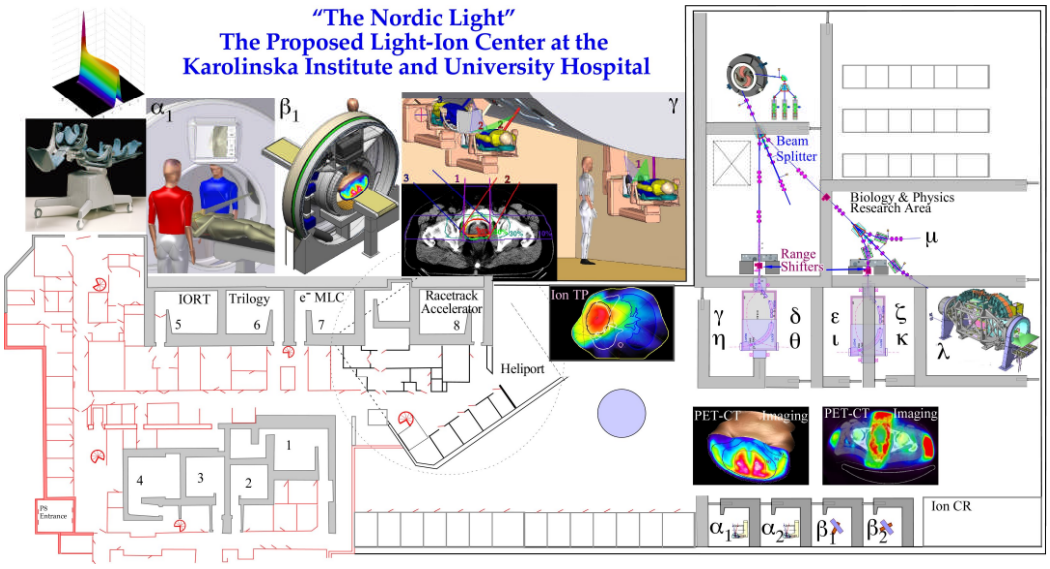

Figure 3. The planned layout of the treatment area of the planned Nordic light Ion Therapy Center. The cyclotron and the eight treatment rooms will be installed underground, beyond the eight existing radiation therapy accelerators and the Heliport at the Karolinska University Hospital. Two rotary excentric gantries are foreseen, providing arbitrary light ions from protons to oxygen in any of eight treatment rooms capable of treating as many as 6000 patients per year in full operation. The advanced tumor diagnostic center will be equipped with two high-resolution fully integrated PET-CT cameras to image the dose delivery immediately after the treatment both for scanned light ion and narrow photon beams.

The only practical complication with light ion dose delivery beside the high installation cost is the large size of the bending magnets required to make a gantry for arbitrary orientations of the delivered ion beam in the treatment room. To this end a new very flexible so called excentric gantry design has been developed for the planned Nordic Light ion therapy center in Stockholm (2,4), as illustrated in Fig. 3. By just bending the beam once out from the rotational axis of the incoming beam with a compact pencil beam scanning system 30 x 30 cm2 beams are available in four treatment rooms placed around each excentric gantry as seen in the figure. In this way the beam angle can be varied over a 45-60° degree angular interval in each of the four treatment rooms so by rotating the patient coach, say 180°, a pair of oblique lateral anterior or posterior beam portals will be available with one and the same accurate beam scanning and beam monitoring system. This makes the installation very cost effective and allows even time consuming beam set up and patient care in all treatment rooms using simulator heads, while the real treatment takes place in only one of them. By suitable room locations both straight vertical and horizontal beams will also be available. In Figure 3 two excentric gantries are used with eight treatment rooms where one room in each gantry can be used simultaneously through the introduction of a beam splitter in the primary beam line. The gantry will in this way be less than 6 meters in diameter and weight as little as 100 – 150 metric tons instead of the 14 meters and 650 tons of the isocentric gantry designed for the Heidelberg clinic.

Room α1 and α2 are planned for narrow scanned high energy photon beams (50-70 MV) also allowing PET imaging of the delivered dose distribution through photonuclear reactions on C, N and O in the patient (12,13).

The whole treatment area in Fig. 3 is located underground next to the existing radiotherapy department with two corridors with 4 therapy accelerators each, to integrate well with the hospital site, to reduce costs and improve radiation protection. The synchrotron accelerates most ions from protons up to carbon and oxygen ions up to 400 MeV/u. The dose is delivered to all the patients with *active scanning systems* designed so that the Bragg peaks are always deposited in the tumor within a treatment time of a few minutes. The scan pattern will be optimized radiobiologically by combining different ion species so that the highest probability to achieve complication free tumor cure is obtained. Fig. 1 shows 7 also the experimental and treatment areas. Additional rooms are needed to accommodate oncologists, physicists, treatment planning and diagnostics. In particular a well-equipped diagnostic center is foreseen including advanced PET-CT and MRSI units to allow maximum quality diagnostic information to fully benefit from the accurate therapeutic beams.

Conclusions

The new developments in light ion therapy and treatment delivery techniques have opened up the possibility for as cost-effective cancer care with light ions as with Intensity Modulated Radiation Therapy, IMRT. At the same time improved treatment outcome for many tumor sites makes it even more important to rapidly bring these new radiation modalities into clinical practice. The possibility to perform radiation Quality Modulate Radiation Therapy (QMRT, 3) with low and high LET light ion modalities makes it possible to do truly biologically optimized dose delivery. There is no doubt that the light ions will have an increasingly important role for radiation therapy of cancer in the new millennium.

References

[1] Brahme A. Optimization of stationary and moving beam radiation techniques. Radiother Oncol 1988; 12: 129-140.

[2] Brahme A Recent advances in light ion radiation therapy. Int J Radiat Oncol Bio Phys 2004, in press.

[3] Brahme A.: Development of biologically optimized light ion therapy. Proc. 7th Int. Conf. On Time Dose Fractionation, Madison 2005; 50-67.

[4] Brahme A, Lewensohn R, Ringborg U,Amaldi U, Gerardi F, Rossi S. Design of a centre for biologically optimised light ion therapy in Stockholm. *Nucl Instr Meth B.* 2001; 184:569-588.

[5] Gademann G. Socioeconomic aspects of hadrontherapy. In: Amaldie, Larsson B. eds. Hadrontherapy in Oncology. *Excerpta Medica* 1994; 59-79.

[6] Gérard JP, Remillieux J, Rochat J, et al. ETOILE Project (European Light Ion Oncological Centre), Rapport LYCEN 2002-01 (A,B,C), Université Claude Bernard Lyon CNRS/IN2P3/IPNL, p.1-73.

[7] Vreede P, Brahme A: Development of biologically optimized radiation therapy: Maximizing the apoptotic cell kill. Rad Sci, 52(7), 31-52, 2009

[8] Lax I, Blomgren H, Larsson D, Näslund I. Extracranial stereotactic radiosurgery of localized targets. *J Radiosurg* 1998; 1(2): 135-148.

[9] Meijer AE, Jernberg AR-M, Hedlöf I, et al. Maximum apoptotic response of light ions around 50 eV/nm in P53 wt human melanoma cells. Proc. 32nd Ann M *Europ Soc Rad Biol* 2002; 73.

[10] Möller TR, Brorsson B, Ceberg. J, et al. A Prospective Survey of Radiotherapy Practice 2001 in Sweden. *Acta Oncol* 2003; 42: 388-410.

[11] Svensson H, Möller TR. Developments in Radiotherapy. *Acta Oncl* 2003; 42: 430-442.

[12] Svensson R. Development of a compact high energy treatment unit combining narrow pencil beam scanning and multileaf collimation: *Thesis Med Radiat Physics*, Stockholm University; 1998: 1-37.

[13] Brahme A. Biologically optimized 3-dimensional in vivo predictive assay based radiation therapy using positron emission tomography-computerized tomography imaging. *Acta Oncol* 42; 123-136, 2003.

Carbon Ion Radiotherapy for Skull Base and Head-and-Neck Tumors

Azusa Hasegawa, Masashi Koto, Ryo Takagi, Takamichi Morikawa,
Tadashi Kamada, Jun-etsu Mizoe, and Hirohiko Tsujii

Research Center for Charged Particle Therapy, National Institute of Radiological Sciences, Chiba, Japan.
e-mail: azusa@nirs.go.jp,

1. Skull Base and Paracervical Tumors

Abstract

The goal of this study was to estimate the toxicity and efficacy of carbon ion radiotherapy during clinical trials for patients with skull base and paracervical tumors. A phase I/II dose escalation study for skull base and paracervical tumors was initiated in April of 1997. The phase I/II dose escalation trial was performed up to the fourth-stage dose level. In April of 2004, a phase II clinical trial was initiated under the Highly Advanced Medical Technology scheme with an irradiation schedule of 60.8 GyE in 16 fractions over four weeks. At the time of analysis, there was no evidence of any serious acute or late reactions in the skull base and paracervical tumors. For skull base and paracervical tumors, a carbon ion dose in excess of 57.6 GyE improves local control.

Introduction

The limiting factor for photon radiotherapy conventionally applied to the skull base and paracervical tumors is the adjacent normal tissue, because photon radiotherapy has poor local control. On the other hand, because of its superior physical-spatial distribution, photon radiotherapy has provided a major improvement in local control in view of the possibility of dose escalation. It has been pointed out, however, that in certain patient groups, it is difficult to achieve local control with proton radiotherapy even at elevated doses. It has thus been recognized that 1) chordoma patients have a worse prognosis than chondrosarcoma patients, 2) among the chordoma patients, the prognosis for paracervical chordoma patients is worse than for patients with skull base chordoma, and is worse for non-chondroid patients than for those with chondroid disease, and it is worse for females than for males, and 3) for meningeal tumors, the prognosis for the atypical or malignant types is worse than for the benign type, and the prognosis for the patients age 60 and above is poorer than for those under age 60. Therefore, high RBE obtained using carbon ion radiotherapy has potential for treating these intractable skull base and paracervical tumors.

Patients and Methods

A phase I/II clinical trial (Protocol 9601) was initiated in April 1997. Chordoma, meningioma, chondrosaracoma and other tumors originating from the skull base or paracervical spine located superior to the C2 vertebra were targeted. Only patients with residual tumors after surgery or with inoperable tumors were permitted to enroll in the carbon ion radiotherapy study. The eligibility criteria for enrollment in this clinical trail were the presence of a histologically proven tumor, patient age ranging from 15 to 80 years, a KPS of 60% or more, neurological function of grade I or II, the absence of anti-cancer chemotherapy within the previous four weeks, a survival expectancy of six months or more, and no distant metastasis. The carbon ion dose was escalated in successive stages: 48.0 GyE (4 patients), 52.8 GyE (6 patients), 57.6 GyE (10 patients) and 60.8 GyE (9 patients). The phase I/II clinical trial was concluded in February 2004, and in April 2004 a phase II clinical trial was initiated under the Highly Advanced Medical Technology scheme with an irradiation schedule of 60.8 GyE in 16 fractions over 4 weeks. Thirty-nine patients were enrolled in this trial until its conclusion in February 2010.

Acute toxicity was assessed based on the Radiation Therapy Oncology Group (RTOG) score, and late toxicity was determined based on the RTOG/European Organisation for Research and Treatment of Cancer (EORTC) score. Local control and overall survival rates were calculated according to the Kaplan-Meier method.

The 68 patients included in the analysis between May 1995 and February 2010 consisted of 31 males and 36 females. One female patient with chondrosarcoma had to be excluded because she was treated with surgery for metastasis and her diagnosis was changed to malignant melanoma. The age of the 67 remaining patients ranged from 16 to 78, with a median of 49 years. Histologically, 39 patients had chordoma, 12 chondrosarcoma, 8 olfactory neuroblastoma, 7 malignant meningioma, and 1 had giant cell carcinoma.

Results

Acute reactions were of a minor nature, as one of the patients in the 48 GyE group showed a grade 3 skin reaction, and one patient in the 57.6 GyE group and 2 patients in the 60.8 GyE group developed a grade 3 mucosal reaction. A late grade 2 brain reaction was detected in one of the patients in the 57.6 GyE group and 2 patients in the 60.8 GyE group, but no other adverse reactions were observed. At the time of analysis, there was no evidence of any serious acute or late reactions.

The effect on the tumor was primarily stable disease (SD) within six months after carbon ion radiotherapy, and there were no significant changes in tumor size in most cases during the follow-up periods. Local control was defined as showing no evidence of tumor regrowth by MRI, CT, physical examination, or biopsy. The five-year local control (LC) rates according to histological types were 82% for the 39 chordomas, 100% for the 12 chondrosarcomas, 80% for the 7 malignant meningiomas, and 100% for the 8 olfactory neuroblastomas. The five-year overall survival (OS) rate was 89% for patients with chordomas, 67% for chondrosarcomas, 83% for malignant meningiomas, and 100% for those with olfactory neuroblastomas. Two of the seven malignant meningioma patients died because of a distant metastasis detected 23 months after beginning treatment, and due to local recurrence detected 85 months after beginning carbon ion radiotherapy. The patient that developed local recurrence had experienced a postoperative recurrence and received low-dose carbon ion radiotherapy of 52.8 GyE.

The 39 chordoma patients were divided into two groups, a low-dose group (n=10) who were irradiated with doses ranging from 48 to 57.8 GyE, and a high-dose group (n=29) who were irradiated with 60.8 GyE. The five-year LC rates were 60% for the low-dose group and 95% for the high-dose group (Fig. 1). One patient in the high-dose group developed marginal failure 29 months after receiving the radiotherapy. The five-year OS rates were 90% for the low-dose group and 90% for the high-dose group. Two patients from the high-dose group died due to hepatic failure and marginal failure.

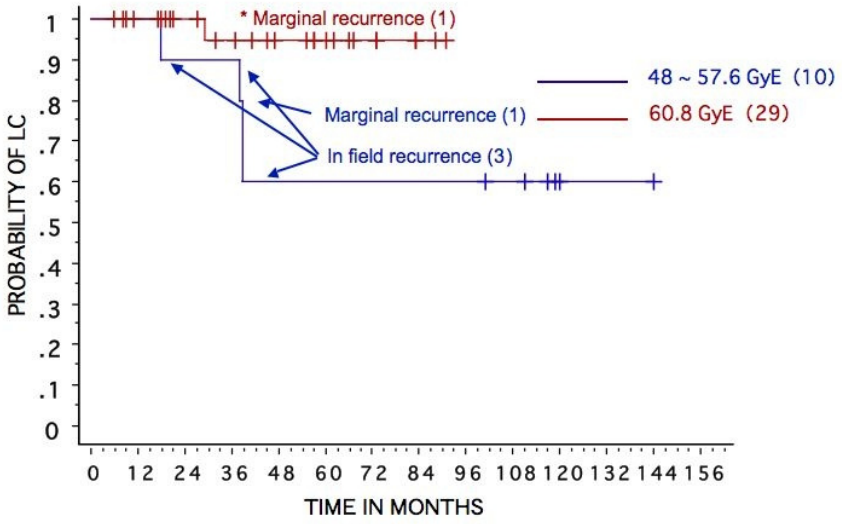

Figure 1. Local Control of 39 Chordomas according to Carbon Ion Dose

Discussion

A carbon ion dose greater than 57.6 GyE improves local control. Additionally, we did not observe any severe toxicity to critical organs such as the brainstem, spinal cord or optic nerves at any of the doses used. Beginning in April of 2004, a phase II trials using carbon ion radiotherapy was initiated under the Highly Advanced Medical Technology scheme with an irradiation schedule of 60.8 GyE in 16 fractions over 4 weeks.

High LET charged particles such as carbon ions have excellent dose localizing properties, and this can cause severe damage to the tumor while minimizing the effects on normal tissues. When the tumor was located close to critical organs, delineation of the clinical target volume was done in an effort to prevent damage to these organs. In particular, when both optic nerves were involved in the high-dose area, treatments were planned to spare the contralateral optic nerve and chiasm according to our previous dose criteria [1]. For tumors close to the brainstem and spinal cord, we recommended surgical resection to create a space between the tumor and brainstem or spinal cord before carbon ion radiotherapy was administered. This allowed for better prevention of severe toxicity to the brainstem and spinal cord. Tumors such as chordomas can only be judged on the results of long-term prognosis. Consequently, it will take more time to reach a definitive conclusion about the efficacy of

the carbon ion radiotherapy. However, it is already clear that, compared with photon or other charged particle radiotherapy, carbon ion radiotherapy will provide higher local control rates with lower toxicity to the surrounding normal tissues (Table 1)[2-14].

Conclusion

In this phase I/II clinical study for skull base and paracervical tumors, dose escalation trials were performed up to the fourth-stage dose level. Because dose escalation is implemented after examining the reactions of the important adjacent organs – the brain and spinal cord – the scheduled enrollment period was exceeded, and therapy was commenced under the Highly Advanced Medical Technology scheme for these patients in April 2004 with a dose fractionation regimen of 60.8 GyE in 16 fractions over 4 weeks. We have demonstrated that a carbon ion dose greater than 57.6 GyE improves local control.

Table1. Clinical characteristics of reported cases of chordoma in the skull base

			Median	Median	Local control rate (%)		
	Authors	N	total dose	f/u (y)	3-y	5-y	10-y
Photon	Catton et al. [4]	24	50.0	5.2		23	15
	Romero et al. [5]	18	50.1	3.1		17	
	Forsyth et al. [6]	39	50.0	8.3		39	31
	Magrini et al. [7]	12	58.0	6.0		25	25
Proton	Munzenrider et al. (MGH) [8]	169	66-83	3.4		73	54
(+/- photon)	Noel et al. (CPO) [9]	100	67.0	2.6	86 (2-y)	54 (4-y)	
	Igaki et al. (Tsukuba) [10]	13	72.0	5.8	67	46	
	Ares et al. (PSI) [11]	42	73.5	3.2 (Mean)		81	
Helium	Castro et al. (LB) [12]	53	65.0	4.3		63	
Carbon	Shults-Ertner et al. (GSI) [13]	96	60.0	2.6 (Mean)	81	70	
	NIRS [14]	39	60.8	4.7		82	82

2. Head-and-Neck Tumors

Abstract

To evaluate the efficacy of carbon ion radiotherapy for malignant head-and-neck tumors. Between April 1997 and February 2010, 378 cases with locally advanced, histologically proven, and new or recurrent malignant tumors of the head-and-neck were treated with carbon ion radiotherapy. The treatment dose was 64.0 GyE in 16 fractions over 4 weeks (or 57.6 GyE when a wide area of skin was included in the target volume). There were no acute reactions worse than grade 3 and no late toxicities worse than grade 2. The five-year local control and overall survival rates were 75% and 54%, respectively, however, the five-year local control rate was 25% for bone and soft tissue sarcomas, and the five-year overall survival rate was 36% for malignant melanomas.

Carbon ion radiotherapy for malignant head-and-neck tumors can be described as presenting no major clinical problems. Although local control using carbon ion radiotherapy was promising for malignant head-and-neck tumors excluding sarcomas, the survival rate was not commensurate with the favorable local control rate of malignant melanoma. On the basis of the results of our analysis, this part of the study was divided into two additional protocols, one for bone and soft tissue sarcomas and another for mucosal malignant melanomas.

2-1. Phase II Clinical Trial for Malignant Head-and-Neck Tumors (Protocol 9602)

Introduction

A clinical trial of carbon ion radiotherapy for malignant head-and-neck tumors was conducted under the "Phase I/II Clinical Trial (Protocol 9301) on Heavy Particle Radiotherapy for Malignant Head-and-Neck Tumors", that was initiated in June 1994 by way of a dose escalation study using18 fractions over 6 weeks. This trial was followed by another dose escalation study that commenced in April 1996 under the title "Phase I/II Clinical Trial (Protocol 9504) on Heavy Particle Radiotherapy for Malignant Head-and-Neck Tumors" using 16 fractions over 4 weeks. Based on the outcome of these two studies [15], the "Phase II Clinical Trial on Heavy Particle Radiotherapy for Malignant Head-and-Neck Tumors (Protocol 9602)" was initiated using 64.0GyE in16 fractions over 4 weeks (or 57.6 GyE in16 fractions over 4 weeks when a wide area of skin was included in the target volume) in April 1997 (Fig. 2).

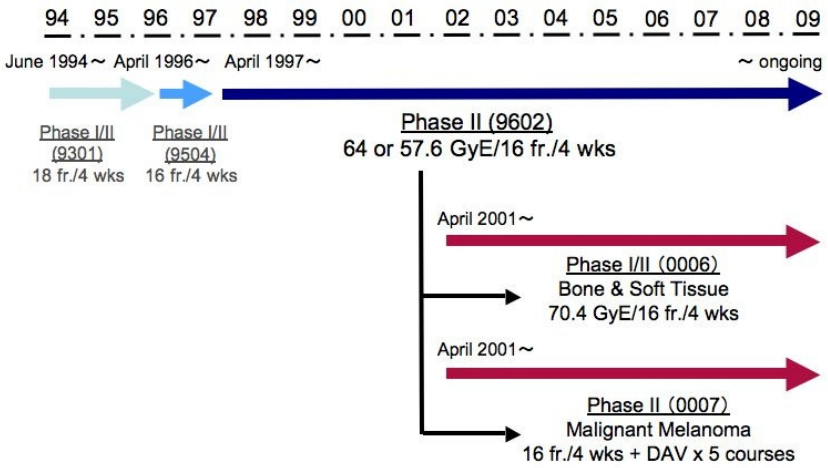

Figure 2. Carbon Ion Radiotherapy for Malignant Head-and-Neck Tumors

Patients and Methods

The eligibility criteria for enrollment in this clinical trial were the presence of histologically proven malignancy, a measurable tumor in the head-and-neck region including N0M0 in the primary tumor, with no co-existent malignant active tumors, no distant metastasis to other parts, an age range from 15 to 80 years, and a prospective prognosis of at least 6 months. The candidates were also required to have a Karnofsky performance status index (KPS) of 60% or higher and to give their written informed consent for inclusion in this clinical study. A further requirement was the absence of prior radiotherapy for the carbon-ion treated area, the absence of an intractable inflammatory lesion, and an interval of at least four weeks from completion of the last chemotherapy.

The clinical trial commenced in April 1997, and by February 2010, a total of 380 patients with 383 lesions were registered (three patients had secondary lesions after the initial treatment). Five of the 380 patients were excluded from the analysis because 1) carbon ion radiotherapy had to be cancelled for two patients with malignant melanoma due to a deterioration of their symptoms, 2) one patient with a lacrimal gland tumor was diagnosed as having a metastasis from the thyroid gland before carbon ion radiotherapy, 3) the ameloblastoma patient was diagnosed as having a benign tumor after histological re-examination and 4) the histological confirmation was done by cytology only. The data for 378 lesions of 375 patients treated until February 2010 were thus are recorded. The patient age ranged from 16 to 80, with a median of 58 years, with 186 males and 192 females. Histologically, the tumors were classified as 134 adenoid cystic carcinomas, 102 malignant melanomas, 46 adenocarcinomas, 22 squamous cell carcinomas, 14 mucoepidermoid carcinomas, 13 papillary adenocarcinomas, 7 undifferentiated carcinomas, 6 osteosarcomas, 6 acinic cell carcinomas, and 28 patient had other histological types. There were five cases of T1, 31 of T2, 58 of T3, and 161 cases of T4 disease, and 86 patients were post-operative, 27 were post-chemotherapy, 9 were post-operative and post-chemotherapy, and one was post-carbon ion radiotherapy. Carbon ion radiotherapy was administered using 16 fractions over 4 weeks. The 378 lesions were irradiated with a dose of 57.6GyE in 249 cases and with 64.0GyE in 129 cases.

Results

Acute reactions were of a minor nature, as only 15 patients (4%) showed a grade 3 skin reaction, and 59 patients (16%) showed a grade 3 mucosal reaction. Late toxic reactions included a grade 2 skin reaction in 8 patients (2%) and mucosal reactions in 12 patients (3%), with no evidence of radiation-induced toxicities worse than these. This therapy can therefore be described as presenting no clinical problems.

The five-year LC and OS rates were 75% and 54%, respectively. The five-year LC rate according to histological type was 79% for the 46 adenocarcinomas, 81% for the 134 adenoid cystic carcinomas, 78% for the 102 malignant melanomas, 73% for the 22 squamous cell carcinomas and 24% for the 14 bone and soft tissue sarcomas. The five-year OS rate was 66% for adenocarcinomas, 72% for adenoid cystic carcinomas, and 36% for malignant melanomas.

Discussion

The overall LC rate for these patients was 75% at 5 years. The therapeutic efficacy was especially good for adenoid cystic carcinoma, a tumor type that is intractable to photon radiotherapy. The treatment results of

surgery with or without radiotherapy ranged from 56% to 93% for the five-year LC rate and from 57 to 77% for the five-year survival rate [16-19] (Table 2). In the present study, the five-year LC rate was 81% for adenoid cystic carcinomas, in spite of including 71 cases (53%) of T4 and 36 cases (27%) that had recurrent tumors after surgery and/or chemotherapy.

Table2. Clinical characteristics of reported cases of adenoid cystic carcinoma

Institutions	N		5-year local control rate (%)	5-year survival rate (%)
Florida [16]	101	Radiotherapy alone	56	57
		Radiotherapy + Surgery	91	77
MGH [17]	23	Proton +/- Surgery	93	77
Washington [18]	151	Neutron	57	77
Heidelberg [19]	29	Neutron +/- Surgery	75	59
NIRS	134	Carbon	81	72

Although the local control of carbon ion radiotherapy was promising for malignant head-and-neck tumors excluding sarcomas, the survival rate was not commensurate with a favorable local control rate for malignant melanoma. Based on the results of preliminary analysis of this protocol (Protocol 9602), two separate protocols were designed and initiated in April 2001 as 1) the "Phase I/II Clinical Trial of Carbon Ion Radiotherapy for Bone and Soft Tissue Sarocomas in Head-and-Neck (Protocol 0006)" designed as a dose escalation study for bone and soft tissue tumors, and 2) the "Phase II Clinical Trial of Carbon Ion Radiotherapy Combined with Chemotherapy for Mucosal Malignant Melanoma in Head and Neck (Protocol 0007)" for the treatment of malignant melanoma with concomitant chemotherapy.

2-2.Phase I/II and II Clinical Trials for Bone and Soft Tissue Sarcomas in Adult Head-and-Neck (Protocol 0006)

Introduction

The phase I/II protocol was initiated in April 2001 for the purpose of a dose escalation study against bone and soft tissue sarcomas in the head-and-neck, since the preliminary analysis of the phase II clinical trial for malignant head-and-neck tumors (Protocol 9602) suggested that the local control and survival of bone and soft tissue sarcomas in the head-and-neck was clearly worse than for other malignant tumors. Kamada et al. described that 4 of 17 patients had grade3 late toxicities in the trunk with more than 70.4 GyE [20], we used 70.4 GyE in 16 fractions over 4 weeks as an initial prescribed dose for this present study. Based on the observed toxicities, it might be possible to proceed to the next irradiation dose. However, the 70.4 GyE used in the present study led to a local control rate of approximately 100%, and a dose higher than 70.4 GyE is certain to cause many unacceptable adverse effects. Thus, we elected to continue using the 70.4 GyE dose. This phase I/II study was completed in February of 2008. In April of 2008, a phase II clinical study was started using the same dose fractionation.

Patients and Methods

The 37 patients included in the analysis between April 2001 and February 2010 consisted of 18 males and 19 females. Two of the 37 patients were excluded from this analysis because 1) one female patient had past history of whole body irradiation for her acute lymphocytic leukemia, 2) another female patient with MFH was diagnosed as having a benign tumor after histological re-examination. The age of the 35 remaining patients ranged from 17 to 78, with a median of 47 years. There were 11 patients with osteosarcoma, 5 with MFH, 3 with chondrosarcoma, 3 with hemangiopericytoma, 2 with myxofibrosarcoma, 2 with leimyosarcoma, 2 with small round cell sarcoma, and 7 with other histological types.

Results

With regard to the acute and late radiation morbidities, most of the 35 patients presented with less than grade 2 acute reactions; however, four patients developed a grade 3 mucosal reaction. All late skin and mucosal reactions were grade 1 or less. The local tumor reactions within six months consisted of a CR for 3 patients, a PR for 10 patients, SD for 22 patients, and none of the patients developed PD. The overall response rate was 37%. The five-year LC and OS rates were 83% and 39%, respectively (Fig. 3).

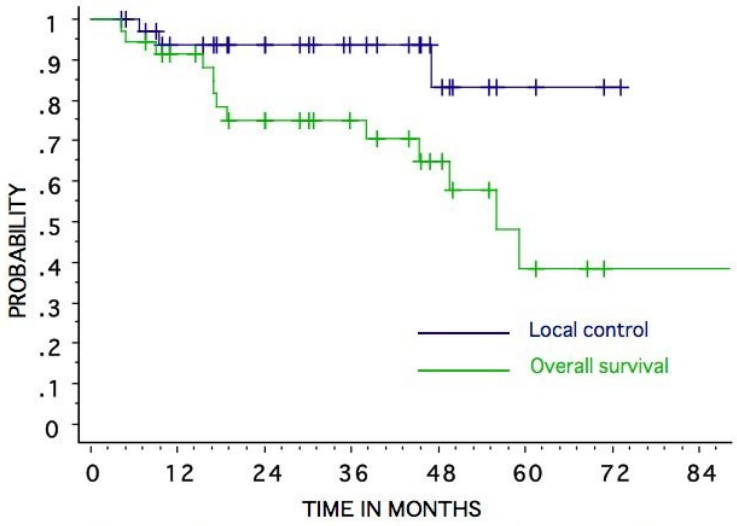

Figure 3. Local Control and Overall Survival of Bone and Soft Tissue Sarcomas

Discussion

Bone and soft tissue sarcomas of the head-and-neck are rare mesenchymal malignant neoplasms accounting for less than 10% of all bone and soft tissue sarcomas, and approximately 1% of all head-and-neck neoplasms. Willers et al. reported that wide resection margins are anatomically difficult to achieve, and the delivery of a high dose of radiation can be limited by the vicinity of critical normal tissue structures (spinal cord, brain stem, optic chiasm, eyes). Accordingly, the local control rates for head-and-neck sarcomas are lower compared to those for the extremities [21]. The five-year LC rate of combined surgery and radiotherapy is 60-70%. The LC of surgery alone is around 54% and that of radiotherapy alone is 43- 50% [22]. However, in unresectable sarcomas, the LC and survival prognosis are very poor. Conventional radiotherapy with a total dose less than 65 Gy showed no local control [23-25].

The results of carbon ion radiotherapy in our previous study (9602) for patients with bone and soft tissue sarcomas of the head and neck, in which study patients were treated using 64.0 or 57.6 GyE in 16 fractions, showed a five-year LC rate of 24%. By increasing the dose of radiation in the current study (0006), we were able to achieve a five-year LC rate of 83%. This result showed a tendency toward improvement compared with surgery with or without radiotherapy.

2-3.Phase II Clinical Trial for Mucosal Malignant Melanoma in Head-and-Neck Combined with Chemotherapy (Protocol 0007)

Introduction

Although the phase II clinical study for malignant head-and-neck tumors (Protocol 9602) had achieved a satisfactory local control rate for mucosal malignant melanomas, the survival rate was not commensurate with the favorable local control rate of malignant melanomas. In view of this result, another protocol was started in April 2001 for the purpose of prophylactic therapy against distant metastasis, the major cause of death from malignant melanoma of the head-and-neck region.

Patients and Methods

The carbon ion dose used for this study was 57.6 GyE in 16 fractions over 4 weeks. Concomitant chemotherapy (DAV: Day 1: DTIC 120mg/m2 + ACU 70mg/m2 + VCR 0.7mg/m2; Days 2~5: DTIC 120mg/m2, 4 weeks' interval, a total of 5 courses) was administered as two courses before, and three courses after carbon ion radiotherapy. The results for the seven patients treated until February 2002 show that at the time of completion of the two courses of DAV chemotherapy prior to carbon ion radiotherapy, there were PR for 2 patients, NC for 2 patients and PD for 3 patients, necessitating the early commencement of carbon ion radiotherapy. From April 2002, carbon ion radiotherapy and DAV chemotherapy were carried out concurrently.

The 96 patients included in the analysis between April 2001 and February 2010 consisted of 42 males and

54 females. Their age ranged from 26 to 74 years, with a median of 62 years. Their KPS ranged from 70% to 100%, with a median of 90%. There were 78 tumors of the nasal cavity and paranasal sinus, 11 of the oral cavity, 4 of the pharynx and 3 of the orbit.

Results

Of the 96 patients who have been followed-up for more than 6 months, one patient developed a grade 3 skin reaction and 20 patients (21%) developed a grade 3 mucosal reaction, while the other toxicities that were observed were grade 2 or less. Almost of all patients presented with less than grade 1 late skin and mucosal reactions; however, one patient presented with a grade 2 mucosal reaction.

The local tumor responses within six months consisted of a CR for 20 patients, PR for 44 patients, SD for 31 patients, and no PD was observed for any of the patients. The efficacy rate was 67%. The five-year LC and OS rates for all patients were 80% and 59%. In the 89 patients treated with concomitant chemoradiotherapy, the five-year LC and OS rates were 83% and 64%, respectively.

Discussion

The reported local failure of systemic therapy including surgery, radiotherapy and chemotherapy is very high (45-54%) [26, 27]. The five-year LC rate of carbon ion radiotherapy was found to be 80% in this protocol. These results indicate that carbon ion radiotherapy is effective for the local control of mucosal malignant melanoma of the head-and-neck. The review articles [28-34] reported five-year survival rates of 17-35% (Table 3), which are attributed mainly to distant metastasis. The five-year OS rate after carbon ion radiotherapy was 36% in protocol 9602 and 59% in protocol 0007. Therefore, it appears that there can be improvement in treatment response when concomitant or adjuvant chemotherapy is used (Protocol 0007) (Fig. 4).

Table3. Clinical characteristics of reported cases of mucosal malignant melanoma

	Authors	N	5-year OS (%)
Radiotherapy	Gilligan [28)]	28	18
(+/- Surgery)	Shibuya [29)]	28	25
Surgery	Chang [30)]	163	32
(+/- RT, +/- Chemo)	Shah [31)]	74	22
	Patel [32)]	59	35
	Lund [33)]	58	28
	Chaudhry [34)]	41	17
Carbon ion alone	NIRS	102	36
Carbon ion + Chemo	NIRS	89	64

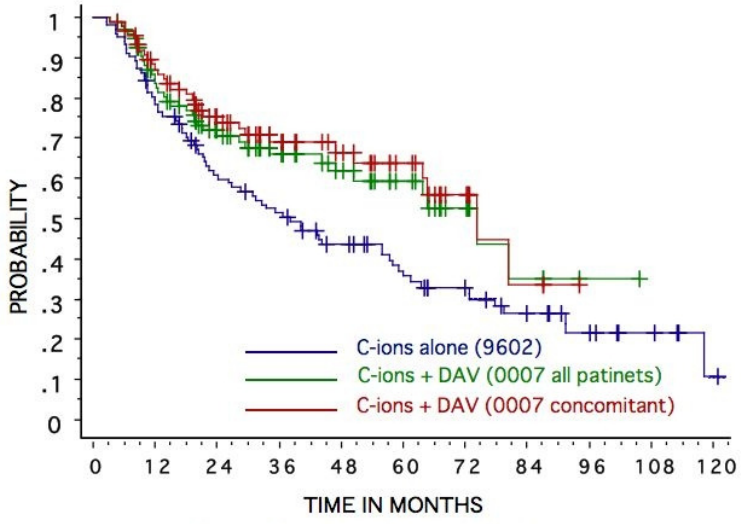

Figure 4. Overall Survival of Mucosal Malignant Melanomas

Conclusion

Malignant head-and-neck tumors are therapeutically diverse because of the many important organs present in this region and the variety of tissue types that can be involved. Carbon ion radiotherapy also requires considerable versatility in terms of the use of a specific radiation dose suited for the particular histological type and the application of concurrent chemotherapy. At present, efforts are being made to increase the number of patients enrolled in clinical trials in order to produce results that can provide cogent clinical evidence.

References

[1] Hasegawa A, Mizoe J, Mizota A, Tsujii H. Outcomes of visual acuity in carbon ion radiotherapy: analysis of dose–volume histograms and prognostic factors. *Int J Radiat Oncol Biol Phys*, 2006; 64 (2): 396-401.

[2] Tsujii H, Mizoe J, Kamada T, *et al*. Overview of clinical experiences on carbon ion radiotherapy at NIRS. *Radiother Oncol* 2004;73:41–49.

[3] Tsujii H, Mizoe J, Kamada T, *et al*. Clinical results of carbon ion radiotherapy at NIRS. *Radiat Res* 2007;48:A1–13.

[4] Catton C, O'Sullivan B, Bell R, *et al*: Chordoma: Long-term follow-up after radical photon irradiation. *Radiother Oncol.* 1996; 41: 67-72.

[5] Romero J, Cardenes H, la Torre A, *et al*: Chordoma: Results of radiation therapy in eighteen patients. *Radiother Oncol.* 1993; 29: 27-32.

[6] Forsyth PA, Cascino TL, Shaw EG, *et al*: Intracranial chordomas: A clinicopathological and prognostic study of 51 cases. *J Neurosurg.* 1993; 78: 741-747.

[7] Magrini SM, Papi MG, Marletta F, *et al*: Chordoma- natural history, treatment and prognosis. The Florence Radiotherapy Department experience (1956-1990) and a critical review of the literature. *Acta Oncol.* 1992; 31: 847-851.

[8] Munzenrider JE, Liebsch NJ: Proton therapy for tumors of the skull base. *Strahlenther Onkol.* 1999; 175: 57-63.

[9] Noël G, Habrand JL, Jauffret E, *et al*: Radiation therapy for chordoma and chondrosarcoma of the skull base and the cervical spine. Prognostic factors and patterns of failure. *Strahlenther Onkol.* 2003; 179(4): 241-248.

[10] Igaki H, Tokuuye K, Okumura T, *et al*: Clinical results of proton beam therapy for skull base chordoma. *Int J Radiat Oncol Biol Phys.* 2004; 60: 1120-1126.

[11] Ares C, Hug EB, Lomax AJ, *et al*: Effectiveness and safety of spot scanning proton radiation therapy for chordomas and chondrosarcomas of the skull base: first long-term report. *Int J Radiat Oncol Biol Phys.* 2009; 75(4): 1111-1118.

[12] Castro JR, Linstadt DE, Bahary JP, *et al*: Experience in charged particle irradiation of tumors of the skull base: 1977-1992. *Int J Radiat Oncol Biol Phys.* 1994; 29: 647-655.

[13] Schulz-Ertner D, Karger CP, Feuerhake A, *et al*: Effectiveness of carbon ion radiotherapy in the treatment of skull-base chordomas. *Int J Radiat Oncol Biol Phys.* 2007; 68(2): 449-457.

[14] Mizoe J, Hasegawa A, Takagi R, , *et al*: Carbon ion radiotherapy for skull base chordoma. *Skull Base,* 2009; 19 (3): 219-224.

[15] Mizoe J, Tsujii H, Kamada T, *et al*: Dose escalation study of carbon ion radiotherapy for locally advanced head-and-neck cancer. *Int J Radiat Oncol Biol Phys*. 2004; 60: 358-364.

[16] Mendenhall WM, Morris CG, Amdur RJ, *et al*: Radiotherapy alone or combined with surgery for adenoid cystic carcinoma of the head and neck. *Head Neck*. 2004; 26(2): 154-162.

[17] Pommier P, Liebsch NJ, Deschler DG, *et al*: Proton beam radiation therapy for skull base adenoid cystic carcinoma. *Arch Otolaryngol Head Neck Surg*. 2006; 132(11): 1242-1249.

[18] Douglas JG, Laramore GE, Austin-Seymour M, *et al*: Treatment of locally advanced adenoid cystic carcinoma of the head and neck with neutron radiotherapy. *Int J Radiat Oncol Biol Phys.* 2000; 46(3): 551-557.

[19] Huber PE, Debus J, Latz D, *et al*: Radiotherapy for advanced adenoid cystic carcinoma: neutrons, photons or mixed beam? *Radiother Oncol.* 2001; 59(2): 161-167.

[20] Kamada T, Tsujii H, Tsuji H, *et al*: Efficacy and safety of carbon ion radiotherapy in bone and soft tissue sarcomas. *J Clin Oncol.* 2002; 20: 4466-71.

[21] Willers H, Hug EB, Spiro IJ, *et al*: Adult soft tissue sarcomas of the head and neck treated by radiation and surgery or radiation alone: patterns of failure and prognostic factors. *Int J Radiat Oncol Biol Phys.* 1995; 33: 585-593.

[22] Mendenhall WM, Mendenhall CM, Werning JW, *et al*: Adult head and neck soft tissue sarcomas. *Head Neck.* 2005: 27: 916-922.

[23] Le QT, Fu KK, Kroll S, *et al*: Prognostic factors in adult soft-tissue sarcomas of the head and neck. *Int J Radiat Oncol Biol Phys.* 1997; 37: 975-984.

[24] Barker JL Jr, Paulino AC, Feeney S, *et al*: Locoregional treatment for adult soft tissue sarcomas of the head and neck: an institutional review. *Cancer J.* 2003; 9: 49-57.

[25] Chen SA, Morris CG, Amdur RJ, *et al*: Adult head and neck soft tissue sarcomas. *Am J Clin Oncol.* 2005; 28: 259-263.

[26] Mendenhall WM, Amdur RJ, Hinerman RW, *et al*: Head and neck mucosal melanoma. *Am J Clin Oncol.* 2005; 28: 626-630.

[27] Lengyel E, Gilde K, Remenár E, *et al*: Malignant Mucosal Melanoma of the Head and Neck -a Review-. *Pathology Oncology Research.* 2003; 9: 7-12.

[28] Gilligan D, Slevin NJ: Radical radiotherapy for 28 cases of mucosal melanoma in the nasal cavity and sinuses. *Br J Radiol*. 1991; 64:1147-1150.

[29] Shibuya H, Takeda M, Matsumoto S, *et al:* The efficacy of radiation therapy for malignant melanoma in the mucosa of the upper jaw: an analytic study. *Int J Radiat Oncol Biol Phys.* 1992; 25: 35-39.

[30] Chang AE, Karnell LH, Menck HR: The National Cancer Data Base Report on cutaneous and noncutaneous melanoma. *Cancer.* 1998; 83: 1664-1678.

[31] Shah JP, Huvos AG, Strog EW: Mucosal melanomas of the head and neck. *Am J Surg.* 1977; 134: 531-535.

[32] Patel SG, Prasad ML, Escrig M, *et al*: Primary mucosal malignant melanoma of the head and neck. *Head Neck*. 2002; 24: 247-257.

[33] Lund VJ, Howard DJ, Harding L, *et al*: Management options and survival in malignant melanoma of the sinonasal mucosa. *Laryngoscope*. 1999; 109: 208-211.

[34] Chaundhry AP, Hampel A, Gorlin RJ: Primary melanoma of the oral cavity. *Cancer.* 1958; 11: 923-928.

Carbon Ion Radiotherapy in a Hypofraction Regimen for Stage I Non-Small Cell Lung Cancer

Masayuki Baba, Naoyoshi Yamamoto, Mio Nakajima, Horino Takeshi, Kyosan Yoshikawa, Reiko Imai, Naruhiro Matsufuji, Shinichi Minohara, Tada-aki Miyamoto, Hiroshi Tsuji, Tadashi Kamada, and Hirohiko Tsujii

Hospital, Research Center for Charged Particle Therapy, National Institute of Radiological Sciences, Chiba, Japan
e-mail address: baba@nirs.go.jp

Abstract

From 1994 to 1999, we conducted a phase I/II clinical trial for patients with stage I non-small cell lung cancer (NSCLC) using carbon ion beams alone, demonstrating optimal doses of 90.0GyE in 18 fractions over 6 weeks (Protocol #9303) and 72.0GyE in 9 fractions over 3 weeks (Protocol #9701), which led to more than 95% local control with minimal pulmonary damage. In the present study, the total dose was fixed at 72.0GyE in 9 fractions over 3 weeks (Protocol #9802), and at 52.8GyE for stage IA and 60.0GyE for stage 1B in 4 fractions in 1 week (Protocol #0001). Following this schedule, we conducted a phase II clinical trial for stage I NSCLC from 1999 to 2003. We also conducted a phase I/II single fractionation clinical trial (Protocol #0201) as a dose escalation study. The total dose was initially 28.0GyE in 2003, and it was increased to 46.0GyE in 2008. This article describes the intermediate steps. Most targets were irradiated from four oblique directions. A respiratory-gated irradiation system was used for all sessions. Local control and survival were assessed by the Kaplan-Meier method. For statistical testing, the Log-rank test was used.

The local control rate for all patients (#9802 and #0001) was 91.5%, and for those with T1 and T2 tumors was 96.3% and 84.7%, respectively. While there was a significant difference (p=0.0156) in the tumor control rate between patients with T1 and T2 tumors, there was no significant difference (P=0.1516) between squamous cell carcinomas and non-squamous cell carcinomas. The 5-year cause-specific survival rate was 67.0% (IA: 84.4, IB: 43.7), and overall survival was 45.3% (IA: 53.9, 1B: 34.2). No adverse effects greater than grade 2 occurred in the lungs. In a single fractionation trial, the 3-year local control rate for 117 patients was 81.9%, and the control rates for patients with T1 and T2 tumors were 84.7% and 78.0%, respectively. No adverse effects greater than grade 2 occurred in the lungs. Carbon beam radiotherapy, an excellent new modality in terms of high QOL and ADL, was proven to be a valid alternative to surgery for stage I cancer, especially for elderly and inoperable patients.

Introduction

In 1998, lung cancer became the leading cause of cancer-related death in Japan, as it is in Western countries. Surgery plays a pivotal role in the curative treatment for non-small cell lung cancer (NSCLC), but it is not necessarily the best treatment for elderly persons and/or patients with cardiovascular and pulmonary complications. Conventional radiotherapy as an alternative, however, produces a five-year survival rate for merely 10-30% of the patients due to poor control of the primary tumor. Dose escalation is essential to improve the efficacy of radiotherapy, but this involves increasing risk of pulmonary toxicity. Carbon ion radiotherapy (CIRT) is a promising modality because of its excellent dose localization and high biological effect on the tumor. Our clinical trials led us to conclude that irradiation with heavy particle beams, notably carbon ion beams, offers a significant potential for improving tumor control without increasing toxicity risks.

Between 1994 and 1999, a phase I/II study of the treatment of stage I NSCLC by CIRT was first conducted using a dose escalation method to determine the optimal dose. An additional purpose was to develop correct, reliable and safe irradiation techniques for CIRT. As reported in our phase I/II study [1], the following results (Table 1) were obtained: 1) The local control rate was dose-dependent, reaching more than 90% at 90.0GyE with

a regimen of 18 fractions over 6 weeks and at 72.0GyE with 9 fractions over 3 weeks. Both doses were determined to be optimally effective. It was also found that setting the provisional target by allowing for the difference with the CT value can prevent marginal recurrence [2]. 2) Damage to the lungs was minimal, with grade 3 radiation pneumonitis occurring in 2.7% of the cases. Respiratory-gated and 4-portal oblique irradiation directions, excluding opposed ports, proved successful in reducing the incidence of radiation pneumonitis. 3) Survival was strongly influenced by local control and the size of the primary lesion. The early detection of nodal and intralobar metastasis, followed by irradiation with carbon beams, can help increase the survival rate. Local failure, distant metastasis and malignant pleurisy were responsible for decreases in survival.

Table 1 The results of a phase I/II study of carbon beam radiotherapy for stage I

Adverse reactions in the lungs 1) Minimal damage to the lungs (grade 3 radiation pneumonitis: 2.7%) 2) Influenced by dose, respiration movement, and port direction and number
Local control 1) Dose-dependent, but less dependent on tumor size and histological type 2) More than 90% by the optimal dose, and demonstrated by pathological CR
Survival 1) Influenced by the local control state and tumor size 2) Nodal and intralobar metastasis are less important, but local failure, malignant pleurisy and distant metastasis play a major role in decreasing survival

In the present manuscript, a phase II clinical trial and a phase I/II dose escalation clinical trial are reported. In the phase II clinical trial, the total dose was fixed at 72.0GyE in 9 fractions over 3 weeks [3], and at 52.8GyE for stage IA NSCLC and 60.0GyE for stage IB NSCLC in 4 fractions in one week [4]. Using this optimal schedule, the phase II clinical trial was initiated in April in 1999 and closed in December in 2003, accruing a total of 127 patients.

The phase I/II dose escalation clinical trial was initiated in April 2003. The initial total dose was 28.0GyE administered in a single fraction using respiratory-gated and 4-portal oblique irradiation directions, with the total irradiation dose being escalated in increments of 2.0GyE each, up to 46.0GyE. This clinical trial is still in progress. This article describes the intermediate steps of the phase I/II clinical trial and the preliminary results of the phase II clinical trial in terms of local control and survival after CIRT.

Materials and Methods

[Phase II clinical trial]

One hundred and twenty-nine patients with 131 primary lesions were treated with CIRT. Fifty-one primary tumors of 50 patients were treated by carbon ion beam irradiation alone using a fixed total dose of 72GyE in 9 fractions over 3 weeks (#9802 protocol [3]). The remaining 79 patients had 80 stage I tumors (#0001 protocol [4]). A total of 127 patients were evaluated for survival, as 2 patients had been treated twice, one in the first protocol #9802, and one in the second protocol #0001. The IA and IB stage tumors were treated with fixed doses of 52.8GyE and 60.0GyE in 4 fractions in one week, respectively. The mean patient age was 74.5 years, and gender breakdown was 92 males and 37 females. There were 72 T1 and 59 T2 tumors. The mean tumor size was 31.5 mm in diameter. By type, there were 85 adenocarcinomas, 43 squamous cell carcinomas, 2 large cell carcinomas and 1 adenosquamous cell carcinoma. Medical inoperability stood at 76%.

[Phase I/II clinical trial (single fractionation)]

One hundred and seventeen patients were treated in this clinical trial between April 2003 and August 2009. As mentioned above, the intermediate steps of this still ongoing phase I/II clinical trial included a total dose of 36.0GyE or more, and the follow-up time was 6 months or more after CIRT. The local control ratio of T1 tumors (□30mm in diameter) was as high as 90% at the total dose of 36.0GyE. The 117 primary tumors of the 117

patients were treated by carbon ion beam irradiation alone using a total dose of 36.0GyE (n=18), 38.0GyE (n=14), 40.0GyE (n=20), 42.0GyE (n=15), 44.0GyE (n=44) or 46.0GyE (n=6) per single fractionation. The mean patient age was 73.4 years, and gender breakdown was 40 females and 77 males. There were 68 T1 and 49 T2 tumors. The mean tumor size was 29.1 mm in diameter. By type (cancer type was determined by biopsy), there were 79 adenocarcinomas, 37 squamous cell carcinomas, and one large cell carcinoma. Medical inoperability was 58% (Table 2).

Table 2 Treatment and characteristics of 117 patients with stage I NSCLC

Age (mean)		46-87 (73.4)
Gender	Female	40
	Male	77
PS	0	87
	1	29
	2	1
Tumor size (mean)		10-62 (29.1)*
Stage	IA	68
	IB	49
Histology	Adenocarcinoma	79
	Sq cell caracinoma	37
	Large cell carcinoma	1
Reason why poor candidate for surgery		
	Refusal	49 (42)**
	Medically inoperable	68 (59)**
Total dose (GyE)		
	36.0	18
	38.0	14
	40.0	20
	42.0	15
	44.0	44
	46.0	6

*mm, **percent Aug. 31, 2009

[Carbon ion beam irradiation]

The same system of carbon ion beam irradiation was used in both phase II and phase I/II clinical trials. The targets were usually irradiated from four oblique directions without prophylactic elective nodal irradiation (ENI). A greater than 10-mm margin was set outside the gross target volume (GTV) to determine the clinical target volume (CTV). The planning target volume (PTV) was established by adding an internal margin (IM) to the CTV. The IM was determined by extending the target margin in the head and tail direction by a width of 5 mm, leading to more successful prevention of marginal recurrence, possibly because it ensured that the target was still being irradiated during respiratory movement [2]. Fig. 1 shows the dose distribution maps for a representative case. A respiratory-gated irradiation system was used in all irradiation sessions. Fig. 2 shows the CIRT room. We used vertical or horizontal beams in 2 oblique positions including 4 direction total irradiation.

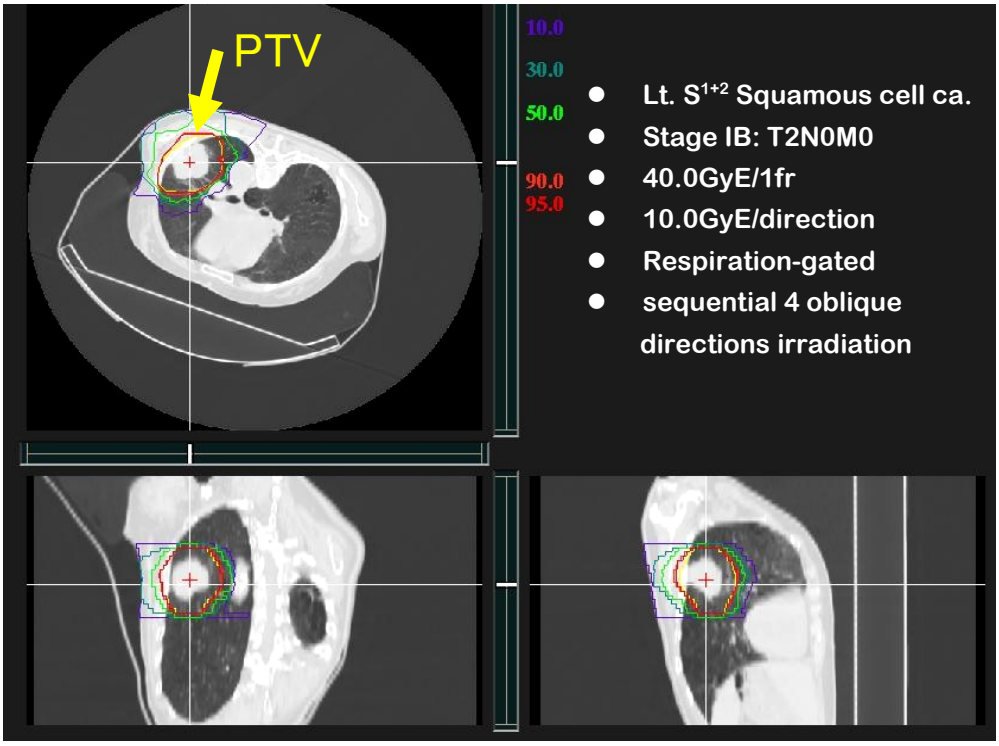

Fig. 1 Dose distribution maps of a 71-yr-old female

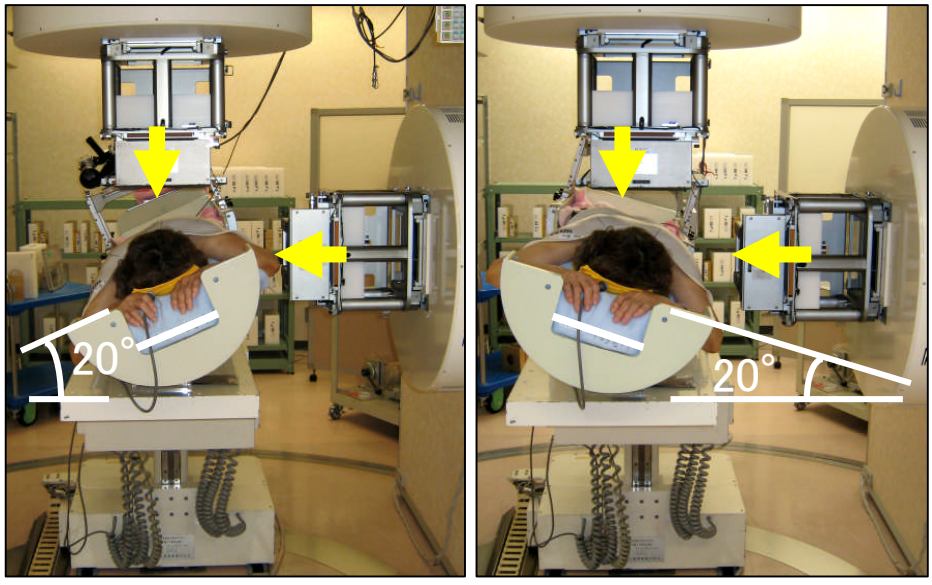

Fig. 2 Treatment room

[Statistical analysis]

Local control and survival were assessed by using the Kaplan-Meier method. For statistical analysis, the Log-rank test was used.

Results

[Phase II clinical trials (#9802, #0001)]

All patients were followed up until death, with a median follow-up time of 50.8 months, ranging from 2.5 months to 70.0 months. The local control rate for the 131 primary lesions was 91.5% (Fig. 3), those for T1 (n=72) and T2 (n=59) tumors were 96.3% and 84.7% and for squamous cell type (Sq) (n=43) and non-squamous cell type (Non-Sq) (n=88) tumors were 87.1% and 93.8%, respectively. While there was a significant difference (p=0.0156) in the tumor control rate between T1 and T2 tumors, there was no significant difference (P=0.1516) between squamous and non-squamous (T1/T1), nor between T1 and T2 for the different types. However, with respect to the squamous cell type cancer, the local control was 100% for T1 (n=17) and 78.0% for T2 (n=26) tumors, which was approaching significance (p=0.0518). The local control of non-squamous tumors was 95.3% for T1 (n=55) and 91.0% for T2 (n=33) tumors, which was not significantly different (p=0.3364).

The 5-year cause-specific survival rate of the 127 patients was 67% (Fig. 3), breaking down into 84.8% for stage IA and 43.7% for stage IB tumors (Fig. 4A). The 5-year overall survival rate was 45.3% (Fig. 3), breaking down into 53.9% for stage IA and 34.2% for stage IB tumors (Fig. 4B).

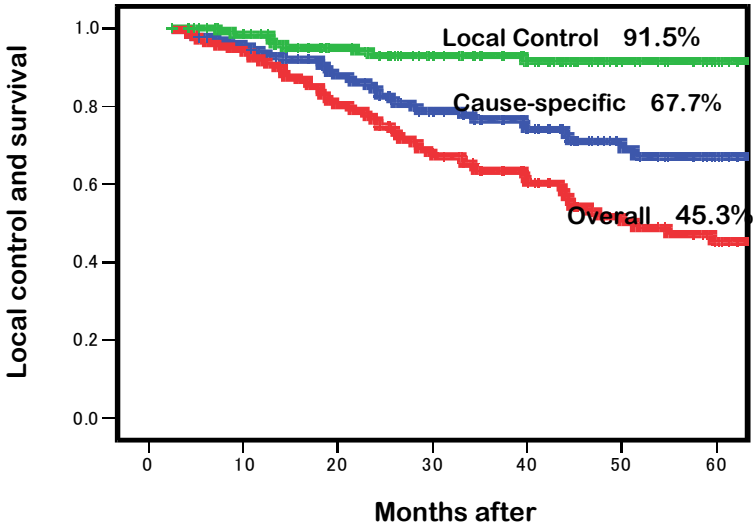

Fig. 3 Local control (n=131) and survival (n=127) following CIRT

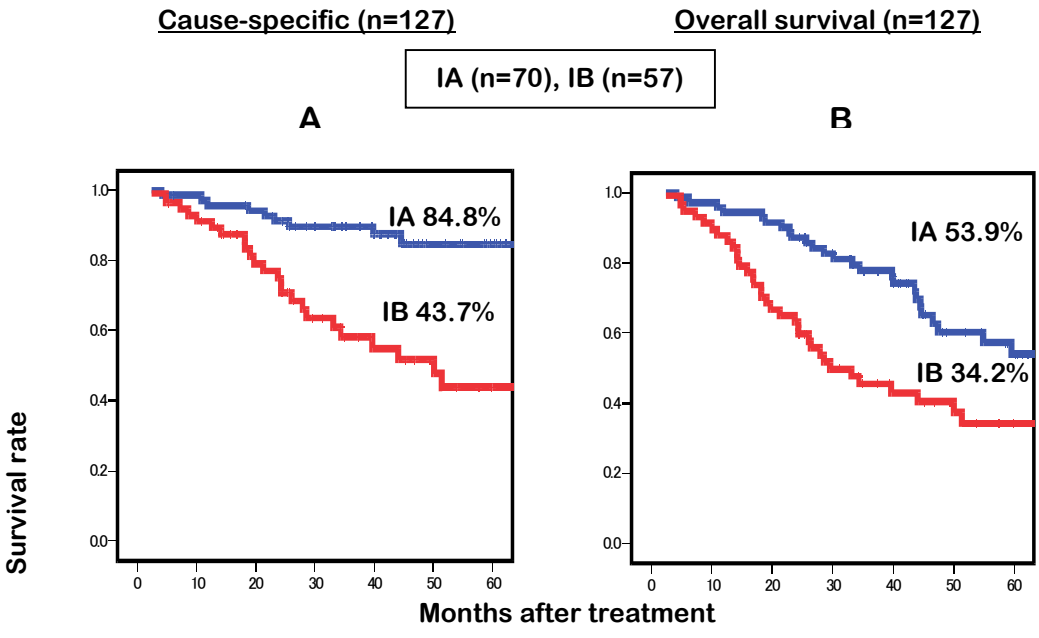

Fig. 4 Survival of patients by stage (IA and IB)

Toxicities to the skin and lungs caused by CIRT were assessed according to RTOG (early) and RTOG/EOTRC (late) as shown in Tables 3 and 4. Early skin reactions were assessed for 131 lesions and late skin reactions for 128 lesions. Of the early reaction lesions, 125 were grade 1 and 6 were grade 2. Among the late reaction lesions, 126 were grade 1, 1 was grade 2, and 1 was grade 3. Lung reaction was clinically assessed in all 129 patients. One hundred twenty-seven had grade 0 and 2 had grade 2 early reactions. Late effects were followed-up in 126 patients: 7 patients had grade 0, 116 patients had grade 1, and 3 patients had grade 2 responses. No higher than a single grade 2 reaction was observed.

Table 3. Adverse skin reactions after CIRT

Skin		Early reaction (RTOG)						Late reaction (RTOG)					
		Lesion	Grade					Lesion	Grade				
		No.	0	1	2	3	≥4	No.	0	1	2	3	≥4
	#9802	51	0	50	1	0	0	51	0	49	1	1	0
	#0001	80	0	75	5	0	0	77*	0	77	0	0	0
	Total	131	0	125	6	0	0	128	0	126	1	1	0

* 3 cases were not observed due to early death

Fifty-three of the 127 patients (41.7%) had recurrence, all occurring between 1 and 54 months (median, 10.5 months) after the commencement of therapy. No recurrence was observed in the other 74 patients (58.3%). The 9 primary recurrences (7.1%) and 11 regional metastases (8.7%) consisting of 7 regional nodes (5.5%), one intrabronchial (0.8%), and 3 intralobar metastases (PM1) (2.4%) occurred in the loco-regional site. In one patient, primary recurrence was seen at the margin, while in another it occurred in-field.

Table 4. Adverse lung reactions following CIRT

Lung		Early reaction (RTOG)						Late reaction (RTOG)					
		Lesion	Grade					Lesion	Grade				
		No.	0	1	2	3	≥4	No.	0	1	2	3	≥4
	#9802	50	49	0	1	0	0	50	0	48	2	0	0
	#0001	79	78	0	1	0	0	76*	7	68	1	0	0
	Total	129	127	0	2	0	0	126	0	116	3	0	0

* 3 cases were not observed due to early death

By sub-stage classification, the incidence of loco-regional recurrence, pleural dissemination, and distant metastasis for stage IB (63%) was much higher than for IA (24%). The total incidence of first recurrence for stage IB (63%) tended to be higher than for stage IA (24%). However, verification by χ^2 test showed no significant difference (χ^2=1.63).

The causes of death were as follows: 62 out of the 127 patients (48.8%) died, half of disease progression. Among the patients with recurrence, 5 of 9 with primary recurrence (55%) died from disease progression. Ten of the 11 patients with regional metastases were re-treated, 9 with CIRT and 1 with photons. Seven of these patients, although they had no further recurrence, died due to intercurrent disease, and 1 with node metastasis but no re-treatment died of disease progression. Eight of the 11 patients with regional metastases (72%) died, and 9 of the 10 patients (90%) with malignant pleurisy and 17 of the 23 patients (74%) with distant metastases died of disease progression. Five of them died due to primary recurrence, and 26 due to metastasis and dissemination. For the remaining 31 patients, intercurrent diseases were the cause of death [3, 4].

[Phase I/II clinical trial (single fractionation)]

All patients were followed up until death, with a median follow-up time of 30.3 months, ranging from 1.6 months to 56.9 months. The overall local control rate for the 117 primary lesions was 81.9%, and those for the patients with T1 (n=68) and T2 (n=49) tumors were 84.7% and 78.0%, respectively (Fig. 5). The 3-year overall survival rate was 73.1% and the cause-specific survival rate was 83.3%.

Toxicities of CIRT to the skin and lung were assessed according to NCI-CTC (early) and RTOG/EOTRC (late) as shown in Tables 5 and 6. Early skin reactions were assessed for 117 lesions and late skin reactions for 114 lesions. Of the early reaction lesions, 115 were grade 1 and one was grade 2. Among the late reaction lesions, 110 were grade 1 and one was grade 2. Lung reactions were clinically assessed in the 117 patients. Forty-six had grade 0, and 70 had grade 1 early reactions. Late reactions were followed up in 114 patients, with 101 showing grade 1 and one developing a grade 2 reaction.

The clinical course of a 71-year-old female is shown in Fig. 6 and Fig. 7. Tumor shrinkage and slight lung fibrosis is apparent, and a grade 1 skin reaction was observed.

Discussion

In the present study, local control, cause-specific, and overall survival rates for the 127 patients in the phase II clinical trial were 91.5%, 67.0%, and 45.3%, respectively. The overall local control, local control of T1 tumors, and local control of T2 tumors were 81.9%, 84.7%, and 78.0%, respectively, by single fractionation. Toxicities to the skin, lungs and bone were minimal.

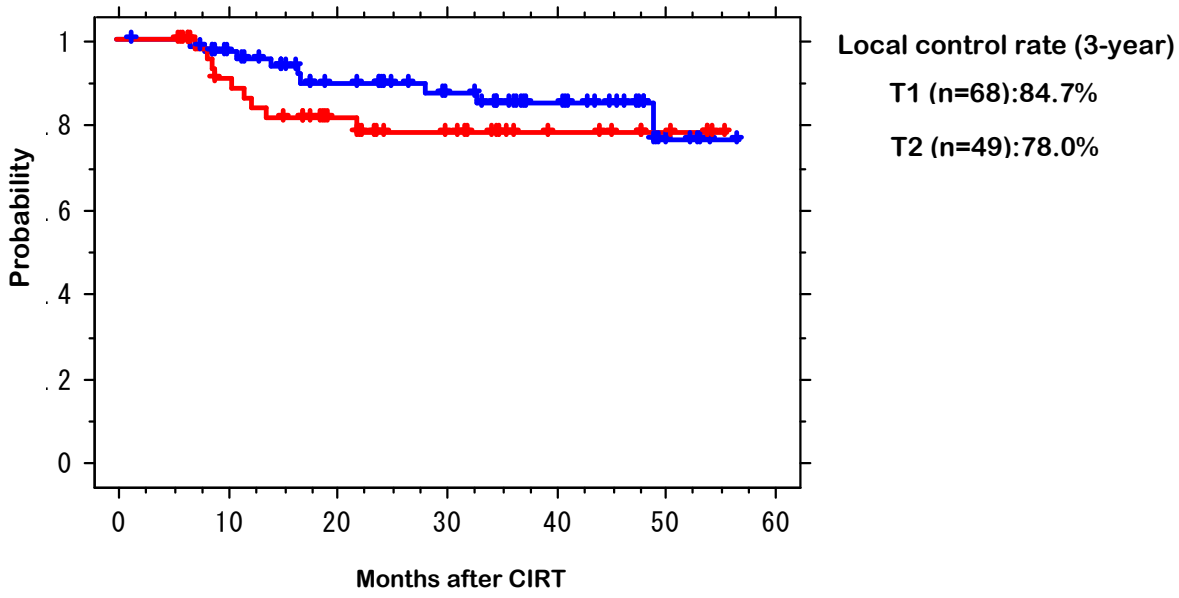

Fig. 5 Tumor control rates after single fractionation ICRT

Table 5. Adverse skin reactions after single fractionation CIRT

Skin	Total dose (GyE)	Early reaction (NCI-CTC)						Late reaction (RTOG/EORTC)					
		No. of Cases	Grade					No. of Cases	Grade				
			0	1	2	3	≥4		0	1	2	3	≥4
	36.0	18	0	18	0	0	0	17*	0	17	0	0	0
	38.0	14	0	14	0	0	0	13*	0	13	0	0	0
	40.0	20	1	18	1	0	0	20	2	17	1	0	0
	42.0	15	0	15	0	0	0	14*	0	14	0	0	0
	44.0	44	1	44	0	0	0	44	1	43	0	0	0
	46.0	6	0	6	0	0	0	6	0	6	0	0	0
	Total	117	2	115	1	0	0	114	3	110	1	0	0

*One case was not observed in each group

Table 6 Adverse lung reactions after single fractionation CIRT

Lung	Total dose (GyE)	Early reaction (NCI-CTC)						Late reaction (RTOG/EORTC)					
		No. of Cases	Grade					No. of Cases	Grade				
			0	1	2	3	≥4		0	1	2	3	≥4
	36.0	18	12	6	0	0	0	17*	3	14	0	0	0
	38.0	14	9	5	0	0	0	13*	2	11	0	0	0
	40.0	20	10	10	0	0	0	20	4	16	0	0	0
	42.0	15	9	6	0	0	0	14*	1	13	0	0	0
	44.0	44	6	37	1	0	0	44	2	41	1	0	0
	46.0	6	0	6	0	0	0	6	0	6	0	0	0
	Total	117	46	70	1	0	0	114	12	101	1	0	0

*One case was not observed in each group

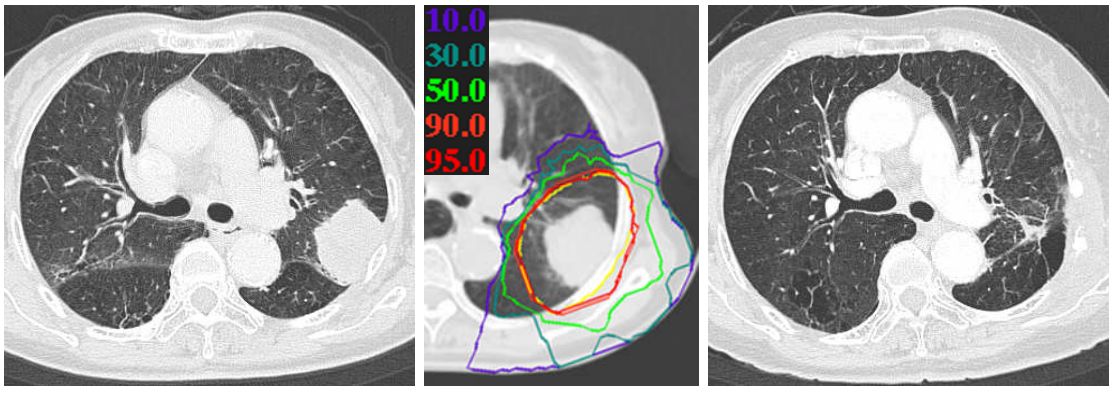

Fig. 6 The clinical course of a 71-year-old female (T2N0M0 squamous cell carcinoma) after CIRT (40GyE/ single fractionation). The initial CT (A), dose distribution map (B), and CT (C) at18 months after CIRT are shown. Apparent tumor shrinkage was observed without severe lung fibrosis.

Out of the 131 primary cancers in 127 patients, local recurrence occurred in 9 patients (6.8%). The average recurrence time was 17.2 months, ranging from 7 to 39 months. According to our previous study, the observation period required to determine local control of the irradiated lesions was at least 3 years post therapy [1]. However, the present study suggested the need for a longer observation period. It is evident that prolonged survival guarantees more reliable observation of local control results.

For the correct assessment of local control in patients who could not be observed for such a long duration because of death resulting from metastasis/dissemination or intercurrent disease, a histological approach based on repeated bronchoscopy was used, providing evidence of the absence of viable tumor cells in the collected specimens [3].

Furthermore, definite tumor control was also confirmed by the autopsies of CIRT-treated patients and in cases treated by surgery [5]. Such high and definite tumor control appears to be an outstanding feature of CIRT. Presumably, this is primarily due to the radiobiological nature of the high LET beams, which may account for the higher survival rate of patients with stage I NSCLC, since the failure of local control for primary tumors directly affects the poor survival of stage I NSCLC patients [1, 3]. Among our cases, 5 of 9 patients with primary recurrence (55%) died due to disease progression.

Eleven regional recurrences occurred. This incidence was close to that of surgery (7.5% [6], 11% [7]). Eight of these patients (72%) died. Only one patient, with no retreatment, died due to disease progression. The other 7 retreated patients died due to intercurrent disease. Martini et al. [7] reported that any resection less than a lobectomy coupled with no lymph node dissection had adverse effects on recurrence and survival of patients who underwent surgery. Our CIRT strategy for regional recurrence was thus validated to be as safe and effective as the standard surgical procedure for stage I NSCLC.

Nine of the 10 patients (90%) with malignant pleurisy and 17 of the 23 patients (74%) with distant metastasis died of disease progression. The poor prognosis of stage IB cases was based on the high incidence of pleural and distant metastasis.

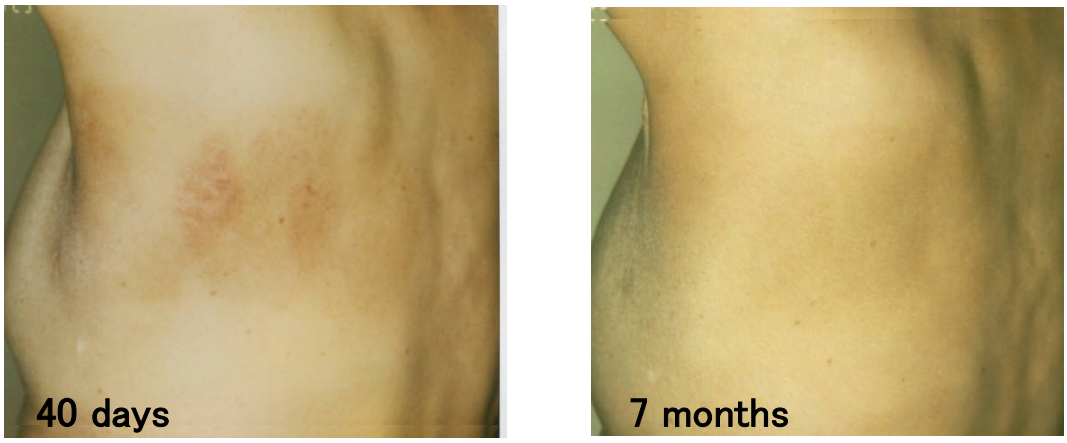

Fig. 7. A patient Grade I skin reaction after CIRT (40.0GyE/1fr).

With clinical stage I NSCLC, our 5-year overall survival results were somewhat inferior to the surgery [Author: significantly, or just a trend toward being inferior?] [3, 5]. This difference may have been due to the significant age gap between the two groups. The incidence of death due to recurrence in the surgical groups was 29% or 36%, whereas that due to intercurrent diseases was 19% or [a few-Author: add the actual number] % [6, 7]. In contrast, our patients showed a higher incidence of death due to intercurrent diseases (60%) than death due to recurrence (40%). Comparison of stage IA with stage IB patients revealed a large difference between overall (53.9%) and cause-specific (84.8%) survival for those with stage IA disease, while there was a smaller difference in the stage IB overall (34.2%) and cause-specific (43.7%) survival. Such survival differences in the two stage I subgroups might well be explained by the low incidence of recurrence-related deaths in the stage IA (24%) patients and the high incidence of recurrence-related death in stage IB patients (63%). Generally, such a high

frequency of intercurrrent death might be related to the advanced age of our patients, as they were on average 10 years older than the surgical patients [6, 7]. As we have reported, elderly patients 80 years and older can be treated safely by CIRT [8], but the survival rate was lower in our study because these patients were more likely to die of other causes than the younger patients.

Compared with pulmonary damage reported for stereotactic radiotherapy for stage I NSCLC [9-11], the incidence and severity in our patients seem to be remarkably low. This decrease in adverse effects on the lung were achieved as a result of the small volume irradiated. This advantage is a result of the excellent dose distribution property unique to carbon ion beams and lies in the formation of a Bragg peak, which is not present when X-rays are used as the permeating beam.

Conclusions

One hundred twenty-seven stage I NSCLC patients with 131 primary tumors were treated with CIRT using a total dose of 72GyE in a regimen of 9 fractions over 3 weeks, and 52.8GyE for stage IA and 60GyE for stage IB at 4 fractions in one week. In addition, 117 stage I NSCLC patients with 117 primary tumors were treated with single-fraction CIRT using total doses ranging from 36.0GyE to 46.0GyE. These studies have led to seven major findings:

1. The local control rate of the 131 primary lesions was 91.5%. There was statistically significant differences between the local control rates for T1 and T2 tumors, and near significance between the rates for squamous cell carcinoma and non-squamous cell carcinoma (stage T2).
2. The five-year overall and cause-specific survival rates of the 127 patients were 45.3% and 67.0%, respectively.
3. The five-year overall survival rates of the patients with stage IA and stage IB were 53.9% and 34.2%, while five-year cause-specific survival rates with stage IA and stage IB were 84.8% and 43.7%, respectively.
4. There was high incidence of intercurrent death in our patients due to advanced age and related complications.
5. Adverse effects on the skin and lungs were minimal, indicating the safety of the modality. Carbon beam radiotherapy, which is an excellent new modality in terms of a high QOL and ADL, is a valid alternative to surgery for stage I cancer, especially for elderly and inoperable patients.
6. In CIRT using single fractionation with a total dose range from 36.0GyE to 46.0GyE, the local control rate for the 117 primary lesions was 81.9%, and those for the T1 (n=68) and T2 (n=49) tumors were 84.7% and 78.0%, respectively.
7. Single fractionation CIRT is effective, viewed at this intermediate step, and is a safe modality for stage I NSCLC.

References

[1] Miyamoto T, Yamamoto N, Nishimura H, et al. Carbon ion radiotherapy for stage I non-small cell lung cancer. Radiother Oncol 2003;66:127-140.

[2] Koto M, Miyamoto T, Yamamoto N, et al. Local control and recurrence of stage I non-small cell lung cancer after carbon ion radiotherapy. Radiother Oncol 2004;71:147-156.

[3] Miyamoto T, Baba M, Yamamoto N, et al. Curative treatment of stage I non-small cell lung cancer with carbon ion beams using a hypo-fractionated regimen. Int J Radiat Oncol Biol Phys 2007;67:750-8.

[4] Miyamoto T, Baba M, Sugane T, et al. Carbon ion radiotherapy for stage I non-small cell lung cancer using a regimen of four fractions during 1 week. J Thorac Oncol 2007;2:916-26.

[5] Yamamoto N, Miyamoto T, Nishimura H, et al. Preoperative carbon ion radiotherapy for non-small cell lung cancer with chest wall invasion - pathological findings concerning tumor response and radiation induced lung injury in the resected organs. Lung Cancer 2003;42:87-95.

[6] Harpole DH, Herndon JE, Yung WG, et al. Stage I nonsmall cell lung cancer. A multivariate analysis of treatment methods and patterns of recurrence. Cancer 1995;76:787-796.

[7] Martini N, Bains MS, Burt ME, et al. Incidence of local recurrence and second primary tumors in resected stage I lung cancer. J Thorac Cardiovasc Surg 1995;109:120-129.

[8] Sugane T, Baba M, Imai R, et al. Carbon ion radiotherapy for elderly patients 80 years and older with stage I non-small cell lung cancer. Lung Cancer (2008), doi:10.1016/j.lungcan.2008.07.007.

[9] Nagata Y, Takayama K, Matsuo Y, et al. Clinical outcomes of a phase I/II study of 48Gy of stereotactic body radiotherapy in 4 fractions for primary lung cancer using a stereotactic body frame. Int J Radiat Oncol Biol Phys 2005;63:1427-1431.

[10] Onishi H, Shirato H, Nagata Y, et al. Hypofractionated stereotactic radiotherapy (HypoFXSRT) for stage I non-small cell lung cancer: updated results of 257 patients in a Japanese multi-institutional study. J Thorac Oncol 2007;2 (7 Suppl 3):S94-100

[11] Timmerman R, McGarry R, Yiannoutsos C, et al. Excessive toxicity when treating central tumors in a phase II study of stereotactic body radiation therapy for medically inoperable early-stage lung cancer. J Clin Oncol 2006;24:4833-4839

Carbon Ion Radiotherapy in Bone and Soft Tissue Sarcomas

Tadashi Kamada, Reiko Imai, Hiroshi Tsuji, Takeshi Imaizumi,
Akira Matsunobu, Tohru Okada, and Hirohiko Tsujii

Research Center for Charged Particle Therapy, National Institute of Radiological Sciences, Chiba, Japan
Corresponding Author: Tadashi Kamada, e-mail address: t_kamada@nirs.go.jp

Abstract

The Heavy Ion Medical Accelerator in Chiba (HIMAC) is the world's first heavy ion accelerator complex dedicated to medical use in a hospital environment. Heavy ions have superior depth-dose distribution and greater cell-killing capability than other forms of radiation. In June 1996, clinical research for the treatment of bone and soft tissue sarcomas was begun using carbon ions generated by the HIMAC. As of February 2010, a total of 507 patients with bone and soft tissue sarcoma were enrolled in these clinical trials. Most of the patients had locally advanced and/or medically inoperable sarcomas. The clinical trials revealed that carbon ion radiotherapy provided definite local control and offered a survival advantage without unacceptable morbidity for patients with bone and soft tissue sarcomas that were hard to cure using other modalities.

1. Introduction

Tumors arising from bones, muscles, and vessels are referred to as bone and soft tissue sarcomas. While the incidence of these tumors is low, they are capable of occurring ubiquitously throughout the body. For this reason, they are occasionally detected too late for surgery, or their accurate diagnosis presents difficulty and incomplete treatment is administered on the false recognition of their being benign.

While tumor resection is the most common treatment modality for such bone and soft tissue sarcomas, major progress has been made in their management, thanks to the development of combined therapy modalities in recent years, and in the wake of advances made in surgical techniques. The new combined modalities use chemotherapy and radiotherapy with new imaging diagnostics such as MR, CT, and PET. Among these tumors, osteosarcomas originating in the limbs account for the majority of malignant bone tumors, and limb-sparing surgery not requiring arm or leg amputation has become possible through a combination of surgical resection and chemotherapy. The therapeutic results have also shown a dramatic improvement in recent years. While the five-year survival rate was only 10-20% in the 1970s, the latest data show that the survival rate is as high as 50-80%. Similarly, soft tissue sarcomas developing in muscle or other soft tissues have meanwhile been shown to be responsive to treatment with a combination of chemo-radiotherapy modalities and functional preservation surgeries to achieve five-year survival rates in more than 70% of patients. In the case of tumors that have developed in or near the spinal cord or in the pelvis, as well as advanced limb tumors and postoperative recurrent tumors, however, chemotherapy is often not be very effective, and curative surgery may be difficult to perform. Moreover, most bone and soft tissue sarcomas are known to be resistant to conventional radiation. Thus, despite the significant progress seen in the treatment of bone and soft tissue sarcomas in recent years, patients judged to be intractable to surgery are less likely to find an effective treatment option.

However, the introduction of carbon ion radiation, with its superior dose conformity and potent biological effects has promise for also achieving outstanding results in radio-resistant bone and soft tissue sarcomas. This article presents our experiences with carbon ion radiotherapy using the Heavy Ion Medical Accelerator in Chiba (HIMAC) at NIRS for patients with bone and soft tissue sarcomas.

2. Patients and Methods

1) Patients

A dose escalation trial (phase I/II trial) using carbon ion beams was carried out on 64 lesions in 57 patients with bone or soft tissue sarcomas during the period from June 1996 until February 2000 [1]. A fixed-dose phase II trial was then initiated in April 2000, and records as of February 2010 show that 463 lesions in 444 patients have been treated. Both of these trials included bone or soft tissue sarcoma patients for whom surgical resection was contra-indicated. The main eligibility criteria are listed in Table 1. While the phase II trial included patients with radiation-associated sarcoma, it did exclude patients with intravascular tumor embolus. Four hundred and sixty-seven patients (493 lesions) in these 2 trials have been followed for 6 months or longer after carbon ion treatment as of February 2010. Their clinical characteristics are summarized in Table 2. There were 289 males and 178 females, and their age ranged from 11 to 87 years, with a median of 52 years. Tumor locations were as follows: 98 lesions were in the spine or paraspinal region; 361 in the pelvis, and 34 in the extremities and other sites. The tumors were categorized as 365 primary bone and 102 primary soft tissue sarcomas. Histological classification showed that chordoma was the most frequent tumor, accounting for 156 patients, followed by osteosarcoma in 86 patients, chondrosarcoma in 73 patients, MFH (including 17 bone primaries) in 35 patients and Ewing/PNET in 35 patients (including 5 soft tissue primaries). For pathological confirmation, central pathological review of surgical or biopsy specimens was carried out. All patients enrolled in the trials gave their written informed consent.

Table 1. Eligibility criteria

• Histologically confirmed bone or soft tissue sarcomas
• Unresectable tumor or the patient declines surgery
• Gross measurable lesion
• Lesion size <15cm in maximum diameter
• KPS 60~100%
• No prior radiotherapy of the lesion
• Signs informed consent statement

Abbreviations: KPS, Karnofsky performance status

Table 2. Patient characteristics

Characteristic			No. (N =467)
Age, years			
Median (range)			57 (11~87)
Sex			
Female/ Male			178/289
Tumor sites (493 lesions)			
Pelvis			361
Spine/para-spine			98
Extremities etc			34
Histology			
Bone		365	
Chordoma			156
Osteosarcoma			86
Chondrosarcoma			73
PNET			30
MFH			17
Others			3
Soft tissue		102	
MFH			18
MPNST			18
Synovial sarcoma			10
Liposarcoma			9
PNET			5
Leiomyosarcoma			6
Rhabdomyosarcoma			5
Others			31
Clinical target volume, cm^3			
Mean (range)			502 (16~2900)

Abbreviations: PNET, primitive neuroectodermal tumor; MFH, malignant fibrous histiocytoma; MPNST, malignant peripheral nerve sheath tumor

2) Carbon ion radiotherapy

The features of the Heavy Ion Medical Accelerator in Chiba (HIMAC) and the carbon ion beam have been previously described [1]. In brief, the accelerated carbon ion beam energies used for treatment during our clinical trial were 290, 350, and 400 MeV. The range of the beams was a depth of 15–25 cm in water. An appropriately sized ridge filter corresponding to the tumor size was selected to form the spread-out Bragg peak (SOBP). A compensation bolus was fabricated for each patient to make the distal configuration of the SOBP similar to the shape of the target volume. A multi-leaf collimator defined the margins of the target volume. The patients were placed in customized cradles and immobilized with a low-temperature thermoplastic sheet. A set of 5-mm-thick CT images was taken for the treatment planning. Three-dimensional treatment planning was performed with HIPLAN software (National Institute of Radiologic Sciences, Chiba, Japan) for the planning of carbon ion therapy. A margin of 5 mm was usually added to the clinical target volume to create the planned target volume. When the tumor was located close to critical organs such as the spinal cord, skin or bowel, the margin was

reduced accordingly. The clinical target volume was covered by at least 90% of the prescribed dose. The dose was calculated for the target volume and any nearby critical structures and expressed in Gray-Equivalent (GyE = carbon physical dose (Gy) x Relative Biological Effectiveness {RBE}). Carbon ion radiotherapy was given once daily, 4 days a week (Tuesday to Friday), for a fixed 16 fractions over 4 weeks. The patients were treated with two to eight irregularly shaped ports (median, 3 ports). One port was used in each session. At every treatment session, the patient's position was verified with a computer-aided on-line positioning system. The patient was positioned on the treatment couch with the immobilization devices, and digital orthogonal X-ray TV images in that position were taken and transferred to the positioning computer. They were compared with the reference image on the computer screen and the differences were measured. The treatment couch was then moved to the matching position until the largest deviation from the field edge and the isocenter position was less than 2 mm. For all of these patients, a total dose ranging from 52.8 GyE to 73.6 GyE was administered by a fractionation regimen of 16 fractions over four weeks (with single radiation doses of 3.3 - 4.6 GyE).

3. Results

A dose escalation trial (phase I/II trial) with a total dose ranging from 52.8 GyE to 73.6 GyE administered in 16 fractions over four weeks (single radiation doses of 3.3 - 4.6 GyE) was carried out on 64 lesions of 57 patients with bone and soft tissue sarcoma between June 1996 and February 2000. As 7 of the 17 patients treated with 73.6 GyE were found to have grade 3 RTOG acute reactions (skin), dose escalation was halted at this dose level. No other grade 3 or worse acute reactions were detected. These findings made it clear that with a fractionation regimen of 16 fractions over four weeks, a total dose of 70.4 GyE was the maximum applicable dose in cases in which the skin presented a problem, and a total dose of 73.6 GyE was possible in other cases. The overall local control rate was 89% at 1 year, 63% at 3 years, and 63% at 5 years. A significant difference was found between the local control rates achieved with a total dose of 57.6 GyE or less and those with 64.0 GyE or more. The median survival was 31 months (2-96 months), and the 1-, 3- and 5-year survival rates were 82%, 47%, and 37%, respectively. A fixed-dose phase II trial was then initiated in April 2000, and as of February 2010, 448 patients have been enrolled for treatment. The number of lesions and patients analyzed six months or longer after therapy stands at 427 lesions of 404 patients, with 10 of these lesions having been treated with a dose of 73.6 GyE (4.6 GyE per fraction), 27 with 64 GyE (4.0 GyE per fraction) and 53 with 67.2 GyE (4.2 GyE per fraction). The remaining 336 lesions were treated with a dose of 70.4 GyE (4.4 GyE per fraction). As of the present, the 2- and 5-year local control rates are 89% and 74%, and similarly, the overall survival rates are 80% and 62%, respectively (Figure 1).

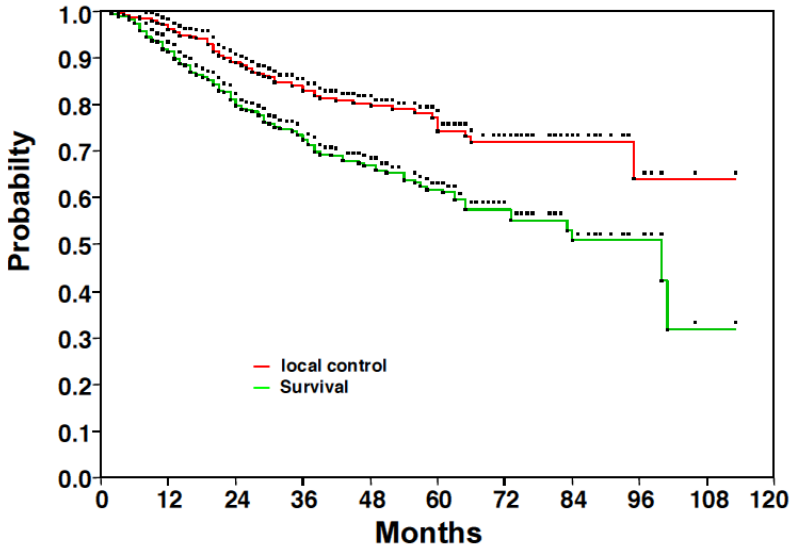

Figure 1. Actuarial local control and overall survival in the 404 phase II study patients with bone or soft tissue sarcomas. Local control rate at 5 years was 74%, and overall survival rate at 5 years was 62 %.

Radiation morbidities are summarized in Table 3. Grade 3 or worse toxic reactions included 2 patients with acute skin toxicities (grade 3) and 7 patients with late skin toxicities (grade 3: 6 patients; grade 4: 1 patient). These late skin reactions suggest that the following may be risk factors in addition to the total dose: 1) subcutaneous tumor invasion, 2) tumor volume, 3) sacral involvement, 4) previous surgery, 5) additional chemotherapy, and 6) irradiation from two portals. It was possible, however, to prevent these reactions by aiming for a standard dose of 70.4 GyE and by modifying the irradiation method so that it may include irradiation from three portals, in order to reduce the dose delivered to the skin [2]. The acute and late skin reactions at each dose level are listed in Table 4. The incidence of severe skin reactions in the patients receiving 70.4 GyE was within the acceptable level for the past several years.

Table 3. Radiation morbidities in the phase II study

		Grade					
	No.	0	1	2	3	4	5
Skin							
Early	427	1	385	38	3	0	0
Late	420	4	389	20	6	1	0
GI tract							
Early	380	375	5	0	0	0	0
Late	374	373	1	0	0	0	0
Lung							
Early	33	33	0	0	0	0	0
Late	33	31	2	0	0	0	0
Edema	18	14	3	1	0	0	0
Spinal cord	39	38	0	1	0	0	0

Early: RTOG, Late: RTOG/EORTC, SOMA/LENT

Table4. Skin reactions by dose level

		Grade : Early (RTOG)					
Total Dose (/Fr.)	No.	0	1	2	3	4	5
64.0 (4.0)	28	0	26	1	1	0	0
67.2 (4.2)	53	0	53	0	0	0	0
70.4 (4.4)	336	1	306	28	1	0	0
73.6 (4.6)	10	0	0	9	1	0	0
	427	1	385	38	3	0	0

		Grade : Late (RTOG/EORTC)					
Total Does (/Fr.)	No.	0	1	2	3	4	5
64.0 (4.0)	27	1	25	1	0	0	0
67.2 (4.2)	53	0	53	0	0	0	0
70.4 (4.4)	330	3	299	13	3	1	0
73.6 (4.6)	10	0	3	4	3	0	0
	420	4	389	20	6	1	0

/Fr.: per fraction

The entire evaluable population for both of the above clinical trials amounted to 493 lesions in 467 patients, and their aggregate 5-year local control rate presently stands at 73% and their 5-year overall survival rate at 57% (Figure 2). The 156 chordoma patients (excluding patients with the base of the skull primaries) from this population have a 5-year local control rate of 84% and a 5-year overall survival rate of 86% (Figure 3) (A report on the 30 sacral chordoma patients who were observed for a period of two years or longer was previously published in Clinical Cancer Research [3]). The reported 5-year local control rates of surgical treatment with or without radiations for chordoma were 44 to 77 % [4-8], while the 5-year local control rate of our series was 84% (Table 5). Our follow-up period was rather short, however, so additional follow-up will be necessary to confirm whether carbon ion radiation represents a promising alternative to surgery. Nevertheless, we believe the method will be useful because a large number of the lesions treated in our study were already at an advanced stage.

The 5-year local control rate and 5-year overall survival rate for the 78 patients with osteosarcoma of the trunk were 64% and 29%, respectively (Figure 4). Five year survival rates for unresectable osteosarcoma of the trunk in the literature were 10 % or less [9-12], while that of our 78 patients treated with carbon beam was 29% (Table 6). Tumor size has been pointed out one of the most significant prognosticators in the surgical series of osteosarcoma of the trunk [14]. Similarly, in our present series, we found that local control and survival depended on the tumor volume. Forty-five lesions with the volume of less than 600 cc showed a 5-year local control rate of 91 %, while 33 lesions with a volume of more than 600 cc had a rate of 21%. The five-year survival rate in the 45 patients with smaller tumors (less than 600cc) was 40%, but was only 12% in the group with larger tumors. For the evaluable 70 chondrosarcoma patients, the 5-year local control rate and 5-year overall survival rate were 60% and 60%, respectively. (Figure 5)

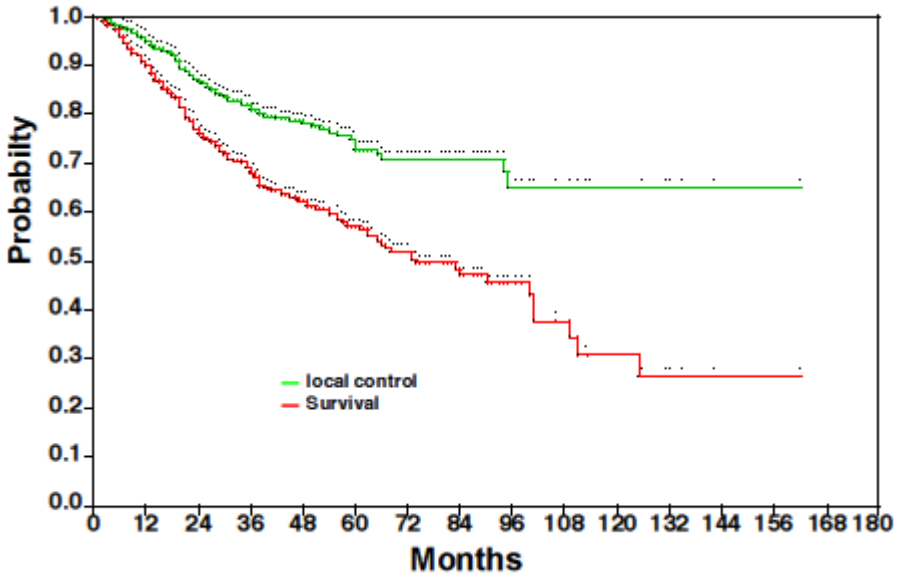

Figure2. Actuarial local control and overall survival in the 467 patients (493 lesions) with bone or soft tissue sarcomas. Local control rate at 5 years was 73%, and overall survival rate at 5 years was 57%.

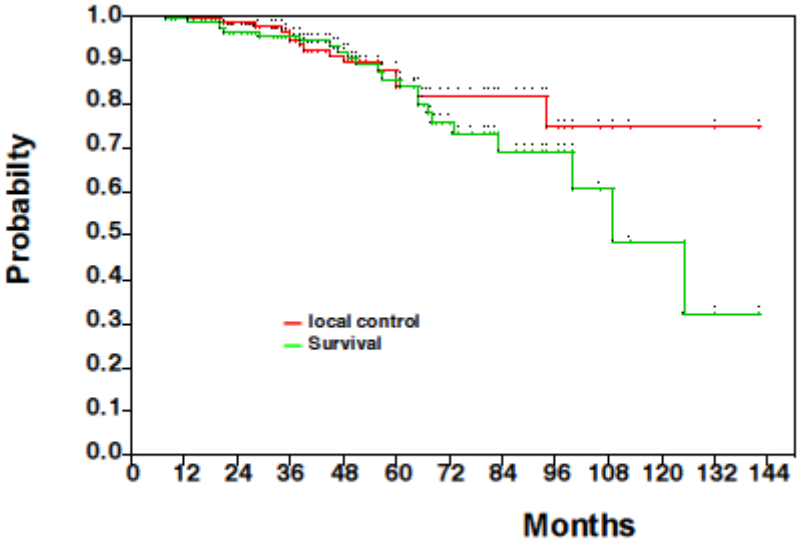

Figure3. Actuarial local control and overall survival in the 156 patients with chordoma. Local control rate at 5 years was 84%, and overall survival rate at 5 years was 86%.

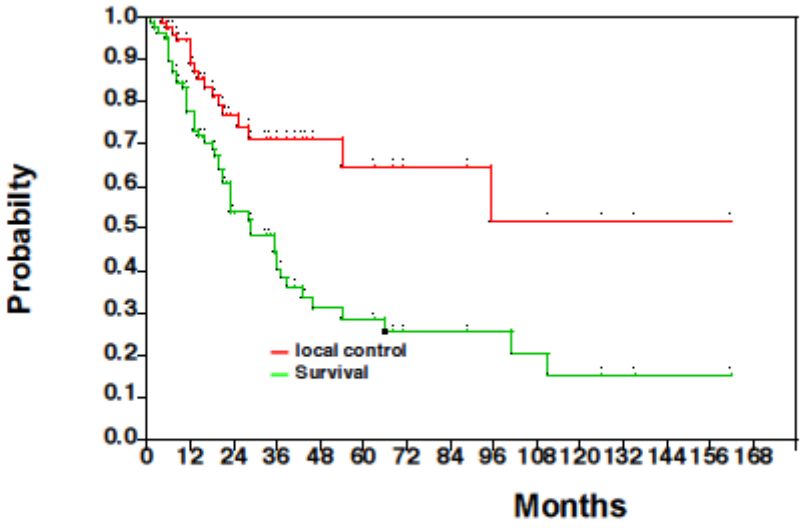

Figure4. Actuarial local control and overall survival in the 78 patients with osteosarcoma. Local control rate at 5 years was 65%, and overall survival rate at 5 years was 29%.

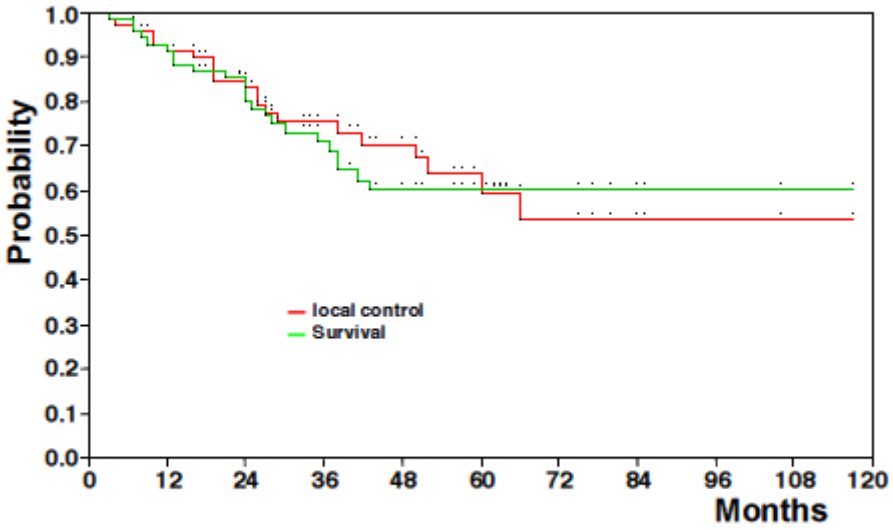

Figure5. Actuarial local control and overall survival in the 70 patients with chondrosarcoma. Local control rate at 5 years was 60%, and overall survival rate at 5 years was 60%.

Table 5. Local control and survival rate of patients with chordoma

	No. of Pts. (new pts /y)	Site	Treatment	Local 5-years	Survival 5-years	10-years
MGH 4) 1972-1992	21 (1.1)	S	Surgery	77%	-	50%
Sweden 5) 1963-1998	39 (1.1)	S+Sp	Surgery	44	84%	64
MGH. 6) 1982-2002	27 (2.7)	S	Surgery + Proton	72	82	62
LBL 7) 1977-1989	14 (1.2)	S	Surgery + He-ion	55	85	22
Mayo 8) 1980-2001	52 (2.5)	S	Surgery	56	74	52
NIRS 1996-2009.8	156 (11)	S+Sp	C-ion	84	86	48

S: sacrum, Sp: mobile spine

Table 6. Survival rate in patients with osteosarcoma

	No. of Pts.	Site	Overall 5year	Surgery yes 5year	none 5year
MSKCC 9) (1977-1994)	40	Pelvis	34 %	41 %	10 %(1/10)
Royal Ortho Hosp 10) (1971-1996)	36	Pelvis	18	41	0
COSS 11)12) (1979-1998)	67 22	Pelvis Spine	27 30	34 40	0 0
NCBT 13) (1978-1995)	40	Pelvis	21	26	-
University of Zurich14)	43	Pelvis	38	38	-
NIRS, C-ion (1996-2009.8)	78 45 (600 cc or less)	Pelvis + Spine	29 40	- -	29 40

4. Discussion

In this study, carbon ion radiotherapy was well tolerated and demonstrated substantial activity against sarcomas [1,3,15]. These results were obtained in patients with advanced and/or chemo-resistant gross lesions not suited for surgical resection and located mainly in the trunk. Irradiation with a total dose ranging from 64 to 73.4 GyE in 16 fractions over four weeks resulted in a local control rate of 75% for bone and soft tissue sarcomas disqualified from surgery. Although treatment results after carbon ion radiotherapy have so far been quite satisfactory, it is imperative to continue with long-term follow-up and carry out further analyses to assess local control, toxicities, survival rate and QOL as a function of such criteria as histological type, location, tumor size, irradiation field and dose, to design a safe and effective therapy regimen. For small lesions, in particular, the possibility of using a shorter irradiation regimen should be explored. Systematic analyses will be essential to determine the optimum dose and irradiation field setting in accordance with the patient's histological type and tumor location and to shed light on the problems involved. Research will also be needed to clarify the role of heavy particle radiotherapy in the context of combined therapy modalities for bone and soft tissue sarcomas. In addition to patients disqualified from surgery, elderly patients and patients with major functional loss subsequent to surgical resection, would also benefit from the use of carbon ion radiotherapy as a valid alternative to surgery. While previous experience with carbon ion radiotherapy to the extremities has so far been rather limited, the combination of carbon ion radiation and surgery could offer a promising strategy for patients intractable to limb-sparing surgery as a modality for widening the scope of limb-retaining therapy (Figure 6).

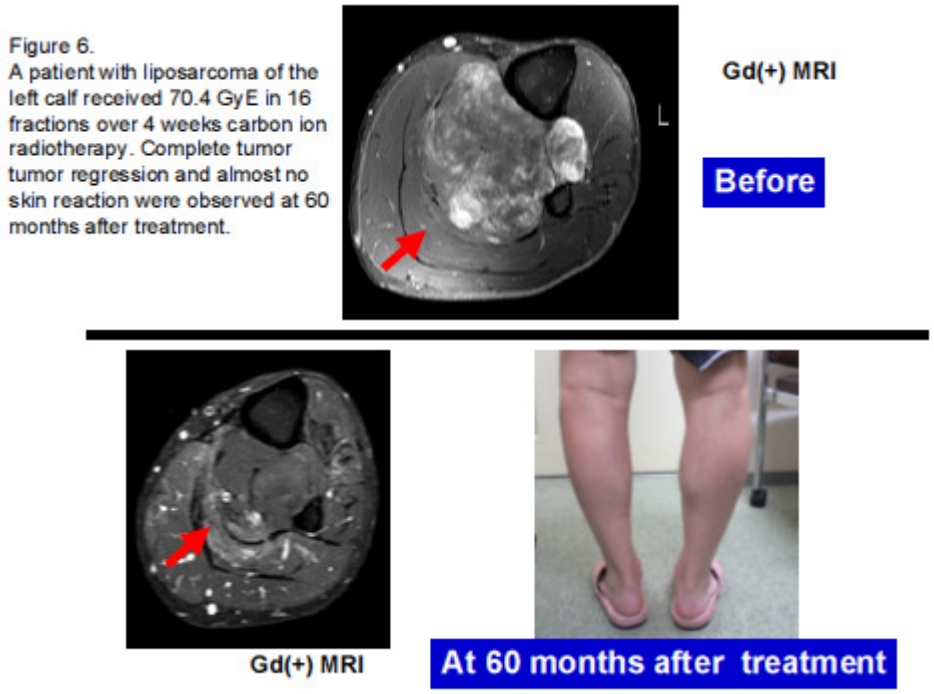

Figure 6.
A patient with liposarcoma of the left calf received 70.4 GyE in 16 fractions over 4 weeks carbon ion radiotherapy. Complete tumor tumor regression and almost no skin reaction were observed at 60 months after treatment.

5. Conclusion

Carbon ion radiotherapy is an effective local treatment for patients with bone and soft tissue sarcomas for whom surgical resection is not a viable option, and it shows great promise as an alternative to surgery. The morbidity rate of carbon ion radiotherapy has so far been acceptable, although the long-term safety of this approach for patients with sarcomas will need to be monitored.

References

[1] Kamada T, Tsujii H, Tsuji H, et al. Efficacy and Safety of Carbon Ion Radiotherapy in Bone and Soft Tissue Sarcomas. Journal of Clinical Oncology. 2002;20:4466-4471.

[2] Yanagi T, Kamada T, Tsuji H, et al. Dose-volume histgram and dose-surface histgram for skin reactions to carbon ion radiotherapy for bone and soft tissue sarcoma. Radiother Oncol. 95(1):60-5. 2010

[3] Imai R, Kamada T, Tsuji H, et al. Carbon Ion Radiotherapy for Unresectable Sacral Chordomas. Clinical Cancer Research. 2004;10:5741-5746.

[4] Samson I.R., Springfield D.S., Suit H.D. et al. Operative treatment of sacrococcygeal chordoma. A review of twenty-one cases. J Bone Joint Surg Am., *75:*1476-1484,1993

[5] Bergh P., Kindblom L.G., Gunterberg B. et al. Prognostic factors in chordoma of the sacrum and mobile spine: a study of 39 patients. Cancer, *88:*2122-2134,2000.

[6] Park L, Delaney TF, Liebsch NJ, et al. Sacral chordomas: Impact of high dose proton /photon-beam radiation therapy combined with or without surgery for primary versus recurrent tumor.Int J Radiat Oncol Biol Phys. 65(5):1514-21, 2006

[7] Schoenthaler R., Castro J.R., Petti P.L., et al. Charged particle irradiation of sacral chordomas. Int J Radiat Oncol Biol Phys., *26:291*-298,1993.

[8] Fuchs B, Dickey ID, Yaszemski MJ, et al. Operative management of sacral chordoma. J Bone Joint Surg Am. 87(10):2211-6, 2005

[9] Kawai A, Huvos AG, Meyers PA, et al. Osteosarcoma of the pelvis. Oncologic results of 40 patients. Clin Orthop Relat Res. (348):196-207. 1998.

[10] Ham SJ, Kroon HM, Koops HS, et al. Osteosarcoma of the pelvis--oncologic results of 40 patients registered by the Netherlands Committee on bone Tumors. Eur J Surg Oncol. 26(1):53-60. 2000.

［11］ Grimer RJ, Carter SR, Tillman RM, et al. Osteosarcoma of the pelvis. J Bone Joint Surg Br. 81(5):796-802. 1999.
［12］ Bielack SS, Kempf-Bielack B, Delling G, et al.Prognostic factors in high-grade osteosarcoma of the extremities or trunk : an analysis of 1702 patients treated on neoadjuvant cooperative osteosarcoma study group protocols.J Clin Oncol. 20(3):776-90. 2002.
［13］ Ozaki T, Flege S, Kevric M, Lindner N, et al. Osteosarcoma of the pelvis. :experience of the Cooperative Osteosarcoma Study Group. J Clin Oncol. 21(2):334-41. 2003.
［14］ Fuchs B, Hoekzema N, Larson DR, et al. Osteosarcoma of the pelvis: outcome analysis of surgical treatment. Clin Orthop Relat Res. 467(2):510-8. 2009.
［15］ Serizawa I, Kagei K, Kamada T, et al. Carbon ion radiotherapy for unresectable retroperitoneal sarcomas. Int J Radiat Oncol Biol Phys. 2009;75(4):1105-10.

Carbon Ion Radiotherapy: Clinical Study and Future Prospect

Tadashi Kamada, Hirohiko Tsujii

Research Center for Charged Particle Therapy, National Institute of Radiological Sciences, Chiba, Japan
e-mail address: t_kamada@nirs.go.jp

1. Introduction

The pioneering work in carbon ion radiotherapy by US, Japanese and European investigators has generated great enthusiasm. However, as a particle therapy center is certain to be an extremely complex and expensive medical facility, it may become a source of disagreement in the radiation oncology community.

The paradigm of drug development in medical oncology from phase I to phase II to phase III trials remains unaltered, but this is not the case in radiation oncology.

According to the presentations at the NCI "Workshop on Advanced Technologies in Radiation Oncology" in December 2006, there were only a few level-I trials of implemented new technologies in radiation oncology. (1)

For protons, the physical proof of better depth dose characteristics, virtually identical biological effects compared with X-rays, and the fact that decreased doses to normal tissues always result in decreased toxicity, argue against conducting phase III trials comparing protons with X-rays. (2)

Radiation oncology has not, until this decade, seen such dramatic changes in technological innovations, and they give rise to new and complicated issues. What kind of studies should be carried out to sort out the indications, advantages, and disadvantages? In this presentation, the issue of the evaluation of the clinical results of carbon ion radiotherapy and their comparison with other modalities will be discussed.

2. Carbon Ion Radiotherapy Clinical Trial at HIMAC

The carbon ion radiotherapy program was initiated based on the rationale of exploiting the high physical selectivity of carbon ions, as well as their high LET, with the attendant potential radiobiological advantage for selected tumor types. From the beginning all carbon ion radiotherapies were carried out as prospective phase I/II and II clinical trials in an attempt to identify tumor sites suitable for this treatment, including radio-resistant tumors, and to determine optimal dose-fractionation, and especially for hypo-fractionation, in common cancers. Our ultimate goal is to prove the efficacy and safety of carbon ion radiotherapy in cancer treatment.

Conducted carbon ion radiotherapy protocols and their time lines are summarized in Table 1. A total of 46 protocols have been conducted. The number of patients receiving carbon ion radiotherapy has already reached more than 5,000, and in the year 2009 more than 750 patients were treated in such protocols at NIRS.

Clinical studies revealed that intractable cancers such as advanced head and neck cancer, large skull base tumors, pelvic recurrence of operated rectal cancer, and inoperable sarcomas can be cured, and cancers in the lung, liver, and prostate can be cured safely with a shorter treatment period. (3)

Table 1

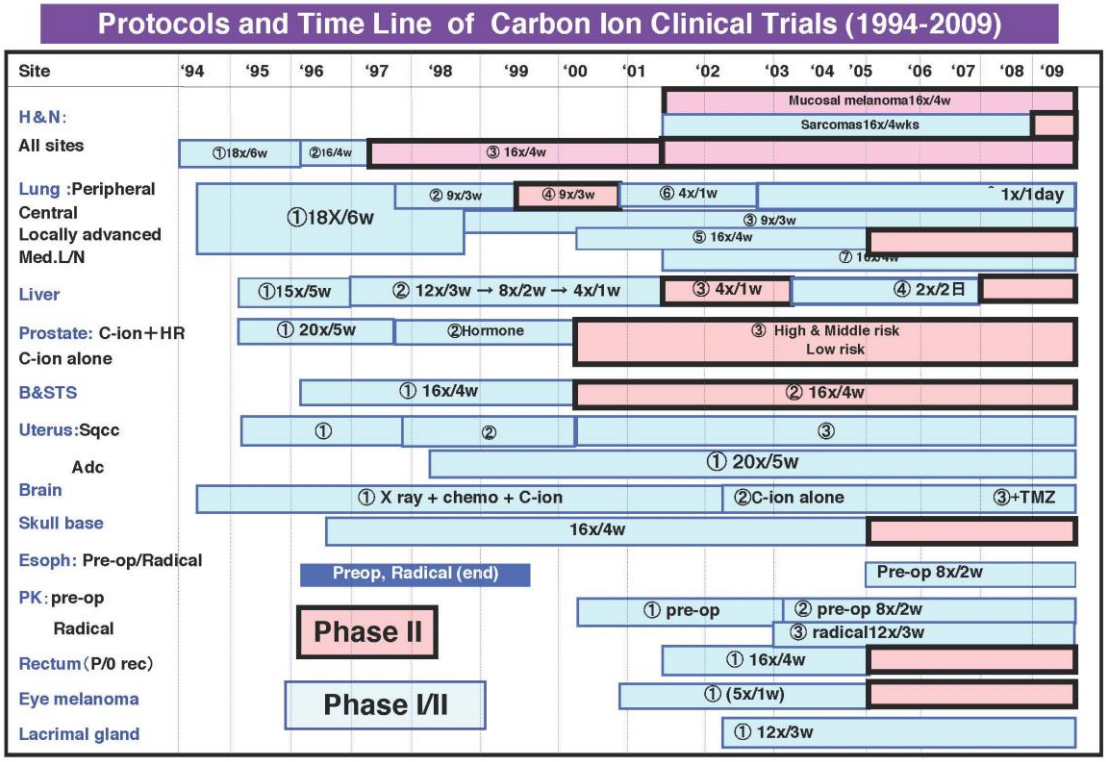

3. Should Carbon Ion Radiotherapy be Subjected to Randomized Clinical Trials?

When comparing various therapies, the results of randomized controlled studies provide the strongest evidence. Dr. Lawrence, the chief editor of the Journal of Clinical Oncology, has made the following statement about the need for phase III (randomized controlled studies) when comparing different therapies, or different types of therapeutic equipment, in the field of radiation oncology: "*In medical oncology, there is a need to compare drug treatment A to drug treatment B. It is not possible to determine which is better without carrying out a randomized trial. In radiation oncology, one can know, based on physics, that protons deliver a better dose distribution than photons or that IMRT is superior to three-dimensional conformal therapy. If treatment planning and delivery are carried out using consistent methodology, there is no debate; this is a matter of physics. The big question is: is any observed difference clinically meaningful enough to justify the added expense? What kind of trial needs to be designed to answer this question? Would it be difficult to run a randomized trial in the United States asking whether a treatment that is superior based on physics translates into superior patient survival and/or quality of life? Would patients permit themselves to be randomly assigned to the standard but less expensive therapy?*" [(4)]

Progress in radiation oncology is inextricably linked to the development of treatment facilities, however almost no randomized controlled study has been conducted for the purpose of the introduction of any new modality. In fact, no randomized controlled study was conducted in the shift from cobalt to LINAC, but if there had been there would have been little difference between cobalt and LINAC in the treatment results in patients

with early glottic cancer. Cobalt irradiation has advantages in terms of both cost and equipment maintenance, and the results of LINAC may be poor unless a suitable energy is selected. Cobalt is sufficient to treat laryngeal cancer, and it may be unnecessary to introduce LINAC to achieve successful treatment for this cancer. In recent years, however, treatments with cobalt have been significantly reduced in developed countries. The distribution of the very-high-energy x-rays of LINAC allows safer treatment of deeply situated targets, and the design of a study to determine the difference between cobalt and LINAC in patients with glottic cancer is itself a problem.

In any case, the question remains "Should Carbon Ion Therapy be Subjected to Randomized Clinical Trials?" What must be seen in a phase II study to justify moving to phase III? No matter how exciting the laboratory technique and how great the improvement in animal models, there must be evidence that the method is transferable to humans and that successes in the laboratory can be reproduced in humans. Further, there must be real promise of improvement in phase II studies in human tumors. There is real promise of improvement in our carbon ion radiotherapy results presented at this meeting, and it justifies the move to phase III.

4. From Phase II Clinical Trials to Randomized Clinical Trials (RCT)

However, before moving to a phase III study, several questions are raised. First, are there comparable phase II results in other modalities? If the answer to the first question is yes, do those modalities use the same eligibility criteria? And third, how do we recruit the patients for the phase III trial? Our patients often travel long distances to Chiba seeking carbon therapy. Finally, we charge patients more than $35,000 USD for carbon ion therapy; how do we fund such a trial? Carbon ion radiotherapy is successful in advanced head and neck cancer, large skull base tumors, recurrent rectal cancer and inoperable sarcomas that are not treatable by other means. For these intractable diseases, it is clear that there are no ample data with other modalities. For these diseases, there is no idea how to conduct a phase III study and to obtain consent from patients. Hence, the answer to the question, should carbon ion therapy be subjected to randomized trials, is "No" in these intractable diseases. In lung, liver, and prostate cancer, promising results have been obtained with carbon ion radiotherapy. A randomized controlled study might be possible in these rather common cancers. However, as described above, patients are traveling long distances to Chiba to obtain carbon ion therapy. It will be very hard to obtain consent from these patients for a randomized trial. Thus, our answer to the question is that it is untenable. RCT provides the firmest evidence in various clinical settings, but it is too difficult to conduct RCT for assessment of new radiation therapy technologies.

5. Methodologies for Critical Assessment of New Health Technologies

We radiation oncology researchers need to develop new methodologies for critical assessment of new health technologies as a complement to RCT. Possible future comparative studies of carbon ion radiotherapy may include the following: 1) multi-institutional prospective clinical studies using the same protocols that can be applied to other therapies (non-randomized concurrent clinical trial), 2) matched-pair controlled studies in subjects matched to those receiving other therapies, and 3) RCT between carbon ion and proton or other high-tech radiotherapies.

Comparative studies, feasible at present, to further clarify the usefulness of carbon ion radiotherapy at various indications, include those in which the same protocol applied to other therapies is followed, the backgrounds of

the subjects are matched, and the treatment desired by the study participants is performed. In this case, consent from study participants can be easily obtained, the study cost is low, and an agreement among the participating facilities is relatively easily obtained, as the treatment desired by the patients is provided by the co-operating institutions. For realizing this type of comparative study, a project team has been organized to conduct a multi-institutional prospective prostate cancer study in all particle therapy facilities in operation in Japan. This study is expected to start within 1 or 2 years. This could represent a new methodology for the assessment of new radiotherapy technologies. Another method would be to determine the inclusion criteria for patients already treated and then to comparatively analyze the therapeutic results in a matched-pair study. This is feasible if consent is obtained from the institutions that performed the treatments being compared. We conducted a matched-pair study of sacral chordoma with patients treated at the Massachusetts General Hospital in Boston with proton therapy.[(5)] However, there were only a few matched cases in both institutions and were not able to carry out the comparison. Nonetheless, this can be retried with other institutions or performed with more common cancers.

6. Summary

At present, most of the patients receiving carbon ion radiotherapy at NIRS visit the clinic seeking this specific modality, and it is difficult to obtain consent for a randomized controlled study from these patients and it may be unnecessary to conduct a phase III trial. However, in selected tumors where the high-LET benefit could be appreciated, we can participate in randomized studies. Finally, studies aimed at clarifying the usefulness of carbon ion radiotherapy and elucidating any advantages from hypo-fractionation should be considered. A multi-institutional prospective non-randomized concurrent phase II clinical trial is one such new approach, and it will be proposed not only to the Japanese, but also to the international community of particle therapy and radiation oncology.

References

1) http://www3.cancer.gov/rrp/workshop/2006AdvancedRadiationTech/presentations.html

2) Goitein M, Cox JD: Should randomized clinical trial be required for proton radiotherapy? J Clin Oncol 26:175-176(2008)

3) Tsujii H, Mizoe J, Kamada T et al: Clinical results of carbon ion radiotherapy at NIRS. J Radiat Res 48: Suppl., A1-A13 (2007)

4) Lawrence TS, Petrelli NJ, Li BD, Galvin JM: Think globally, act locally. J Clin Oncol 25:924-930(2007)

5) Park L, Delaney TF, Liebsch NJ et al: Sacral chordomas: Impact of high-dose proton/photon-beam radiation therapy combined with or without surgery for primary versus recurrent tumor. Int J Radiat Oncol Biol Phys 65: 1514-1521(2006)

Recent Advances in Carbon Ion Therapy

Hirohiko Tsujii, M.D.

National Institute of Radiological Sciences, Chiba, JAPAN
e-mail: tsujii@nirs.go.jp

Carbon ion radiotherapy (C-ion RT) has the beneficial property of superior physical dose distribution (Bragg peak curve) as well as a higher RBE compared with protons or photons. The rationale for selection of carbon ions is based on comparative evaluation of other ion species. As the mass of the particle increases the RBE also increases, but the ratio of RBE between the peak to plateau becomes worse when using a particle with a higher mass, therefore when considering both the physical and biological effect, the carbon ion comes to the most balanced particle. At present, there are a total of 7 facilities for charged particle therapy in Japan. Among them, carbon therapy facilities include 3 centers in operation and one center has just started the project. In other countries, there are two facilities in operation including Heidelberg and Lanzhou. The CNAO in Italy is to start treatment soon. Three other facilities are constructing carbon facilities, two in Germany and one in China. There are still more facilities planning to introduce carbon facilities in the world. In Japan, the government has approved it as Advanced Medical Technology, which has enabled us to put C-ion RT in general practice. More recently we have established the Japan Clinical Study Group of Particle Therapy (JCPT) for the purpose of advancing the practice of particle therapy by the individuals who are interested in charged particle therapy. As an activity for comparing clinical efficacy of different modalities, we are designing protocols to be shared by facilities for both proton and C-ion RT.

Regarding clinical results of C-ion RT, it has been mainly applied to tumors of the head and neck, lung, liver, prostate, bone/ soft-tissue, uterine cervix, and pelvis (post-ope pelvic recurrences of rectal cancer). So far, more that 5,100 patients have been treated at NIRS. Although the total number of patients is much smaller, similar types of tumors have been treated in other two facilities in Japan. GSI/Heidelbeg has been focusing on treatment of head and neck, skull base, and intracranial malignancies. It has been possible to complete the treatment in a short time. For example, stage 1 lung cancer and liver cancer can now be treated with only one or two fractions, respectively. Even for prostate cancer and bone and soft-tissue tumors requiring a relatively long course of RT, only 16 sessions have been sufficient, less than half the number of fractions required in the case of standard RT. This means that the carbon therapy facility can be operated more efficiently, offering treatment for a larger number of patients than is possible with other modalities over the same period of time.

The current status and the anticipated future directions of the role of particle therapy in medicine is a complex subject that involves a very intimate interplay of radiobiology, accelerator physics and radiation oncology. In this presentation, together with highlighting the clinical results, we will focus on the technical advances as well as future directions of C-ion RT. It will also be attempted to present a balanced, consensus view of the past achievements and current strategies in particle therapy, in a manner of interest both to long-term experts and to educated newcomers to this field.

References

[1] Tsujii H, Kamada T, Baba M, et al: Clinical advantages of carbon-ion radiotherapy. New J Phys. 10: 1367-2630, 2008.

[2] Tsujii H, Minohara S, Noda K: Heavy-particle radiotherapy: System design and application. Reviews of Accelerator Science and Technology Vol 2 (ed. by Chao AW), Imperial College Press, UK, pp1-19, 2009.

[3] Okada T, Kamada T, Tsuji H, et al.: Carbon ion radiotherapy: Clinical experiences at National Institute of Radiological Sciences (NIRS). J Radiat Res. 51: 355-364, 2010.

[4] Schulz-Ertner D, Tsujii H: Particle radiation therapy using proton and heavier ion beams. J Clin Oncol. 25(8): 953-964, 2007.

New Treatment Facility Project at HIMAC

Koji Noda, Takuji Furukawa, Taku Inaniwa, Yoshiyuki Iwata, Mitsutaka Kanazawa, Nobuyuki Kanematsu, Ken Katagiri, Atsushi Kitagawa, Shinichi Minohara, Kota Mizushima, Shinichiro Mori, Takeshi Murakami, Masayuki Muramatsu, Shinji Sato, Toshiyuki Shirai, Eiichi Takada, Eri Takeshita, Yuka Takei

Research Center for Charged Particle Therapy, National Institute of Radiological Sciences, Chiba, Japan
e-mail address:noda_k@nirs.go.jp

Abstract

The first clinical trial with carbon beams generated from HIMAC was conducted in June 1994. The total number of patients treated was 5,196 as of February 2010. The impressive advance of carbon-ion therapy using HIMAC has been supported by high-reliability operation and by the development of accelerator technology. Based on more than ten years of experience with HIMAC, we have proposed a new treatment facility for the further development of therapy with HIMAC. The new facility, as an extension of the existing one, has been designed, and the related R&D work has been carried out. The building of the new treatment facility was already completed in March 2010, and the 1st treatment is scheduled in March 2011. The following description gives a summary account of the design study and the related R&D work for this new treatment facility at HIMAC.

1. Introduction

Heavy-ion beams are very suitable for the treatment of deeply seated cancer because of an excellent physical-dose distribution and high-LET characteristics around the Bragg peak. Therefore, NIRS decided to carry out heavy-ion cancer therapy with HIMAC [1]. The first clinical trial of cancer treatment with carbon beams was conducted in June 1994. The total number of patients treated until June 2008 was more than 4,000. Based on more than ten years of experience with HIMAC, we have proposed a new treatment facility toward adaptive cancer therapy [2] with heavy ions, making the one-day treatment of lung cancer possible. Further, the new treatment facility should accurately treat a fixed target, a moving target with breathing and/or a target near a critical organ. For these purposes, a 3D-scanning method with a pencil beam is employed in the new treatment facility. A phase-controlled rescanning (PCR) method [3] has been proposed and studied, especially for treating a moving target. A rotating gantry with the PCR method [4] is also employed in order to reduce the patient's load, such as face-downward position during patient positioning, and to increase treatment accuracy for a tumor near a critical organ through multi-field optimization [5]. In addition, we have designed the beam-delivery system, the rotating gantry system, the treatment flow including patient positioning and the facility planning. The related R&D work has also been carried out with HIMAC since 2006. We review the design study and the related R&D work for the new treatment facility at HIMAC.

2. Design consideration

2.1 Specification

In HIMAC treatments, we have observed shrinkage of the target size as well as a change in its shape during the entire treatment. In order to keep the sophisticated conformations of the dose distributions even in such cases, it has been required that treatment planning is carried out just before each fractional irradiation, which we

call adaptive cancer therapy. For this purpose, 3D scanning with a pencil beam should be employed, because it does not use any bolus and patient collimators, which take a long time to be manufactured. It is also well-known that 3D scanning has brought about a highly treatment accuracy in the case of a fixed target [6]. However, this method has not yet been applied to treating a moving target with breathing in practical use. Therefore, we have developed the PCR method to treat a moving target, as mentioned in 3.1.

A main specification such as ion species and irradiation-field size in the new treatment research facility [7] was determined by using the clinical statistics for the more than ten-year treatment period at HIMAC, as summarized in Table 1. A ^{12}C beam is mainly used for treatments that have been carried out in the existing HIMAC treatment. Different ion species will also be employed for the further development of HIMAC therapy. Thus, the maximum ion energy is designed to be 430 MeV/n in both the horizontal and vertical beam-delivery systems, in order to obtain more than the residual range of 30 cm in a ^{12}C beam and more than that of 22 cm in an ^{16}O beam. The maximum lateral field and SOBP sizes are 25 cm × 25 cm and 15 cm, respectively, in order to cover almost all treatments with HIMAC. On the other hand, the rotating gantry system employs a maximum energy of 400 MeV/n, a maximum lateral field of 15 cm × 15 cm, and a maximum SOBP size of 15 cm in order to downsize the gantry. Further, positron-emission beams, such as ^{11}C and ^{15}O, will be used to verify the irradiation area and their ranges in a patient's body. At HIMAC, R&D work has been carried out in order to obtain positron-emission beams accelerated directly through the HIMAC accelerator [8], instead of using the projectile-fragmentation method.

Table 1. Specification of the new treatment facility

1. Basic parameters	
Ion species	^{12}C, ^{16}O (^{11}C, ^{15}O)
Delivery beam intensity	10^7 – 10^9 pps at ^{12}C
Treatment room	2 fixed-beam rooms (Hori&Vert), 1 rotating-gantry room
2. Fixed beam-delivery system	
Energy	140 - 430 MeV/n
Irradiation method	Fixed target: 3D raster scanning with pencil beam
	Moving target: PCR method
Scanning speed	H:100mm/ms, V: 50 mm/ms
Spot size	2 – 4 mm at 1-sigma
Lateral-field/SOBP/Range size	22 cm in square/ 15 cm/ >25 cm at ^{12}C
Irradiation-port length	9 m
3. Rotating-gantry system	
Type	Iso-centric rotating gantry
Energy	140 – 400 MeV/n
Irradiation method	as same as the fixed beam-delivery system
Scanning speed	H:100mm/ms, V: 50 mm/ms
Spot size	2 – 4 mm at 1-sigma
Lateral-field/SOBP/Range size	15cm×15cm/ 15 cm/ >25 cm at ^{12}C
Displacement of iso-center	< 1 mm
Size and weight	Length: 16.5 m, Radius: 7.1 m, Weight:350 ton

2.2 Irradiation method

The new facility should employ a pencil-beam scanning method for a fixed target, a moving target and/or a target near critical organs, toward adaptive cancer therapy. It is also well-known that 3D scanning has brought about a highly treatment accuracy in the case of a fixed target. However, this method has not yet been applied to treating a moving target with breathing in practical use. Therefore, we have developed the PCR method, especially for treatment of moving target. In the PCR method, rescanning completes the irradiation of one slice during a single gated period corresponding to the phase between the end of expiration and the beginning of inspiration, because the organs are most stable during this gated period. Further, since the average displacement of the target over a single gated period is close to "zero", we can obtain uniform dose distribution even under irradiation of a moving target. The PCR method requires mainly two technologies: (1) intensity-modulation technique for a constant irradiation time on each slice having a different cross-section as described in the section 3.2 and (2) fast pencil-beam scanning technique for completing several-times rescanning within a tolerable time. The following key technologies have been developed in order to realize the fast scanning.

A new treatment planning system

The raster scanning has been chosen in order to save the irradiation time, instead of the spot scanning, because the raster-scanning does not require the beam-off period during the raster-position movement. In the raster scanning, however, it is inevitable to deliver an extra-dose on the position between the raster-points. It is noted that the extra-dose is proportional to the delivered intensity. Owing to the high reproducibility and uniformities in the time structure of the extracted beam from the HIMAC synchrotron, we can predict the extra-dose and incorporate its contribution to the treatment planning. Consequently we can increase the beam intensity and shorten the irradiation time by factor of around 5. Further, since the path length is optimized through applying a travelling- salesman problem, the scanning time can be decreased by 20-30%.

An extended flattop operation of the HIMAC synchrotron

A synchrotron operation has generally dead time such as the beam injection, acceleration and deceleration periods, and the duty factor is around 50% in the HIMAC synchrotron. In order to increase the duty factor to almost 100%, an extended flattop operation has been carried out in the HIMAC synchrotron.

High-speed scanning magnet

The scanning speed is designed to be 100 mm/ms and 50 mm/ms in the horizontal and vertical directions, respectively, which are faster by around one order than that in the conventional spot scanning. In order to increase the scanning speed, we designed the scanning magnet having slits in both the end of magnetic pole, according to a thermal analysis including both the eddy-current and hysteresis losses. The power supply of the scanning magnet was designed for the fast scanning, and this consists of two stage circuits; the first stage for voltage forcing by IGBT switching elements and the second stage for the flattop-current control by FET switching ones. As a result of the test, a temperature rise was measured to be around 30 degree at maximum, which is consistent with the thermal analysis.

2.3 Facility planning

The new treatment research facility is connected with the upper synchrotron at HIMAC. In the treatment hall, placed underground of the facility, three treatment rooms are prepared in order to treat more than 800 patients per year. Two of them are equipped with fixed beam-delivery systems in both the horizontal and vertical directions, and the other is equipped with a rotating gantry. Two treatment-simulation rooms are also prepared for patient positioning as a rehearsal, and for observing any change of the target size and shape with X-ray CT during the entire treatment. Further, six rooms are devoted to patient preparation before irradiation. A schematic view of the new treatment research facility with the HIMAC facility is shown in Fig. 1. A patient will be taken by medical staff to a waiting room in the treatment hall and will be in the preparation room just before a treatment. After the preparation, the patient on a patient capsule is transported to the treatment room, and the patient capsule is automatically caught up by a robotic couch and is set at an irradiation position. The building of the new facility was completed in March 2010, and a photograph of the building is also shown in Fig. 1.

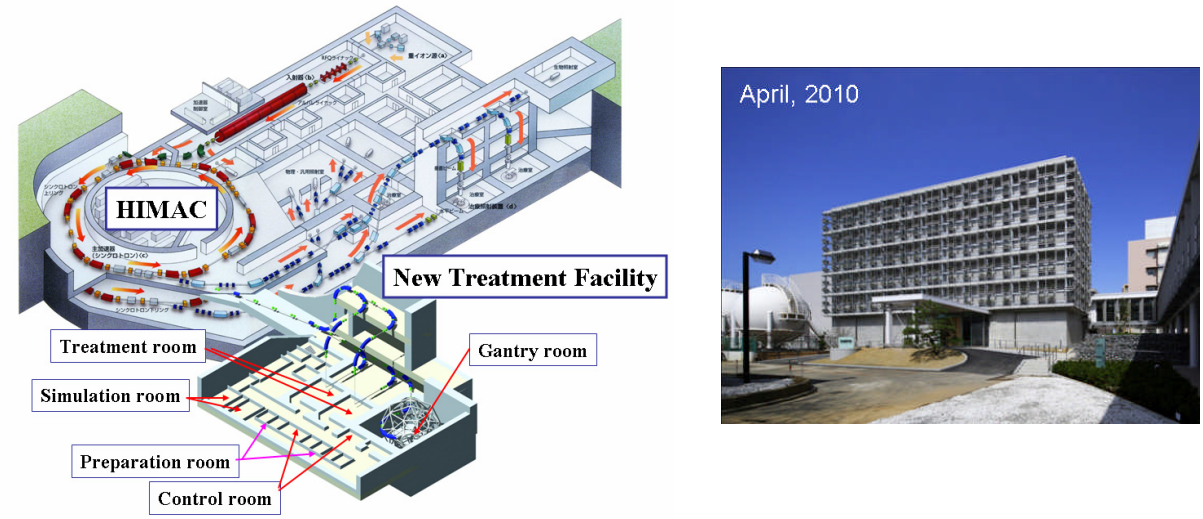

Fig. 1. Schematic view of the HIMAC and the new treatment facility with photograph of the new building completed (Left). The completed building of the new treatment research facility.

3. Design study and R&D work

3.1 Design of the beam transport and beam delivery systems

In the new treatment research facility, beam transport (BT) lines are designed to make energy scan [6] possible. Thus all of the magnets will be manufactured with laminated iron plates. The beam optics is designed to realize dispersion free in the fixed beam-delivery system, and the beam size can be changed from 2 to 8 mm at one-sigma by using the final Q-triplet. The beam-position changes due to undesirable parameter change of the synchrotron, which can be corrected by using a pair of steering magnets and non-destructive screen monitors in both horizontal and vertical directions in the beam-delivery system.

The fixed beam-delivery system is designed to realize the PCR method with the fast raster scanning and to be same configuration in both the horizontal and vertical directions. The system consists of a pair of scanning magnets, dose monitors, a ridge filter and a range shifter. The total length of the system is around 9 m. Two dose monitors, which are parallel-plate ionization chambers with an effective area of 250 mm^2, are used for dose management. The beam position and size are monitored by multi-wire proportional counters. Considering the slice thickness, the Bragg peak is slightly spread out by a mini ridge filter. The range shifter is utilized to change the slice in the target. Thus, the range shifter should be as close as possible to the iso-center in order to avoid any change of the beam size by multiple scattering through the range shifter. The layout of the beam-delivery system is shown in Fig. 2.

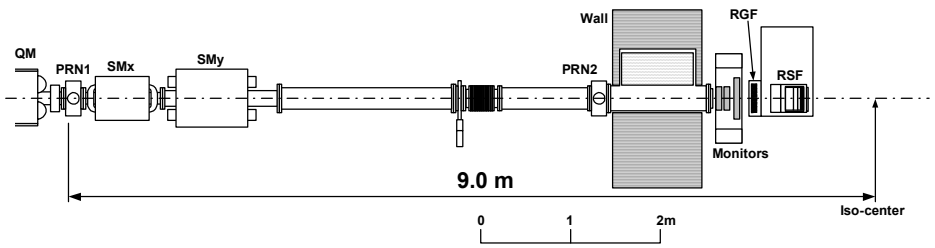

Fig. 2. Layout of the beam-delivery system. PRN: Beam-profile monitor, SMx,y: Horizontal and vertical scanning magnet, respectively, Monitors: Dose and position monitors, RGF: Mini ridge filter, RSF: Range shifter.

In the present design, the rotating gantry employs a pencil-beam raster scanning, which is identical to the one used for the horizontal and vertical beam-delivery systems. It is important for the gantry design to avoid any change in beam size in accordance with the rotation angle. Thus, we will adapt a compensation method of asymmetric phase-space distribution [9]. This method is based on multiple scattering by a thin foil placed at the position with optimum beam-optical parameters in the beam-transport line. In order to decrease the gantry weight, the final dipole magnet is divided into 30-degree and 60-degree magnets. Further, two scanners are placed between the two magnets in order to extend the effective length from the scanners to the iso-center. The total weight of the gantry system is around 350 tons. Figure 3 shows a rotating gantry schematically.

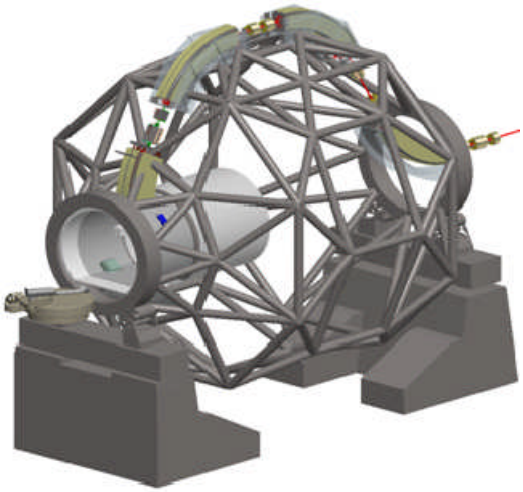

Fig. 3 Schematic view of the rotating gantry. Diameter: about 15 m, Length: about 17m, Weight: about 350 ton.

3.2 Intensity modulation

We have developed a spill control system [10] in order to deliver the beam with intensity modulation, based on improvement of the RF-KO slow extraction method [11]. The core part of this system requires the following functions: (1) calculation and output of an AM signal according to request-signals from an irradiation system, (2) real-time processing with a time resolution less than 1 ms, and (3) feed-forward and feedback controls to realize the extracted intensity as requested. This system allows us to dynamically control the beam intensity almost as required, as shown in Fig. 4.

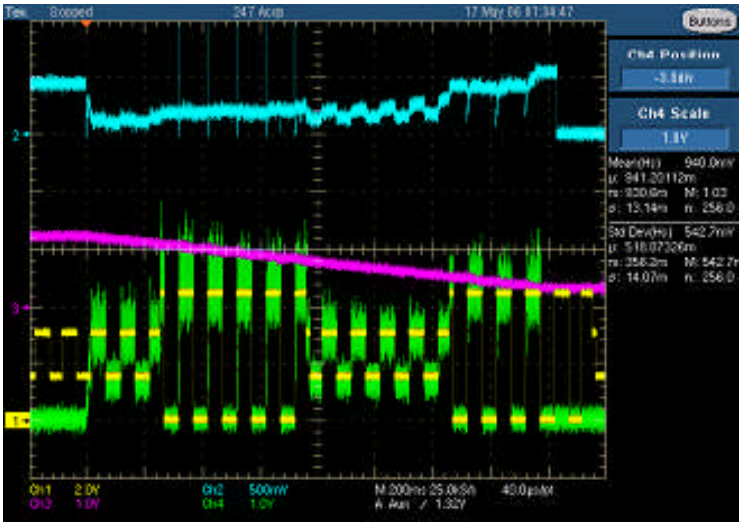

Fig. 4. Intensity modulation by spill control system. Yellow and green show the signal of the required intensity and actual beam intensity, respectively.

3.3 Intensity upgrade and extended flattop operation

The beam intensity extracted from the HIMAC synchrotron has been increased in order to complete single-fractional irradiation with one operation cycle. In this case, applying the efficiency of the gated irradiation is increased by a factor of about 2, applying a synchrotron operation with an extended flattop infinitely in principle. The extended flattop operation will save considerably irradiation time. In order to increase the beam intensity, we have thus developed a correction method of the third-order resonance that causes the strong beam loss just after a beam injection into the synchrotron. In addition, the multi-harmonics operation of the RF acceleration system can also increase the intensity, because of suppressing the space-charge effect after bunching. Consequently, around 2×10^{10} carbon ions can be accelerated to the final energy. This intensity is sufficiently high to complete single-fractional irradiation for almost all tumours treated with HIMAC when using the 3D-scanning method with beam-utilization efficiency more than 90%. The extended flattop operation was successfully tested at the HIMAC synchrotron, as shown in Fig. 5.

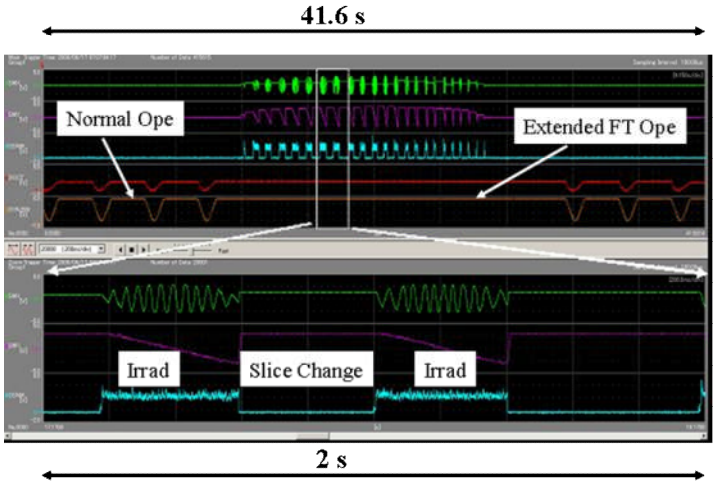

Fig. 5. Extended flattop operation of the HIMAC synchrotron.

3.4 Fast raster-scanning experiment

We designed and constructed a test irradiation port for the fast raster-scanning experiment in order to verify the design goal as mentioned in the section 2, which was the same configuration as the fixed beam-delivery system adapted to the new treatment research facility. The test irradiation port is shown in Fig. 6. We have adapted the measured dose response of the pencil beam with various energies for the new treatment planning system. The beam size at the entrance and the width of the Gaussian-shaped mini-peak were 3.5 and 4 mm at one standard deviation, respectively. As a result of the experiment, the validity of the beam model and the optimization calculation was already verified [12, 13]. In the experiment, further, we obtained a uniform physical dose field not only for a fixed target, but also for a moving one. The irradiation time was significantly shortened by around 100 times compared with that of the conventional spot scanning [14]. The experimental result is described in the Ref [15] in detail.

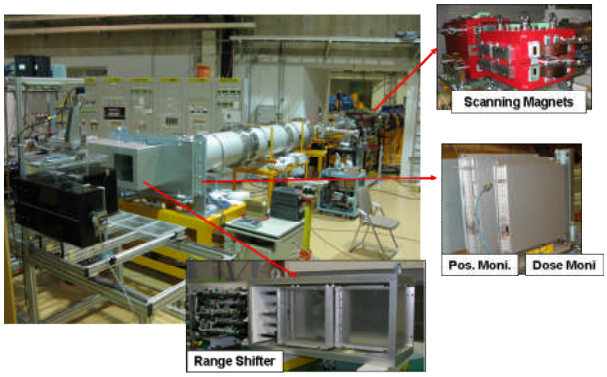

Fig. 6 Test irradiation port for fast 3D scanning, which was installed in the HIMAC facility.

4. Summary

During the more than ten-year of clinical trials with HIMAC, both the beam-delivery and the accelerator technologies have been significantly improved. It has brought the good result of the clinical trial. Therefore we proposed the new treatment facility project for further development of the HIMAC treatment. In this project, a patient handling system including patient positioning with a robotic couch, treatment planning system for the PCR method and Carbon-radiotherapy information system have been developed as well as that of the accelerator and beam delivery systems since April 2006. At December 2007, the Japanese government approved this project. The facility building was already completed in March 2010, and the first-patient treatment is scheduled in March 2011.

References

[1] Y. Hirao et al., Nucl. Phys. A 538, 541c–550c (1992).

[2] K. J. Halverson et al., Int. J. Radiat. Oncol. Bio. Phys. 21:1327-1336 (1991).

[3] T. Furukawa, T. Inaniwa, S. Sato, T. Tomitani, T. Minohara, K. Noda, T. Kanai, Med. Phys. 34 (3), 1085-1097 (2007).

[4] T. Furukawa, T. Inaniwa, S. Sato, Y. Iwata, S. Minohara, K. Noda, T. Kanai, in these proceedings.

[5] A. Lomax, Phys. Med. Biol. 44:1219-1226 (1999).

[6] Th. Haberer, W. Becher, D. Schardt, G. Kraft, Nucl. Instrum. Meth. A 330, (1993) 296-305.

[7] K. Noda et al., J. Rad. Res., 48 (2007) A43-A54.

[8] S. Hojo, T. Honma, Y. Sakamoto, S. Yamada, Nucl. Instrum. Meth. B 240 (2005) 75.

[9] T. Furukawa and K. Noda, Nucl. Instrum. Meth. A 565 (2006) 430.

[10] S. Sato, T. Furukawa, K. Noda, Nucl. Instrum. Meth. A 574, (2007) 226-231.

[11] K. Noda et al., Nucl. Instrum. Meth. A 374 (1996) 269.

[12] T. Inaniwa et al., Med. Phys. 34 (8) 3302-3311(2007).

[13] T. Inaniwa et al., Nucl. Instrum. Meth. B 266 (2008) 2194.

[14] T. Furukawa et al., Proc of 1st IPAC, Kyoto, Japan, 2010, pp.76-78.

[15] E. Urakabe et al., Jpn. J. Appl. Phys. 40 (2001) 254.

New Treatment Facility at Gunma

T.Kanai, M. Sakama, K. Yusa, M. Tashiro, H. Shimada, K. Torikai, J. Koya, T. Ishii, Y. Yoshida, S. Yamada, T. Ohno, T. Nakano

Heavy-ion Medical Center, Gunma University, Maebashi, Japan
Corresponding Author: Tatsuaki Kanai, e-mail address: kanai@showa.gunma-u.ac.jp

Abstract

For treatment of cancer patients by carbon beams, broad beam techniques were developed at LBNL and also at NIRS. Scanning techniques were followed in order to improve dose distributions. Although the scanning technique was already applied to carbon therapy at GSI and Heidelberg and also a new scanning technique is developed at NIRS, the broad beam technique is still attractive because of its simplicity and well established technique for moving targets. This broad beam technique has been adapted at a new hospital-based carbon therapy facility installed at Gunma University. In the new carbon facility, the main accelerator is a slow-cycling synchrotron with an average diameter of around 20 m, and it accelerates carbon ions up to an energy range from 140 to 400 MeV per nucleon. We have four treatment rooms, three of which will have a fixed horizontal beam line, both fixed horizontal and fixed vertical beam lines, and a fixed vertical beam line, respectively. The fourth room will be used for developmental studies for advanced irradiation techniques. The design details of the facility are based on design and R&D studies performed at the National Institute of Radiological Sciences.

The construction and commissioning of the new carbon therapy facility were completed and the first clinical treatment of the carbon therapy has been executed at Gunma-University Heavy-Ion Medical Center on March 16, 2010. In this symposium, we will discuss about the commissioning of the new facility.

1. Introduction

Design and R&D studies have been carried out at NIRS to obtain a cost-effective design for the compact carbon therapy facility. In the design of the new carbon therapy facility, only high-energy carbon ions will be used to reduce the size and cost of the apparatus. Beam characteristics should cover the clinical beam characteristics of HIMAC. Our final goal is to establish a cost-effective design of a carbon therapy facility in a hospital environment. Under this basic idea, Gunma University has been collaborating with these studies since 2004. In summer of 2009, the construction of the new facility at Gunma University is completed and the beam test has begun. After two and half month of the beam test, the commissioning of the irradiation system and registrations of basic beam profiles to a treatment planning system has been started. The treatment planning system 'Xio-N', has been developed by NIRS and Mitsubishi Electric Cooperation in the R&D studies of the cost-effective design. On March 16, 2010, the first carbon treatment using the new carbon facility has been executed for a prostate cancer patient. In this symposium, we will report on the new facility and the commissioning of the new irradiation system.

2. The facility outline

Specifications of the facility were determined on the basis of the statistics of clinical treatments at HIMAC. It was decided to accelerate only carbon ions with a maximum energy of 400 MeV/u. This energy ensures a 25-cm residual range in water and, for example, carbon ions can penetrate a human body and reach the prostate through a patient's pelvis. Another important requirement is to have two orthogonal beam lines directed toward the same isocenter. This beam line configuration is required in order to realize sequential beam irradiation from different directions with single positioning of a patient. A fast beam course and energy switching are required for the purpose. The major specifications of the facility are summarized in Table 1. The layout of the new facility is shown in Fig.1.

Table 1. Major specifications of the therapy facility

Items	Contents
Ion Species	Carbon ions only
Range	25 cm max. in water (400 MeV/u)
Field Size	15 cm × 15 cm max.
Dose Rate	5 GyE/min. (1.2×10^9 pps)
Treatment Rooms	3 (H, V, H&V)
	No rotational gantries
Fourth Room	Prepared for future developments
Irradiation Techniques	Respiration Gated
	Single & Spiral Wobbling Methods
	Layer-Stacking Method

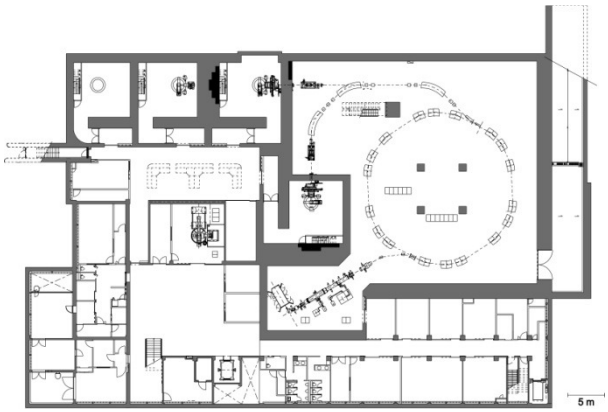

Fig.1 Plan view of the facility.

The accelerator of the facility consists of an Electron Cyclotron Resonance (ECR) type ion source, a Radio-Frequency Quadrupole (RFQ) linac, an Interdigital-H (IH) linac with Alternating Phase Focusing (APF) structure and a synchrotron ring followed by a high-energy beam transport system. C^{4+} ions will be produced by the ECR source and pass through a thin carbon foil installed downstream of the IH linac. Output energy of the linac is determined at 4 MeV/u so that more than 90% of C^{4+} ions are converted to fully stripped ions. An averaged diameter of the synchrotron is about 20 m and will accelerate C^{6+} ions up to 400 MeV/u.

In the ECR source, permanent magnets are adopted to generate magnetic fields both for sexta-pole and mirror fields [1], [2]. Based on experimental studies with a conventional 10 GHz ECR source at HIMAC, the field distribution of the mirror magnet is designed so that a charge distribution of carbon ions is optimized at 4+.

A linac system is composed of a conventional four-vane type RFQ linac and an interdigital-H type linac with alternating-phase focusing (APF) structure [3], [4]. The RFQ accelerates carbon ions from 10 to 600 keV/n. The output energy of the APF-IH linac is 4 MeV/u. Since both linacs need no extra focusing element in the linac cavities, the tuning procedure of the linac system is very simple and easy. The operation frequency is chosen to be 200 MHz, and the cavity diameter is about 35 cm for both linacs. Cavity lengths are 2.4 m for RFQ and 3.4 m for IH. A 50 $\mu g/cm^2$ thick carbon foil stripper is installed at the output of the IH linac.

The synchrotron has a conventional FODO type lattice structure and accelerates fully stripped carbon ions from 4 up to 400 MeV/u [5], [6]. The circumference of the ring is 63.3 m and the average diameter is about 20 m. The bending field changes from 0.13 to 1.48 T. There are 18 bending magnets in the ring, each of which is about 6 t, making the total weight over 100 t.

The injection and extraction methods are conventional multiturn injection and slow extraction using 1/3 resonance, respectively. Acceleration rf frequency varies in a range from 0.88 to 6.77 MHz with a harmonic number of two. A single-gap acceleration cavity is loaded with Fe-based amorphous cores and generates a maximum voltage of 2 kV. The maximum output power of the power amplifier is 8 kW.

The wobbler method was adopted for our beam delivery system based on more than 10 years experience at HIMAC. In order to improve the beam efficiency in a large irradiation field size, we adopted a spiral wobbler technique [7]. By single wobbler technique, the beam size is required to satisfy a definite relation with the radius of the circular wobbling orbit at an isocenter. At first phase of the facility operation, the energy of the treatment is limited to 380 MeV per nucleon and also we can use only single wobbler method for broadening the accelerated carbon beams because of regulation of government. The distance between the iso-center and the final beam transport element of the bending magnet was chosen to be 9 m. We can make a maximum 15 cm × 15 cm irradiation field with a dose distribution error better than ±2.5%. A horizontal beam delivery system is installed in treatment rooms A and B, whereas a vertical system is installed in rooms B and C.

3. Justification of fixed RBE system

Clinical trials for carbon therapy have been safely studied under strict clinical protocols at NIRS for over 15 years. Dose escalation studies for treating various tumor sites are included in this clinical protocol studies to estimate appropriate dose level for the carbon therapy. And a fixed RBE system is adopted through the all clinical trials. The results of the clinical trials were very good [8]. Because of the fixed RBE system, clinical results can be expressed by a function of physical dose under an equivalency assumption for various SOBP treatments. We defined the equivalency assumption so that the tumor responses are assumed to be the same as those expected for the clinical dose (GyE) irrespective of SOBP width. That is to say, all treatments can be represented by the treatment using SOBP 6 cm [9].

Height and shape of the optimized SOBP depth dose distributions will vary due to LET and fractionation size dependences of RBE. However, the variation of the optimized SOBP shape are not different so much, when normalizing dose distributions at the center of the SOBP, Fig. 2 shows physical dose distributions of spread out Bragg peaks, which are optimized for realizing uniform survival fraction at survival levels from 0.1 to 0.000001.

In the analysis of local control rate of carbon therapy for non-small cell lung cancer with linear quadratic model, we had to introduce variation in radiation sensitivity, ($\alpha \pm \Delta\alpha$) [9]. Fig. 3 shows results of tumor control probability of carbon therapy for chordomas [10], non-small cell lung cancer[11], and bone and soft tissue sarcomas[12]. The treatment schedule is 4 fractions per week, total 16 fractions. Horizontal axis shows total physical dose, which is the dose at the center of 6 cm SOBP beam under the equivalency assumption. The analysis introducing the variation in radiation sensitivity using LQ model can be practically reproduced the clinical results.

For hypo-fractionation treatments less than 4 fractionations, however, reliable data of survival fractions less than 0.001 in LQ model will be required. In the cell survival experiments, there will be large uncertainty for survival fractions below 0.001. And biological dose distribution used in the treatment planning system is in the uncertainty region of tumor responses ($\alpha \pm \Delta\alpha$) for various fractionation sizes. At present stage of carbon therapy, it can be justified to use fixed SOBP for various fractionation sizes in some extent. Detail analysis of carbon clinical trial should be required in order to step further.

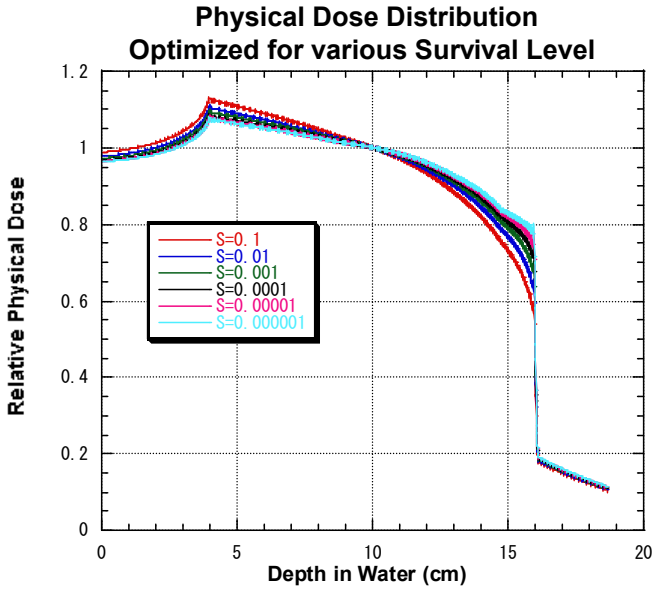

Fig. 2. Physical dose distributions of spread out Bragg peaks, which are optimized for realizing uniform survival fraction at survival levels from 0.1 to 0.000001

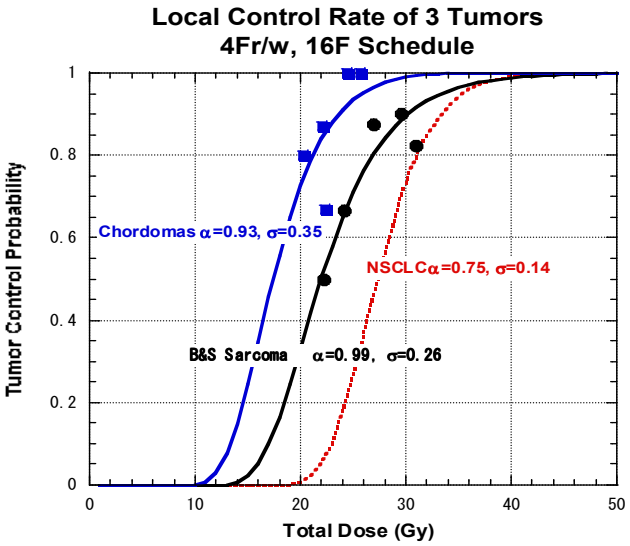

Fig. 3. Results of tumor control probability of carbon therapy for chordomas, non-small cell lung cancer, and bone and soft tissue sarcomas.

4. Design of spread out Bragg peak

In the designing ridge filter for spread out Bragg peak, we decided our plan to keep NIRS experiences of carbon therapy and also to use recent developments of heavy-ion radiation physics. (1) Tumor responses can be represented by survival curves of human salivary grand tumor cell (HSG cell). (2) For the LET dependence of alpha and beta in the LQ model, we will use the same data as those used at NIRS. The LET dependences of the coefficients, α and β, are shown in Fig. 4. (3) Biological responses for the all fragmented particles, protons to Boron, are assumed to be the same as alpha particles. (4) Detail LET distributions should be taken into account for SOBP design. (5) Fragmentations in aluminum material which is ridge filter material, should be taken into account.

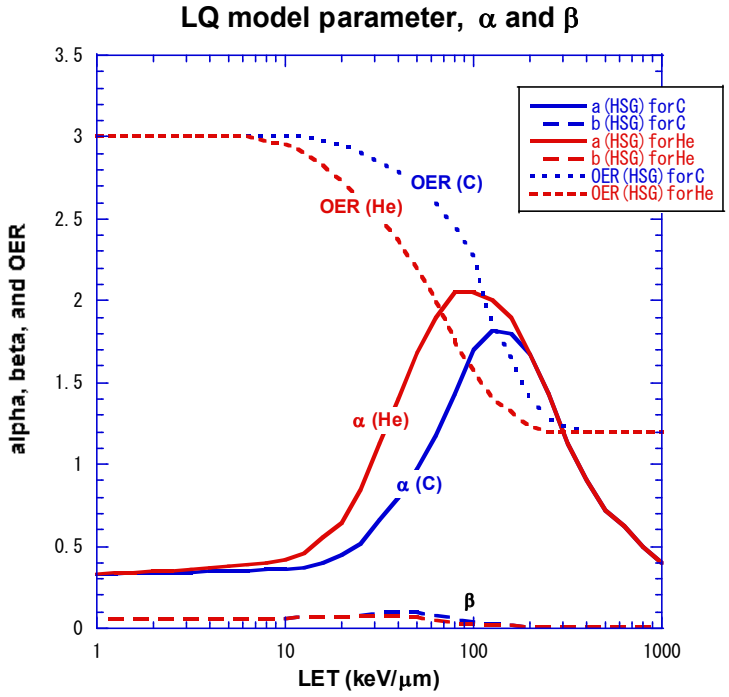

Fig. 4. LET dependences of the coefficients, α and β,in LQ model of survival curve.

We use Monte Carlo code, Geant 4, for calculation of physical beam characteristics of the therapeutic beam. Placing various thickness of aluminum plates at the ridge filter position, depth dose distributions in water were

calculated using the Geant 4 code. The results of the depth dose distributions are compared with the measured distributions. Geometry of the irradiation course is shown in Fig. 5. The measured depth dose distributions are shown in Fig. 6. The overall yield of fragmentation particles should be corrected for the Geant 4 results in order to coincident with the measured depth dose distributions.

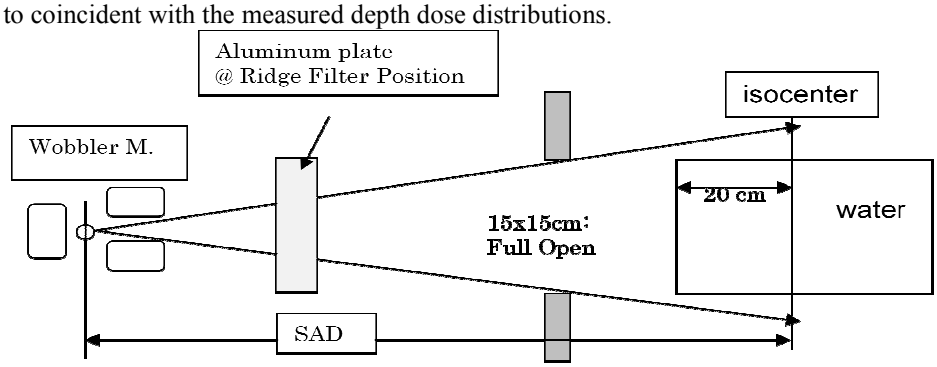

Fig. 5. Geometry of the irradiation course

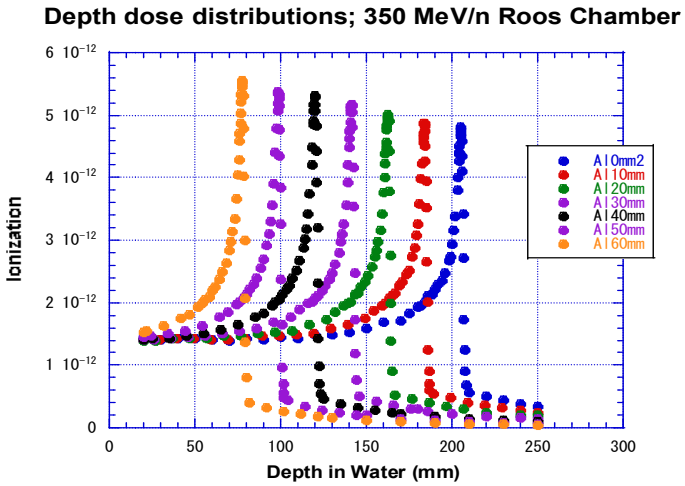

Fig. 6. Measured depth dose distributions in water phantom

Obtained SOBP curves for 80 mm width are shown in Fig. 7. Initial energy of the carbon beams are 290, 350 and 380 MeV/n.

5. Conclusions

We designed therapeutic carbon beams based on NIRS experiences of clinical trials. In order to take over the NIRS treatments, physical dose at SOBP center should be kept. It can be justified to use fixed SOBP for various fractionation size in some extent. Detail analysis of carbon clinical trial should be required in order to step further. We introduced Geant 4 Monte Carlo simulation for calculating LET distributions of fragmented particles produced in the ridge filter and water phantom.

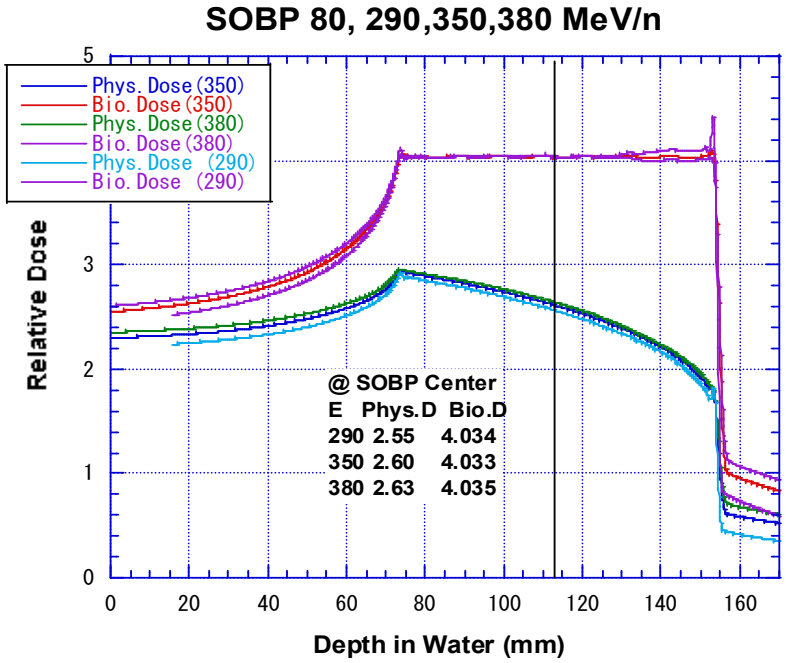

Fig. 7. Designed depth dose curves for 80 mm SOBP width

6. Acknowledgements

Design and R&D studies have been performed under the strong initiative of the HIMAC group at NIRS. The authors give their sincere thanks to Dr. K. Noda and other members of the HIMAC group.

References

[1] M. Muramatsu, A. Kitagawa, Y. Sakamoto, et al. Compact ECR ion source with permanent magnets for carbon therapy. Rev. Sci. Instr., 75(5), 1925, 2004.

[2] M. Muramatsu, A. Kitagawa, S. Sato, et al., Development of a compact electron-cyclotron-resonance ion source for high-energy carbon-ion therapy, Rev. Sci. Instr. 76, 113304, 2005.

[3] Y. Iwata, S. Yamada, T. Murakami, et al., Alternating-phase-focused IH-DTL for an injector of heavy-ion medical accelerators, Nucl. Instr. & Meth. in Phys. Res., A569, 685, 2006.

[4] Y. Iwata, S. Yamada, T. Murakami, et al. Performance of a compact injector for heavy ion medical accelerator, Nucl. Instr. & Meth. in Phys. Res., A572, 1007, 2007.

[5] K. Noda, K., T. Furukawa, Y. Iwata, et al. Design of carbon therapy facility based on 10 years experience at HIMAC, Nucl. Instr. & Meth. in Phys. Res., A562, 1038, 2006.

[6] K. Noda, T. Furukawa, T. Fujisawa, et al. New Accelerator Facility for Carbon-Ion Cancer-Therapy, J. Rad. Res., 48, Suppl. A, A43, 2007.

[7] M. Komori, T. Furukawa, T. Kanai and K. Noda, Optimization of Spiral-Wobbler System for Heavy-Ion Radiotherapy, Jpn. J. Appl. Phys. 43, 6463, 2004.

[8] H. Tsujii, J. Mizoe, T. Kamada, et al. Clinical Results of Carbon Ion Radiotherapy at NIRS, J. Radiat. Res., 48, A1, 2007.

[9] T. Kanai, N. Matsufuji, T. Miyamoto, J. Mizoe, T. Kamada, H. Tsuji, H. Katou, M. Baba, H. Tsujii, Examination of GyE System for HIMAC Carbon Therapy, Int. J. Radiat. Oncol. Biol. Physics, 64(2), 650-656, 2006.

[10] J. Mizoe, H. Tsujii, T. Kamada, et al., Dose escalation study of carbon ion radiotherapy for locally advanced head and neck cancer. Int. J. Radiat. Oncol. Biol. Phys. 60, 358-364, 2004.

[11] T. Miyamoto, N. Yamamoto, H. Nishimura, et. al., Carbon ion radiotherapy for stage I non-small cell lung cancer. Radiother. Oncol. 66, 127 – 140, 2003.

[12] T. Kamada, H. Tsujii, H. Tsuji, et. al., Efficacy and safety of carbon ion radiotherapy in bone and soft tissue sarcomas. J. Clin. Oncol. 22, 4472 – 4477, 2002.

Secretariat

NIRS

National Institute of Radiological Sciences
Education and International Cooperation Section
4-9-1 Anagawa, Inage-ku, Chiba 263-8555, Japan
E-mail: kokusai@nirs.go.jp
Tel: +81-43-206-3025
Fax: +81-43-206-4061

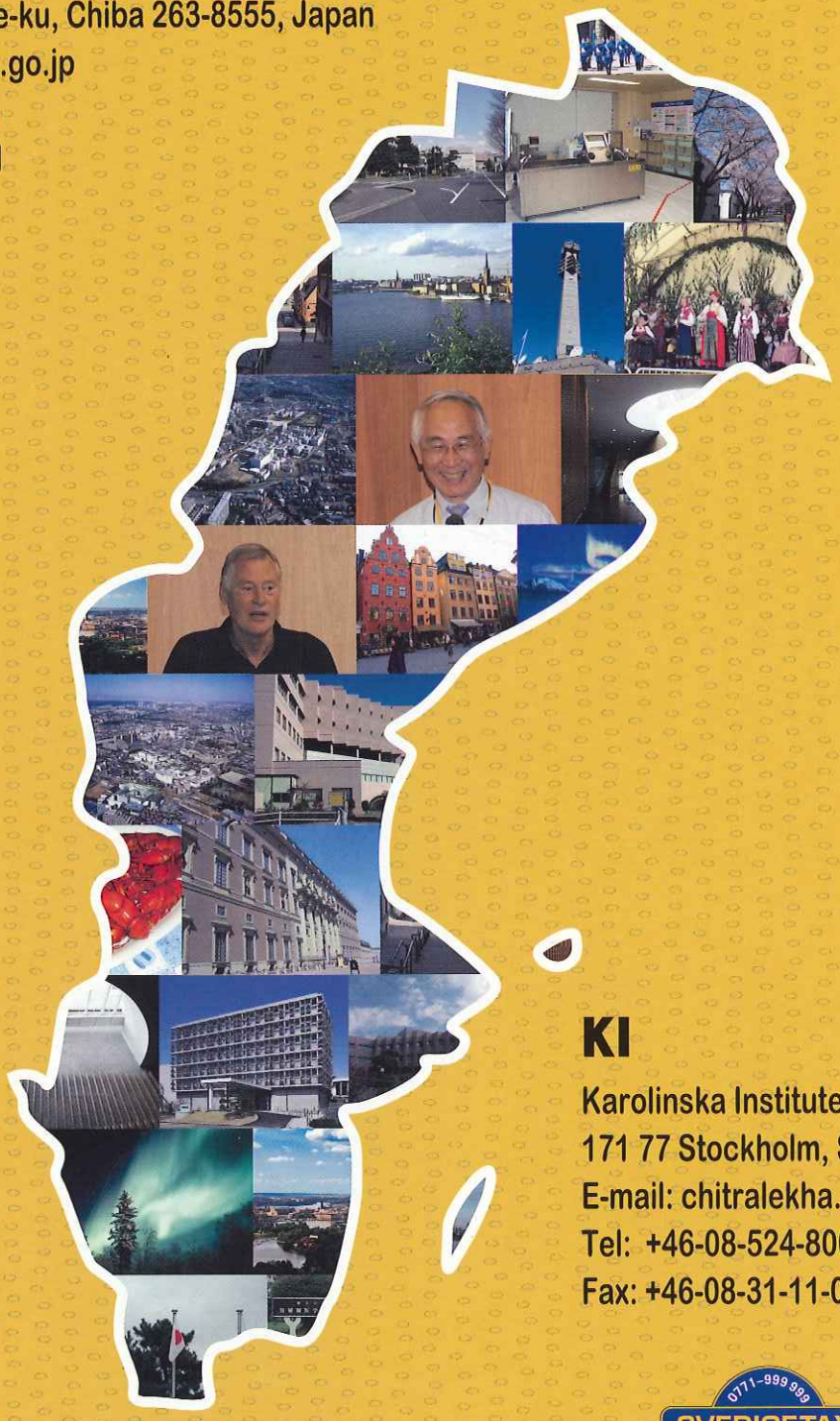

KI

Karolinska Institute
171 77 Stockholm, Sweden
E-mail: chitralekha.mohanty@ki.se
Tel: +46-08-524-800-00
Fax: +46-08-31-11-0

Recyclable paper

This booklet uses paper that meets
Japan's Green Purchasing Law Requirements.